Integrating Crystalline-Silicon Photovoltaic Cells into Decorative Glazing

Dorothy Anne Hardy

Submitted for the degree of Doctor of Philosophy

Heriot-Watt University

School of Engineering and Physical Sciences

March 2015

ABSTRACT

Photovoltaic cells are often perceived as an ugly addition to glazing. Improvements could make photovoltaics more attractive for use in architecture, increasing the opportunities to generate electricity on the surfaces of buildings. This research demonstrates methods of integrating crystalline-silicon photovoltaic cells into decorative glazing. The aim was to explore the use of a combination of opaque, reflective and coloured materials with crystalline-silicon photovoltaic cells in glazing designs, to enhance appearance whilst maintaining good photovoltaic generation. Colour was incorporated through the use of Lumogen F dyes (BASF) added to the photovoltaic encapsulants Sylgard 184 (Dow Corning) and EVA (ethylene vinyl acetate: Solutia Vistasolar Fastcure 486.00). The absorption and emission properties of these new material combinations were measured. The dyes degraded quickly under both accelerated and outdoor testing. Glazing designs were created that incorporated Lumogen dyes, plus opaque and reflective materials. The opaque and reflective materials were used to disguise the square photovoltaic cells. This demonstrated that crystalline-silicon photovoltaic cells could be assimilated into a wide variety of architectural glazing. Reflective materials and fluorescent dyes were shown to improve maximum electrical current from widely-spaced crystalline-silicon photovoltaic cells. Further work is recommended to establish durable material combinations for use with photovoltaics in decorative glazing.

ACKNOWLEDGEMENTS

I am particularly grateful to my PhD supervisors: Sue Roaf's enthusiasm for the project, and encouragement of the artistic side of my work has been key to the success of the project. Gudrun Kocher's enthusiastic assistance and Tadhg O'Donovan's cheerful support have been vital. Bryce Richard's interest in the project proposal and work on the funding application allowed the project to start in the first place. Many thanks are also due to Abdelfateh Kerrouche, the RA on the project, for work on luminescent solar concentrator modelling. Sigrid Blekastad showed great keenness and dedication by making luminescent solar concentrator artworks the focus of her MfA studies, and then joining the project to organise the 'Light Bright Electric' exhibition and workshop.

I am deeply grateful to the Leverhulme Trust for funding this project that combines artistic and scientific methodology.
Additional funding was invaluable in enabling travel to expand the artistic side of the research. This came from the Michael Ventris Memorial Award, presented by the Architectural Association, and from the Spires Network.

The assistance of many members of staff and students in the departments of Engineering and Physical Sciences has been invaluable. In particular, I would like to thank Amanda Hughes, Sean MacDougall and Nabin Sarmah, who were my first office mates at Heriot-Watt University. Brenda Rowan, Gavin Park, Efthymios Klampaftis, Serena Ciorba, Aruna Ivaturi, David Ross, Jonathan Morton, Alessandro Boccolini, Yiorgos Arnaoutakis, Daniel Rylatt, Amber Ityona and Anne-Marie Fuller, have also given great support and friendship. Neil Ross cheerfully cut many photovoltaic cells. Andreas Heipieper was very helpful in assisting in development of EVA sample making. Richard Kinsella and all in the Mechanical and Electrical Engineering workshops provided crucial, ongoing support.

The steering committee for the project freely gave advice, questions, time and enthusiasm: Colin Gilmour, Lucy Hall, Steve McQueen, Keiko Mukaide, Inge Panneels, John Stephen and Crichton Wood.
Peters Glass Studios, Paderborn, Germany was especially important in provision of studio space, expertise and the idea to combine glass painting with crystalline silicon photovoltaics. Special thanks are due to Jan and Wilhelm Peters and to Britta Vormoor.

Solar Capture Technologies supplied materials and useful information on lamination.
Sunovation GmbH supplied PV encapsulation materials, and advice.
Newcastle Optical supplied borofloat glass.
E. Jordan Brookes donated tabbing strip.
Mark McCallum at Edinburgh Instruments assisted with an experiment.

Very many thanks are due to my family and friends, especially to my parents, Catherine and Michael Hardy, for great support for my career and for this research. My father did not live to see the end of this project, but was always encouraging.

And very many thanks to Graham Middlemass for being superb.

ACADEMIC REGISTRY
Research Thesis Submission

Name*:*	Dorothy Anne Hardy		
School/PGI:	Engineering and Physical Sciences		
Version: *(i.e. First, Resubmission, Final)*	Final	Degree Sought (Award **and** Subject area)	PhD Mechanical Engineering

Declaration

In accordance with the appropriate regulations I hereby submit my thesis and I declare that:

1) the thesis embodies the results of my own work and has been composed by myself
2) where appropriate, I have made acknowledgement of the work of others and have made reference to work carried out in collaboration with other persons
3) the thesis is the correct version of the thesis for submission and is the same version as any electronic versions submitted*.
4) my thesis for the award referred to, deposited in the Heriot-Watt University Library, should be made available for loan or photocopying and be available via the Institutional Repository, subject to such conditions as the Librarian may require
5) I understand that as a student of the University I am required to abide by the Regulations of the University and to conform to its discipline.

* *Please note that it is the responsibility of the candidate to ensure that the correct version of the thesis is submitted.*

Signature of Candidate*:*	D. A. Hardy	Date:	11/08/15

Submission

Submitted By *(name in capitals):*	
Signature of Individual Submitting:	
Date Submitted:	

For Completion in the Student Service Centre (SSC)

Received in the SSC by *(name in capitals):*			
Method of Submission *(Handed in to SSC; posted through internal/external mail):*			
*E-thesis Submitted (**mandatory for final theses)***			
Signature:		Date:	

Please note this form should bound into the submitted thesis.

Updated February 2008, November 2008, February 2009, January 2011

TABLE OF CONTENTS

LIST OF TABLES

LIST OF FIGURES

All figures and photos are by the author, unless otherwise stated in information adjacent to the illustration. All drawings, mock-ups and test pieces shown in Chapter 3 and subsequent chapters were designed and made by the author.

GLOSSARY

AM1.5 Air mass coefficient 1.5. This is a standard way of defining the solar spectrum, taking into account the path that light takes from the sun to the surface of the earth through the atmosphere.

BIPV Building-integrated photovoltaics

c-Si Crystalline silicon

EVA Ethylene vinyl acetate

GW GigaWatt (10^9 Js^{-1})

IV Current-voltage

kW_{peak} Maximum amount of power in kW (1000 Js^{-1}) units

kWh kilowatt Hours: A product of energy and time with energy measured in units of 10^3 Watts, with time in hours (kJs^{-1} x hours)

LSC Luminescent solar concentrator

mW milliwatts (mJs^{-1})

P_{max} Maximum power

PMMA Poly(methyl methacrylate), also known as acrylic

PLQY Photoluminescent Quantum Yield

PV Photovoltatic

TWh Terrawatt Hours: a product of energy and time with energy measured in units of 10^{12} Watts, with time in hours

U-value A measure of the insulation level of a material (Wm^{-2})

UV Ultraviolet

W Watts (mJs^{-1})

Wh Watt-Hours: a product of energy and time with energy measured in units of Watts (Js^{-1}) and time in hours

W_{peak} Peak power in units of Watts (Js^{-1})

LIST OF PUBLICATIONS

Material from these papers is included in this thesis.

Journal paper

Hardy, D. A., Roaf, S. C. & Richards, B. S. 2015. Integrating Photovoltaic Cells into Decorative Architectural Glass Using Traditonal Glass-Painting Techniques and Fluorescent Dyes. *Recently accepted by Wessex Institute of Technology Press for inclusion in the International Journal of Sustainable Development and Planning.* [1]

Conference papers

Hardy, D., Kerrouche, A., Roaf, S. & Richards, B. S. 2011. The Search for Building-Integrated PV Materials with Good Aesthetic Potential: A Survey. *In:* Hutchins, M. G. & Pearsall, N. (eds.) *PVSAT-7: 7th Photovoltaic Science, Applications and Technology Conference.* Heriot-Watt University: The Solar Energy Society. [2]

Hardy, D., Kerrouche, A., Roaf, S. & Richards, B. 2012. A Silicone Host for Lumogen Dyes. *In:* Hutchins, M., Pearsall, N. & Cole, A. (eds.) *PVSAT-8: 8th Photovoltaic Science, Applications and Technology Conference.* Northumbria University, Newcastle: The Solar Energy Society. [3]

Hardy, D. A., Blekastad, S., Kerrouche, A., Roaf, S. C. & Richards, B. S. 2012. Creative Use of BIPV Materials: Barriers and Solutions. *27th European Photovoltaic Solar Energy Conference and Exhibition.* WIP. [4]

Hardy, D., Kerrouche, A., Roaf, S. C. & Richards, B. S. 2013. Improving the Aesthetics of Photovoltaics Through Use of Coloured Encapsulants. *PLEA2013 - 29th Conference: Sustainable Architecture for a Renewable Future.* Munich: Technische Universität München. [5]

Hardy, D. A., Roaf, S. C. & Richards, B. S. 2014. Improving the aesthetics of photovoltaics in decorative architectural glass. *In:* Brebbia, C. A. & Pulselli, R. (eds.) *Eco-architecture V: Fifth international conference on harmonisation between architecture and nature.* Siena: Wessex Institute of Technology Press. [6]

CHAPTER 1: INTRODUCTION AND PRECEDENT

1.1 The problem of integrating photovoltaics into architecture

Conventional, crystalline-silicon photovoltaics (c-Si PV) are proving difficult to integrate into a wide range of architectural styles in ways that are both functional and aesthetically pleasing [7, 8]. The reflective surfaces of rectangular PV modules, filled with rows of shiny, square cells, differ strongly from the appearance of many traditional building materials such as roof tiles. It is important to solve this problem, as solar energy is an ideal form of renewable energy for use in built-up areas, since PV can be incorporated onto both the roofs and walls of building structures [9]. More widespread use of solar energy could greatly assist in minimising the use of fossil fuels, and so reducing carbon dioxide emissions and the damaging effects of climate change [10-12]. The UK government has set a target 'of reducing carbon emissions 80% by 2050 compared with a 1990 baseline', which will involve 'emissions from all buildings' being 'reduced to practically zero' [13]. The total amount of electricity generated by all sources in the UK in the first quarter of 2015 was 94.9 TWh [14]. Photovoltaic use is growing rapidly, with UK installed capacity now at 7.265 GW at the end of May 2015, which is an increase of 0.5% of capacity from the previous month and is a marked rise since the end of 2011 when installed PV capacity was 1 GW [15]. The capacity of photovoltaic installations to generate electricity is usually described in terms of peak power (W_{peak}). This is an indication of the maximum amount of power that can be produced with the photovoltaic panels at ideal orientation, with 1000 Wm^{-2} irradiance. Power that has been generated by a PV panel is expressed in terms of Watt hours (Wh): a multiple of the power and the time over which it was generated. Comparison of the peak power and actual power generated over time gives a measure of the effectiveness of a PV system. For example, a standard domestic 4 kW_{peak} system in Stirling, Scotland could be expected to generate 3180 kWh per year [16].

This rapid increase in uptake means that PV is an established part of the UK renewable energy mix, with 'feed in tariffs' providing an incentive to further installation of PV through payments for each unit of electricity generated through use of PV [17]. PV now needs to be demonstrated to be an attractive and fashionable proposition for architects and building owners in order to contend in the very competitive market for building envelope materials [18, 19]. Improving the aesthetics of PV can assist in this, ensuring that negative perceptions of the technology do not cause problems with the uptake of the technology as has happened with wind energy in the UK [20, 21]. There is

a need to establish innovative use of PV as an appropriate building material before standard blue, rectangular PV panels become the only known norm [22].

1.1.1 Choosing crystalline silicon photovoltaics (c-Si PV) from the range of PV materials

There are many types of PV cell. Figure 1.1 is the main section of a conference poster by the author [2] showing the range of PV, from the most efficient and expensive, single-junction PV cells, made from gallium arsenide, that are used mostly in space.

PV material	Maximum Module Efficiency*	Warranty %	Price	In BIPV?
Mono-crystalline silicon	19.7% [2]	Normally 80% at 25 years	Low <2 €/W_p	Yes
HIT (Hetero-junction with intrinsic thin layer)	19.0% [2]	76% after 25 years	Medium	Yes
Multi-crystalline silicon (including ribbon and sheet)	15.4% [2]	80% at 25 years	Low	Yes
Micro-crystalline silicon	13.7% [2]	80% at 25 years	Low	Yes
Amorphous silicon	7.3% [2]	80% at 25 years	Low	Yes
CIS (Copper Indium Selenide) and CIGS (Copper Indium Gallium (di)Selenide)	12.7% [2]	80% at 25 years	Medium >2 €/W_p	Yes
CdTe (Cadmium Telluride)	11.1% [2]	80% at 25 years	Low	Yes
GaAs (Gallium Arsenide)	*28% [5]	At least 15 years [5]	High	In space and on solar cars
Organic	*8.3% for 1cm^2 [6]	1 to 3 years [7]	Low	Bus shelters[7]
Dye-sensitised	*9.9% for 17.1 cm^2 [6]	1 year: indoor applications [8]	Low	Yes, experimentally
LSC (Combined with Gallium Arsenide PV)	7.1% [9]	Not available	High	Small area experimental designs only
LSC (With silicon PV)	2% [10]	Not available	Low	Experimental designs only

* denotes cell efficiency % indicates percentage of nominal power [2]

References

1. Gaiddon, B., H. Kaan, and D.M. (editors), 2009. *Photovoltaics in the Urban Environment.* London: Earthscan.
2. PI. *Market Survey on Solar Modules 2011.* Photon International, 2011. **2**: p. 184 - 221.
3. http://www.gintech.com.tw/en/product.php?prekey=1258349638.
4. Wuerth_Solar, *The CIS technology in buildings.*
5. http://www.spectrolab.com/solarcells.htm.
6. Green, M.A., et al., *Solar cell efficiency tables (version 37).* Progress in Photovoltaics: 2011. **19**(1): p. 84-92.
7. http://www.solarmer.com/productbipv.php.
8. http://www.g24i.com/filebase/G24i_Indoor_Specification_Sheet.pdf.
9. Slooff, L.H., et al., *A luminescent solar concentrator with 7.1% power conversion efficiency.* physica status solidi (RRL), 2008. **2**(6).
10. Wilson, L.R., 2010. *Luminescent Solar Concentrators: A Study of Optical Properties*, PhD, Heriot-Watt
11. Bates, R. and B. Faircloth, *Assessing the applicability of building integrated organic photovoltaic modules through a surface area approach*, in *Solar Building Skins* 2010: Bressanone, Italy. p. 31-41 .

Figure 1.1: Types of PV with efficiency and lifetime details, from the poster to accompany 'The Search for Building-Integrated PV Materials with Good Aesthetic Potential' [2]

At the other end of the scale are organic PV cells which can be made at very low cost, but have short lifetimes leading to unsuitability in many architectural applications. The majority of standard PV modules contain PV cells made from squares of crystalline silicon (c-Si) [23] which generally appear blue or black due to the addition of anti-reflection coatings, so that maximum amounts of light are absorbed. This type of PV offers the best combination of efficiency, durability and cost [2], and have been developed over several decades [24]. There is continual improvement of all types of PV, leading to gradual increases in efficiency for PV materials [25, 26]. The maximum, recorded efficiency of a monocrystalline c-Si PV module has increased from 19.7% when the information in Figure 1.1 was compiled in 2011, to 22.9 ± 0.6% in 2014, with similar increases in efficiency for other types of PV [27]. In parallel with these PV efficiency increases, there is an ongoing discussion about better methods for integrating PV into the built environment [28, 29]. Large-scale incorporation of PV into clusters of buildings has already taken place [30]. This leads to the possibility of a backlash against this change in appearance of the built environment [22]. If PV is to become a desirable addition to architecture, the development of functional building-integrated PV with good aesthetics requires as much attention as improvements in PV efficiency [1, 18].

1.2 Photovoltaics in architecture

PV can be applied over entire building envelopes, with c-Si PV modules now established for use in both roof and façade-mounted installations. Figure 1.2 shows roof-mounted PV in the UK and Germany.

Figure 1.2: Roof-mounted PV in Newcastle-upon-Tyne, UK (left); and in Paderborn, Germany (right)

There is a mismatch between the red roof tile colours and the blue, reflective surfaces of the PV panels. The panels are applied to the existing building skin, rather than being

integrated into the architecture. Panels with red backings are available, to overcome the colour contrast [31]. The entire roof surface can also be covered with PV [29], especially when there are no obstructions such as chimneys or roof lights. Products such as c-Si PV roof tiles and slates are also available to disguise the appearance of PV on roofs [32]. These replace existing roofing materials, and are more expensive than standard c-Si PV panels, so are less-commonly used [33].

Table 1.1 shows a selection of inventive uses of roof-mounted PV. The first photo shows the Sunovation headquarters, where matching of colour and shape between the roof and façade ensures that the square shapes of the PV modules fit in with the colour of the structure.

Table 1.1: Examples of roof-mounted PV

Photo of installation	Description, location and comments
	Sunovation GmbH, Elsenfeld, Germany A good match between the PV colour and shapes and that of the dark glazing below.
	Smartcity Barcelona provisional Control Centre, Barcelona, Spain Eye-catching installation attracts attention to the PV. Panels at different angles to incident sunlight cause shading that will reduce power outputs.
	Bus shelter, Edinburgh, UK Flexible, amorphous-silicon PV cells fit the curved roof shape. The lower efficiency of amorphous silicon compared with c-Si PV are viable structures with low power requirements.

The use of a circular roof highlights the square PV module shapes. The second photo is a playful installation in which the PV modules are highlighted by the angles at which they are placed, as well as the contrast in colour and texture between the wooden structure and PV. The photo at the bottom of the table shows flexible, amorphous silicon panels on a bus shelter. These are visible only from above, so there is little need

to blend their colour in with that of the bus shelter roof. These examples show that PV can be fitted onto many different types of structure, but that the blue and black, rectilinear modules tend to dominate the appearance of structures into which they are incorporated.

1.2.1 Integrating PV into architecture

PV can be integrated in any position on a building envelope that is not shaded: roofs and façades are the most common. Table 1.2 (below) shows examples of c-Si PV mounted on vertical surfaces. The first photo shows PV covering a section of wall, providing a strong contrast with the white wall and the green creeper. In the second photo, one wall is completely covered in PV panels whilst another has spaces between the modules. The photos in Table 1.2 show the tendency to arrange PV modules geometrically, which is similar to the method of application of many building materials, but is limiting when attempting to use c-Si PV artistically, as discussed in section 1.2.2 below. The examples show c-Si PV retrofitted to building surfaces. The photo at the bottom of the table shows retrofitted c-Si PV modules used to create a curtain wall. In new build, PV modules can replace other materials such as glass panels that are often used to create curtain walls [18, 28, 34]. Innovative examples of design with building-integrated PV have been extensively documented [9, 29, 28, 30, 35, 36]. The IEA (International Energy Agency) task 7 developed a set of guidelines for good practice in integration of PV into architecture [37]. These included a requirement for PV to be 'in harmony' with other building materials [18]. The guidelines indicate that PV should be both an integral part of the building, and an 'eyecatching' feature. More recently, the findings of IEA task 41 state that PV products are required that can replace other building components [38]. These building-integrated PV components must have all the characteristics of the required building materials, including structural properties. PV module design should also be adaptable if PV is to be integrated into a wide variety of building styles. Kanters [39] describes a need for PV and with good aesthetics, and Farkas [40] points out that PV integration into a building should take place at all levels, from cell to array. One method of ensuring that PV is more widely used in architecture is to aim for 'visual mediocrity' of the PV elements, as suggested by Lüling [41]. This is particularly difficult due to PV products being complex assemblies of several materials [42] with a very different appearance from many building materials. Scognamiglio described an approach that capitalised on this, in which traditional building styles were complemented by the addition of photovoltaic elements [43].

Table 1.2: Examples of vertically-mounted c-Si PV

Photo of installation	Description, location and comments
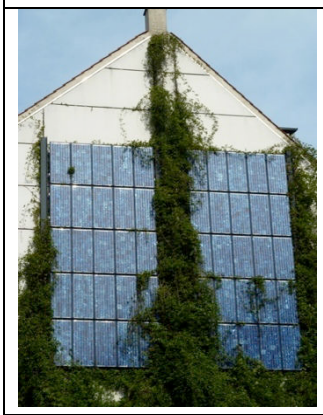	Building in Hedebygade, Copenhagen, Denmark PV on a wall that would otherwise be plain white or covered in foliage. Creeper is shading parts of the PV.
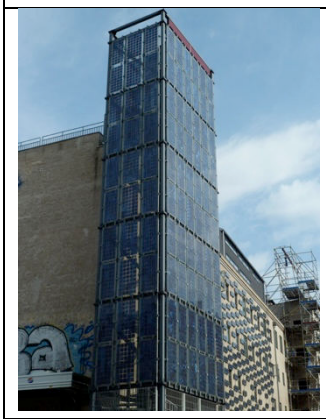	Building in Eskildsgade, Copenhagen, Denmark Two different patterns of PV array provide a contrast whilst covering a plain wall.
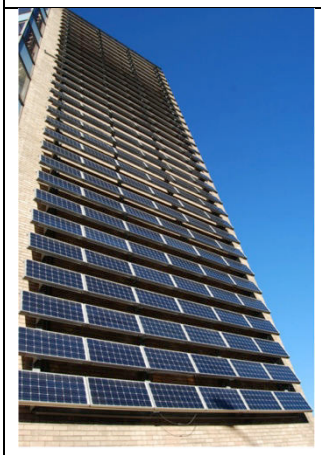	Napier University, Edinburgh, UK Standard, rectangular PV panels highlighting an end wall of a tower block.
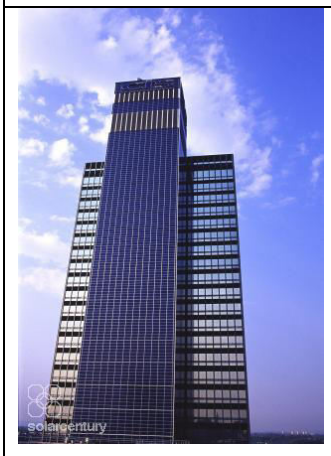	The CIS tower, Manchester, UK c-Si PV modules are retrofitted to the central section of the tower, forming a cladding. Photo by Oliversb (Own work) [CC BY-SA 3.0 (http://creativecommons.org/licenses/by-sa/3.0)], via Wikimedia Commons

In contrast, Hermannsdörfer and Rüb describe projects where the approach was often to disguise PV materials added to traditional buildings [44]. This included screen-printing on the glass covering PV cells, which reduces module efficiencies. An approach is required in which improved aesthetics can be combined with maintenance of good PV efficiencies.

1.2.2 The use of artistic techniques to improve the aesthetics of PV

The use of art offers one way of resolving the conflict between the need to make PV desirable, and ensuring that PV products do not clash with other building elements. This approach is recommended by both Claus [45] and Farkas [40]. Investigations such as the BIMODE [46] and HAVEMOR projects [47] demonstrated that variation in colour and shape of PV cells and modules could be achieved. In both of these projects, the anti-reflection coating thickness of c-Si PV cells was altered to change the surface colour, but this led to decreases in efficiency compared with standard blue or black c-Si PV. Coloured c-Si PV cells are commercially available [48], but are rarely used [49] due to the lower efficiencies. Table 1.3 shows some examples of standard blue or black c-Si PV used artistically. The first photo in Table 1.3 contains an example of PV applied over the surface of a gable end. Neon lighting covers the PV and is visible at night, as shown in the second photo of the building. The other photos show c-Si PV incorporated into structures. The rectilinear nature of the c-Si PV cells and arrays dominates all the examples in Table 1.3. This greatly limits the artistic application of c-Si PV. Alternative approaches are required.

1.2.3 c-Si PV in glazing

The advantage of light-transmitting PV is that it is straightforward to incorporate into new-build or to retrofit into architecture [50]. Baum has amassed extensive databases of innovative structures that contain PV [7, 49]. He concludes that many innovative PV installations are part of light-transmitting structures. These typically comprise c-Si PV cells sandwiched between layers of translucent glass or polymer, and arranged so that there are gaps through which light can pass, as shown in Table 1.4.

Table 1.3: Examples of artworks incorporating PV

Photo of installation	Alternative view or detail of installation	Description, location and comments
 By day	 At night (with neon lighting)	Provehallen, Valby, Denmark: Black, mono-crystalline PV with neon lighting. Designed by Anita Jørgeson [51]
 'Stele' by Celia Mendoza. Photos included with permission from Derix Glasstudios GmbH, Taunusstein, Germany.		Detail of 'Stele' screen incorporating c-Si PV cells. Square elements within the screen match the size and shape of the c-Si PV cells.
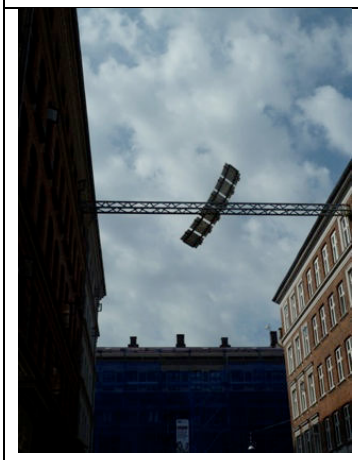	 Detail showing c-Si PV array (with birds' nest underneath).	Eriksgade, Copenhagen, Denmark. A small c-Si PV array is mounted between buildings. This minimises any possible shading of the PV.

The first example in Table 1.4 (below) shows c-Si PV modules that are mounted in front of windows. Light is transmitted through the gaps between the c-Si PV cells. The second photo shows a retrofitted glass façade incorporating monocrystalline c-Si PV modules [52]. The photo on the right shows the detail of the opaque, square c-Si PV

cells that are laminated into clear glass-glass modules. There is a large area of glazing at the top of each window aperture that does not contain PV cells, in both this and the first example in the table. The strong light-dark contrast between the dark c-Si PV cells and surrounding areas of glass leads to a grid pattern of light reaching the building interior, as shown in the photo on the bottom, right of Table 1.4. This can be acceptable for an outdoor structure such as the canopy shown at the bottom of the table. But the rectilinear patterns could be intrusive if transmitted to a building interior, as shown by Gunnarshaug-Lien [53].

Table 1.4: Examples of light-transmitting c-Si PV installations

Photo of installation	Description, location and details
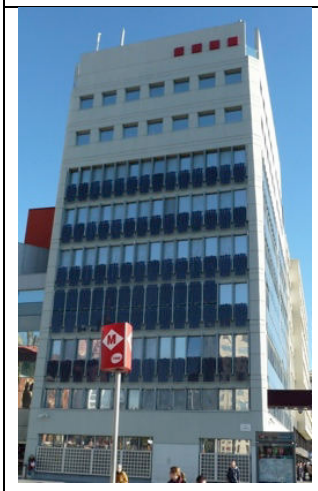	Tower block, Placa d'Espagna, Barcelona, Spain PV partially covers the glazing, as shown in this detail: 
	NTNU (Norges teknisk-naturvitenskapelige universitet), Trondheim, Norway  Retrofitted glass with integrated c-Si PV
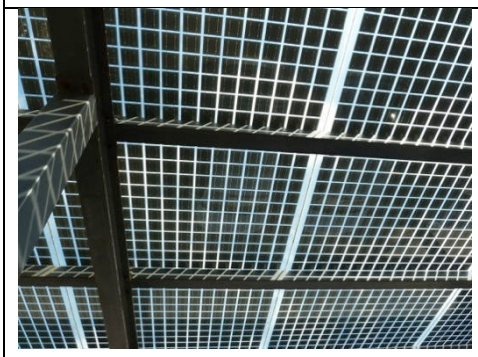	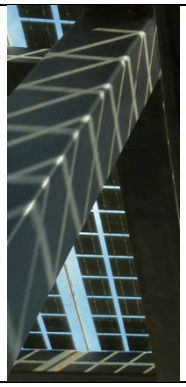 Solar Capture Technologies, Blyth, UK Light-transmitting canopy incorporating c-Si PV cells. This detail shows the patterns of light transmitted onto a supporting post of the canopy.

The first two examples in Table 1.4 show c-Si PV module placement limited to the bottom of the window apertures to ensure that most light reaching the building interior is not transmitted through rows of c-Si PV cells. PV glazing is commercially available, such as that from Onyx solar, which has a 'pixellated' appearance [54]. The ASI-thru glass used on the Schott-Iberica building also demonstrated that dark PV elements contrast with sections of transparent glazing [55]. For all PV glazing, the proportion of glass that needs to be covered by PV cells depends on the amount of electricity that is required from a given area of glazing. This has to be balanced with the amount of transmitted light that is required. A method is required to reduce the strong contrast between light-transmitting areas of glazing and dark areas covered by PV cells.

1.2.4 Artistic development of light-transmitting PV

Current PV module rectilinear production and assembly systems constrain architectural glass artists into working with the contrast between geometric PV and translucent, coloured or patterned areas of glazing, as discussed in section 1.2.2. The decorative PV glazing in Figure 1.3 is an example of this.

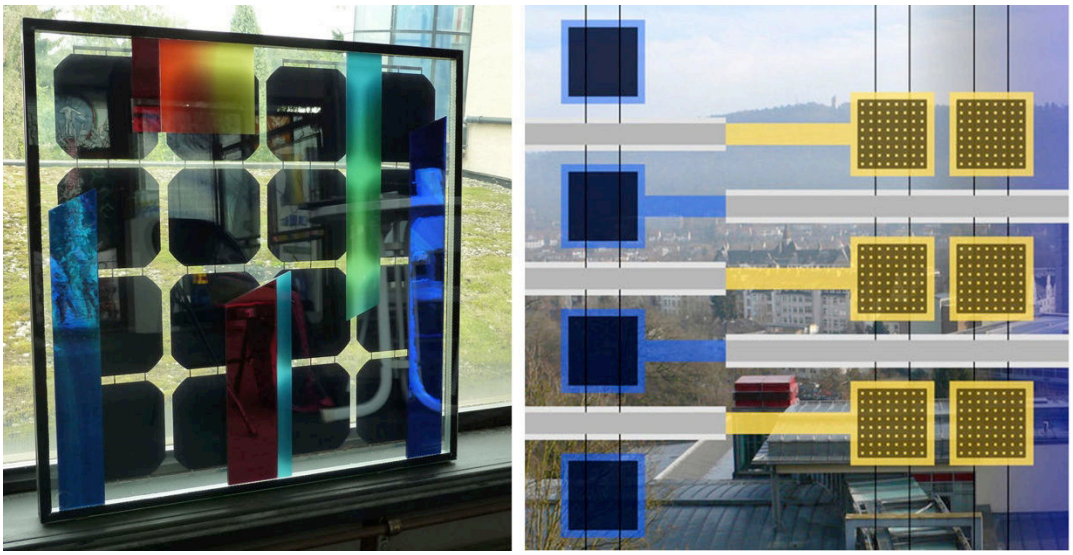

Figure 1.3: Glass panel incorporating c-Si PV cells by Raphael Seitz (on the left). Photo included with permission from Derix Glasstudios, Taunusstein, Germany. Detail of Jochem Poensgen's c-Si PV glazing at Parkhaus Pilgrimstein, Marburg (on the right). Photo reproduced with permission from Jochem Poensgen.

There is rich tradition of decorative architectural glass, which has been used to enhance architecture artistically, and to alter light levels and colours within buildings for centuries [56-58]. The traditional design of architectural glass shown in Figure 1.4 is one example of the level of sophistication and detail that has been reached in this medium. Many artists are keen to increase the sustainability of their work [59] with a

need to work to benchmarks such as BREEAM® [60] when designing glazing for use in buildings. Work with PV can assist in this, and some artists are already working with PV, as discussed in sections 1.2.2 and 1.2.4. Increasing the range of styles and materials for design of decorative PV glazing will facilitate this development, leading to a wider variety of building-integrated PV.

Figure 1.4: A traditional example of decorative architectural glass at Peters Studios, Paderborn, Germany. Photo reproduced courtesy of Peters Studios.

A variety of architectural glass artworks have been created, using c-Si PV [49, 40]. Baum developed a series of light-transmitting PV designs [61]. These utilise the rectilinear nature of the PV modules and strings. Colour, lettering and other artistic forms have been introduced into novel module designs, from Jochem Poensgen's minimalist use of a few PV cells and some colour [62], shown on the right in Figure 1.3, to use of colour and text in conjunction with PV cells, in Lynn Goodpasture's PV windows in Pearl Avenue Branch Library, San José, California [63] (shown on the left in Figure 1.5), and Sarah Hall's c-Si PV designs, such as Lux Nova, at Regent College, University of British Columbia, Canada [64], shown on the right in Figure 1.5. These examples all explore the strong contrasts between the opaque, square PV cell shapes, and other aspects of the designs. They also contain straight strings of PV cells in rectilinear groupings. Methods are required to create curvilinear as well as rectilinear designs, as well as disguising the opaque squares of c-Si PV.

Figure 1.5: Solar Illumination 1 / Evolution of Language ©2008 Lynn Goodpasture Art & Design at Pearl Avenue Library, San Jose, CA (on the left). Photo by Lucas Fladzinski reproduced with permission from Lynn Goodpasture. On the right is Sarah Hall's Lux Nova installation at Regent College, Vancouver, Canada. Photo reproduced with permission from Sarah Hall.

1.2.5 Use of colour

Photovoltaic cells function by converting light to electricity [9]. Light is perceived by the human eye as colour, with white light being a mixture of primary light colours [65]. Colour can be defined as the way in which the human eye experiences light [66]. Colour is a vital component of much artistic design, including stained and decorative glass, in which changes in the transmitted and reflected light provide changing displays of colour observed as part of the artwork itself and transmitted into the surroundings [58, 67]. Perception of colour varies between individuals [68], and accurate description of colours is vital to ensure consistency in reproduction of colour in applications from TV screens to preparation of glass paints [66, 56]. Colour can be described accurately through use of colour space as defined by CIE 15 [69, 70]. Each point in the CIE colour space indicates a different perception of colour. The colour space is broken down into three components:

Hue: The wavelength of the light, giving the position in the electromagnetic spectrum

Lightness: The amount of light incident on the human eye

Saturation: The amount of white light included in the mixture [66]

The hue can be described by the name of the colour, such as red or yellow. The lightness and saturation values give precise details of the intensity and paleness of the

colour. Colour difference can therefore be described accurately through use of separate sets of coordinates in colour space.

Colour is such as important component of much decorative, architectural glass [57] that its use in combination with photovoltaic cells was seen as an important part of this PhD research. The following section gives details of addition of colour to PV through use of luminescent solar concentrators (LSC's).

1.2.6 The use of luminescent solar concentrators

Colour can be added to PV modules by addition of coloured films or backsheets [31]. These alter the colour of the areas surrounding the PV elements as well as the appearance of the backs of the PV cells. These materials do not alter the appearance of the fronts of the PV cells. Another method of creating coloured PV modules is to use luminescent solar concentrators (LSC's). These are devices in which thin strips of PV are applied to the edges of translucent plates that contain fluorescent dye [71]. Light is emitted by the dyes and can be guided to PV cells [72]. The principle is illustrated in Figure 1.6. This shows light incident on a PV cell that is covered by a material containing Lumogen Red 300 fluorescent dye. The dye molecules absorb light, particularly in the green to yellow area of the visible spectrum (500 – 580 nm). They then emit red light (585 – 670 nm). This process is called luminescent downshifting. Some of the emitted light is reflected between the surfaces of the dye-doped materials, in a process of total internal reflection. This process transports light to the PV cell from adjacent areas. LSC's can function in diffuse light, making them useful in regions where cloud cover is common [73]. A variety of materials can be used to absorb and re-emit light within LSC's including fluorescent dyes, which are available in a range of colours [72, 74]. Lumogen F dyes are established from among the available fluorescent dyes as suitable for use in LSC's [75, 76]. These dyes absorb light over narrow ranges of wavelengths, altering the colour of encapsulants whilst still allowing light at other wavelengths to reach underlying PV cells [72, 77, 78]. LSC's offer possibilities for artistic use, because of the colour of the dyes, and the fact that the PV cells can be concealed at the edges of modules, leaving coloured areas of translucent, dye-doped material, through which light can be transmitted.

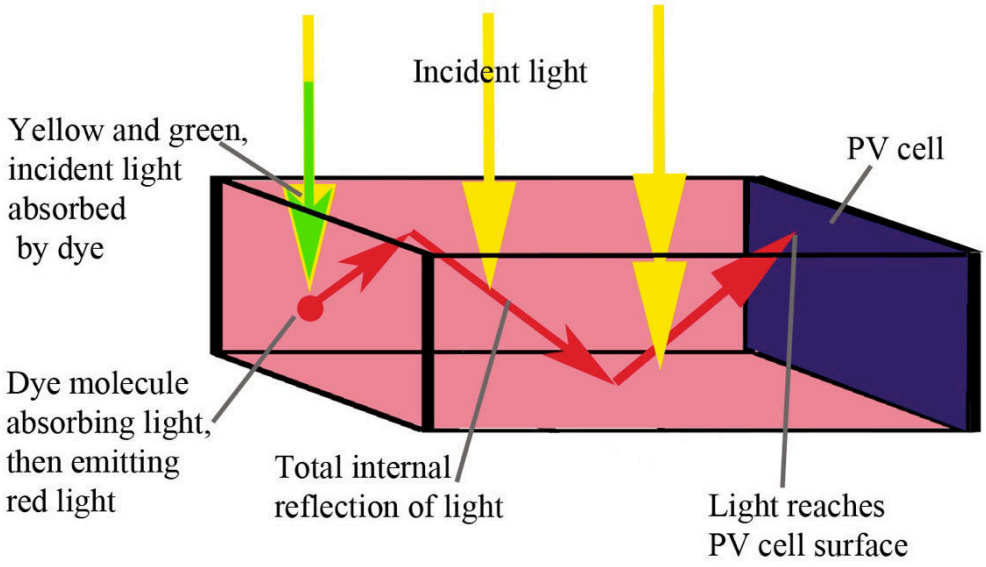

Figure 1.6 Schematic of a luminescent solar concentrator, with light being absorbed by a Lumogen Red 300, fluorescent dye molecule; emitted at a longer wavelength; then moving through the encapsulant material, until it reaches the surface of a PV cell.

1.2.7 Measurement of the properties of light-transmitting materials for use with PV

The performance of the dyes used in LSC's is normally measured by investigation of the way in which the dyes absorb and emit light [73, 76]. Use of CIE colour measurements (as discussed in section 1.2.5) could also be used, but this does not provide detail about the fluorescence of the dyes. Fluorescence of light can be measured using spectrometers or fluorospectrometers. The materials are placed within the machines so that light within precise wavelength bands can be measured as it is directed towards the material, or as it is output. The setup can be varied so that the fractions of light that are absorbed, transmitted, reflected or emitted by materials are measured [79].

LSC's are primarily intended for use in glazing [71]. Glazing is used mainly to transmit light to the interior of buildings. The methods of measurement of the performance of glazing are designed to give details about the amount and quality of transmitted light [80]. Light can be lost through absorption within materials such as glass, or by reflection or scattering. BS EN 410 [80] sets out the method of calculation of the fractions of incident light that are absorbed, reflected and transmitted by glazing. Building glazing systems should also be designed to provide as much insulation as possible. U-values define the amount of insulation provided by each element within a glazing system. U-values can be calculated from the properties of the glass and additional materials [81] or measured using the 'guarded hot plate method' [82].

The standard test method of performance of PV modules involves measurement of current-voltage (IV) characteristics [83], which is a measure of the power output of

the PV over a changing load. This shows the maximum power that can be generated by the module at a given irradiance, as well as being a test of the performance of the circuit of connected PV cells. The method of IV testing is ideal for comparison of performance of PV glazing modules.

1.3 Chapter conclusion

Increased use of building-integrated photovoltaics can provide an alternative to alleviate reliance on fossil fuels. There is a wide range of inventive architecture and art that incorporates PV, especially the most widely used crystalline-silicon (c-Si) PV. Use of c-Si PV in architectural glass is one important area of evolvement, as glazing is relatively straightforward to retrofit into buildings. There is a rich tradition of architectural glass art, but rows of opaque, square c-Si PV cells are difficult to blend into translucent glazing. Development of more design options would enable PV to be integrated into a wider variety of decorative glazing. Use of luminescent solar concentrator technology is one possible area of development. This is discussed further in Chapter 2, which also gives details of the choice of methodologies to move on from the precedent.

CHAPTER 2: CHOICE OF METHODOLOGIES

2.1 Chapter synopsis

This chapter gives details of the chosen methodologies and materials for this PhD research. The aim was to integrate c-Si PV into a range of glazing designs. An approach was chosen in which improved aesthetics could be combined with maintenance of good PV performance. The use of front-facing luminescent solar concentrators (LSC's) with dye incorporated within the encapsulant layer was chosen, combined with traditional and modern methods of applying coatings to glass.

2.2 Research aims for this PhD

Chapter 1 showed that one problem with current development of building-integrated PV is the difficulty in blending c-Si PV cells into a wide variety of glazing designs. There has been extensive discussion of good practice in integration of photovoltaics into architecture, as described in section 1.2. Building and glazing designers have incorporated c-Si PV into architecture, working with the rectilinear PV cell and array shapes. This PhD advances the research by establishing practical methods of integrating c-Si PV cells into a wide range of decorative architectural glass styles. This can already be achieved by sacrificing some PV efficiency, as discussed in section 1.2.2 and in Hermannsdörfer and Rüb's study of projects in which the PV was integrated into traditional architecture [44]. The aim of this PhD research is to blend c-Si PV into glazing whilst optimising electrical power production from the PV. This involves creation of designs and selection of materials that will enhance the appearance of the architectural glass whilst ensuring that optimal amounts of light reach the c-Si PV cells. This practical approach combines use of scientific methodology with techniques from architectural glass art practice.

Figure 2.1 shows the decisions to be made when designing a piece of decorative glazing that incorporates PV. The section highlighted in green illustrates the main areas covered by this PhD research. The top of the diagram shows that the first steps are to establish the need for glazing and the need for PV. Glazing is usually required for light transmission. This function can be combined with creation of a dramatic statement through design of architectural glass that demonstrates the aspirations of the building users or owners [56, 58]. This can incorporate promotion of 'green' credentials [1, 44]. This may mean that the PV cells are to be displayed prominently, in which case a scheme incorporating lines of square c-Si PV cells can be ideal. But if PV is to be

assimilated into an increasingly wide range of decorative glazing, including curvilinear designs, then additional approaches are required, as discussed in chapters 3, 7 and 9. This development could also prevent a backlash against widespread use of building-integrated PV [22], as has occurred for wind turbine generators [21].

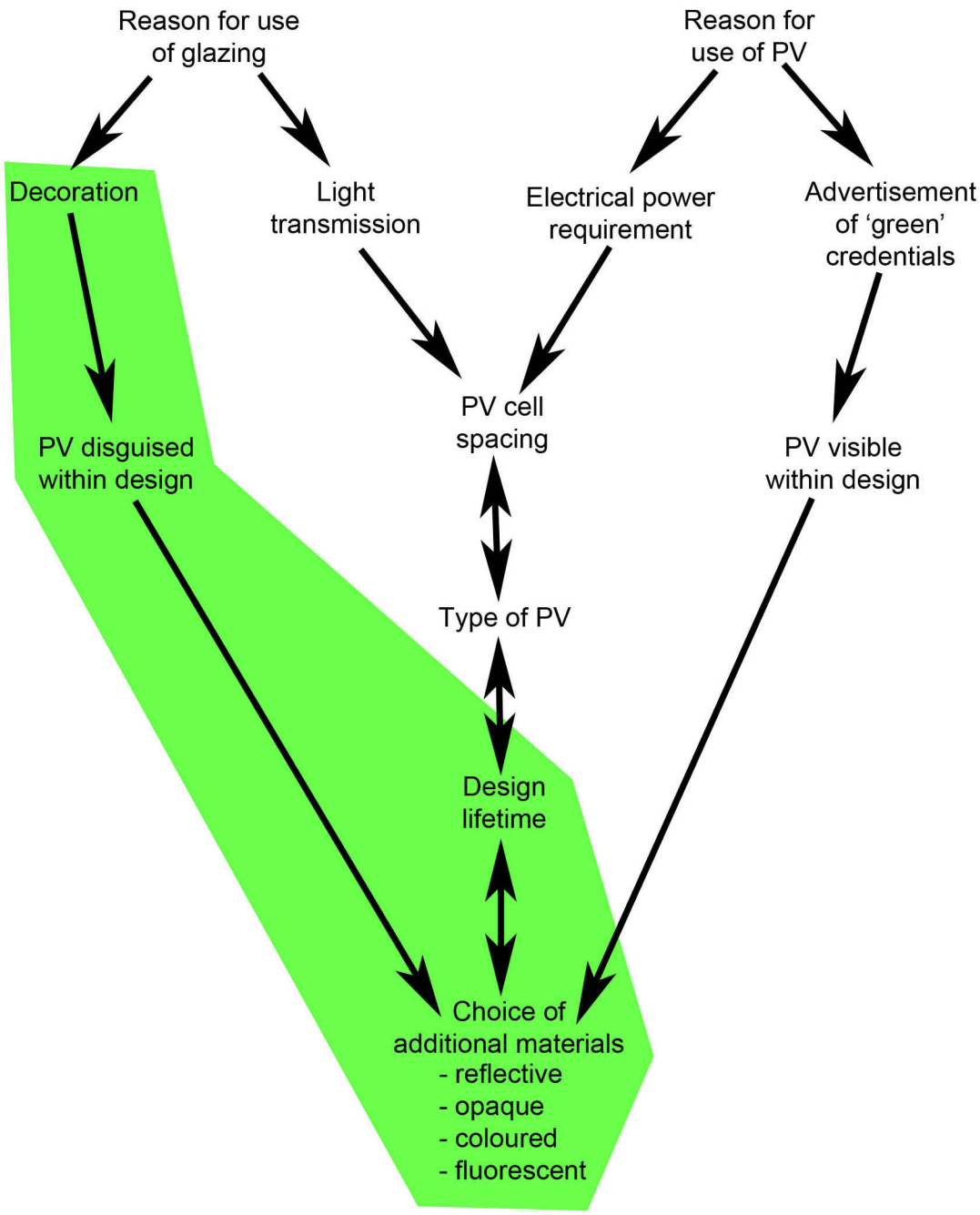

Figure 2.1: Decisions to be made when designing decorative PV glazing

The centre of the second row of Figure 2.1 shows that a balance has to be achieved between sections of glazing through which light can be transmitted and areas covered by opaque or semi-translucent PV from which electricity can be generated. This

balance dictates the spacing of PV cells, which is also dependent on the choice of PV, as different types of PV generate dissimilar amounts of electricity per unit area.

The most widely-used type of PV is c-Si PV, as discussed in section 1.1.1. The research in this PhD focuses on use of c-Si PV in order to make the work relevant for use now. An alternative is to apply thin-film PV directly to substrates during manufacture of the PV [84]. If the efficiencies and lifetimes of thin film PV become suitably competitive with those of c-Si PV, then the method of manufacture of decorative glazing can be altered, so that PV can be applied to substrates in a wide variety of configurations. It is important to establish a precedent for good aesthetics and extensive design variety in PV before use of thin film PV becomes more widespread. This can ensure that building-integrated PV glazing is shown to be an adaptable and desirable architectural component.

This PhD research focuses on establishment of an initial range of designs and material combinations that can be used to create decorative glazing into which c-Si PV cells are blended. This precedent can then become a start point for further development of designs that will fit into a variety of architectural styles. Placing PV within architectural glass is a compromise between the need to generate as much electricity as possible from closely-spaced PV cells, and the need for areas of glazing through which light can be transmitted. The ideal balance between electricity generation and light transmission will vary according to the location in which glazing is to be installed, the electricity requirements and the design style constraints for the given piece of architecture. There is some discussion of this balance in chapters 3 and 9, but the main aim is to establish design variety.

2.2.1 Summary of thesis aims

The main aim of this thesis is to establish that great variety in design of c-Si PV glazing is possible, and to create designs that demonstrate this. The principles can then be applied widely through use of a range of materials and by variation of PV cell layout. The secondary aim of this research is to ensure that power outputs from c-Si PV cells are optimised through use of designs and materials that enhance the amount of light incident on the PV. This provides some compensation for reduced electricity production per unit area due to wide PV cell spacing within light-transmitting glazing.

2.3 Initial designs

Section 1.2.6 described two main methods for incorporating c-Si PV cells into glazing:

- By sandwiching c-Si PV cells between layers of glass or polymer
- By placing strips of c-Si PV at the edges of fluorescent materials to make luminescent solar concentrators

To experiment with both of these methods, two initial designs were made up by the glass artist Sigrid Blekastad, with assistance from the author [4]. These are shown in Figure 2.2. Both artworks incorporated engraving on glass: to add detail around the standard array and to provide a focal point in the LSC artwork. In the design of the artwork with a conventional c-Si PV array, the aim was to detract attention from the central, square PV cell shapes by use of a curved piece of blue glass behind the c-Si PV cells, and by incorporating broken PV cells into the array shape. When the panel was placed in front of a light source, the translucent, blue glass also transmitted light, so that the opaque c-Si PV cell shapes still dominated the design. In the LSC artwork (on the right in Figure 2.2) sections of metal tabbing strip were used decoratively. These reflected light, especially in conditions of low lighting, adding interest to the artwork.

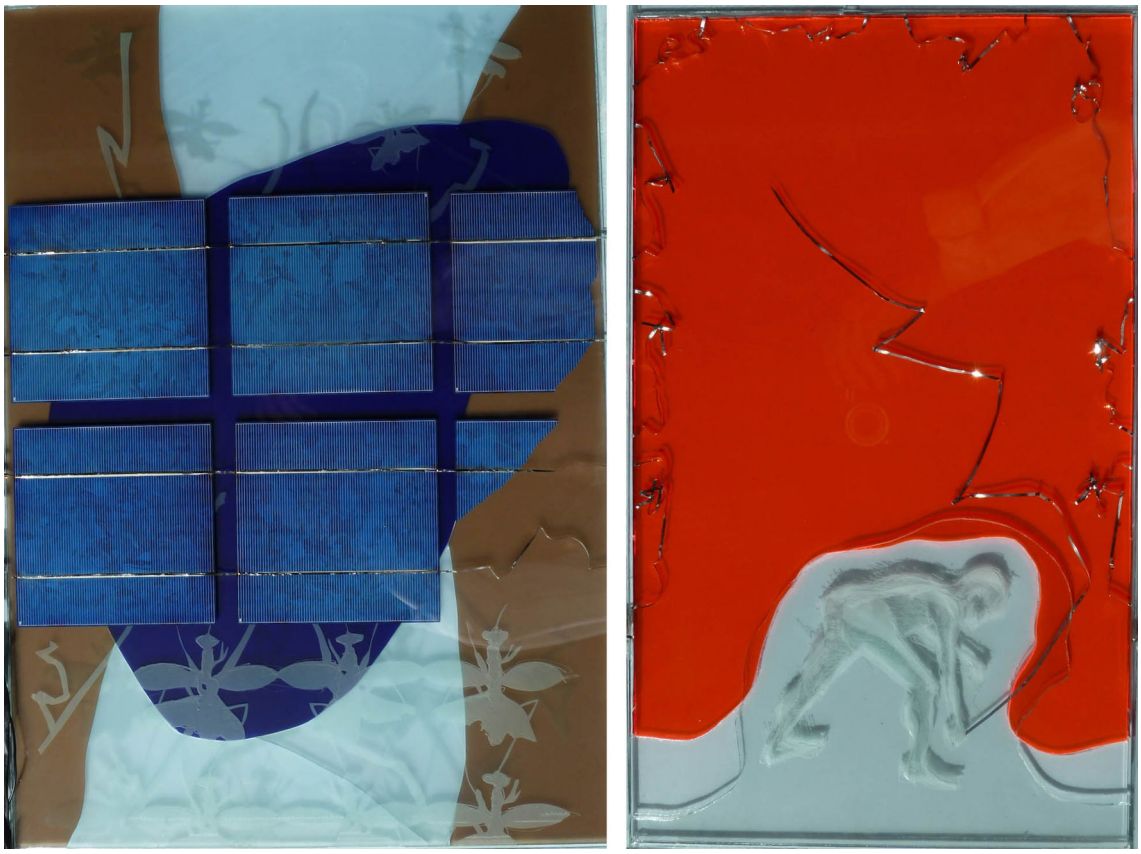

Figure 2.2: Decorative glass panels incorporating c-Si PV, made by Sigrid Blekastad. Left: with front-facing PV; Right: luminescent solar concentrator with edge-mounted c-Si PV strips

Testing of power outputs from both artworks showed that the conventional c-Si PV

array produced a maximum power per unit area of 7.3 Wm^{-2}, and the LSC artwork produced a maximum power per unit area of 2.2 Wm^{-2} [4]. These values are low, due to faults in fabrication of both modules, but it is clear that the front-facing PV configuration, as shown on the left of Figure 2.2, produced a greater maximum power per unit area than the LSC panel with side-mounted c-Si PV strip cells. A similar conclusion was reached by Wilson after a thorough analysis [85].

The advantages of both panels could be combined through use of coloured, fluorescent dyes, as in the LSC panel, used with front-facing PV. This principle has been demonstrated by Klampaftis [77] and Corrado [86]. Light incident on areas of fluorescent material covering c-Si PV cells is transported to the PV cell surfaces by a process of total internal reflection. The process is as shown in the schematic of a luminescent solar concentrator in Figure 1.6, but with the PV cell underneath the fluorescent waveguide, rather than at the edge. Some incident light is absorbed by the fluorescent dye before reaching the PV cells, but this is compensated for by transport of light from areas surrounding the PV cells [86]. Light that is not absorbed by the dye is transmitted through the translucent areas surrounding the PV cells. This technology is therefore appropriate for use in glazing schemes where light transmission is required. The fluorescent dyes add colour whilst transporting light to PV cells. Development of front-facing luminescent solar concentrators provides one method of fulfilling the aims of this PhD research, by enhancing the appearance of c-Si PV within architectural glass whilst maintaining good PV efficiency.

2.4 Material selection

The choice of materials used to construct light-transmitting PV glazing affects both the appearance and durability of the finished products. To create light-transmitting panels that act as front-facing LSC's, fluorescent dye can be contained within a material such as polymethyl methacrylate (PMMA), which is placed over PV cells, as shown by Corrado [86]. PMMA is unsuitable for many architectural applications as it is easily abraded and can be a fire hazard [87]. An alternative is to incorporate the fluorescent dyes within the PV encapsulant materials as shown in Figure 2.3, below. This has been demonstrated by Klampaftis [77], and was chosen as the approach for this PhD research. The approach was developed by incorporation of fluorescent dyes into commercially-available EVA sheet, instead of pure EVA as used by Klampaftis [78]. This is discussed in section 4.2.2. Fabrication of c-Si PV modules with EVA requires use of a PV lamination process in which heat and pressure are applied in order to cross-

link the EVA [88]. Ideally, the techniques developed in this PhD research would be feasible for artists working in a studio setting. To fulfil this requirement, an alternative encapsulation method was also required, without the need for specialist PV lamination equipment. A wet-lamination technique was selected, in which PV cells are placed between sheets of glass, and then liquid encapsulant is poured into the gap between the glass sheets, so that the encapsulant surrounds the PV cells. There is precedent for use of this method in architectural glass [89], and in photovoltaic module manufacture [90]. The silicone encapsulant Sylgard 184 Dow Corning) [91] was chosen for this, due to a precedent for use as a photovoltaic encapsulant [92], and an ability to tolerate addition of the solvent toluene, in which Lumogen F dyes can be dissolved [93], as discussed in section 4.2.2. A precedent for use of Lumogen F dyes within LSC's was discussed in section 1.2.6. This included the addition of the dyes to EVA (ethylene vinyl acetate) [77]. For this PhD research, the addition of Lumogen F dyes to PV encapsulants was chosen as an appropriate method of creating front-facing LSC's.

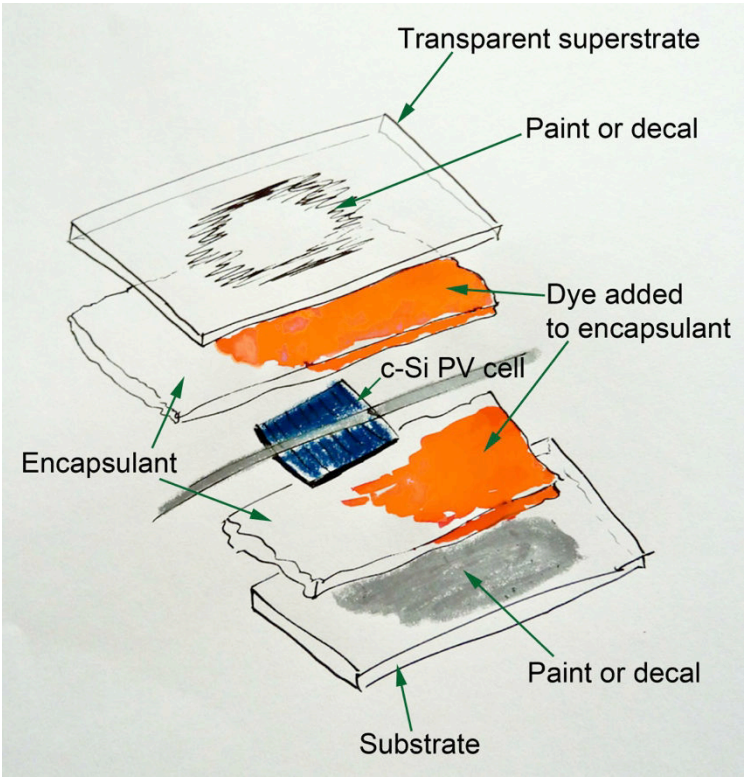

Figure 2.3: Exploded view of c-Si PV encapsulation with added materials

Figure 2.3 is an exploded view showing the materials used to encapsulate a c-Si PV cell. The transparent superstrate and substrate are shown at the top and bottom of the diagram. The superstrate and encapsulant are required to transmit light to underlying PV whilst protecting the cells from breakage and ingress of moisture. Rigid superstrates

and substrates such as glass are ideal for use in wet-lamination processes with c-Si PV. The c-Si PV can be attached to the back glass with stickers, preventing movement or breakage of the fragile cells. During a wet lamination process, the front glass remains in position as the liquid encapsulant is poured into place and cures. Glass is known to be durable [94], and there is an established precedent for application of materials such as paint to glass surfaces [95]. Glass was therefore chosen as both superstrate and substrate for the c-Si PV modules that were fabricated as part of this PhD research. Low-iron glass such as Optiwhite™ [96] and borofloat glass [97] were chosen for use as superstrates to ensure that maximum amounts of light were transmitted to the PV. The substrates were made using soda-lime float glass, as this is cheaper than low-iron glass [98].

The design on the left of Figure 2.2 shows that opaque c-Si PV cells stand out when combined with translucent materials. A method is required to blend the c-Si PV into glazing designs. The square c-Si PV cells could be disguised by applying opaque materials to the superstrate in areas surrounding the PV cells as shown at the top of Figure 2.3. Translucent c-Si PV modules can be made with glass [99] or polymer as superstrate or substrate [100]. Methods of creating opaque areas on glass include firing compatible materials such as paints or frit onto the glass surfaces [95]; sticking decals to the glass surface (including decals that can then be fired onto the surface [101]); and inserting films or coloured backsheets behind PV cells [31]. Firing of glass paints onto float glass is a well-established method that creates very durable results [56]. This method was chosen due to the accessibility to architectural glass artists, and the ease with which a variety of designs could be created. A second method, involving application of decals to glass surfaces was also selected. With this approach, a variety of finishes could be applied to both superstrate and substrate. The method could be developed further through use of more permanent media such as decals or print that can be fired onto the glass [101], or through use of glass coatings [102].

Mirrors can be used to reflect light back into LSC's in order to increase efficiency [71, 72]. The bottom of Figure 2.3 shows reflective material applied to the substrate of encapsulated c-Si PV, so that light can be redirected back towards the central PV cell. The reflective material also covers the back of the PV cell, so can be used to improve the appearance of the assembly. Mirrored surfaces can be applied selectively in any required pattern, offering good opportunities for creation of a wide variety of design styles. Reflective surfaces were applied using the two chosen design methods of glass painting and application of decals. Platinum paint was fired onto glass

(as described in Chapter 3), and reflective 'solar film 65' [103] used as a decal (as shown in Chapter 9).

2.5 Choice of measurement methods

The research described in this thesis includes fabrication of combinations of materials that are designed to transmit light and to fluoresce. The performance of these material combinations was best investigated through use of spectrometry, in order to establish whether the dyes are performing as expected within the novel material combinations, as discussed in section 1.2.7. When the novel material combinations were used to encapsulate PV cells, then current-voltage (IV) testing was used in order to find if the materials were enhancing the electricity production of underlying PV cells.

2.6 Thesis structure

Figure 2.4, below, summarises the thesis structure in diagrammatic form. The research aim was to establish methods of integrating crystalline silicon photovoltaic cells (c-Si PV) into decorative glazing designs. Details of the precedent and the reasons for carrying out the work are discussed in Chapter 1. The approach to the research and choice of methodologies are then described in this chapter (Chapter 2). The following chapters give details of a parallel development of glazing test pieces and of coloured, photovoltaic encapsulant materials. These materials and methods are brought together in Chapter 7 and Chapter 9. Chapter 10 contains conclusions and details of areas in which further work is recommended.

2.7 Chapter conclusion

Materials and methods were selected to fulfil the aims of enhancing the appearance of c-Si PV within translucent glazing whilst maintaining good PV performance. The chosen methodology was addition of coloured, fluorescent Lumogen F dyes to the encapsulant materials within front-facing LSC's (luminescent solar concentrators). Applications of paint or decals to glass were also selected as methods of adding opacity and reflectivity to the areas around and behind the PV. This gave scope for disguising opaque, square c-Si PV cells within a wide range of light-transmitting designs. Chapter 3 gives details of an initial investigation into the use of opaque and reflective materials plus c-Si PV within a glazing test piece.

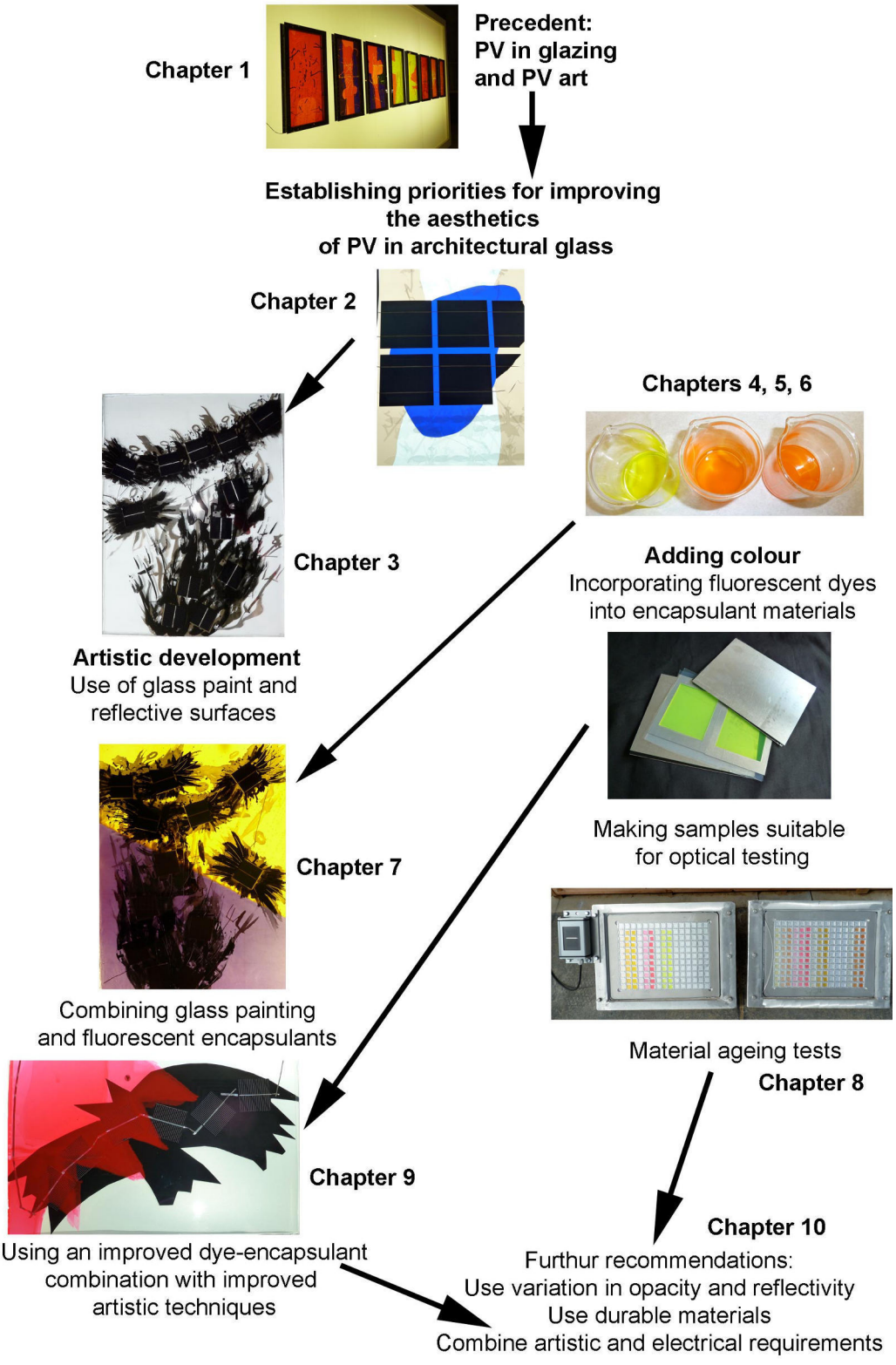

Figure 2.4: Thesis structure diagram showing links between sections

CHAPTER 3: USE OF GLASS PAINT TO INTEGRATE PV CELLS INTO AN ARCHITECTURAL GLASS TEST PIECE

3.1 Chapter synopsis

A piece of architectural glass art was constructed by blending crystalline-silicon photovoltaic cells (c-Si PV) into a curvilinear design. Fluid paintwork was used to soften the strong light-dark contrast between the edges of the c-Si PV cells and the surrounding clear glass. Platinum paint applied to the glass placed behind the PV cells led to a slight increase in the current generated by the PV.

3.2 Aims

The PV glazing shown on the left in Figure 2.2 showed that the opacity of c-Si PV cells contrasts strongly with light-transmitting materials when incorporated into glazing. This led to the aim of integrating c-Si PV cells into a piece of architectural glass, by:

- Disguising the square PV cells within a curvilinear design
- Covering grey cell backs
- Creating a design that enabled some light to be transmitted through the glazing
- Incorporating mirrored surfaces to:
    - Add visual interest through reflection of light and movement
    - Increase the amount of light reaching PV

3.3 Materials and method

Techniques and materials were chosen so that assembly could be carried out in a glass studio, without the use of specialist PV lamination equipment. This ensured that the methodology was applicable to those with access to studio facilities, as opposed to PV module manufacturing plants. The only exception was the use of a wafer-dicing saw, to cut c-Si PV cells into small pieces. Use of smaller PV cell pieces meant that small-scale test pieces could be fabricated. It would be possible to scale up the designs, using full-size c-Si PV cells, with no cell cutting required. Materials were chosen as follows:

- Monocrystalline silicon PV cells (Topsky Electronics Technology (HK) Co. Ltd.) were cut into 52mm × 52mm pieces with central busbars, so that they could be connected with pieces of tabbing strip.
- Tabbing strips (E Jordan Brookes) were soldered to the c-Si PV, using 60/40 tin/lead solder, after application of VOC-free, no-clean flux.

- 4mm-thick, low-iron glass was used in front of the c-Si PV to optimise the light spectrum reaching the surface of the PV.
- Standard, 4mm-thick, soda lime float glass was used behind the PV. Translucent layers behind and in front of the PV ensured that light could be transmitted.
- Glass paints (Rüger and Günzel GmbH) were mixed with water and a few drops of gum arabic solution, and then applied to the low-iron glass with a brush, using sticks to scratch through the painted surface. Some softening of the paint edges was achieved by applying a fine spray of water to the edges of painted areas. Masking was used to leave square areas clear of paint, so that c-Si PV cells placed underneath would be exposed to light. Once dry, the paints were fired in a gas oven, and held at 606°C for 10 minutes, then allowed to cool *in situ*.
- Platinum paint (Ferro Corporation) was mixed with ceramic thinning medium (Hans Wolbring GmbH), then applied with a brush to the soda lime float glass that was to be placed behind the PV cells. Once dry, the paint was fired onto the glass at 650°C for 40 min. This gave a semi-translucent, mirror finish that covered the grey backs of the c-Si PV cells, and reflected a fraction of the incident light, whilst allowing some light to be transmitted through areas not covered by PV cells. The mirrored surface also reflected movement and colour, adding interest for viewers, whilst matching the silver tabbing strips used to connect the PV cells (Figure 3.1).

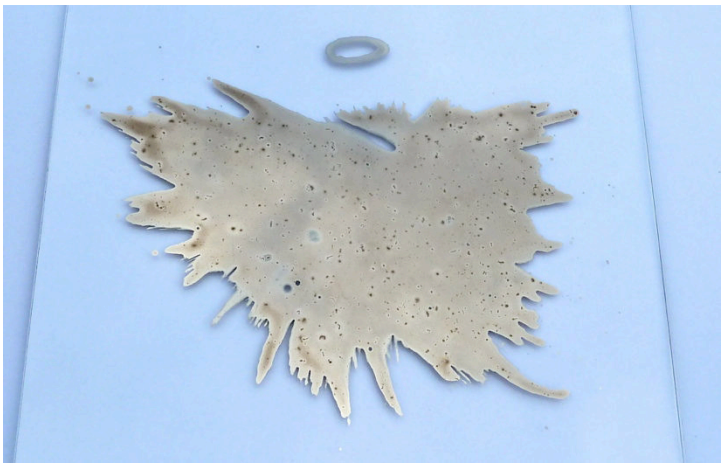

Figure 3.1: Platinum paint fired onto soda-lime glass, giving a reflective, semi-translucent surface finish

Further details of the development of the design are given in appendix 1.

3.3.1 Development of painted designs

Opaque glass paints are traditionally used to create variation in light transmission in stained and decorative architectural glass [56]. Stained glass was often used for church windows [94], with frequent depictions of heaven and hell, which often show particularly imaginative use of painted designs and colour [104]. Painting techniques were chosen for this work, as glass paint can be applied at varying levels of opacity, and a range of test pieces could be made up quickly in a studio setting. Ideally, the materials used with c-Si PV should last at least as long as the PV cells themselves. Glass paints are known for their durability, with many painted windows surviving for several centuries [58]. For both the front and back glass, paint was applied to the side of the glass that was to be placed nearest the c-Si PV, so that no paint was on the outside surfaces of the glass. This gave maximum protection for the paint layer. Float glass has tin on one side, due to the production method, in which molten glass is poured onto molten tin [105]. To avoid a reaction with the tin, paint was applied to the non-tinned side of the glass. The paint was used to build up layers of opacity around c-Si PV cells. A brush was used to apply the paint rapidly in a fluid style, to contrast with the solid, rectilinear shapes and patterns that are normally associated with c-Si PV cells and arrays. Masking was used to keep square areas of glass free from paint, so that light could reach the PV placed underneath. Figure 3.2 shows an initial test in which a painted piece of glass is placed over a c-Si PV cell on a lightbox. There is a gradation from the opaque PV cell and darker areas of paint to semi-translucent areas. This softens the transition from dark PV cell edge to the surrounding areas of clear glass.

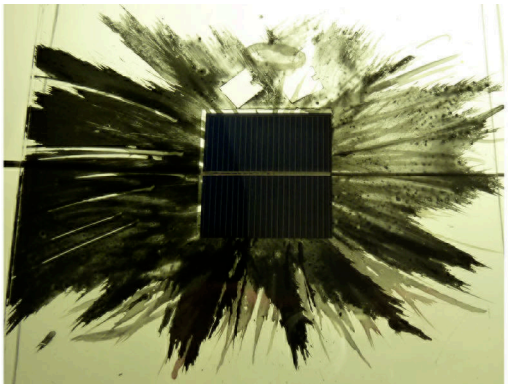

Figure 3.2: Use of glass paint to create opacity variation on a piece of glass placed over a PV cell

An interpretation of the heaven and hell theme was elaborated in the designs in order to remain in agreement with themes used in traditional stained glass practice [104]. The streaks of paint that were built up around the PV cells in the initial tests were

made to resemble either wings or fire. Clear lines were scraped through the paint to add detail, whilst resembling the lines of reflective tabbing strip that join the PV cells, ensuring that the tabbing strip did not remain an anomaly amongst the rest of the design. Masking was used to add small, rectangular shapes mimicking the rectilinear PV cell shapes and symbolising eyes in the design; adding detail and humour. Figure 3.3a shows a paint test with insufficient paint around a PV cell to disguise the square shape within the surroundings. In Figure 3.3b more paint coverage is used, to ensure that the PV cell shape becomes part of an area of opacity when lit from behind. Clear glass is still visible adjacent to the PV cell edges, due to the need to prevent painted areas of the front glass from obscuring light that could otherwise reach the PV cell.

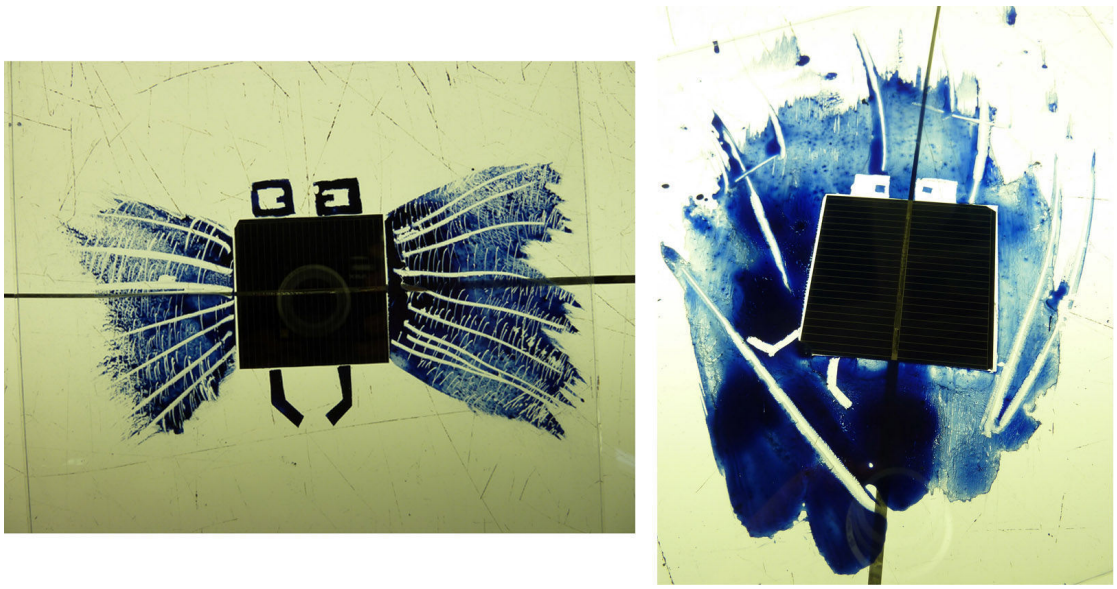

Figure 3.3: Development of paint tests, from left to right: (a) Paint test with insufficient paint to disguise the central PV cell; (b) Paint test with fluid paintwork surrounding a PV cell

3.3.2 A larger test piece, incorporating PV cell strings

The structure of PV panels should be clear, ensuring no shading of the PV elements. c-Si PV cells are normally connected in straight, equally-spaced lines, within modules. Cell strings of any shape can be created by soldering individual c-Si PV cells together by hand. A cartoon was created in which PV cells were connected together in two strings of six cells, to fit into a curvilinear design (Figure 3.4) for a 600 x 450 mm test piece. Additional pieces of the silver-coloured tabbing strip were incorporated into the design, to demonstrate the potential of this material for use in PV artworks. The design was kept as fluid as possible, to demonstrate the possibilities for incorporation of c-Si PV into curvilinear designs. Although many of the initial tests were carried out using blue paint, to match the unencapsulated cell colour, black paint was chosen for use on

the front glass in the final designs, as encapsulation of the cells gave them a black appearance in many lighting conditions. The black paint would remain neutral when compared with the coloured dyes that were used later, within the PV encapsulant (described in Chapter 7).

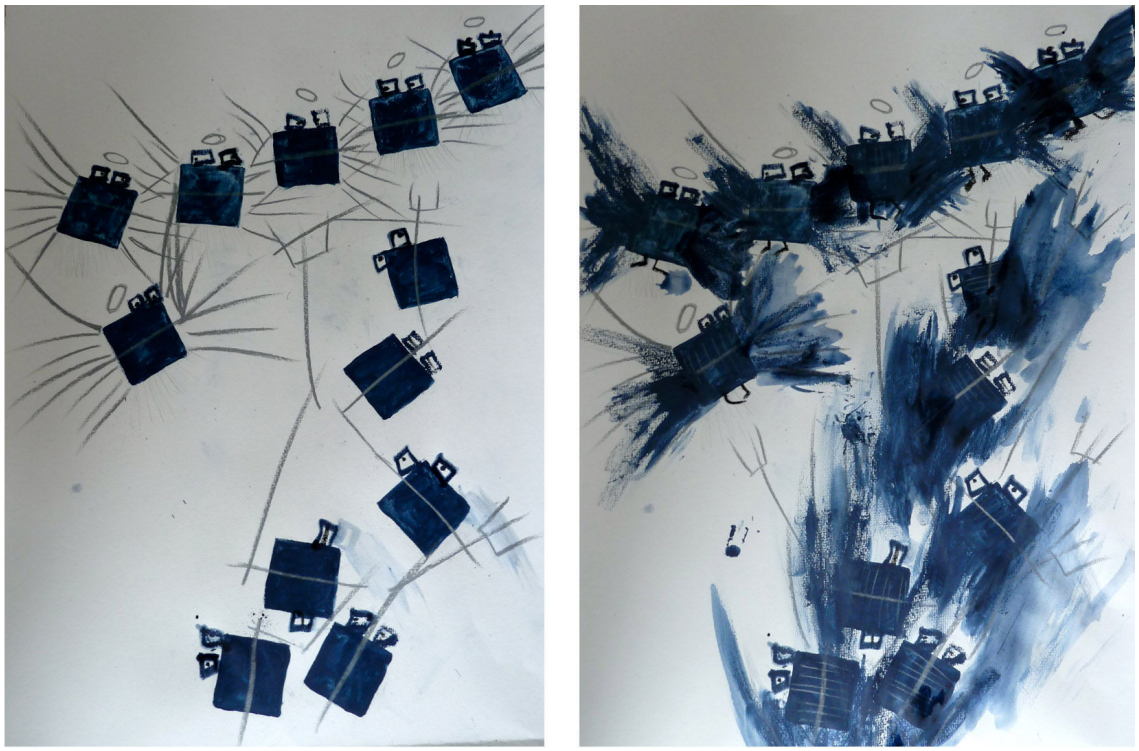

Figure 3.4: Development of the paper cartoon for the test piece, from left to right: (a) PV cell placement in non-linear string shapes, plus use of tabbing strip within the design; (b) Addition of opaque areas to be painted on the front glass

Platinum paint was applied to the back glass, to cover the backs of the c-Si PV cells, and to create a pattern similar to that on the front glass. The extent of the painted area was increased, so that some platinum paint would be visible around the edges of the black paint when viewing the test piece from the front. The translucent nature of this paint meant that it could be used over a larger area of glass with minimal loss of light transmission.

3.3.3 Placing and encapsulating the PV cells

A wet lamination process was chosen to bond c-Si PV and glass. Use of a liquid encapsulant meant that the encapsulation process could be carried out in a studio setting, without the need for a PV laminator that is necessary when using PV encapsulants such as EVA (ethylene vinyl acetate). Circular stickers (obtained from Sunovation GmbH) were used to secure the backs of the PV cells 1 mm above the back glass, allowing liquid encapsulant to flow around the cells. Layers of double-sided tape

were used to attach the front and back glass together, keeping a thin gap (approximately 3mm wide) between them. Hot-melt adhesive was applied to seal any gaps. Sylgard 184 was not available at the time of fabrication of this test piece. A small, reference test piece, was also fabricated in which Sylgard 184 was used as the encapsulant, to provide a comparison with the Sylgard 184 used as an encapsulant for Lumogen dyes in Chapter 7. This small test piece contained a single piece of c-Si PV, encapsulated between 200 x 200 mm pieces of glass, with paint applied to the front glass (Figure 3.5). The wet lamination of the larger test piece was carried out with an alternative two-part silicone, specifically formulated for use with c-Si PV, supplied by Sunovation GmbH. The encapsulant was poured into the gap between front and back glass.

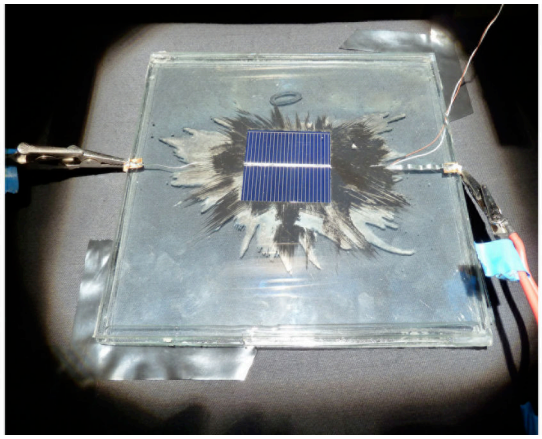

Figure 3.5: A single PV cell, encapsulated in clear Sylgard 184, under the light from a solar simulator. Black paint is applied to the front glass, and a piece of glass with applied platinum paint is placed underneath

3.3.4 Use of platinum paint as a reflective surface to increase electrical output

Measurements were carried out to find if the use of platinum paint increased the electrical power production from a c-Si PV cell placed over glass to which platinum paint had been applied. A current-voltage (I-V) curve tracer (EKO MP-160) was used to show the variation of voltage plotted against current, under a changing electrical load. The power from the PV cells was also measured in this process, as power is a product of voltage and current [106]. The single c-Si PV cell piece encapsulated in clear Sylgard 184 was placed on a black backing, under the light from a xenon-based solar simulator (ABET Technologies Sun2000 11044, class AAB, 1000W continuous). Measurements were also taken with a piece of platinum-painted glass placed behind the PV (Figure 3.5), and with a mirror placed behind the PV. The temperature of the test piece was measured using a thermocouple. This is the thin white and brown cable in the top, right of Figure 3.5. Current-voltage tests were carried out when the reading on the

thermocouple was 25 °C. The thermocouple was placed under the glass, behind the encapsulated PV cell. The encapsulation of the PV meant that direct contact between the PV cell and the thermocouple was not possible, so the cell temperature was likely to be different from that measured on the thermocouple, due to the layer of encapsulant and glass between the thermocouple and the PV cell. The similar values of open-circuit voltage, shown on the x-axis in Figure 3.9, indicate that similar temperatures were achieved for each test [107].

3.4 Results and discussion

c-Si PV cell pieces were successfully fitted into a curvilinear design through use of glass paints (shown in Figure 3.6).

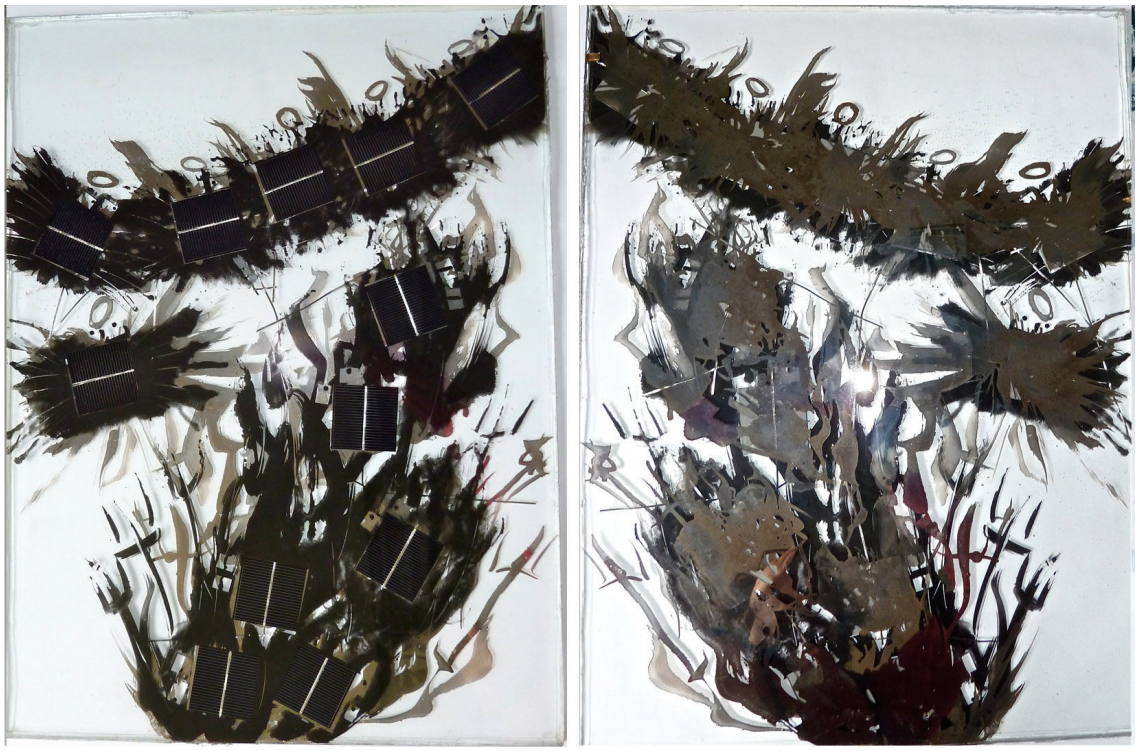

Figure 3.6: Views of the large test piece, from left to right: (a) Front view, with opaque, square PV cells blended into a painted design; (b) Rear view, with platinum paint covering PV cell backs

The design demonstrated that it is possible to disguise square, opaque cell shapes through use of paint on the front and rear surfaces of the glass surrounding each PV cell. The test piece is likely to be viewed more frequently from the back, as the PV faces outwards, towards the sun. The platinum paint on the back glass created a covering for the cell backs whilst transmitting some light, as shown in Figure 3.6. Figure 3.7 is a detail of the front of the test piece placed in a window aperture. This shows the translucency of the platinum paint in transmitted light, and also the contrast between the

blue surface colour of the c-Si PV and the surrounding black paint, which was visible under some lighting conditions. The main aim of disguising the opacity of the c-Si PV was still fulfilled.

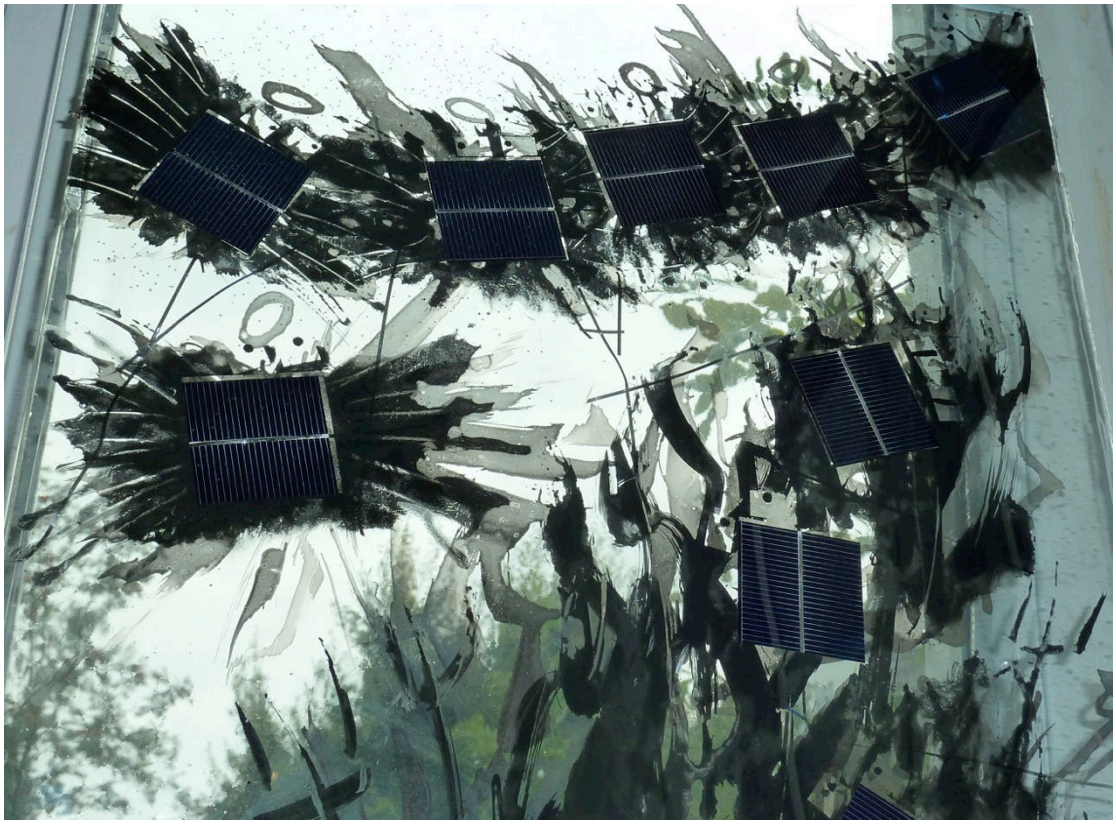

Figure 3.7: Detail of the front of the test piece shown in a window aperture. Under this lighting condition, the blue PV colour of the PV cells contrasts with the surrounding black paint

3.4.1 Details of the painted design

Table 3.1 lists aspects of the painted design that require further work, together with possible solutions. Most of the problems listed in Table 3.1 were only visible when the design was viewed close up. The gaps between paint and c-Si PV cell edges could also be viewed at a distance. This could be overcome by applying both black and platinum paint only to the glass to be placed behind the PV cells. Tests showed that it was possible to fire black and platinum paint onto the same sheet of glass, at 610°C, so that this design modification is possible (Figure 3.8), but that this reduces the reflective surface area on the back glass when compared with the design in Figure 3.6. An ideal covering for the back glass would have a large reflective area to maximise light incident on the PV combined with opaque areas to disguise the c-Si PV in transmitted light. The most difficult aspect of the test piece fabrication was the positioning of the c-Si PV cells so that they were underneath the clear areas of the top glass. c-Si PV cells would not

need to be placed so accurately in designs made with paint applied only to the glass to be placed behind the PV. For designs that are to be viewed close-up, on the side facing the light source, back-contact c-Si PV cells, with no front surface patterning [108], could be used to avoid the clash between the rectilinear metallization pattern of the PV cells and the surrounding painted patterns. This would also remove the bright, reflective strips of tabbing strip, across the centre of each c-Si PV cell front, as all connections would be made to the back.

Table 3.1: Details of problems with the test piece design, with suggested solutions

Problem	Photo	Solution
Gaps between the edges of the c-Si PV cells and the dark painted surface, causing a light stripe to highlight the edges of each PV cell	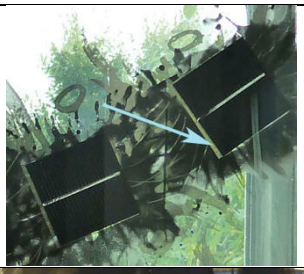	Put dark paint on the glass behind the c-Si PV, instead of applying paint to the glass in front of the PV.
Some shadowing of c-Si PV cells by paint	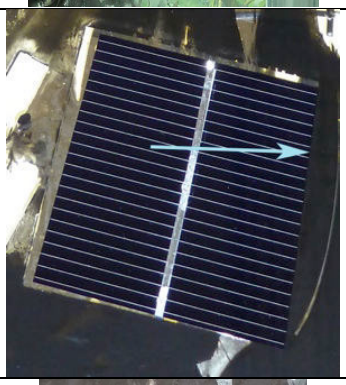	Apply dark paint mainly to the glass behind the PV cells. Ensure that paint applied to the front glass does not cover areas where PV cells are placed, to prevent shading of the PV cell surfaces.
Reflective tabbing strip across the centre of each c-Si PV cell is very prominent	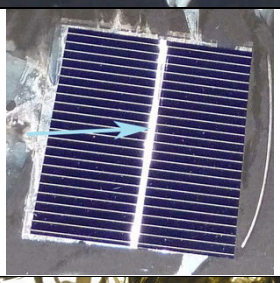	Use back-contact c-Si PV cells, where the tabbing strip is attached only to the back of the PV
Patterns on the surfaces of the c-Si PV cells did not match the painted design	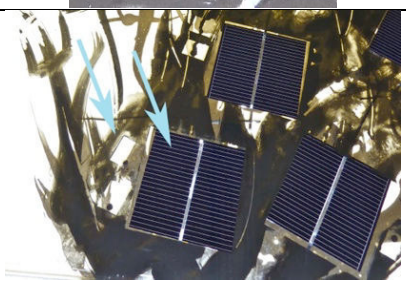	Use back-contact c-Si PV cells with no front metallization patterns, or adapt the paint finish to a coating that gives a similar pattern to that on the surface of the PV cells.

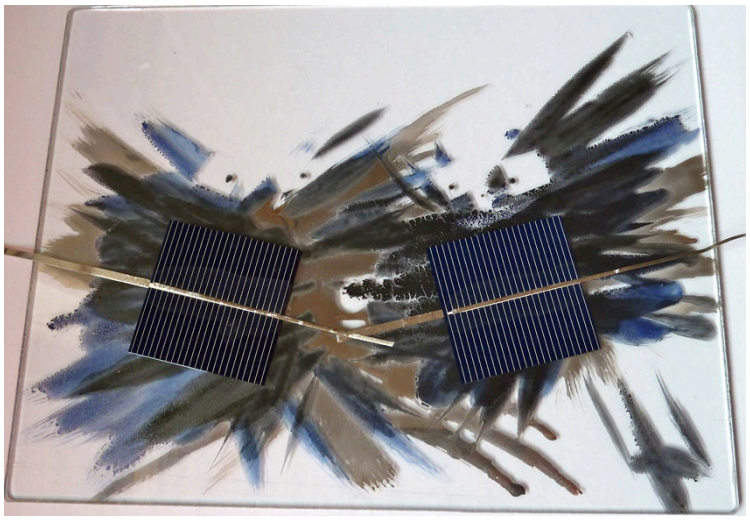

Figure 3.8: Black, blue and platinum paint fired onto a single sheet of glass, with PV cells placed on the front of the glass

3.4.2 Increase in power production due to the use of platinum paint

Platinum paint is sufficiently opaque to hide the backs of c-Si PV cells, when it is applied to the glass placed behind the PV cells. It also reflects light back towards the PV. The paint is can be applied at varying degrees of thickness, so that it can be made semi-translucent, giving a surface that is a combination of a light-transmitter and reflector. The paint costs £883 for 250 g [109], but is applied in small quantities, diluted with thinning medium, so that the cost per square metre of application is likely to be less than £50. A test was carried out to see how a piece of back glass with platinum paint altered the performance of a c-Si PV cell placed over it (Figure 3.9). A comparison was made with a black backing behind a c-Si PV cell, and a mirror backing. When a platinum-painted piece of glass was placed behind an encapsulated PV cell, the maximum current from the PV increased slightly, compared with the maximum current from the same PV cell with a black backing. The dashed line in Figure 3.9 shows the current-voltage (IV) curve for the c-Si PV cell with a platinum-painted piece of glass placed beneath it. The curve with the continuous black line shows that without any mirror finish underneath the PV, less power is generated. A piece of mirror glass placed behind the PV cell, shown by the dotted line, leads to more light reaching the PV, giving a further increase in peak current. This shows that maximum current is increased slightly through application of a mirror coating behind a c-Si PV cell. The points at which maximum power (P_{max}) are achieved are also shown on each I-V curve. The positions of these maximum power points also indicate the increase in power due to use of increasingly reflective materials. When reflective surfaces are incorporated into a design, a balance has to be achieved between letting light through and reflecting light

back towards c-Si PV cells.

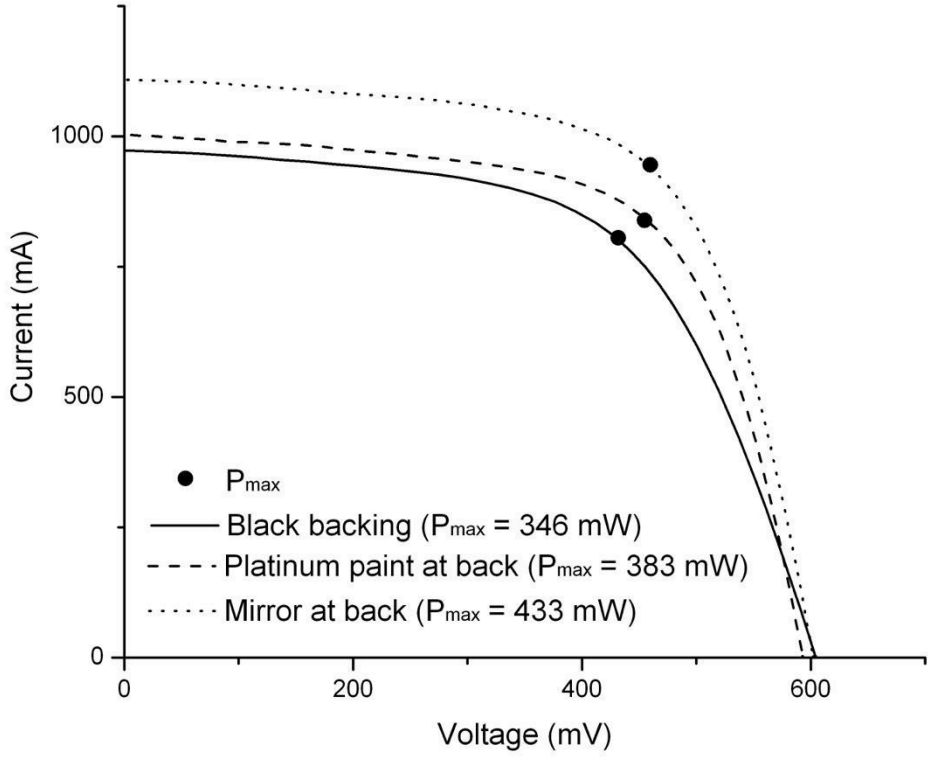

Figure 3.9: Comparison of the current/voltage (IV) curves from an encapsulated PV cell with a black backing; a platinum-paint backing; and a mirror backing, with maximum power points (P_{max}) highlighted

The large test piece was constructed to test the visual aspects of the design. No IV test facilities were available at the studio where this was fabricated and installed, so it was not feasible to carry out an IV test on the large test piece. The fabrication of a second, large test piece is described in Chapter 7. This was made up with a similar painted design, but with coloured encapsulant, instead of clear encapsulant. IV tests were carried out on this, second test piece and are compared with the results from the 200 x 200 mm test piece in Chapter 7.

3.4.3 Alternative design ideas

For each new design incorporating PV within architectural glass, decisions will need to be made about the degree to which c-Si PV cells are to be made visible or disguised. The methods described in this paper give a starting point, showing that it is possible to incorporate c-Si PV cells within a variety of architectural glass designs, with choice as to the level of prominence of the c-Si PV cell shapes and string patterns. There is limited light transmission through the large test piece described in this chapter, due to the opacity of the c-Si PV, plus large areas of paint. Paint areas could be minimised, by making sharp gradations from opaque to transparent areas, as in Figure 3.10.

Figure 3.10: Rectilinear design incorporating c-Si PV and reflective material

Modifications to this design could enable it to be used in PV glazing where light reaching the interior is to be maximised, or where views to the exterior need to be maintained. If shading were only required in one part of the window, then designs such as that in Figure 3.11 could be used. This could be modified to place the reflective materials underneath the c-Si PV, to maximise light incident on the PV. The designs described in this chapter demonstrate that variety can be achieved whilst integrating c-Si PV into glazing.

Figure 3.11: Concept design for c-Si PV cells, glass paint and reflective medium, with opacity limited to one area

3.5 Chapter conclusion

A large test piece with curvilinear paintwork and c-Si PV cell strings was constructed; showing that c-Si PV cells can be blended into a wide range of architectural glass styles. The use of reflective paintwork on the back glass was shown to be beneficial in disguising c-Si PV cell backs and increasing current production and maximum power from the PV cells that were placed on top of the surface. Colour is added to the encapsulant in a similar design described in Chapter 7. The following chapter (Chapter 4) gives details of methods of addition of colour to two photovoltaic encapsulant materials.

CHAPTER 4: SYLGARD 184 AND ETHYLENE VINYL ACETATE (EVA) AS HOSTS FOR LUMOGEN DYES

4.1 Chapter synopsis

Colouring of PV encapsulants was chosen as a method of increasing variety in PV module design. Suitable PV encapsulant materials were required to act as hosts for the chosen Lumogen F fluorescent dyes. Two contrasting materials were chosen: Sylgard 184 (Dow Corning); and EVA (ethylene vinyl acetate): Solutia Vistasolar Fastcure 486.00. Methods of adding Lumogen F dyes to the two encapsulant materials and making samples suitable for optical testing were developed.

4.2 Choice of materials

4.2.1 Fluorescent dyes

Adding fluorescent dye to PV encapsulants is a way of introducing colour to PV modules at minimal cost and with minimal change in PV efficiency [110]. Fluorescent dyes were selected from several available methods of addition of colour to c-Si PV cells, as described in Chapter 2. Organic, fluorescent, Lumogen dyes (BASF) [111] were used due to the good range of available colours, relative stability [112, 75] and a precedent for their use with EVA [78]. Only a small amount of Lumogen dye is required to obtain strong colouring, so the cost is minimal [77]: for example 2.5 mg dye per 10 g of Sylgard 184 encapsulant for 200 ppm concentration of Lumogen Red 300 dye would cost €0.025 [113]. These coloured dyes can also enhance the efficiency of underlying PV cells [4, 77]. The chosen Lumogen F dyes were: Red 300; Orange 240; Yellow 083; Violet 570, as these are available from BASF, with published details of solubilities in a range of solvents [111]. Lumogen F Yellow 170 dye was also used initially, due to a precedent of successful incorporation into PMMA [76], although it is not commercially available [85]. The chosen dyes are listed in Table 4.1, together with the wavelengths at which peak absorbance and emission occur within a PMMA (polymethyl methacrylate) host, as measured by Wilson [76].

Table 4.1: Peak absorbance and emission values for Lumogen F dyes within PMMA [76]

Lumogen F dye	Wavelength (nm) at peak absorbance within PMMA at 25-70 ppm	Wavelength (nm) at peak emission within PMMA at 1.2 – 3.5 ppm
Orange 240	527	534
Red 300	574	597
Yellow 170	502	516
Yellow 083	475	483
Violet 570	376	425

4.2.2 PV encapsulants

Encapsulant materials were used as hosts for the chosen Lumogen dyes, and to transmit light to underlying c-Si cells. PV encapsulants can be divided into those supplied in liquid form, and sheets of flexible polymer that require application of heat and pressure in a PV lamination process. Each type has distinct advantages, including different possible artistic applications, so one of each was chosen:

- Sylgard 184 (Dow Corning) is a two-part, silicone elastomer from a group of polymers known as polydimethylsiloxanes (PDMS). This polymer will be referred to as Sylgard or Sylgard 184. Mixing the two Sylgard components together in a 10:1 ratio, gives a viscous liquid that can be poured over PV cells, then allowed to cure to form a transparent, tacky solid. Silicones with good adhesive qualities and excellent optical properties have been developed for use with PV [114]. Sylgard 184 is a silicone with a precedent as a PV encapsulant [90], and use as a host for fluorophores [115]. In order to incorporate Lumogen dyes within a silicone, a solvent containing the dyes has to be added, then evaporated off, leaving the dyes within the silicone. Toluene can be used to dissolve Lumogen dyes [111, 3], and is known to be straightforward to evaporate out of polydimethylsiloxanes (PDMS) [116]. It has been shown that toluene can be evaporated out of Sylgard 184 without damaging it [93]. Encapsulation of c-Si cells with silicones such as Sylgard does not require the use of specialist equipment [92], so can be carried out in a studio setting. Having a method that does not require application of pressure or heat, makes Sylgard suitable for use with uneven glass surfaces, including the painted, fired glass used in Chapter 3. This glass would have been likely to crack when pressure was applied to the uneven surfaces in a PV laminator.

- EVA (ethylene vinyl acetate: Solutia Vistasolar Fastcure 486.00) is a copolymer that is supplied in the form of flexible, thin sheets. These are placed over and under PV cells, between sheets of glass or polymer (Figure 4.1). A PV laminator is used to apply heat and pressure, cross-linking the molecules to form a clear, sticky encapsulant [88]. The advantages of EVA are a precedent for addition of Lumogen dyes to pure EVA pellets [77]. This allowed intricate designs to be produced, in colour, within PV modules by cutting images from flexible EVA sheets, with the details preserved during PV lamination [117]. The method is developed in this PhD research through addition of Lumogen dyes to commercially-available EVA sheets that contain compounds including UV-inhibitors, to ensure good resistance to degradation [118, 119].

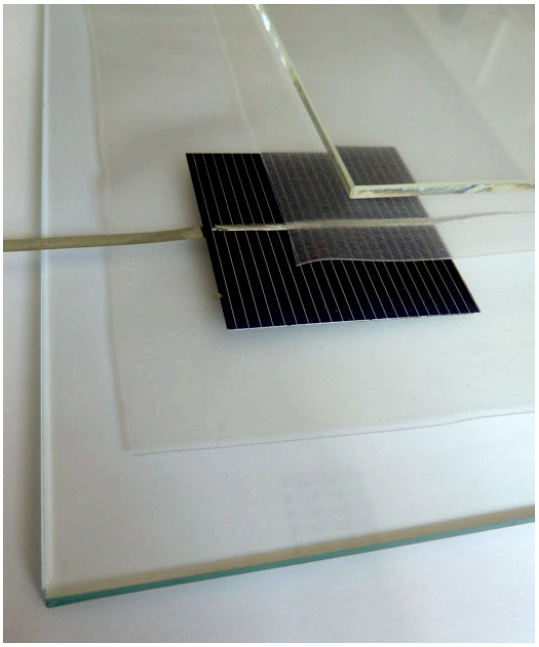

Figure 4.1: The layers of glass and semi-translucent EVA sheet that are placed either side of a PV cell before lamination.

Additional benefits are the short processing times for EVA, which takes a few minutes to process in a PV laminator. This is very different from use of Sylgard, which is poured into place, then allowed to set over several hours. Vistasolar 486.00 [120] was the chosen type of EVA, as this has adequate sheet thickness and processing temperatures for the method of sample fabrication. This involved laminating several sheets of EVA together. Use of thinner EVA sheets would have required a larger total number of sheets to be soaked in dye solutions, then laminated together to make up samples of sufficient thickness to compare with Sylgard samples that were made initially.

4.2.3 Method: Adding Lumogen dyes to Sylgard 184 and developing sample-preparation techniques

Sylgard 184 was assessed first, as this PV encapsulant material does not require the use of a PV laminator, giving the greatest flexibility for use by artists. (See Chapter 7 for details of use on the use of Lumogen dyes, within Sylgard, in a piece of decorative glass.) Lumogen dyes are not directly soluble in Sylgard 184, so it was necessary to dissolve the dyes in a solvent first and mix the solution with Sylgard 184 part A; followed by an evaporation step to remove the solvent but retain the dye within the Sylgard. Toluene causes an initial swelling of Sylgard 184, but discussions with the manufacturer confirmed that this solvent could be evaporated off [93] at temperatures well below those which would cause damage to the Sylgard [91].

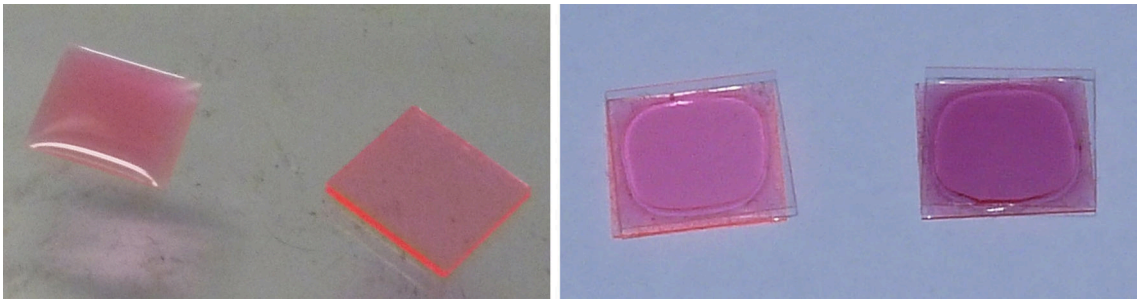

Figure 4.2: From left to right: A piece of glass with Sylgard plus Lumogen Red 300 on the surface; A complete sample with glass placed on top; Two samples showing an air gap around the edges due to over-curing before placing the glass on top.

Initial experiments were made using dyes at a range of concentrations, from 20 to 2000 ppm, to assess the limits of solubility of Lumogen dyes within Sylgard 184. Small quantities of Lumogen dye were weighed out on a microbalance. Any lumps of dye were crushed with a spatula; 30 ml of toluene was added, and the mixture was then placed in an ultrasonic bath for at least 5 minutes, to ensure that the dye was dissolved. The dye solution was added to 17g of Sylgard part A. The solution was placed on a magnetic stirrer for 48 hours with 60 °C heat applied for the first 24 hours, to ensure evaporation of the toluene. Sylgard 184 part B was then added and stirred in for 2 minutes before de-gassing the mixture in a vacuum oven for 20 minutes.

The first sets of samples were made up by allowing the Sylgard to start to cure for approximately 2 hours at ambient temperature and pressure. Drops of the viscous liquid were then placed onto 11 x 11 mm pieces cut from borosilicate cover slip. Surface tension held the Sylgard solution in place. The mixture was then allowed to cure further, for 8 to 14 hours at room temperature, before using tweezers to position a

second piece of microscope cover slip onto the top of each sample. This created a sandwich of Sylgard 184 between thin pieces of cover slip (Figure 4.2). The method was difficult to implement successfully, as variations in ambient temperature and humidity influenced the curing state. As a result, it was hard to define conditions that would ensure that the top piece of glass remained in place. The curing process could be accelerated by placing drops of Sylgard onto pieces of cover slip, then placing the pieces of cover slip in a vacuum oven at 40 °C. The top slide was then placed on each sample, however the time to achieve ideal viscosity was still inconsistent. This led to samples with some adhesion in the centre, but none at the edges, leaving an air gap between glass and Sylgard at the edges (Figure 4.2, right side). Reference samples of Sylgard 184 were also made up, without the addition of dye. A range of completed samples are shown in Figure 4.3. These samples were used for an initial assessment of the performance of Lumogen dyes within Sylgard 184. The sample preparation method was then improved, as described in section 4.2.5.1.

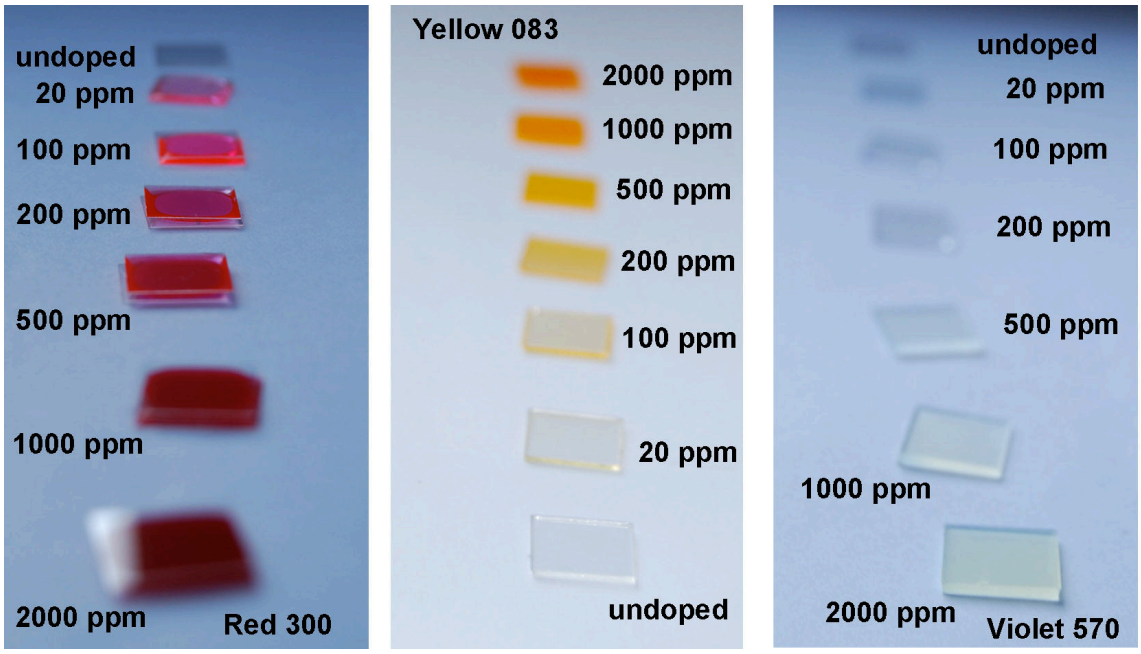

Figure 4.3: Samples made with Sylgard 184; borosilicate glass; and Lumogen dyes, from left to right: Red 300, Yellow 083 and Violet 570

4.2.4 Assessing light absorbance of the dyes within Sylgard 184

Absorbance spectra of the Sylgard samples were measured (Figure 4.4) to discover whether Lumogen dyes were absorbing light as expected within a Sylgard host. The spectra were compared with known spectra for Lumogen dyes in poly(methyl methacrylate) (PMMA) [76], which is an established host material for Lumogen dyes [74, 85, 121]. A Perkin Elmer (PE) Lamda 950 spectrometer was used to pass light

through each Sylgard sample, at wavelengths from 300 to 800 nm. A detector recorded sample absorbance in each wavelength band. The light sources were a deuterium lamp, for light from 300 to 319 nm, and a tungsten-halogen source for wavelengths above 319 nm. Losses occurred due to scattering of light and reflection from the sample [66]. Table 4.2 and Figure 4.4 show that Orange and Red dye have well-defined spectral absorbance peaks. There is a shift of spectral peaks to shorter wavelengths compared with the spectra for the same dyes in PMMA. These results concur with BASF data that show peak absorbance values differing according to host material [111]. Both Yellow 083 and Yellow 170 dye have flattened absorbance peaks, and Yellow 170 has a particularly low value of absorbance, indicating that the dye is not well assimilated within the Sylgard host, so has become ineffective at absorbing light. The flattened absorbance peaks are likely to be due to reabsorption of light by the dye, leading to absorbance over a wide range of wavelengths. Violet 570 dye within Sylgard 184 shows a shift of peak absorbance to a higher wavelength than in PMMA. This could be due to the different molecular structure of Lumogen Violet 570 which is a naphthalimide, unlike the other dyes which are perylenes [74]. The effect of this on the fluorescence emission is shown in Chapter 6. Clear, un-doped, reference samples were also measured. The results showed low levels of absorbance, with no peaks.

Table 4.2: Comparison of absorbance spectra of Lumogen dyes in Sylgard 184 and PMMA

	PMMA	Sylgard 184	
Lumogen F dye	**Wavelength (nm) at peak absorbance for Lumogen dyes in PMMA at 25-70 ppm [76]**	**Wavelengths (nm) at peak absorbance values for Lumogen dyes in Sylgard 184 at 20 – 2000 ppm**	**Absorbance intensity range**
Orange 240	527	519 – 520	0.174 – 2.043
Red 300	574	565 – 567	0.125 – 3.283
Yellow 170	502	478 – 547	0.096 – 1.909
Yellow 083	475	463 – 508	0.079 – 2.680
Violet 570	376	378 – 379	0.473 – 2.534

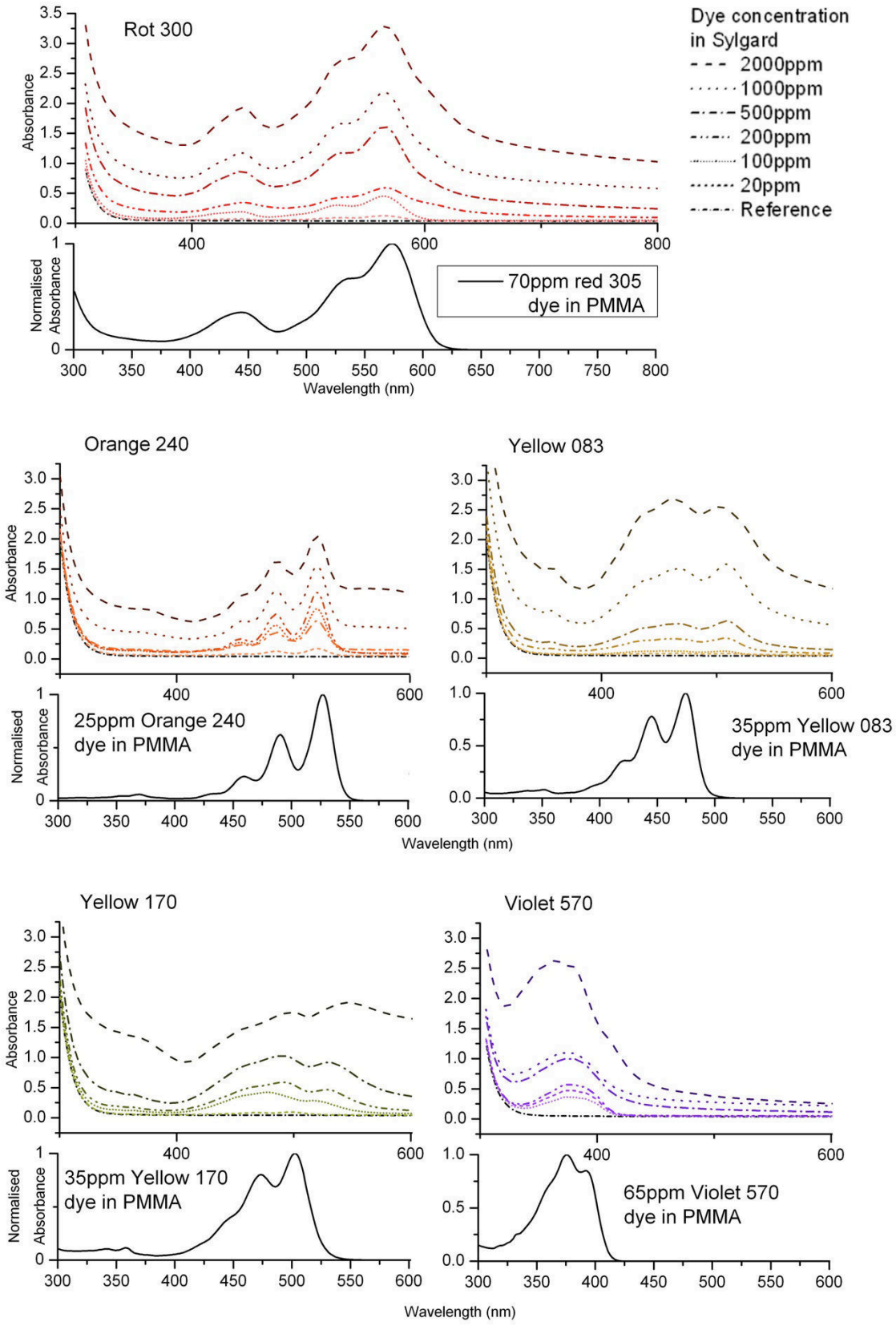

Figure 4.4: Absorbance Spectra for Lumogen Dyes in Sylgard 184, compared with Lumogen Dyes in PMMA

4.2.5 Assessing Lumogen dye solubility within Sylgard 184

The Sylgard samples with concentrations above 500 ppm appeared opaque: they were not transparent when held up to a light source (Figure 4.5). Samples were inspected with an optical microscope (Leica DMRM) to find the cause of the opacity. Figure 4.6 shows images of violet samples taken at a magnification of 50. The two images show a great difference in the amount of dark flecks that obscure the backlighting of the microscope, with many more dark flecks visible in the 1000 ppm sample (Figure 4.6 on the right). The most likely explanation is that these flecks appear due to a larger amount of undissolved dye within the 1000 ppm sample, as the concentration is the only difference between the two samples.

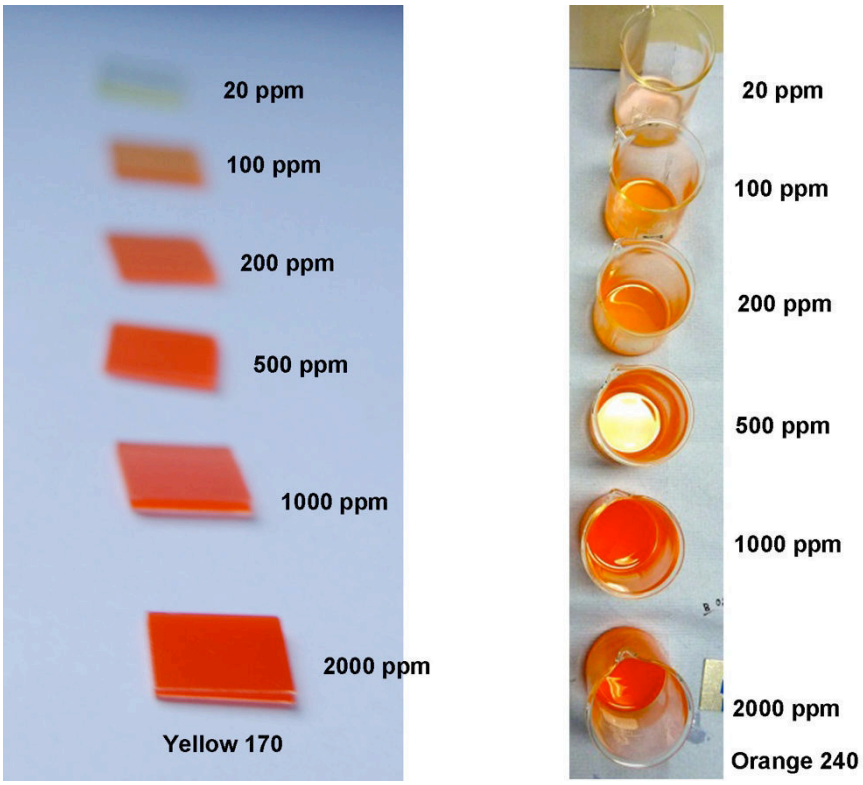

Figure 4.5: Sylgard with Yellow 170 dye (left) and Orange 240 dye (right), showing the increase in opacity from the lowest to the highest dye concentration. (Concentration increases from top to bottom of the figure)

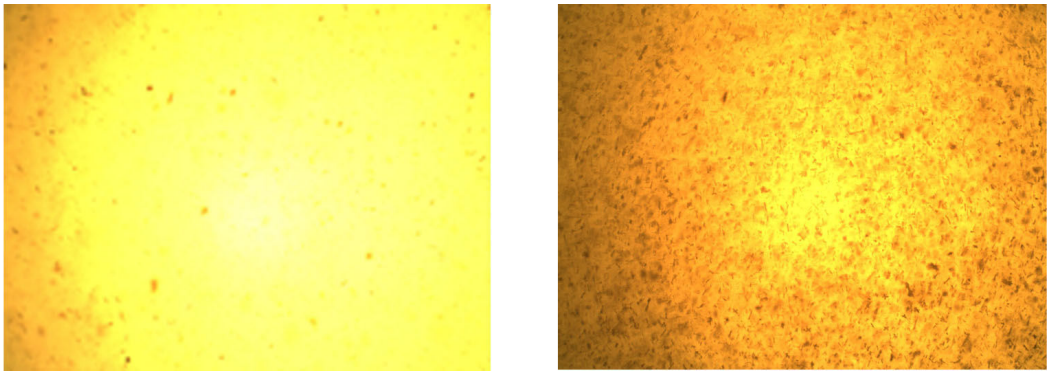

Figure 4.6: Images from an optical microscope at 50x magnification. Violet 570 Lumogen dye in Syglard 184: 500 ppm on the left and 1000 ppm on the right

A photograph of the samples is shown in Figure 4.7. The increased opacity in the 1000 ppm sample (Figure 4.7 right) can be seen clearly as compared with the 500 ppm sample on the left of Figure 4.7.

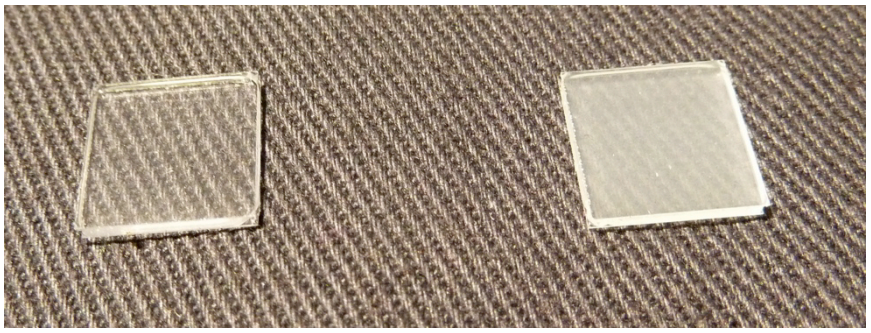

Figure 4.7: Opacity variation in samples of Violet 570 dye in Sylgard. Dye concentrations are 500ppm on the left and 1000 ppm on the right

For the other Lumogen dyes, the lowest concentrations at which flecks of undissolved dye were clearly visible were found to be 500 ppm for Orange 240 and Yellow 083, and 200 ppm for Red 300 and Yellow 170 dyes. In contrast, Lumogen dye in PMMA is fully dissolved at all these concentrations [85, 74]. The low solubility of Red 300 dye in Sylgard was particularly surprising, as this dye has a high solubility in toluene: 80 g/l as opposed to 10 g/l or less for the other dyes [111]. The sample preparation method was examined further, and it was found that insufficient solvent was being used to dissolve the dyes, so that the higher concentrations of dye were not fully dissolved on addition to Sylgard.

The highest concentration samples in which dye appeared to be well dissolved were investigated further. The aim was to find if a significant proportion of the dye that was used to prepare the samples was in solution within the Sylgard, and absorbing light as expected. The concentration of a translucent material such as the Sylgard samples can

be measured by transmitting light through the material. As light passes through a translucent material, such as the Sylgard samples, some of the light is absorbed. The change in intensity of the transmitted light can be used to measure the concentration of the sample. The relationship between light absorbed by a sample and the dye concentration within the sample is given by the Beer-Lambert law [79]:

$$\text{Log}\,(I_d / I_o) = \mu\, d\, C \qquad \text{(Equation 1)}$$

Where: C = dye concentration in gl^{-1}

I_o = the intensity of the light before passing through a sample of thickness d

I_d = the intensity of the light after transmission the sample.

d = sample thickness in cm

μ = dye mass absorbtivity $lg^{-1}cm^{-1}$ [122]

The logarithm of the ratio of incident and transmitted light is known as absorbance, A, so:

$$A = \text{Log}\,(I_d / I_o) \qquad \text{(Equation 2)}$$

The peak absorbance A_p for each sample was taken from the curves in Figure 4.4. The mass absorptivities of the dyes were known, and the sample thicknesses were measured with vernier calipers, so using equations 1 and 2 and these values, the concentration, C, of dye within each sample could be calculated from:

$$C = A_p / d\mu \qquad \text{(Equation 3)}$$

The resulting calculated values of dye concentration are shown in the right column of Table 4.3. These values are all much lower than the initial amounts of dye that were weighed out at the start of sample preparation. These, initial, amounts of dye are shown in the third column of Table 4.3. This apparent loss of dye could have been due to a problem with the solubility of Red dye within Sylgard, or to dye being incompletely dissolved within toluene before addition to Sylgard. Greater volumes of toluene were required, to ensure that the dyes were in solution, not suspension, before addition to Sylgard. Improvements to the method of sample preparation are discussed in Section 4.2.5.1. Further samples were made with a maximum dye concentration of 200 ppm, to ensure that all samples were translucent, with dyes dissolved as fully as possible.

Table 4.3: Measured Lumogen dye concentrations (ppm) in Sylgard samples at the lowest concentrations at which dye particles are visible

Lumo-gen dye	Dye mass absorbtivity ($lg^{-1}cm^{-1}$)	Concentration of dye used to make the samples (ppm)	Peak absorbance from absorbance spectra	Sample thick-ness without glass (mm)	Concentration calculated from absorbance spectra peaks (ppm)
Red 300	44.2	200	0.592	0.84	160
Orange 240	118.8	500	0.634	0.49	108
Yellow 170	88.5	200	0.590	0.68	97
Yellow 083	88.8	500	0.627	0.45	266
Violet 570	48	500	0.999	0.78	266

4.2.5.1 Improving the Sylgard 184 sample-preparation method

Many of the initial Sylgard samples had an uneven cross-sectional area, due to the top layer of glass settling unevenly on top of the Sylgard as it cured. The variable thickness of the samples led to uncertainty in measurements of absorbance, which are dependent on the thickness of the sample at the point of measurement. The sample-making method was improved by making flat samples that contained no glass. A mould with a glass base was used. The Sylgard samples could be peeled from this after curing. The amount of toluene used in sample preparation was increased to 100 ml to ensure full dissolution of the dye. The solution of dye in toluene was added to Sylgard part A, then evaporated by heating and stirring at 70 °C for at least 12 hours, followed by stirring alone, to bring the total time allowed for solvent evaporation to 48 hours. The mixture was then poured into a mould, which was placed in a vacuum oven for 30 minutes to eliminate air bubbles, and then left on a level surface for 48 hours, to cure. A sharp blade was used to cut the samples into squares with side lengths of approximately 11 mm. The Sylgard 184 was not heat cured, as previous experiments showed that this was inclined to lead to irregular spots of colour forming within the material after a few weeks (Figure 4.8), and Dow Corning's datasheets indicated that heat curing is optional [91].

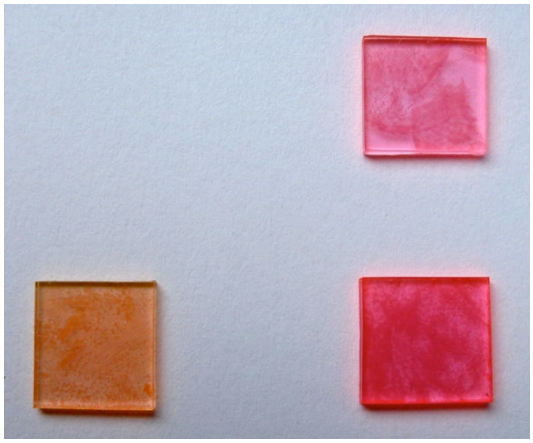

Figure 4.8: Irregular spots of colour in heat-cured Sylgard samples. Left: Orange 240 Lumogen dye, at 200 ppm concentration. Right: Red 300 dye at 100 ppm (above) and 200 ppm (below).

Without heat curing, streaky iridescence formed on the surface of the Orange 240 samples (shown in Figure 4.9). This developed after a few days storage in the dark. (Samples were stored in the dark to eliminate effects caused by the lack of lightfastness of the dyes. These are investigated in Chapter 8.)

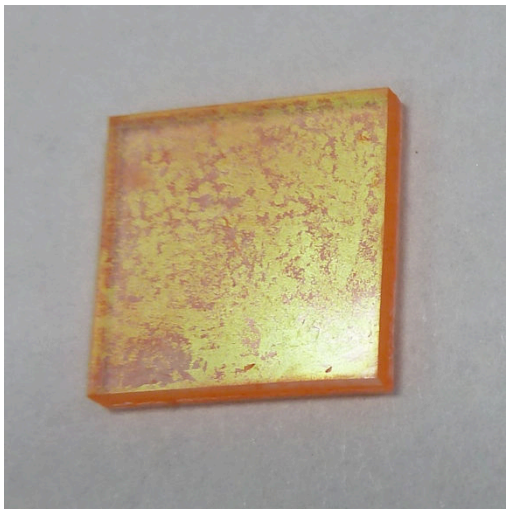

Figure 4.9: Streaky iridescence on the surface of a Sylgard sample containing Orange 240 dye at 49 ppm

These samples still exhibited excellent dye absorbance and emission (discussed in section 6.3), so tests with this dye were continued. The samples containing Red 300 dye were free from dark spots of colour, unlike the heat-cured samples. Figure 4.10 shows the full range of completed Sylgard 184 samples. The maximum concentration of dye used to make the samples was 200 ppm, as this was considered to give the highest levels of opacity that would be useful in fabrication of light-transmitting PV such as the test pieces made in Chapter 7 and Chapter 9.

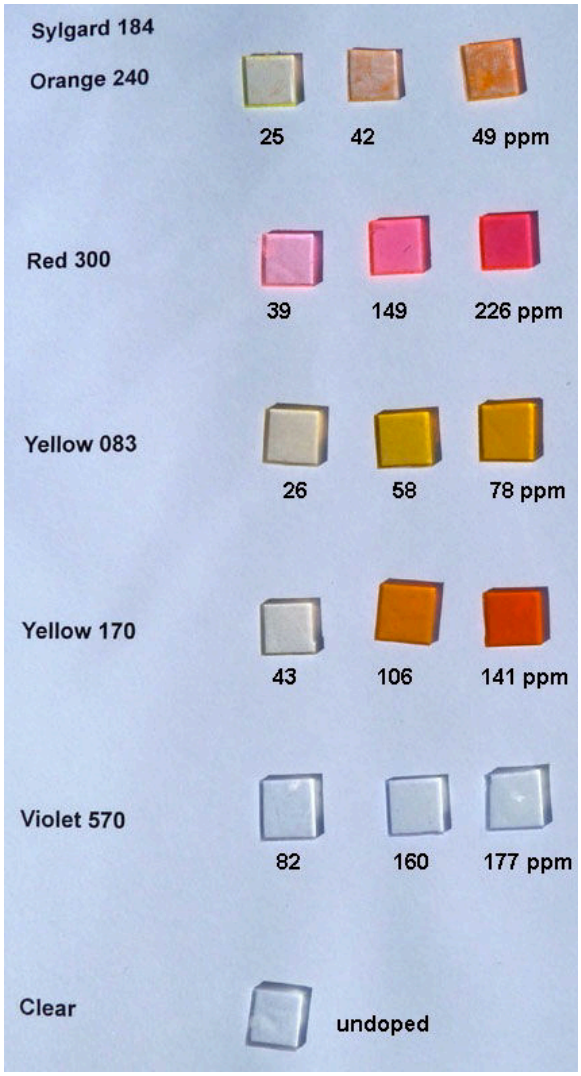

Figure 4.10: Samples of Lumogen F dyes in Sylgard 184 at concentrations from low (left) to high (right)

4.3 Sylgard sample absorbance and concentration measurements

Sample absorbance was measured to determine if the Lumogen dyes were functioning as expected within the new Sylgard samples. Table 4.4 shows the peak absorbance values and calculated dye concentrations. Many of the calculated concentration values are higher than the dye concentrations used to make the samples, with a maximum of a 95% greater concentration measured for the Red sample fabricated with 20 ppm dye. This greater concentration applies to all the Red and two of the Violet samples, as well as the low concentration samples of all the dyes. Red 300 and Violet 570 dyes have higher solubilities in toluene than Yellow 083 or Orange 240 [111]. The solubility of Yellow 170 in toluene is unknown, as this dye is not commercially available [85]. The high values of concentration mean that the Red and Violet dyes are likely to be dissolved fully in toluene before addition to Sylgard part A. It is possible that the Yellow 083 and Orange 240 dyes are incompletely dissolved, despite the increased

amount of solvent used to make these samples. This is supported by the values found for low concentration samples. At low dye concentrations, all the dye molecules are likely to be in solution in toluene, before addition to Sylgard part A. This ensures that a large amount of dye molecules are in solution when added to Sylgard part A. If Sylgard is a poor host for Lumogen dyes, then only a fraction of the available dye molecules will dissolve fully within the host. Other dye molecules may form agglomerates [123]. The higher the solubility of dye within toluene, the greater the amount of dye that is available to form agglomerates on addition to Sylgard part A. If the dye agglomerates absorb more light than single dye molecules, then the greater absorbance values will lead to higher calculated dye concentrations when using the Beer-Lambert equation (in section 4.2.5). The poor solubility of both Orange 240 and Yellow 083 dyes within toluene is likely to cause less dye to be in solution before addition to Sylgard part A, so that less dye molecules are available to form agglomerates. This leads to low absorbance values from the small amounts of dye that are in solution within the Sylgard samples.

Table 4.4: Peak absorbance values and measured dye concentrations for the Sylgard 184 samples with Lumogen F dyes

Lumogen F dye added to Sylgard 184	Initial dye concentration (ppm)	Peak absorbance from absorbance spectra	Wave-length at peak absorb-ance (nm)	Sample thick-ness (mm)	Dye concentration calculated using Beer-Lambert law (ppm)
Red 300	20	0.189	565	1.10	39
	100	0.658	565	1.00	149
	200	1.119	565	1.12	226
Orange 240	20	0.332	520	1.14	25
	100	0.403	523	0.8	42
	200	0.624	523	1.07	49
Yellow 170	20	0.395	462	1.05	43
	100	0.904	481	0.96	106
	200	1.274	486	1.02	141
Yellow 083	20	0.27	464	1.15	26
	100	0.451	456	0.87	58
	200	0.82	457	1.18	78
Violet 570	20	0.418	372	1.06	82
	100	0.683	372	0.89	160
	200	0.814	372	0.96	177

4.4 Adding Lumogen dyes to sheet EVA (ethylene vinyl acetate)

The second encapsulant material investigated as a host material for Lumogen dyes was Vistasolar Fastcure 486.00 EVA [120]. The most effective method of incorporating Lumogen dyes into the flexible EVA sheets found was soaking in solutions of dye. Toluene was tested as a solvent, but it was found that the EVA sheets disintegrated after soaking the sheets for more than one minute [124], so 1-methoxy-2-propanol was selected instead [111], even though the dyes exhibit lower solubility in this solvent. 1-methoxy-2-propanl did not degrade EVA sheets, even after several days immersion in the solution, so decreased solubility of the dye in solution was compensated for by increasing the soak times of EVA sheets in solution.

Initially, samples were made by soaking 100 mm square pieces of EVA sheet in dye solutions. After drying, the sheets were cut into 10 mm squares of EVA sheet, which were placed between thin sheets of borosilicate cover slip. This sandwich construction was compressed in a heated press at 125 °C to laminate the EVA to the glass [124](Figure 4.11).

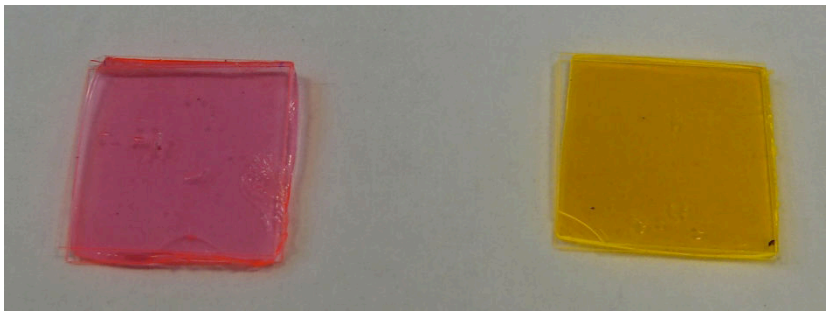

Figure 4.11: EVA samples made with borosilicate glass: Red (left) and Orange (right)

Samples made without glass were required for comparison with the Sylgard samples, which had also been made without glass. It was found that after cross-linking EVA could be peeled from backing materials, especially ‘non-stick’ FEP (fluorinated ethylene propylene). The sheet EVA was 0.46 mm thick, so three dyed sheets of EVA were laminated together to produce samples greater than 1 mm thick. A stack of three, dyed sheets of EVA was placed into a 77 x 88 mm cut-out in a piece of aluminium 1.27 mm thick. FEP sheets were placed above and below this, with sheets of aluminium on the outside, to add rigidity (Figure 4.12). This mould was wrapped in fibreglass cloth, then placed in an EETS PV laminator (PVLAM 0.25), at 150 °C, for 4 minutes; then 3 minutes with 990 kPa pressure.

Figure 4.12: The EVA mould, opened to show two sections containing EVA sheets that have been soaked in Yellow 083 dye. A clear, FEP sheet can be seen protruding from under the two, central aluminium pieces.

After removal from the laminator and fibreglass cloth, the mould was placed directly into a heated press with heat applied at 150 °C for 1 minute. The mould was left to cool in the press, before removing the resulting sheet of clear EVA from the aluminium and FEP, and cutting it into smaller pieces.

Samples were prepared with dye concentrations of approximately 20, 100 and 200 ppm, for comparison with the Sylgard 184 samples made previously at similar concentrations (described in section 4.3). Initial tests showed that soaking the EVA in dye solutions for increasing lengths of time could intensify the dye concentration within the EVA sheets [124]. To establish the correct lengths of soak time to achieve the required concentrations, sheets of EVA were soaked in a 200 ppm solution of Lumogen Red 300 dye in 1-methoxy-2-propanol. Figure 4.13 shows an EVA sheet being removed from solution. The sheets of EVA were laminated together, and the absorbance of these samples was measured in a Perkin Elmer UV-vis-NIR spectrometer. As before, the peak absorbance values were used to give a measure of dye concentration, using the Beer-Lambert law (see section 4.2.5). The length of time required to achieve a measured concentration of 100 ppm was found to be between 2 hours and 2 hours 30 minutes, so a soak time of 2 hours 30 minutes was chosen, to ensure a sufficiently high concentration of dye within all the samples.

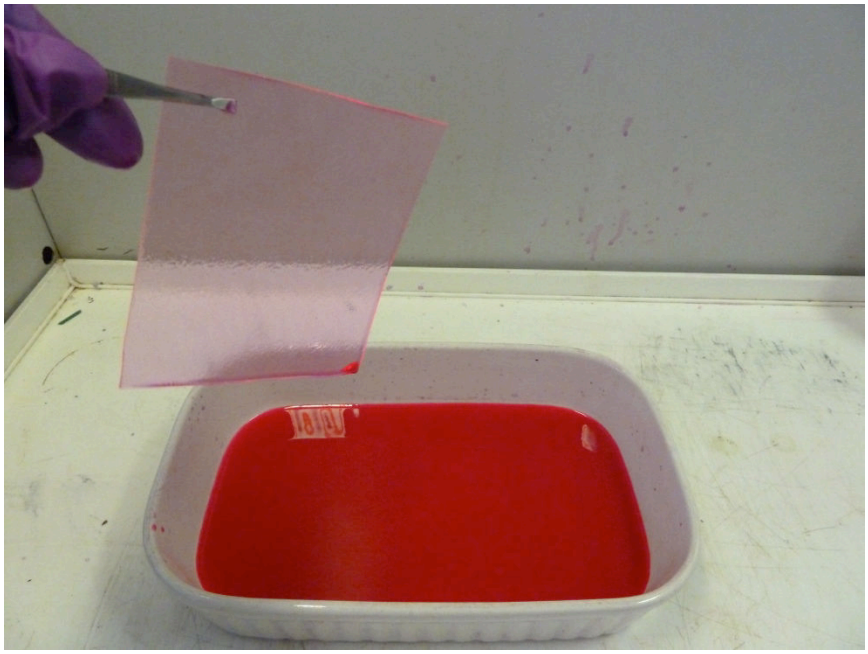

Figure 4.13: An EVA sheet being removed from a 200 ppm solution of Red 300 dye in 1-methoxy-2-propanol

The solubility of Lumogen dyes in 1-methoxy-2-propanol varies from less than 0.5 g/l for Yellow 083 dye to 10 g/l for Red 300. This meant that the same length of time in solution was likely to produce samples with dissimilar dye concentrations for each, separate dye. The Sylgard samples listed in Table 4.4 were made at concentrations of approximately 20, 100 and 200 ppm with a maximum variation of 60% in measured concentration of the samples as fabricated. The EVA samples were intended for comparison with the Sylgard samples, so similar values of dye concentration within the EVA samples were required. The calculated soak times for EVA in Red dye were therefore applied to all the dyes, to give values of dye concentration approximating 20, 100 and 200 ppm within the samples. A soak time of 68 hours in Red dye was found to produce samples with dye concentrations of approximately 200 ppm. To produce samples with 20 ppm dye concentration, EVA sheets were soaked in 200 ppm Red dye solutions for 10 minutes. This led to the EVA becoming covered in spots of uneven colour. The solution strength was changed from 200 to 20 ppm. A soak time of 1 hour 10 minutes was then found to give a dye concentration of 20 ppm within the samples, with an even spread of colour.

Table 4.5 shows the calculated dye concentrations for the final set of EVA samples. Violet 570 dye has a peak absorbance at 374 or 376 nm in PMMA [111, 76]. The following chapter shows that the EVA used for this work contains compounds that block UV light at wavelengths below 360 nm [120]. EVA sheets commonly contain UV blocking compounds [114, 125]. These are designed to minimise light transmission at

the UV end of the spectrum, avoiding damage to the EVA [118]. The UV-blocking compounds lead to a rapid increase in absorbance at wavelengths below 400 nm (Figure 5.4). The measured absorbance of the Violet samples was due to both the dye and the compounds designed to block UV. It was unclear which component of the absorbance was due to the dye. A small peak in absorbance was observed at 390 nm. When the absorbance at this peak was used in the Beer-Lambert equation (in section 4.2.5), dye concentrations of 91, 154 and 252 ppm were calculated. It was unlikely that the resulting high values were a true indication of the dye concentrations within the samples, so they are not recorded in the table. Instead, these samples are simply referred to by the length of time for which they have been soaked in solution: short, medium or long soak; or as low, medium and high concentration.

The measured dye concentrations in Table 4.5 are higher than anticipated for the Red 300 dye, but much closer to the expected values for Orange 240 and Yellow 083 samples. The maximum increase from initial to measured sample concentration was 145% for the Red, low-concentration samples. This is a large difference considering that the calculations of soak time were made using Red 300 dye, and this is greater than the 95% difference measured for the lowest concentration of Red dye within Syglard (in Table 4.4).

Table 4.5: Peak absorbance values and measured dye concentrations for the EVA samples with Lumogen F dyes

Lumogen F dye used in EVA	Peak absorbance from absorbance spectra (*estimated value)	Wavelength at peak absorb-ance (nm)	Sample thickness (mm)	Dye concentration calculated using Beer Lambert law (ppm)
Red 300	0.293	570	1.35	49
	0.946	574	1.64	131
	1.985	572	1.35	333
Orange 240	0.472	524	1.4	28
	1.256	525	1.39	76
	2.988	520	1.41	178
Yellow 083	0.325	445	1.41	26
	1.278	475	1.28	112
	2.434	475	1.36	202
Violet 570	0.57*	390*	1.31	-
	1.067*	390*	1.44	-
	1.585*	391*	1.31	-

The calculated concentrations of dye within the final set of EVA samples (in Table 4.5) show a similar variation to those calculated for Syglard 184 (in Table 4.4), so the affects due to agglomeration of dyes discussed in section 4.3 may apply similarly to EVA and to Sylgard. Dissimilar rates of evaporative loss of solvent or changes in room temperature could have added to the differences between initial and final sample concentrations for the EVA samples. The methodology did give EVA samples with concentrations within a range suitable for comparison with the Sylgard 184 samples described in section 4.3. Again, un-doped, reference samples were made using the same preparation methods as for the doped samples. Completed samples are shown in Figure 4.14. None of the samples showed evidence of dyes precipitating out of the EVA after preparation. Chapter 5 gives details of testing of the un-doped samples of EVA and Sylgard 184. The optical performance of the dye-doped samples is compared with that for Sylgard 184 in Chapter 6.

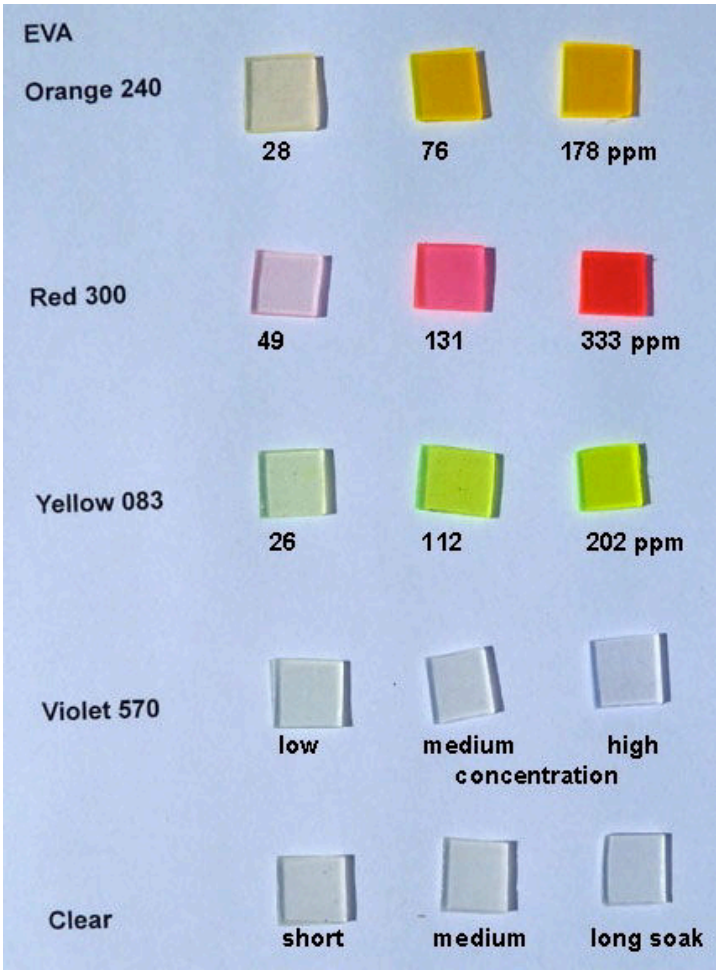

Figure 4.14: Samples of Lumogen dye in EVA (Vistasolar Fastcure 486.00), with weaker dye concentrations on the left, and stronger on the right.

4.5 Chapter conclusion

Lumogen F dyes (BASF) were added to two, dissimilar PV encapsulant materials: Sylgard 184 (Dow Corning) and EVA (ethylene vinyl acetate: Solutia Vistasolar Fastcure 486.00). Methods were developed to make samples suitable for optical testing. Measurements of peak absorbance of the dyes within the host materials were used to calculate the concentrations of dye that were in solution within the host materials. The two sets of samples were found to have similar ranges of dye concentration, so that dye properties within the two host materials could be compared. Having established the sample-making method, Chapter 5 gives details of an investigation to ensure that the use of solvents to add Lumogen dyes to the chosen encapsulant materials does not affect their optical properties.

CHAPTER 5: TESTING THE OPTICAL PROPERTIES OF SYLGARD 184 AND EVA (ETHYLENE VINYL ACETATE)

5.1 Chapter synopsis

Light absorbance and emission of Lumogen-doped and un-doped Sylgard 184 and EVA samples were measured to investigate the influence of the sample preparation methods, specifically the solvents used, on the optical properties of these encapsulants. The optical properties of both encapsulants were found to be similar to those of PMMA, which is a known host material for Lumogen dye. Electrical outputs from PV cells encapsulated with Sylgard 184 and EVA were also compared.

5.2 Method

5.2.1 Power output from silicon cells encapsulated in Sylgard 184 and EVA

PV encapsulants should optimise light transmission to PV cells. Materials such as glass or transparent encapsulants interact with incident light. Some of the light is absorbed within the material, some is scattered and some is transmitted directly through the material. Each material will respond differently to different wavelengths of incident light [66]. Equation 1 in section 4.2.5 shows that the relationship between incident and transmitted light is dependent on the sample properties and thickness. EVA is often specifically designed to exhibit different levels of light transmission at different wavelengths, as discussed in section 4.4. Silicones, in contrast, transmit light at the UV end of the spectrum [114]. The low-iron glass that is commonly used in the fabrication of PV modules is designed to transmit more light in the than the standard soda-lime glass that is traditionally used in many domestic glazing systems [97]. This ensures that maximum amount of light reaches the c-Si PV [126].

Current-voltage (I-V) curves produced by silicon (Si) PV cells were measured to see if encapsulation with the two, chosen encapsulant materials led to any differences in power output, using the method described in section 3.3.4. Monocrystalline silicon PV cells were cut into 52mm × 52mm pieces with central busbars, using a Disco DAD-320 saw. Details of the PV cells are shown in Figure 5.1. These c-Si PV cells were procured from a different manufacturer than those used in Chapter 3 and Chapter 7, and have a higher efficiency. Tabbing strips (E Jordan Brookes) were soldered to the PV cells, using 60/40 tin/lead solder, after application of VOC-free, no-clean flux. 3.3mm-thick borofloat glass (Newcastle Optical) was placed over the fronts of the PV cells. Borofloat glass has a lower iron content than standard soda-lime float glass, leading to a

high light transmittance through the glass to the surfaces of underlying c-si PV cells [97]. After the initial IV test, the same low-iron glass was also used in front of the c-Si PV cells when they were encapsulated. The variation of voltage plotted against current, under a changing electrical load, was then measured using a current-voltage (I-V) curve tracer (EKO MP-160). A solar simulator (ABET Technologies Sun2000 11044, class AAB, 1000W continuous; equipped with quartz optics and both AM1.5G and ultraviolet (UV) edge filters) was used to illuminate each PV cell at 1000 Wm^{-2} (AM1.5) during measurement. I-V curves were measured at 25 °C before and after encapsulation of the PV cells.

Sunways Solar Cells Mono 156 (AH50-H)

The monocrystalline Sunways Solar Cell is provided with three busbars. This reduces the losses during the power generation in the solar module. This contact design, in combination with the constant increase in the efficiency of the Sunways Solar Cells, results in extremely powerful and surface-effective solar modules.

Product description

Category:	monocrystalline, 3 busbars
Format:	pseudo-square
	156 $^{+/-0.5}$ mm x 156 $^{+/-0.5}$ mm
	Diagonal 200 $^{+/-2.5}$ mm
Cell area:	238.95 cm²
Cell thickness:	180 $^{+/-30}$ µm
Temperature coefficients:	Power -19 mW/K
	Open circuit voltage -2.3 mV/K
	Short circuit current +1.1 mA/K

Quality

- 100% camera-based, visual final check for an even appearance of the solar cells in the module
- 100% electric measurement with measuring equipment, calibrated according to ISO 9001:2008

Electrical key data

Current class acc. to I (V_{FIX})	Efficiency rate [%]	Power at V_{FIX} [W]	I (V_{FIX} = 525 mV) [A]	Fill factor [%]	V_{OC} [mV]	I_{SC} [A]
AH508530H	18.7	4.48	8.53	78.0	634	9.05
AH508480H	18.6	4.45	8.48	77.8	633	9.04
AH508430H	18.5	4.42	8.43	77.6	632	9.03
AH508380H	18.4	4.40	8.38	77.3	631	9.02
AH508330H	18.3	4.37	8.33	77.0	630	9.01
AH508280H	18.2	4.34	8.28	76.7	629	9.00
AH508230H	18.1	4.32	8.23	76.4	629	8.99

All figures are averages (Fill factor, V_{OC} and I_{SC} are preliminary), all figures +/- 3 %. Cell class measurement at V_{FIX} = 525 mV.

Figure 5.1: Detail from the Sunways monocrystalline Si-PV cells datasheet with the chosen AH508480H cell details highlighted in yellow [127]

For encapsulation with Sylgard 184, circular stickers (obtained from Sunovation GmbH) were used to secure the backs of the c-Si PV cell 1mm above standard, 4mm-thick, soda lime float glass, to allow the liquid encapsulant to flow around the cells. Layers of double-sided tape were used to attach borofloat front glass to the back glass,

keeping a thin gap (approximately 2mm wide) between them. Sylgard 184 part A was mixed with part B, then placed in a vacuum oven for 30 minutes for de-gassing. The encapsulant was then poured into the gap between the two sheets of glass and left to cure at room temperature. (See the Sylgard sample preparation method discussed in section 4.2.5.1.) For the EVA encapsulation, a sandwich construction was made with sheets of EVA above and below a PV cell, and back and front glass over and under this (Figure 4.1). This assembly was wrapped in fibreglass cloth and placed in a PV laminator at 150 °C for 4 minutes, without pressure, then 3 minutes with applied pressure, as for the EVA sample preparation method. (See the EVA sample preparation method in section 4.4.)

5.2.2 Measurement of absorption and emission spectra

Measuring absorbance of light by EVA and Sylgard 184 ensured that the materials had been processed correctly. These measurements also revealed the effect of the UV-blocking compounds within the EVA. Absorption spectra were measured in a Perkin Elmer Lambda 950 UV-vis-NIR spectrometer (described in section 4.2.4). Clear, undoped samples of Sylgard 184 and EVA were made up using solvents. (See sections 4.2.5.1 and 4.4.) A clear PMMA (poly methyl methacrylate) sample, fabricated by Chilin (Taiwan) [85], was used to compare the optical properties of PMMA with those of the EVA and Sylgard samples, as PMMA is an established host for Lumogen dyes [76].

Fluorescence is common in polymers [115], so it was necessary to check for any fluorescence emission from EVA and Sylgard 184. The aim was to investigate whether un-doped Sylgard and EVA showed any significant fluorescence in the region of the spectrum that could interfere with the emission response from Lumogen dyes. Sylgard 184 is a type of polydimethylsiloxane (PDMS), and it is known that these compounds contain structures that cause light scattering, that could affect fluorescence [128]. It is also known that Sylgard 184 exhibits light scattering [129] and autofluorescence at wavelengths below 570nm [130]. In this research, fluorescence spectroscopy [79] was used to ensure that Lumogen dyes were fluorescing as expected within host materials. Emission spectra were measured using an Edinburgh Instruments FLS920 fluorospectrometer, with a xenon light source, and an extended red-sensitive detector. Samples were held in a sample holder, inside an integrating sphere (Figure 5.2). This ensured that as much of the emitted light as possible reached the detector. This sensitive measurement method [131] was used to quantify light emission when samples were

excited at discrete wavelengths. An excitation wavelength of 365 nm was used. A 395 nm long-wavelength-pass filter prevented excitation light from reaching the detector. The 365 nm wavelength was chosen as it gives an emission response from all the Lumogen dyes used in this research [76]. The aim was to investigate if pure EVA and Sylgard 184 samples showed any significant fluorescence in this region of the spectrum that could interfere with the response of the Lumogen dyes, when these were added to the encapsulant materials. Excitation and emission slits were set to widths of 16 nm and 2 nm, respectively. Similar, substantial slit widths were used when measuring the spectra of Lumogen dyes within these hosts (Chapter 6). 16 nm was the widest available excitation slit width, giving sufficient excitation light to produce response from the samples. This, combined with the narrower emission slit width, ensured that a clear signal of the order of 10^4 to 10^5 photon counts was produced.

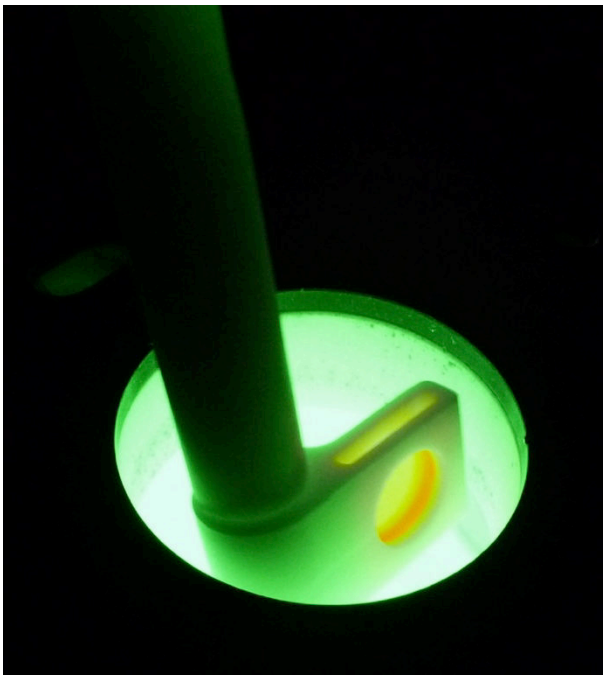

Figure 5.2: The fluorospectrometer sample holder, containing an Orange 240 EVA sample, shown held at the top of the integrating sphere in which it is to be placed.

5.3 Results and discussion

5.3.1.1 Electrical performance of silicon cells encapsulated with EVA and Sylgard

Figure 5.3 and Table 5.1 below, show the results of measuring Si-PV cell performance before and after encapsulation with EVA and Sylgard 184. The top two curves with higher current values and higher maximum power points (P_{max}) show that encapsulation increases the maximum power output. The values in the table confirm that short-circuit current and maximum power both increase on encapsulation. This is expected, as the

encapsulants are designed to optimise the amount of light reaching the PV cells [118]. The results show no significant difference between the two encapsulant materials. The c-Si PV cells used for this experiment produced higher maximum power points than those used in Chapter 3. Both were cut to the same size, so a direct comparison can be made. The maximum power from the c-Si PV used in Chapter 3 was 346 mW for a single, Sylgard-encapsulated cell piece placed on a black backing, as shown in Figure 3.9, whereas the maximum power (Pmax) shown in Figure 5.3, below, for a Sylgard encapsulated cell is 395 mW. Outputs from PV cells or cell strings of different sizes can be compared by use of current density J_c, which is discussed further in section 7.4.2.

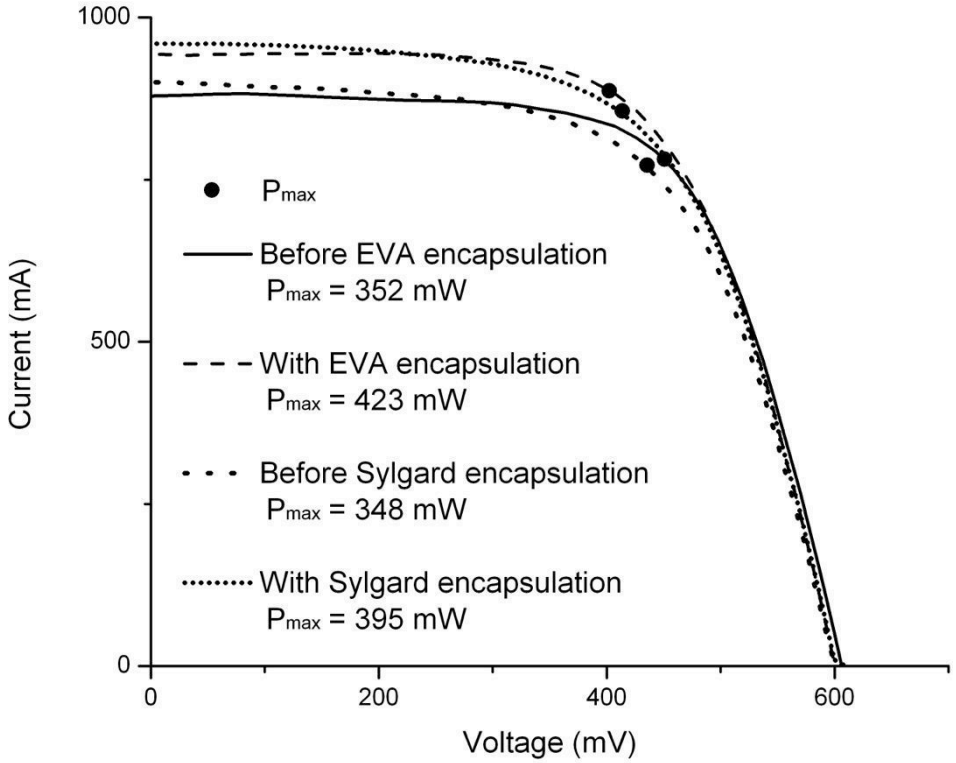

Figure 5.3: Current-voltage curves for two PV cells, before (solid line and widely-spaced, dotted line) and after (dashed line and closely-spaced dotted line) encapsulation with EVA and with Sylgard 184. Maximum power P_{max} values are indicated.

Table 5.1: Maximum current, voltage and power measured before and after Si-cell encapsulation

	Sylgard 184		EVA	
	Before encapsulation	**After encapsulation**	**Before encapsulation**	**After encapsulation**
Maximum short-circuit current (mA)	900	982	879	973
Maximum open-circuit voltage (mV)	613	620	606	616
Maximum power (mW)	348	395	352	422

5.3.2 Comparing light absorbance and emission for EVA, Sylgard and PMMA

Figure 5.4 shows absorbance and emission curves for undoped EVA, Sylgard 184 and PMMA. The EVA absorbance curve (shown in the inset graph) exhibits a rapid increase in absorbance below 400 nm, due to the compounds designed to block UV light, which are included in the EVA [120]. The measured absorbance values correspond to light transmission of 88% for EVA and 93% for Sylgard, at 600 nm. The 88% transmission for EVA is lower than the value of 92% stated in the Vistasolar datasheet [120]. The lower, measured transmission value could be due to abrasion of the surfaces of the EVA when removing it from the FEP moulds that were used when processing the EVA in the laminator. The EVA is intended for adhesion to glass or polymer sheets, so is not designed to be removed from the materials to which it adheres during lamination. The alternative was to make samples with EVA sandwiched between thin pieces of borofloat glass. The glass surfaces were likely to reflect light, increasing inaccuracies in measurement of the optical properties of the EVA and Lumogen dyes. Samples were also required to be comparable with the Sylgard samples made without glass (described in section 4.2.5.1), so further EVA samples were made by removal from moulds, without the use of glass.

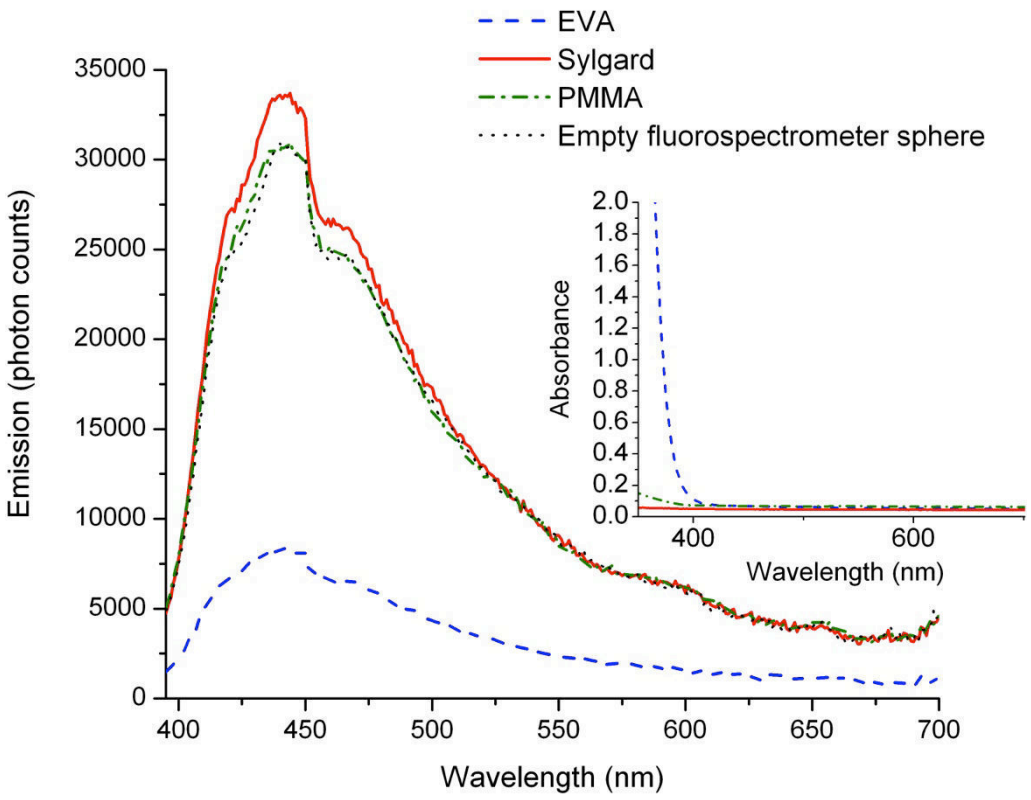

Figure 5.4: Comparing absorbance and emission for EVA, Sylgard 184 and PMMA. The excitation wavelength for the emission scans was 365 nm.

Emission from all three, un-doped samples was compared. Figure 5.4 shows similar intensity and shape of emission curve for all three materials, as well as for the empty integrating sphere. The emission spectrum for the empty fluorospectrometer sphere is almost identical to that from PMMA. This similarity in emission intensity when no sample is present in the integrating sphere indicates that the emission peak is mainly due to the high level of excitation light, not to the presence of the samples. The Sylgard sample shows a slight increase in emission intensity compared with the other samples. This could be due to fluorescence emission, which is known to occur for Sylgard 184 at wavelengths below 571 nm [130]. EVA exhibits a reduction in light emission compared to emission from the other materials and from the empty fluorospectrometer integrating sphere. The excitation light wavelength of 365 nm is within the range of wavelengths at which EVA absorbance of light rises steeply (as shown in Figure 5.4), due to the compounds within the EVA that are designed to block UV light, preventing damage to the material [114, 119]. This increased absorbance of light could be the cause of the reduction in light emission from EVA in comparison with that from Sylgard and PMMA. Although the general level of emission from both EVA and Sylgard is fairly low, emission from undoped samples was still taken into account

when undertaking sensitive photoluminescent quantum yield measurements (section 6.4).

5.3.3 The effects of solvents on EVA and Sylgard

The curves in Figure 5.5 indicate that increasing soak time of EVA in 1-methoxy-2-propanol lead to slight increases in emission intensity. The results appear to be independent of sample thickness. The inset shows that the only significant absorbance of light is at wavelengths below 400 nm. Below 400 nm, there is a decrease in absorbance with increasing length of soak time in 1-methoxy-2-propanol. In this case, greater absorbance of light is leading to decreased emission intensity. The change in absorption below 400 nm, in samples with a longer soak time, could be due to the solvent breaking down the UV-blocking compounds in the EVA. Figure 5.4 shows that soaking in 1-methoxy-2-propanol may cause slight changes to the properties of the EVA. The differences in emission intensity of the order of 10^4 photon counts are taken into account when carrying out the sensitive photoluminescent quantum yield measurements that are discussed in section 6.4.

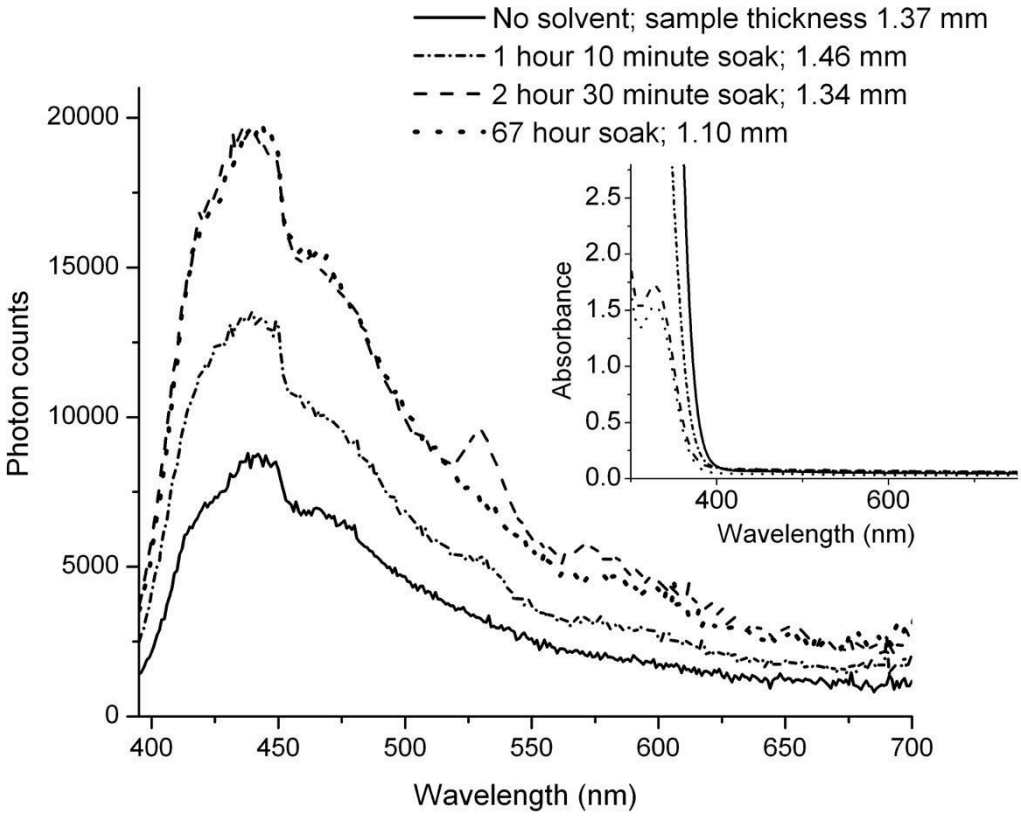

Figure 5.5: Comparison of emission from EVA samples made by soaking EVA sheets in solvent for 1'10"; 2'30" and 67'. Excitation was at 365 nm for the emission curves. The inset shows absorbance measurements for the same samples.

Sylgard 184 exhibits no significant differences in absorbance and emission due to use of toluene in sample making, as shown in Figure 5.6. Toluene is used when adding Lumogen F dyes to Sylgard 184, as described in 4.2.3. Sample thickness, however, appears to have a very small effect on the variations in absorbance and emission. Increasing sample thickness appears to cause a slight increase in absorbance and a small decrease in emission. Clear, control samples that are tested in later chapters are processed with solvents, to ensure that effects due to addition of solvents are not confused with those due to addition of Lumogen dyes to the encapsulant materials. Control samples were made at a similar thickness to doped samples, to ensure that effects due to sample thickness did not become significant.

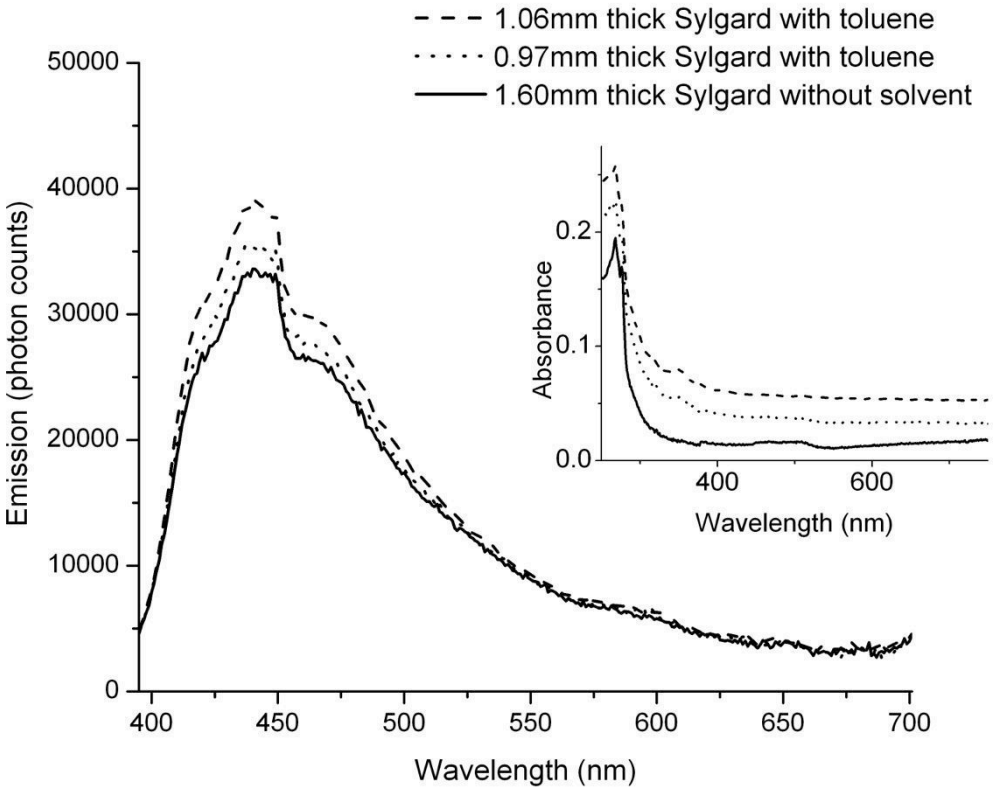

Figure 5.6: Comparison of emission curves for Sylgard 184 samples made with and without solvent. Excitation was at 365 nm for the emission curves. Absorbance spectra are shown in the inset.

5.4 Chapter conclusion

Table 5.2 shows a comparison of the properties of EVA and Sylgard 184, compared with PMMA (poly methyl methacrylate) which is a known host for Lumogen dyes [76]. Both EVA and Sylgard 184 can be used as PV encapsulants, and both cause a slight increase in power output when used to encapsulate Si-PV cells. Absorbance was low for all three encapsulant materials, apart from a rapid rise in absorbance below 400 nm for

EVA, due to UV-absorbing compounds within this material. When measuring emission in the fluorospectrometer, a significant level of emission intensity was observed when testing with the high level of excitation light that is used in later experiments to measure emission spectra from Lumogen dyes. Sylgard exhibited greater emission intensity than EVA. Solvent addition and sample thickness appeared to have small effects on absorbance and emission from samples. Details of absorbance and emission from the doped samples are given in Chapter 6.

Table 5.2: Comparing the properties of EVA, Sylgard 184 and PMMA to assess suitability as PV encapsulants that can act as hosts for Lumogen dyes

	EVA (Solutia Vistasolar 486.00)	**Sylgard 184 (Dow Corning)**	**PMMA (Chilin)**
Used as a PV encapsulant?	Yes	Yes	No
Can be processed without a PV laminator?	No	Yes	Yes
Optical properties	Good light transmission, but not below 360 nm	Good light transmission	Good light transmission
Properties unaffected by the use of necessary solvents for addition of Lumogen dyes?	No (small variations in absorbance and emission are apparent)	Yes	Not applicable: dyes can be added without use of solvents [85]

CHAPTER 6: OPTICAL PERFORMANCE OF LUMOGEN DYES WITHIN SYLGARD 184 AND EVA HOSTS

6.1 Chapter synopsis

The performance of Lumogen dyes within Sylgard and EVA hosts was investigated through measurement of light absorbance, emission and photoluminescent quantum yields.

6.2 Lumogen F Yellow 170 dye in Sylgard 184 encapsulant

Tests were carried out on the samples discussed in Chapter 4, to investigate Lumogen dye characteristics within both Sylgard 184 and EVA. Absorption and emission spectra were measured using a Perkin Elmer UV-vis-NIR spectrometer and an Edinburgh Instruments fluorospectrometer, using the setup described in Chapter 5. Again, the spectra were compared with absorption and emission spectra for PMMA [76] Figure 6.1. shows the comparison of spectra obtained for Yellow 170 dye in Sylgard 184 and in PMMA, respectively. The lowest concentration of dye in Sylgard (43 ppm) gives an emission spectrum with peaks that match those of the dye in PMMA, as shown by the dashed, orange line in the top section of Figure 6.1.

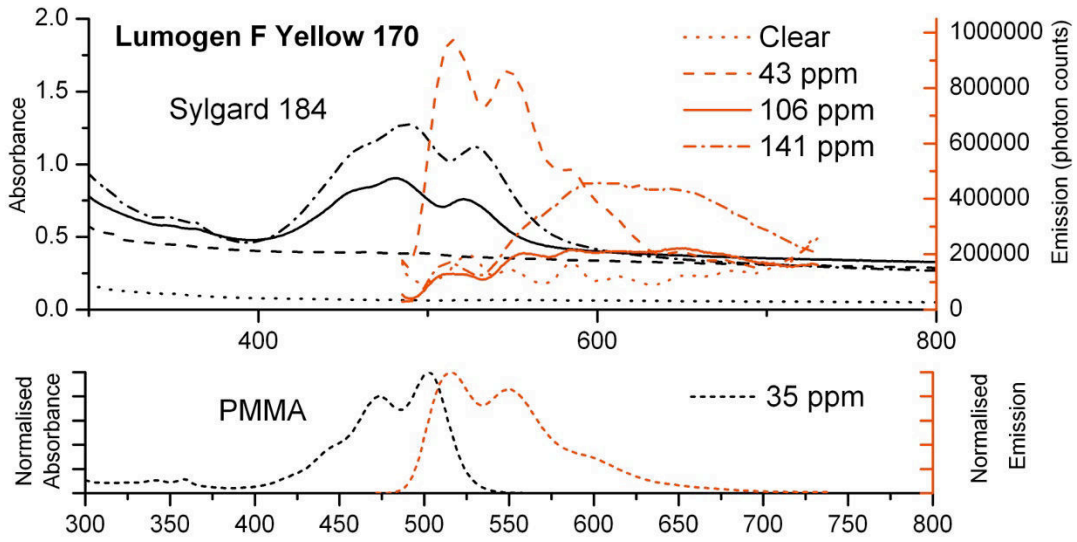

Figure 6.1: Comparing absorption spectra (left axis) and emission spectra (right axis) of Yellow 170 dye in Syglard 184 (top) and PMMA (bottom) [76]

The PMMA emission spectra shown in the lower section of Figure 6.1, and generally in this chapter, are for dyes at very low concentrations of 1.2 to 3.5 ppm [85]. At these low concentrations, the spectra are considered to be optimal spectra, free from the effects of re-absorption of light. These effects shift the spectral peaks to higher wavelengths, due

to light being repeatedly emitted by dye molecules, then re-absorbed by adjacent dye molecules [72]. Each absorption - emission event increases the wavelength of the emitted light, so that dyes at high concentration tend to emit light at longer wavelengths. The Sylgard spectra in Figure 6.1 show this effect, with increasing dye concentration leading to peaks at higher wavelengths. The spectra of the samples doped with 43 ppm Yellow 170 are very similar to the PMMA emission spectrum. At dye concentrations above 43 ppm, the emission spectra become flattened, with reduced emission in the range 510 to 580 nm, where emission occurs within PMMA. The emission from the 141 ppm sample is higher at values above 600 nm, which is a clear indication that the higher concentration of dye is causing re-absorption of light and emission at higher wavelengths. Of the five Lumogen dyes tested, Yellow 170 is the only one that is not commercially available [85]. This dye is similar in colour to Orange 240 dye within a Sylgard 184 host. These facts, combined with fluorescence emission without discernable peaks at useful concentrations (see Figure 6.1), led to a decision not to continue to work with Lumogen F Yellow 170 dye. (This decision is verified in section 6.4.1.1.)

6.3 Comparison of absorbance and emission spectra for Syglard 184 and EVA

Absorption and emission were measured for the four remaining Lumogen dyes that were added to both Sylgard 184 and EVA. Table 6.1 shows the excitation wavelengths used for each dye and the corresponding peak emission wavelengths within each host material. The peak emission values are compared with known values for PMMA [76]. The ratio of excitation to emission slit widths was chosen to give spectra with distinct peaks and a good signal to noise ratio. The ratio of the excitation to detector slit widths was 16:2 nm for the Sylgard samples, but was varied from 16:1.8 nm and 1:0.9 nm for the EVA samples. Narrower slit widths were used when photoluminescent quantum yields could be measured with a lower light input. (Photoluminescent quantum yields are discussed in section 6.4.) Relatively narrow detector slit widths enabled precise measurements of the wavelengths of output light, as slit width is inversely proportional to wavelength resolution. Figure 6.2 to Figure 6.5 (below) are a comparison of absorption and emission spectra compared with the known spectra for these dyes in PMMA.

Table 6.1: Excitation wavelengths and peak emission wavelengths for Lumogen dyes within Sylgard and EVA compared with known peak emission wavelengths for Lumogen dyes in PMMA.

Lumogen dye:			Red 300	Orange 240	Yellow 083	Violet 570
Peak emission in PMMA (nm) [76]			597	534	483	425
Sylgard 184	Excitation wavelength (nm)		525	486	365	350
	Peak emission at dye concentrations:	Low	597	533	-	423
		Medium	604	531	-	424
		High	639	533	-	431
EVA	Excitation wavelength (nm)		530	470	440	360
	Peak emission at dye concentrations:	Low	576	529	425	426
		Medium	601	572	520	426
		High	646	573	523	426

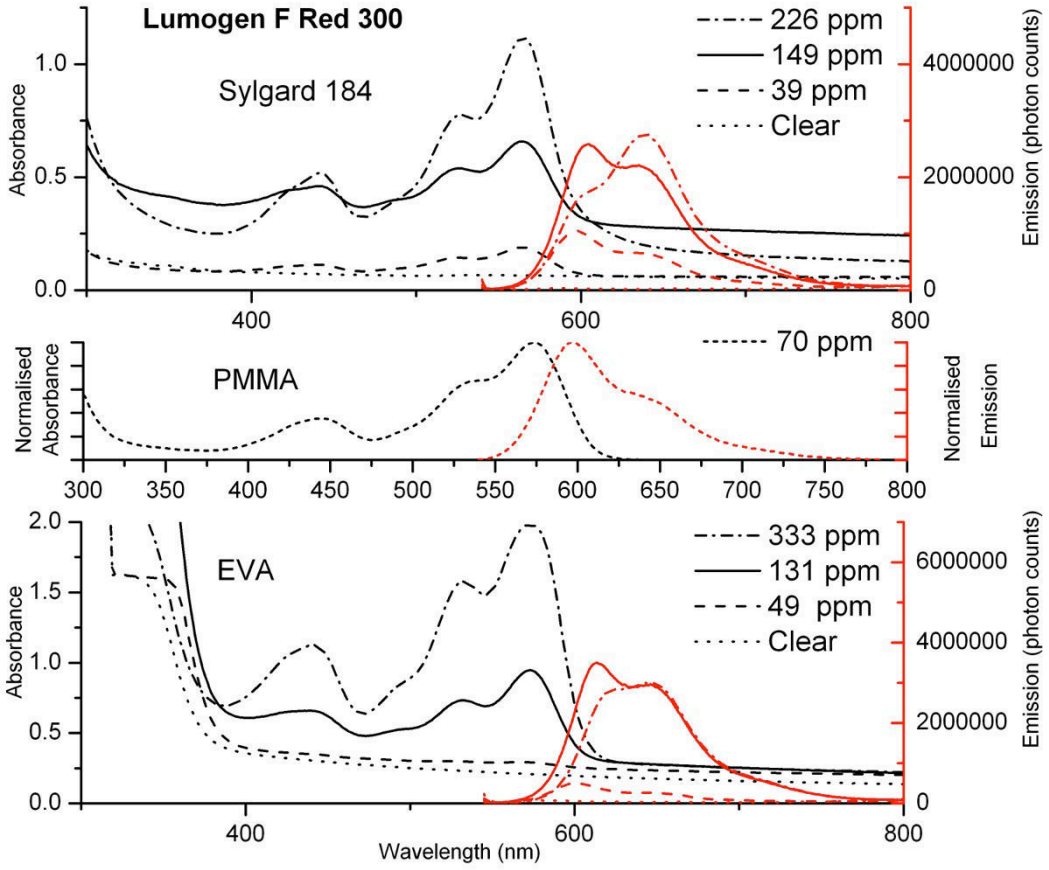

Figure 6.2: Absorption spectra (left axis) and emission spectra (right axis) for Red 300 Lumogen F dyes within Sylgard 184 and EVA, compared with known spectra for the same dyes within PMMA [76]

For Red 300 (Figure 6.2) and Orange 240 dyes (Figure 6.3) many of the peak positions in the Sylgard spectra correspond to peaks in the spectra of the dyes in PMMA. For the highest concentrations of Red 300 dye in both Sylgard and EVA, the relative height of the emission peaks is reversed, compared with those in PMMA. This shift of the greatest emission to a higher wavelength is likely to be due to repeated re-absorption of light increasing the intensity of the longer emission wavelength. The emission curves mirror the absorption curves for medium and lower concentrations, showing good compatibility of the Red 300 dye with the host materials. The absorbance peaks for Orange 240 in Sylgard 184 are flattened when compared with those in PMMA and EVA, but the emission peaks are well defined. The speckled surface of the orange Sylgard samples (discussed in section 4.2.5.1) could have been due to dye being poorly dissolved within Sylgard 184, accounting for the low absorbance compared with the absorbance in EVA. The small fraction of dye that remains in solution within the Sylgard could account for the well-defined emission spectra.

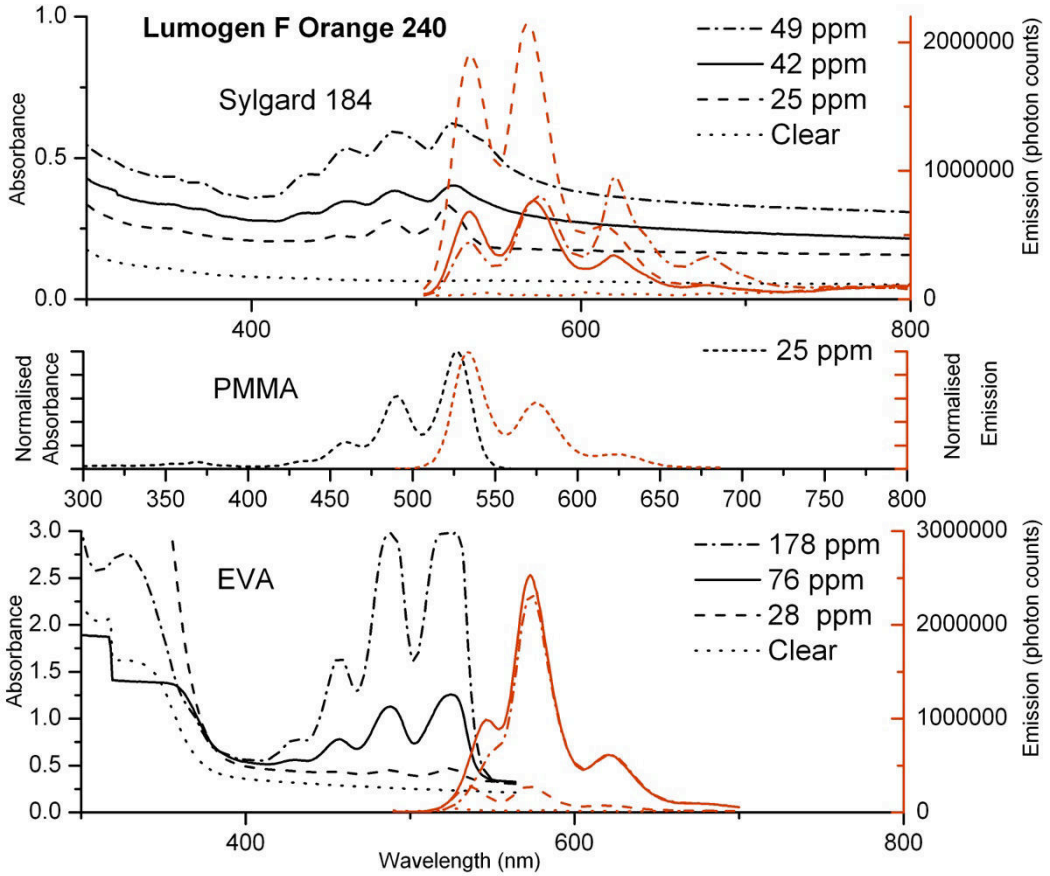

Figure 6.3: Absorption spectra (left axis) and emission spectra (right axis) for Orange 240 Lumogen F dyes within Sylgard 184 and EVA, compared with known spectra for the same dyes within PMMA [76]

Figure 6.3 shows that for Orange 240 dye the relative height of the emission peaks is reversed compared with those in PMMA. Little re-absorption of light is likely at these low dye concentrations. Other mechanisms, such as dye quenching, may be causing the shift. Buffa [132] showed that peak fluorescence emission varies for the same dye at different concentrations within different host materials. She notes that Lumogen dyes exhibit quenching effects at low concentrations within polysiloxane rubbers, which could account for the poor sample emission and quantum yields (discussed in section 6.4) of the Sylgard samples. Sylgard is a polydimethylsiloxane: a siloxane with methyl groups, which is likely to exhibit the same apolarity as the polysiloxanes investigated by Buffa [133], leading to similar low solubility and quenching of Lumogen dyes.

Yellow 083 dye exhibits poor performance within Sylgard, with emission curves without clear peaks (shown in Figure 6.4). It appears that Sylgard is a poor host for Yellow 083.

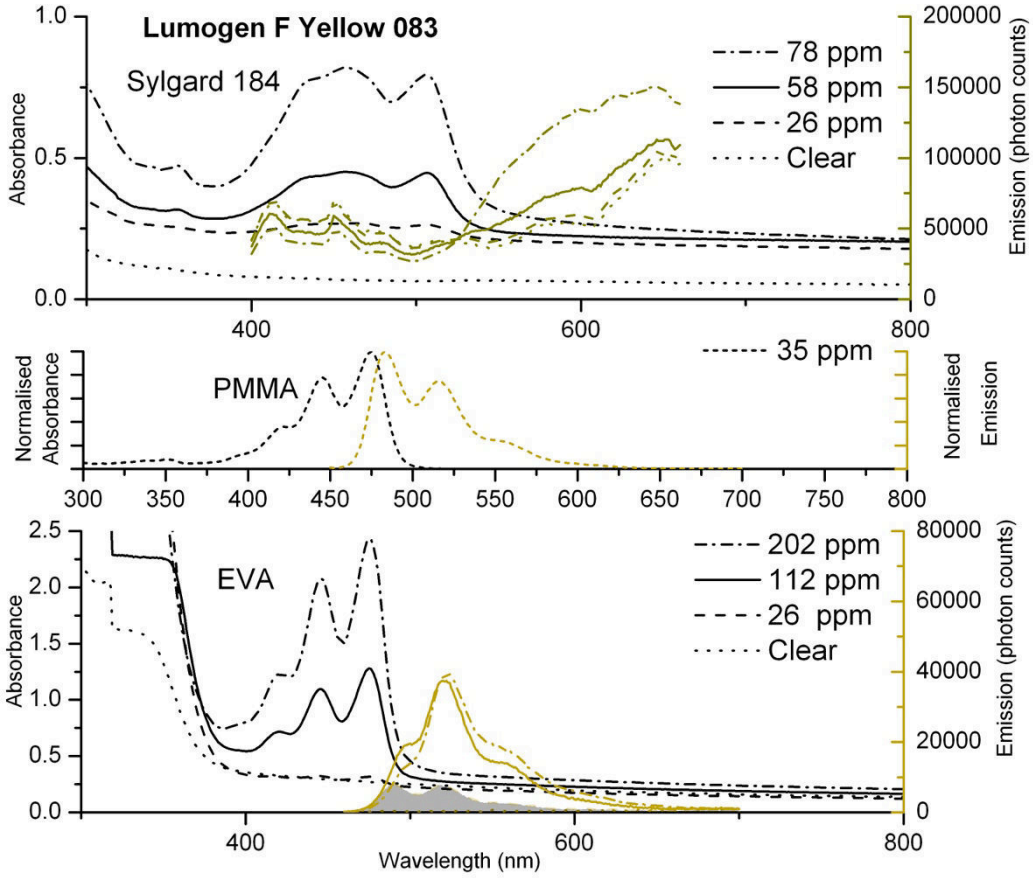

Figure 6.4: Absorption spectra (left axis) and emission spectra (right axis) for Yellow 083 Lumogen F dyes within Sylgard 184 and EVA, compared with known spectra for the same dyes within PMMA [76]

Yellow 083 performs much better within EVA, giving two clear emission peaks at similar wavelengths to those in PMMA for the lowest dye concentration. (The area

under the graph in Figure 6.4 has been shaded to aid viewing.) The emission spectra of 112 ppm and 202 ppm Yellow 083 dye in EVA are similar. This could indicate that a limit of dye saturation within EVA has been reached. These samples are discussed further in section 6.4.

Violet 570 dye, within Sylgard 184, has broad absorbance peaks (shown in Figure 6.5). The peaks are less well defined than those in PMMA, which could again be due to the dyes being poorly dissolved within the Sylgard. There are no clear absorbance peaks in the spectra for Violet 570 dye within EVA, due to the compounds within the EVA that block light below 360 nm. The emission spectra have sharp peaks, however, but overlap at the two highest concentrations in the same way as Violet 570 in Sylgard 184. This could indicate that a limit of saturation of the solubility of dye within the host has been reached for both encapsulant materials.

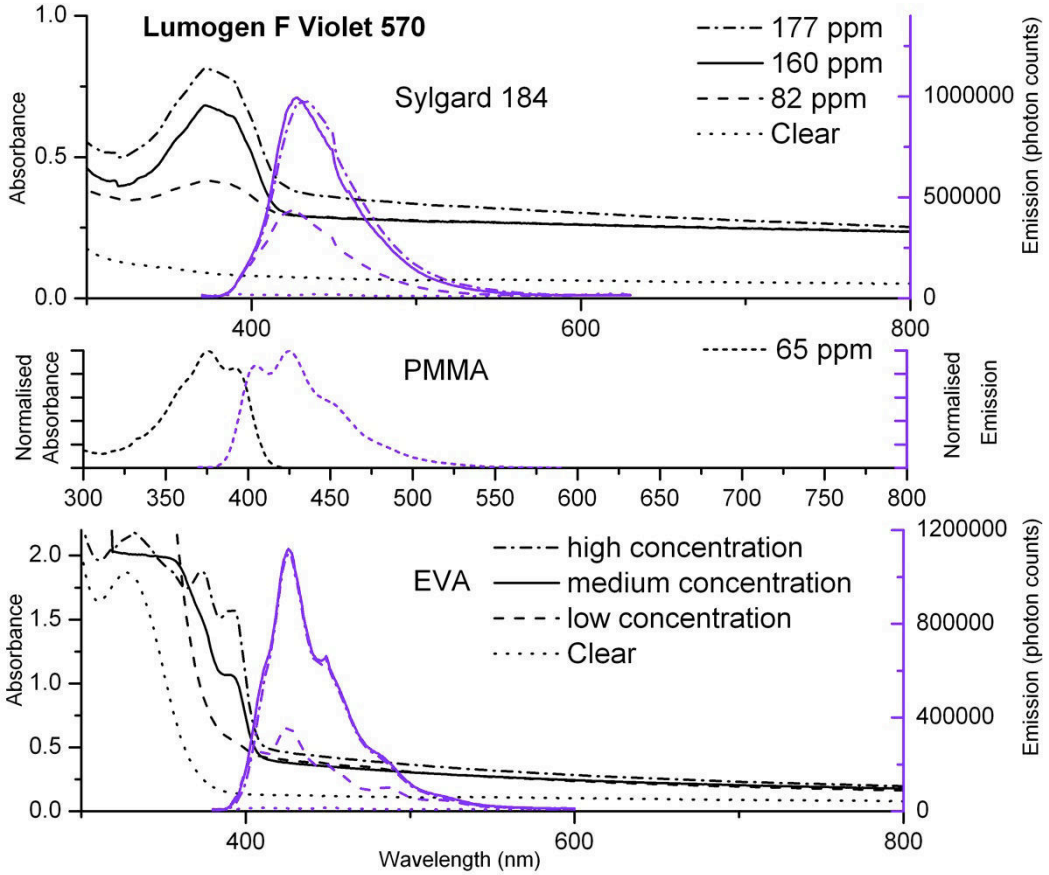

Figure 6.5: Absorption spectra (left axis) and emission spectra (right axis) for Violet 570 Lumogen F dyes within Sylgard 184 and EVA, compared with known spectra for the same dyes within PMMA [76]

6.4 Photoluminescent Quantum Yield (PLQY) measurements

Photoluminescent quantum yields (PLQY) are precise measurements of the performance of fluorophores. They were performed to give an indication of the characteristics of each dye within each encapsulant [134]. Photoluminescent quantum yield is an assessment of the amount of fluorescence emitted by dyes, calculated as a ratio of amount of emitted light divided by amount of absorbed light. Values of PLQY were found by measuring an emission spectrum from each doped sample, using the Edinburgh Instruments fluorospectrometer described in section 5.3.2. A second emission spectrum was then measured at wavelengths around the excitation wavelength. The measurements were repeated for a reference sample without any dye. For each spectrum, a sum of the total photon counts at each wavelength was calculated. Photoluminescent quantum yield was then calculated from:

$$PLQY = (Es - Ec) / (Ac - As) \qquad \text{(Equation 4)}$$

Where:
Es = Total photon counts over the doped sample emission range
Ec = Total photon counts over the control sample emission range
Ac = Total photon counts over the control sample absorbance range
As = Total photon counts over the doped sample absorbance range

The ratio is expressed as a percentage. Ideally a sample absorbs a large amount of light at the excitation wavelength and then emits light strongly at a longer wavelength giving a high ratio of emitted to absorbed light. This is luminescent downshifting, as discussed in section 1.2.6 of the introduction. The chosen Lumogen F dyes have been shown to exhibit PLQY values of over 90% [73]. It has also been shown that the values of PLQY are independent of the wavelength of the excitation light [135].

At least three measurements of PLQY were made for each sample, over at least two days, to establish the variation in measurement accuracy. A PMMA sample, doped with Lumogen F Red 300 dye, was also tested on several different occasions. This sample gave PLQY values of 78% to 80%, thus confirming the consistency of this sensitive method within ± 1%. Table 6.2 shows the measured values of PLQY for each dye at each concentration. An asterisk (*) indicates the use of a paper sample holder to obtain a measurement. This is discussed further in section 6.4.1. At least one measurement was made without a paper sample holder, to ensure no significant effects due to fluorescence from the paper. The maximum discrepancy of the measurements

presented in Table 6.2 was ± 3%, which is between the established measurement error of 10% for this method and Wilson's 2% errors in precise measurements of PLQY in PMMA [76].

Table 6.2 shows that higher dye concentrations lead to lower PLQY values for all the Sylgard samples. This could again be an effect of poorer solubility of dye in Sylgard leading to a decrease in PLQY at higher concentrations.

Table 6.2: Comparison of photoluminescent quantum yield (PLQY) values for Lumogen dyes within Sylgard 184 and EVA

	Sylgard 184 PLQY (%)		EVA PLQY (%)	
Lumogen dye	**Medium dye concentration**	**Highest dye concentration**	**Medium dye concentration**	**Highest dye concentration**
Orange 240	24* ± 1 28	15* ± 2 15	94 ± 3	96 ± 3
Red 300	83* ± 3 81	40 ± 1	87 ± 0	85 ± 1
Yellow 083	Not measureable	Not measureable	Not measureable	100 ± 1
Violet 570	73* ± 1 75	60* ± 3 67	85 ± 3	Not measureable
	* indicates use of a paper sample holder with fluorescence at 440 nm. This is discussed in section 6.4.1			

It is known that PLQY values can vary widely for the same material [136], and that dye concentration affects the value of PLQY [137]. Measured values of PLQY are reduced when samples containing high concentrations of dye are subjected to repeated re-absorption of light, within an integrating sphere [138]. Correction factors to compensate for this were not applied to the PLQY values in table. One method of obtaining these re-absorption correction factors is to scale measured emission spectra. Scale factors are obtained from the emission spectra of very weak concentrations of dye, in which re-absorption events are unlikely to occur [135]. This process could have increased the measured values of PLQY for the Lumogen dyes for all but the 100% PLQY value. Wilson shows increases in PLQY values of Lumogen dyes of up to 5% through application of the re-absorption correction [76]. The correction factors are only valid when reductions in PLQY are due to repeated re-absorption of light by samples tested within the integrating sphere of a fluorospectrometer. This method does not take into account reductions in emission intensity due to agglomeration and quenching. As already mentioned, these can occur as a result of poor solubility of dyes within a host and the Sylgard samples discussed in section 4.3 show some evidence of agglomeration of dyes. Applying re-absorption corrections to the values in Table 6.2 would have given

an indication of the ideal performance of Lumogen dyes within Sylgard and EVA, however the aim of comparing the true performance of the combinations of dye and encapsulants would not have been achieved. Table 6.2 is a therefore a comparison of the performance of each Lumogen dye within each host material without re-absorption correction factors.

The emission spectra of the Yellow 083 dyes within Sylgard were too poor for PLQY values to be measured. It was not possible to measure consistent PLQY values for the lowest dye concentrations within any sample, because the spectra measured at the excitation wavelength were very similar for both doped and clear samples, so that the value (Ac – As) was too small. Any small changes in this value caused large discrepancies in the calculation of PLQY in the above equation, with errors greater than ± 5%. This also occurred for Yellow 083 dye at a medium dye concentration (76 ppm) within EVA, and at the highest concentration of Violet dye within EVA (approximately 200 ppm, as discussed in section 4.4). This is unexpected for a high-concentration sample. Figure 6.6 shows that there is an unanticipated reversal in emission intensity from the high concentration Violet sample, at the excitation wavelength of 360 nm.

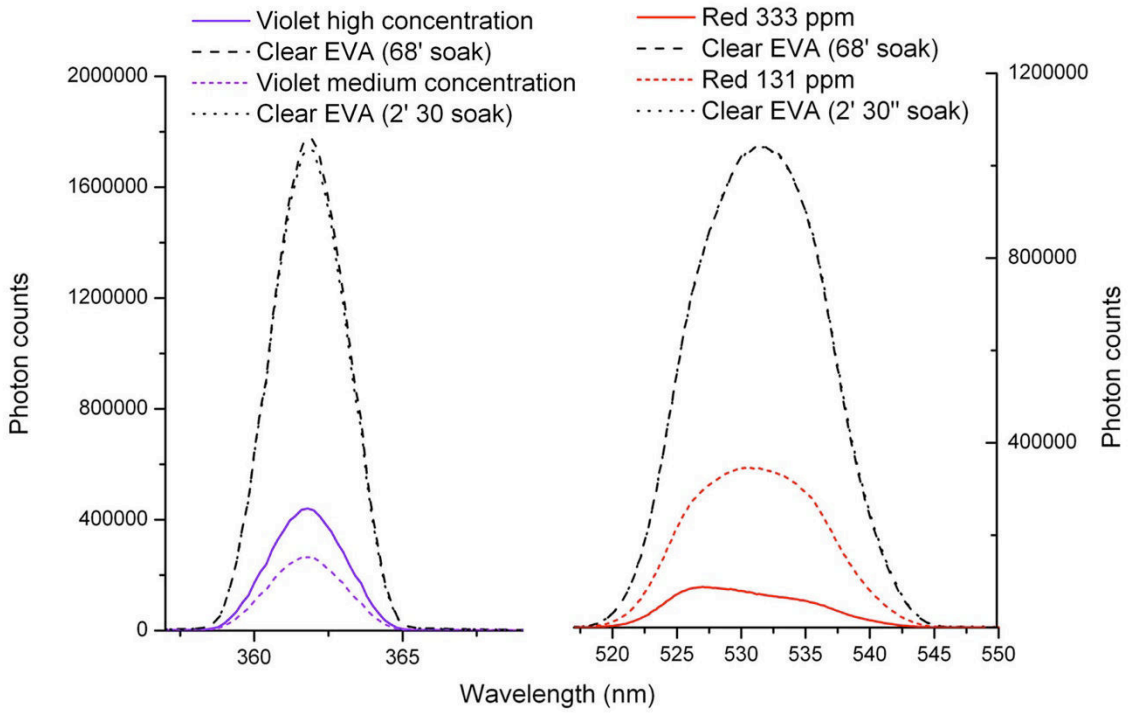

Figure 6.6: Emission scans at the excitation wavelengths of 360 nm for Violet and 530 nm for Red EVA samples, showing the reverse in relative emission intensity between high and medium dye concentrations for the two, different dyes in EVA

A higher concentration of dye would be expected to have lower emission intensity, due to the larger amount of dye molecules absorbing light, as shown by the

emission curves for the Red EVA samples on the right of Figure 6.6. The reversal in emission intensity could be caused by the compounds in the EVA that are designed to absorb and dissipate light at wavelengths below 360 nm [118]. The left side of Figure 6.6 shows a slight difference in peak height for the two undoped samples excited at 360 nm indicating that increased soak time in 1-methoxy-2-propanol leads to greater emission intensity when the samples are excited at 360 nm. It appears that the ability of the EVA to absorb light at 360 nm is being decreased by increased time in solution during sample preparation. Addition of Violet dye appears to amplify this effect, as shown by the two lower curves in the left portion of Figure 6.6, where increased concentration of dye leads to increases in light emission. Addition of dye could be causing further damage to the UV-blocking compounds, so that the EVA and dye combination is less able to absorb light over the measured wavelength range. The measured PLQY values show that Orange, Red and Violet Lumogen dyes were fluorescing within Syglard and EVA. Yellow 083 Lumogen dye appears to perform well only at higher concentrations within EVA. EVA appears to be a better host for Lumogen dyes than Sylgard, showing higher PLQY values for all the EVA samples.

6.4.1 Use of a paper sample holder for Sylgard 184 samples

A white paper sample holder was used to hold some Sylgard 184 samples within the fluorospectrometer sample holder, to avoid contamination due to the tacky surface of the Sylgard samples. The paper was later found, however, to give a strong emission centered at 440 nm, which was much greater than the peaks in emission caused by the dyes. The fluorescence of the paper sample holder is clearly visible in the right section of Figure 6.7. A 365 nm (ultraviolet) source causes the paper to fluoresce brightly in the blue region of the spectrum.

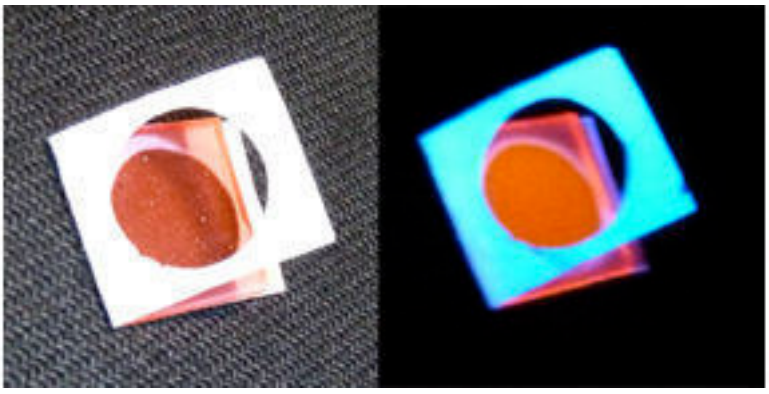

Figure 6.7: A Red Sylgard sample in a paper sample holder: (left) under standard office lighting; (right) under illumination from a 365 nm source

Figure 6.8 shows the emission spectrum from Red 300 dye in Sylgard 184, excited at 380 nm. This wavelength is much lower than the 525 nm excitation used for the other Red 300 emission spectra discussed here, enabling a wide range of light emission to be scanned. (The usual excitation wavelengths for all the Lumogen dyes are shown in Table 6.1.) There is a small fluorescence peak at 597 nm, visible in the red dashed and dotted lines as expected for Red 300 (see Table 6.1). This peak does not occur for the un-doped sample (shown by the black, solid and dotted lines), so is clearly attributed to the Red 300 dye. A large peak at 440 nm dominates the graph. This peak occurs for both dye-doped and undoped samples, and is due to fluorescence from the paper. It is much larger than the fluorescence emission peak due to the Red 300 dye, on the right of Figure 6.8. It was necessary to check the effects of the paper on dye spectra that had been measured with a paper sample holder in place. This is discussed in section 6.4.1.1, below.

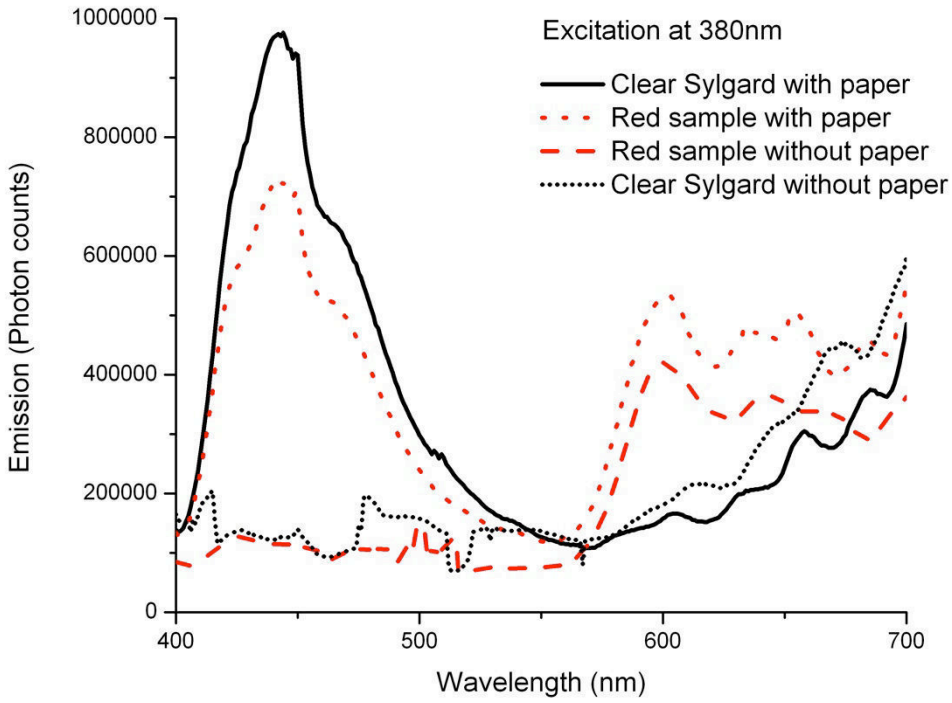

Figure 6.8: Emission from a 20 ppm Lumogen Red Sylgard sample, and a clear Sylgard sample, with a paper sample holder that fluoresces at 440 nm

6.4.1.1 Testing the effect of the paper sample holder on the Sylgard samples

Emission spectra of doped, Sylgard samples, were measured with and without the paper sample holder. Results are shown here for the lowest dye concentrations, as these gave the clearest emission spectra. An exception is made for Yellow 170 dye, where the aim

was to check if removal of the paper sample holder made any significant difference to the poor emission spectrum previously observed in the high concentration sample shown in Figure 6.1.

Figure 6.9 shows that the fluorescence from the paper had little effect on the emission scans for red and orange dyes, where both excitation wavelength and emission peaks are well above 440 nm.

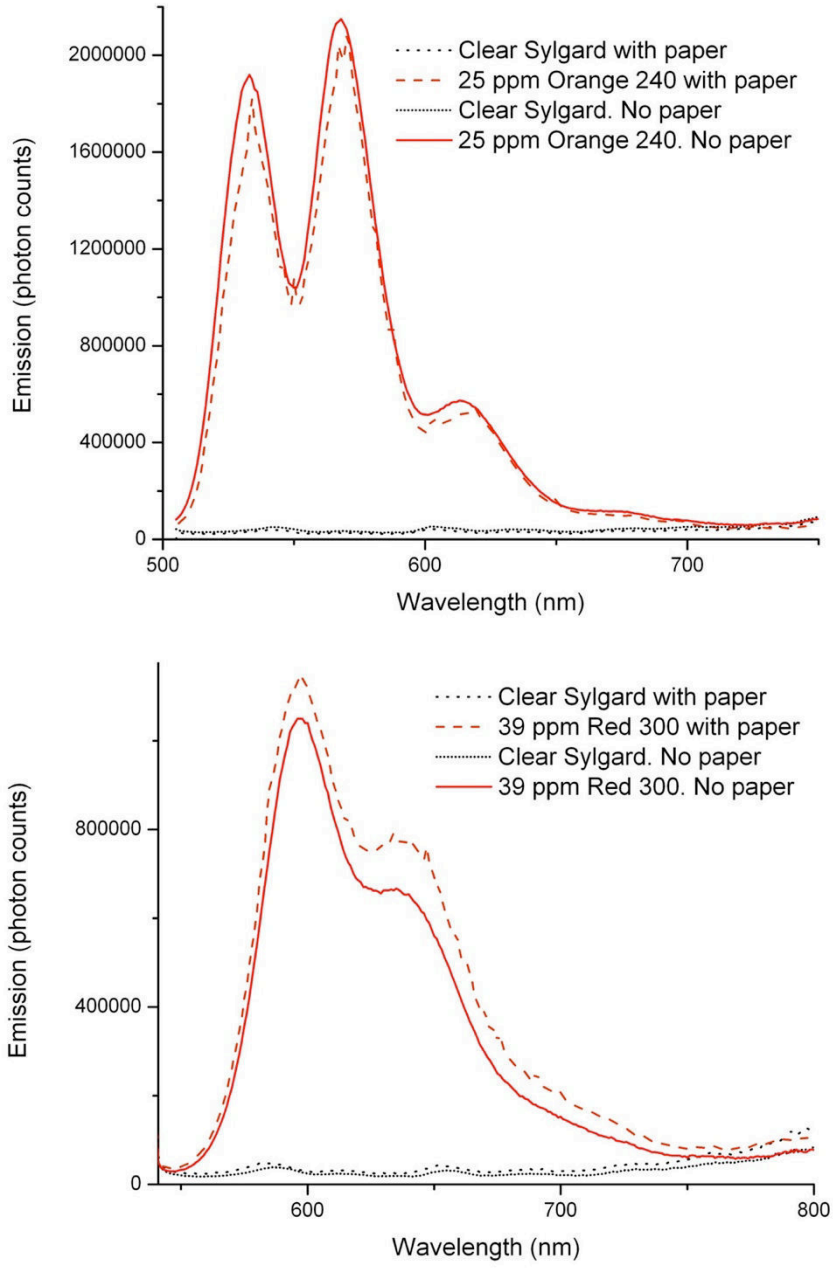

Figure 6.9: Emission scans for Sylgard samples with and without paper sample holders: Orange (above) and Red (below)

Emission scans from both clear and Lumogen Yellow 083 samples however were strongly affected by the use of the paper sample holder (Figure 6.10). The peak at 440

nm disappears when the paper is removed. The subsequent lack of peaks in the dye spectra indicates that the dye was not well assimilated within the Sylgard 184 host (as discussed in section 6.3).

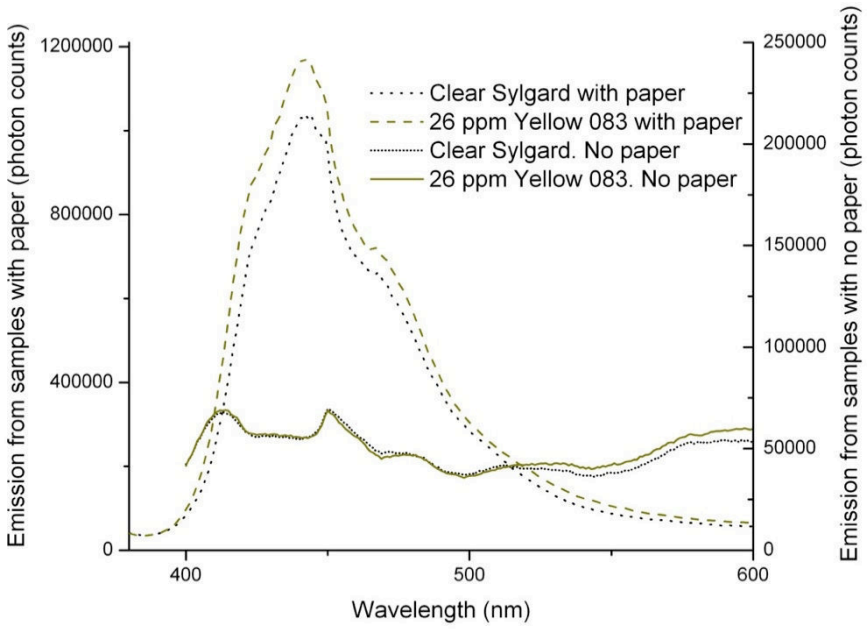

Figure 6.10: Emission scans for Yellow 083 dye in Sylgard, with and without a paper sample holder

The top two curves in Figure 6.11 show that there is a shift in the Violet emission peak from 440 nm to 425 nm when the paper sample holder is removed. There is also a reduction in emission from the Violet 570 sample indicating that the paper was likely to have increased the overall intensity of the peak emission. The change in emission at 440 nm is most apparent for the un-doped sample, as shown by the lower two curves in Figure 6.11.

The paper sample holder was unlikely to cause any change to the emission spectra of the Sylgard samples with Yellow 170 dye, as emission was measured at values well above 440 nm. The highest concentration sample was re-measured without the paper sample holder to ensure that this made no difference to the unexpected shape of the emission spectrum discussed in section 6.2. Figure 6.12 shows that the spectra for both clear and doped samples are similar in shape, both with and without the paper sample holder. The two measurements were carried out at similar excitation wavelengths of 468 nm for the samples with a paper holder, and 460 nm for the later measurement, without paper. The spectra from samples with a paper sample holder were corrected to compensate for a greater slit width of 2.5 nm that was used for these earlier

measurements, compared with a 2.0 nm slit width for the samples without paper sample holders.

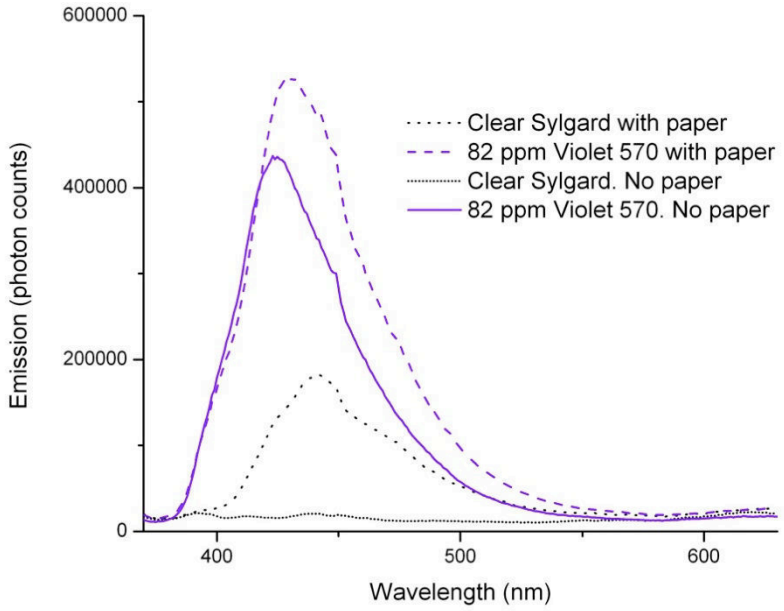

Figure 6.11: Comparison of emission from samples of Violet 570 dye in Sylgard, with and without a paper sample holder

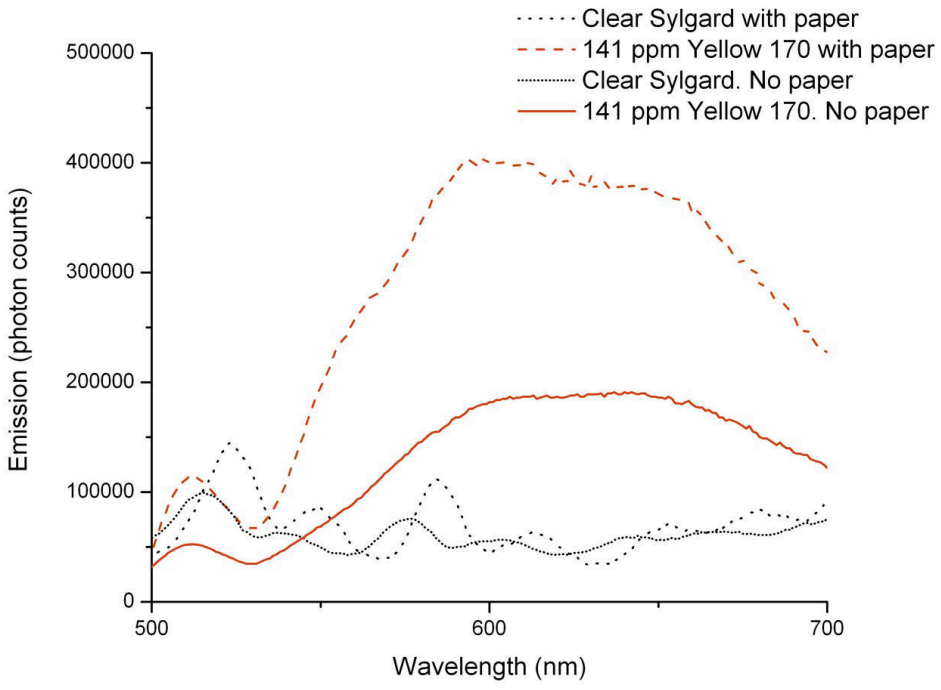

Figure 6.12: Comparison of emission spectra for Yellow 170 dye in Sylgard 184, with and without a paper sample holder

The emission spectra from the clear samples are similar, indicating no effects due to the paper sample holder. Both doped samples exhibit low emission intensities, with a greater emission intensity from the sample measured with a paper sample holder

compared with that measured without a paper sample holder. This could be attributed to use of different samples to carry out the measurements. Both spectra are a similar shape, and exhibit a lack of clear emission peaks. This, combined with the reasons listed at the end of section 6.2, meant that the decision not to carry out further work with Yellow 170 dye was maintained.

In summary, the use of a paper sample holder affected any measurements where emission was measured at or near 440 nm. There was a particularly strong effect on the Sylgard samples containing Yellow 083 and Violet 570 Lumogen dyes. This was taken into account in section 6.4, where measurements of PLQY were repeated without use of a paper sample holder, ensuring that there were no major inconsistencies in measurement due to fluorescence from the paper. There is further discussion of this in Chapter 8.

6.5 Chapter conclusion

Measurement of absorbance and emission spectra, as well as photoluminescent quantum yields (PLQY), showed that Lumogen dyes performed better in an EVA host than when incorporated within Sylgard 184. Low concentrations of dye gave absorbance and emission spectra that approximately matched those for PMMA (a known host for Lumogen dyes), for all the dyes except Yellow 083 within Sylgard, and Violet 570 within EVA. Yellow 083 within Sylgard gave poor emission curves for all dye concentrations, indicating that this dye was not well suited to use within Sylgard 184. The dye absorption spectra for Violet 570 dye in EVA showed that it was not possible to distinguish between effects due to dyes and those due to the UV-absorbing compounds within the manufactured EVA. For the Sylgard samples, where consistent PLQY results could be measured, higher dye concentrations gave lower PLQY values. The range of PLQY values for Sylgard 184 was from 15 ± 2% for high concentration (49 ppm) Orange 240 to 83 ± 3% for medium concentration (149 ppm) Red 300. EVA samples exhibited higher PLQY values, between 85 ± 3% for low concentration Violet 570 to 100 ± 1% for high concentration (202 ppm) Yellow 083. From this, it appeared that Lumogen dyes were better assimilated into an EVA than into a Sylgard host. Work continued with Lumogen dyes in both Sylgard and EVA to provide a comparison of ageing properties of the two material combinations (assessed in Chapter 8), and to assess the differences when using these materials in architectural glass. Chapter 7 gives details of use of Lumogen F dyes within Sylgard 184 in the fabrication of an architectural glass test piece.

CHAPTER 7: ADDING LUMOGEN DYES TO SYLGARD 184 IN AN ARCHITECTURAL GLASS TEST PIECE

7.1 Chapter synopsis

The method of adding fluorescent dyes to the PV encapsulant Sylgard 184 (Chapter 4) was combined with the glass painting techniques described in Chapter 3, to make an architectural glass test piece with added colour.

7.2 Introduction

Colour is a vital feature of much decorative glazing, as discussed in Chapter 1. The method described in Chapter 3 showed that PV cells could be blended into monochrome architectural glass designs through use of glass paint. The first aim of the work described in this chapter was to use a similar design to that developed in Chapter 3 and to enhance this through addition of colour. This could increase greatly increase the range and variety of architectural glass designs that could be produced. Details of the design development, including the fabrication of a small, coloured test piece, are given in Chapter 3 and appendix 1. The second aim of the work was to use luminescent solar concentrator technology to increase electricity output from the PV cells incorporated into the test piece, as described in section 4.2.1. The method of adding coloured, fluorescent Lumogen dyes to Sylgard 184 was chosen, as described in Chapter 4. Use of a silicone encapsulant instead of EVA meant that the work could be carried out in a studio setting, without use of specialist PV lamination equipment. Red 300 and Yellow 083 Lumogen dyes were chosen, as these provided the strongest colour contrast from the four selected Lumogen dyes described in section 4.2.1. (The problems with the fluorescence of Yellow 083 dye within a Sylgard 184 host were only discovered after the test piece was made up (see section 6.3).) The chosen colours fitted with the design theme of heaven and hell that is depicted in the test piece design (shown in Figure 3.6 and Figure 7.1). Reflective, platinum paint was also included in the test piece. It is known that mirrors can be incorporated into luminescent solar concentrators to re-direct light to the dye, and subsequently to attached PV cells [139, 71]. It was anticipated that the platinum paint would act with the fluorescent dyes to enhance the efficiency of electrical power production by the test piece.

7.3 Method

A 600mm × 450 mm test piece was made up using black and platinum glass paints

(Rüger and Günzel GmbH), as described in section 3.3 of Chapter 3. The paints were used to create areas of pattern around the sites in which the PV cells were to be placed. Platinum paint was also applied to the back glass, as described in Chapter 3. This was shown to increase power produced by PV cells placed over the glass.

This test piece was designed to incorporate two strings of six PV cells each: one string to be encapsulated in Sylgard 184 containing Lumogen Red 300 dye, in the lower section, and the other with Lumogen Yellow 083 dye, at the top. The same batch of c-Si PV was used as in Chapter 3, so that the only major difference between the design discussed in this chapter and that in Chapter 3 is the use of coloured encapsulants. The methodology described in section 4.2.5.1 was used when adding the dye to the encapsulant, but was carried out on a larger scale, and in a studio setting. Each Lumogen dye was dissolved in toluene, then added to 1 kg of Sylgard 184 part A at 200 ppm concentration. After taping the front and back glass together, the Sylgard 184, containing Lumogen Yellow 083 dye, was poured into the test piece whilst it was held at an angle. Once this was nearly set, Sylgard 184 containing Lumogen Red 300 was added, so that a little mixing of the dye colours occurred at the interface.

7.3.1 Dye fluorescence

The fluorescence of the dyes was measured by placing an optical fibre against the edges of the test piece. The fibre was connected to a spectrometer (HR2000CG-UV-NIR, Ocean Optics, USA), to give relative values of irradiance in the range 350 - 820 nm, which was the range in which fluorescence emission would be expected to occur from the dyes. Measurements were carried out using an ABET solar simulator at 1000 Wm^{-2} (section 3.3.4), to ensure that each test was made at equal irradiance. The measurements from the edge of the test piece were compared with those from the edges of samples made up in the laboratory (described in section 4.2.5.1). Black masking was used to expose a small, equally-sized area of each sample, and of the test piece, to the light from the solar simulator.

7.3.2 Performance of PV cells with dyed encapsulant

To measure the effects of Lumogen dyes on the performance of PV cells, the electrical output from each string of PV cells in the test piece, was compared with output from a single PV cell, encapsulated in clear Sylgard 184. Black paint was applied to the low-iron glass in front of this PV cell. The current-voltage curve tracer (EKO MP-160) was used to take measurements from each string of PV cells within the test piece, and from the single PV cell, encapsulated in clear Sylgard 184. The tests were carried out with the

test piece and an irradiance sensor positioned vertically, inside a window, as the large test piece was too large to place under the ABET solar simulator. A silicon-based sensor (Mencke and Tegtmeyer Si-01TC-T) was used to ensure that readings were taken at similar levels of irradiance.

7.4 Results and discussion

The appearance of the PV cells was altered by the colour of the dyes within the encapsulant. When viewed from the front, in transmitted light, the PV cells merged into the painted background (Figure 7.1a), as with the test piece with clear encapsulant (Figure 3.6). Figure 7.1b shows the front of the test piece in reflected light. Under this lighting condition, the dye colour caused the PV cells to contrast with the surrounding black paint, making the PV cell shapes stand out. In contrast, Figure 7.2 shows that the platinum paint on the back glass disguises the PV cells in both reflected and transmitted light. The back of the test piece was likely to be viewed more closely, as this would be on the inside of a window aperture, with the PV cells facing outwards. The dye colours did not make the c-Si PV stand out from the rest of the design when viewed from the back.

Figure 7.1: Front views of the 600mm × 450mm testpiece placed in a window aperture, from left to right (a) in transmitted light, and (b) in reflected light

The coloured encapsulants exhibited some opacity within the test piece, as shown on the right side of Figure 7.1 and on the left in Figure 7.2. This was not ideal, as opacity

within encapsulants prevents light from being transmitted to underlying PV cells. The colour of the red dye, within the test piece, was duller and bleached, when compared with the colour of the small, red sample made with 200 ppm of Lumogen Red 300 dye, in the laboratory. The Yellow 083 dye showed little difference between test piece and sample: both exhibited high levels of opacity. This demonstrates that Lumogen Yellow 083 does not fluoresce within Sylgard 184, when the two materials are combined together using the methodology developed in this thesis (as discussed in section 6.3).

Figure 7.2: Rear views of the 600mm × 450mm testpiece placed in a window aperture, from left to right: (a) in reflected light (photographed with a flash); (b) a detail in transmitted light.

7.4.1 Dye fluorescence

Both of the dyes within the test piece appeared to have low fluorescence emission. Figure 7.3 shows measurements of fluorescence made at the edges of the test piece and of the reference samples, using a fibre optic probe. The peaks in the upper graph in Figure 7.3 show that the red dye within the test piece was emitting very little light compared with the small, red sample. The differences in red dye emission, between the small-scale samples made in the lab, and the large test piece, made in the studio, could have been due to contamination or overheating of the materials when working on a larger scale, in the studio. In the lower section of Figure 7.3, the yellow edge of the test piece is shown to have a small emission peak at a similar height to that from the small, yellow sample. Both the peaks for Yellow 083 are small compared with the peak for the Red 300 sample made in the lab. There is also a shift in the peak wavelength from 554 nm for the sample made in the lab to the two peaks shown at 493

nm and 530 nm for the large test piece. This indicates that the sample made in the lab may contain a greater amount of dye in solution or be exhibiting more dye agglomeration than occurs within the large test piece [76]. The two, distinct peaks in the fluorescence from the large test piece indicate that two, different fluorescent compounds may have been formed, possibly due to contamination. The poor fluorescence emission of Yellow 083 within a Sylgard host was discussed in section 6.3. The results shown in Figure 7.3 confirm this. The following chapter shows how improvements in PV performance are achieved through use of an EVA encapsulant.

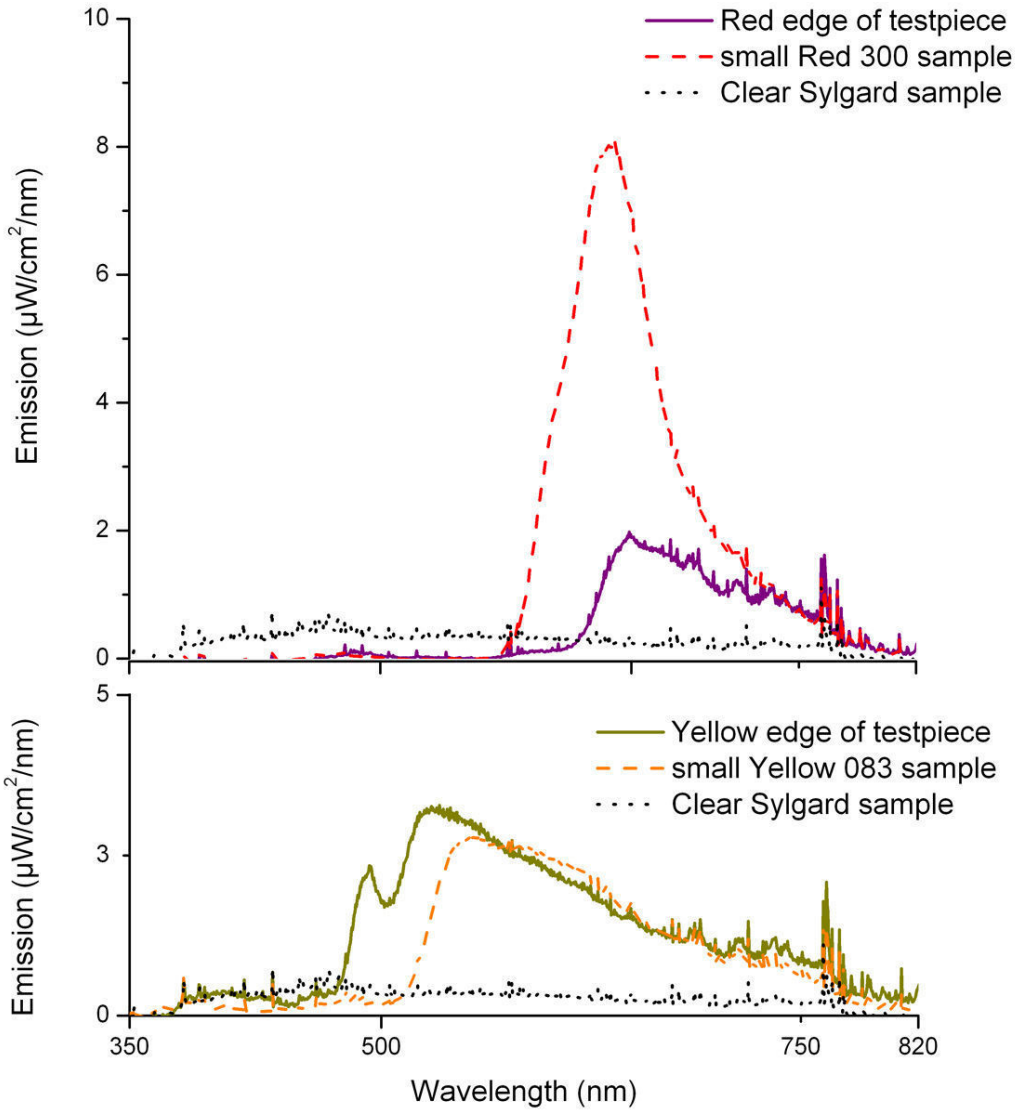

Figure 7.3: Comparison of the light emission from the red and yellow edges of the test piece with that from Sylgard 184 samples made with 200ppm of Lumogen F Red 300 dye (above); Lumogen F Yellow 083 dye (below); and a clear, Sylgard 184 sample.

7.4.2 Power output

The electrical power output from the strings of PV cells within the test piece was compared with that from a single PV cell, encapsulated in clear Sylgard 184, by measuring current-voltage (I-V) curves (Figure 7.4). The x-axis shows, as expected, that the maximum voltage across the six-cell strings is approximately six times that of the voltage across the single cell, encapsulated in clear Sylgard 184. The y-axis shows the difference in current outputs: the current from a single cell, encapsulated in clear Sylgard 184, is greater than that from the cells encapsulated in Lumogen Yellow 083 dye. Cells within the Lumogen Red 300 dye produced even less current. The poor colour intensity and fluorescence emission of the dyes are limiting the electrical performance of the PV cells, due to the dyes absorbing part of the incoming light spectrum, but not emitting as much light as expected. The curvilinear strings of PV cells, with wide spaces between cells, and large areas of paint, also produced minimal electrical power per unit area. For each design, a balance has to be achieved between areas of clear glass, areas of paint and the amount of glass that can be covered by PV, to generate electricity.

The tests were carried out with the test piece placed in a window aperture. The irradiance values of 389 to 404 Wm^{-2} were therefore much lower than the 1000 Wm^{-2} values produced by the ABET solar simulator that were used to produce the I-V curves shown in Figure 3.9, where the same batch and size of PV cells were used. The maximum power (P_{max}) of 109 Wm^{-2} for a single PV cell, shown in Figure 7.4, is therefore much lower than the maximum power of 346 Wm^{-2} for a similar PV cell, shown in Figure 3.9. The current density, J_c, could be used to compare the outputs from the 3 different tests shown in Figure 7.4. This is the Current, I (mA) divided by the surface area of the cell or cell string that has produced that current. Using this comparison for the maximum power values shown in Figure 7.4, gives a current density value of 40 W for the single c-Si PV cell encapsulated with clear Sylgard, compared with 30 W for the red-encapsulated PV and 43 W for the yellow-encapsulated PV. The current density is highest for the yellow-encapsulated PV, even though the Yellow 083 dye has poor fluorescence properties. The encapsulant doped with Yellow 083 did remain translucent, so this, combined with the small amount of fluorescence produced by the dye, is likely to have caused this higher current density.

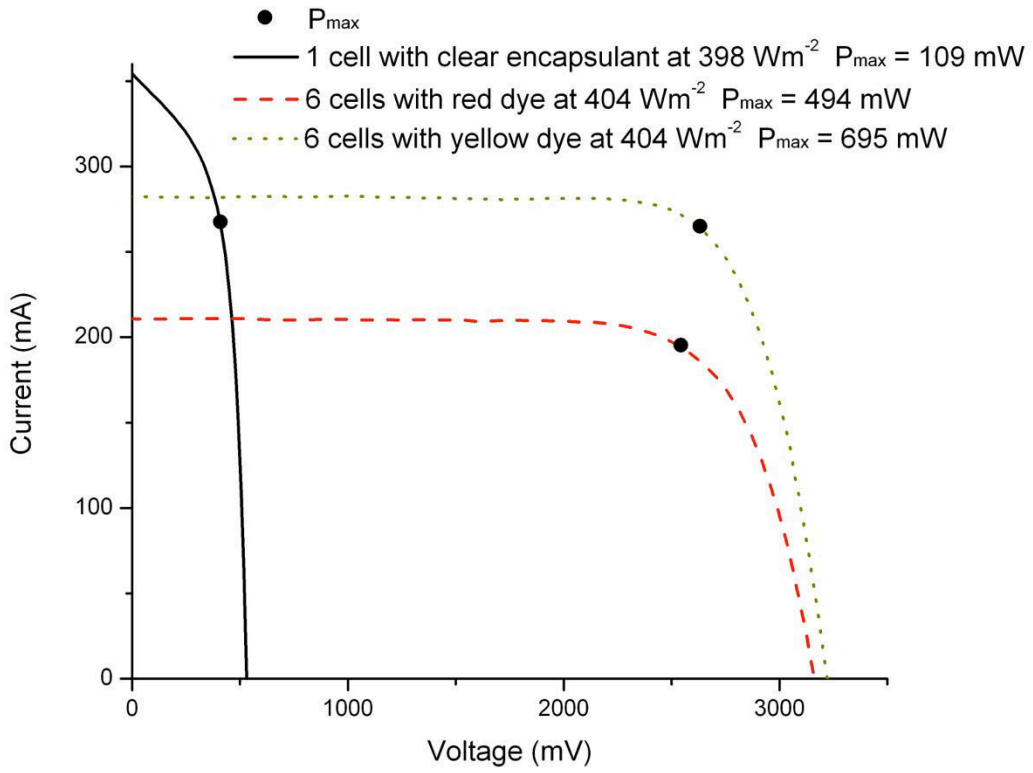

Figure 7.4: Current-voltage (I-V) curves, comparing electrical performance of the PV cells within the Lumogen Red and Yellow dyes, inside the 600 mm × 450 mm testpiece, with performance of a single PV cell encapsulated in clear Sylgard 184. The maximum power points (P_{max}) are shown on each curve.

7.4.3 Details of the testpiece appearance

Table 7.1 shows details of problems with the fabrication and final appearance of the test piece. Accurate placement of the PV cells was particularly difficult. This problem is overcome in the Chapter 9, where fabrication involves placement of all opaque materials behind PV cells, with no need for careful overlay of painted front glass over PV cell strings. Limiting use of opaque materials to the back glass would also prevent the colour contrast between PV cell surface, covered in dyed encapsulant, and the black paint on the front glass, as shown in the central photo in the table. Use of EVA, instead of Sylgard, could minimise the formation of bubbles that occurred when using Sylgard 184. There were difficulties in removing trapped bubbles that occurred during the method of pouring encapsulant between two sheets of glass.

Sheets of EVA can be used as a host for Lumogen dye, as described in Chapter 4. Encapsulation with EVA requires use of a PV lamination process to apply heat and pressure, but the kiln firing processes that were used to fix the glass paint onto the test piece warped the glass surface. Glass that is not perfectly flat would be likely to crack under pressure during the PV lamination process, so alternative methods of coating the glass would need to be found.

Table 7.1: Problems with test piece fabrication and appearance, with possible solutions

Problem	Detail of testpiece	Solution
Difficulties in accurate placement of PV cells beneath square, un-painted areas of glass.	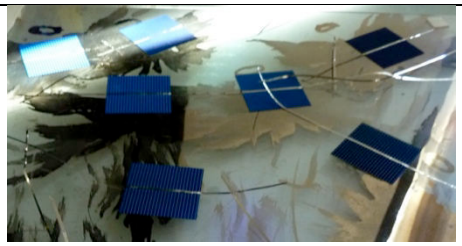 PV cells during string connection	Application of paint only to the back glass would mean that PV cells would not require such accurate positioning.
Colour contrast between painted areas of the front glass and the PV cell surface covered with dyed encapsulant. A few bubbles in the encapsulant	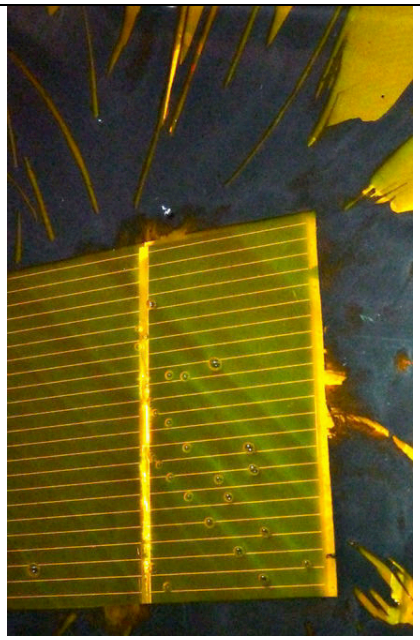	Application of paint to the back glass only, would mean that when viewing from the front, both paint and PV cells would be viewed through a layer of dyed encapsulant, so that colours of the cell surfaces and surrounding areas would appear similar. Use a different encapsulant, where air bubbles will not expand during curing, or a different encapsulation method, such lamination with ethylene vinyl acetate (EVA)
Circular stickers were visible in areas where platinum paint did not cover the cell backs completely	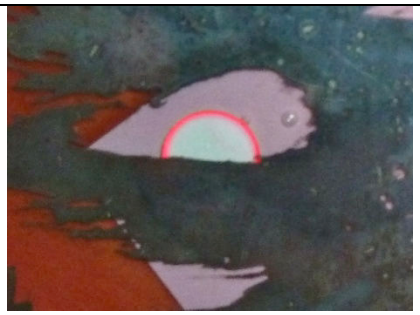	Stickers would not be required when encapsulating with ethylene vinyl acetate (EVA).

Use of glass coatings or decals, instead of traditional glass paint, would remove the need for kiln firing to fix glass paint. This would also make it easier to create designs that conform to safety standards [140]. This is particularly applicable to the platinum paint applied to the back glass, which prevents the glass from being toughened, as the reflective surface prevents the heat treatment from being carried out correctly. An alternative to platinum paint is required: a method of applying a translucent, reflective coating to selected areas of the glass before or after glass toughening. This is explored further in Chapter 9.

7.5 Chapter conclusion

Fluorescent, Lumogen dyes were used to add colour to the Sylgard 184, which was used to encapsulate PV cells within a painted, glass test piece. The translucent red and yellow dye colours altered the test piece appearance, including the apparent colour of the PV cell surfaces. The dye properties were affected by addition to Sylgard 184, so that the Lumogen F Red colour became faded when the mixing process was moved from small-scale laboratory preparation to a larger scale, in the studio. Both dyes exhibited poor fluorescence emission within the Sylgard 184 host. There was a resulting low electrical current produced by the PV cells that were covered by the dyed encapsulant. Alternative materials and methods are required in order to maintain good PV cell efficiency when adding colour to the encapsulant. This is investigated further in Chapter 9, following on from the next chapter (Chapter 8) in which the durability of encapsulant-dye combinations is explored.

CHAPTER 8: DEGRADATION OF LUMOGEN DYES WITHIN SYLGARD 184 AND EVA HOSTS

8.1 Chapter synopsis

The degradation of Lumogen F dyes within Sylgard 184 and EVA hosts was investigated. Accelerated ageing tests were carried out using Suntester CPS+ machines. Samples were also placed outdoors. The absorbance and emission properties of both sets of samples were then compared. The dyes degraded quickly, showing that these combinations of dye and encapsulant are unsuitable for most building-integrated applications.

8.2 Theory

Chapter 4 gave details of addition of Lumogen dyes to PV encapsulant materials. These were intended for use with c-Si PV, within architectural glass. It was important to find if these material combinations were suitably durable for building-integrated applications. Decorative glass is normally designed to last for several decades [56], avoiding costly maintenance. Standard c-Si modules are normally guaranteed for at least 25 years [141]. Ideally, the dyed encapsulants would be similarly robust, so that units containing these materials would require infrequent maintenance or replacement.

There are no guaranteed lifetimes for manufactured polymer sheets containing fluorescent dyes, but it is known that '3 – 5 years' outdoor stability is possible for fluorescent dyes within a PMMA host [112, 142]. BASF gives details of accelerated ageing of Lumogen dyes in PMMA, which show that at least 80 to 95% fluorescence can remain after 2000 hours testing [74]. It was hoped that Lumogen dyes would age at a similar, or slower rate within Sylgard and EVA. It was therefore considered likely that only accelerated ageing tests would cause a high level of degeneration of the dyes, to the point where much less colour was visible within EVA or Sylgard. Any corresponding changes in colour or opacity of the host materials would then be observed. This was important, as any degradation of the host materials could result in loss of transmission of light to underlying PV cells [118].

Hastening of degradation, through use of a Xenon lamp, could cause dissimilar reactions to those produced in sunlight [143]. The combinations of dye and encapsulant were designed for exposure to sunlight, so outdoor tests were carried out in addition to accelerated ageing tests. It was expected that comparison of the accelerated and outdoor

decay of the samples could be used to estimate an expected, useful lifetime for each encapsulant-dye combination.

8.3 Method

Accelerated ageing tests were carried out in Suntest CPS+ machines. Each of these contained a Xenon lamp and filters. The filters modulated the spectrum from the Xenon lamp, to approximate to the solar spectrum [144]. Figure 8.1 shows a Suntest CPS+ with an aluminium tray containing samples placed inside the base of the testing chamber.

Figure 8.1: A Suntest CPS+ with the door open to show an aluminium tray containing samples of EVA doped with Red 300 dye

An aluminium tray with square depressions was designed to hold each set of samples, and to fit into each machine. Figure 8.2 shows a tray filled with Sylgard samples, prior to testing. The top row of the tray contains the undoped reference samples. Each column contains a single dye colour at the same concentration. 3.3 mm borofloat glass was placed over the samples in the trays, as this is a type and thickness of glass commonly used in PV modules [97]. During each test, single rows of samples were removed after 1, 2, 5, 10, 20, 50, 100, 200, 500 and 1000 hours. A reference sample was also removed at each of these times.

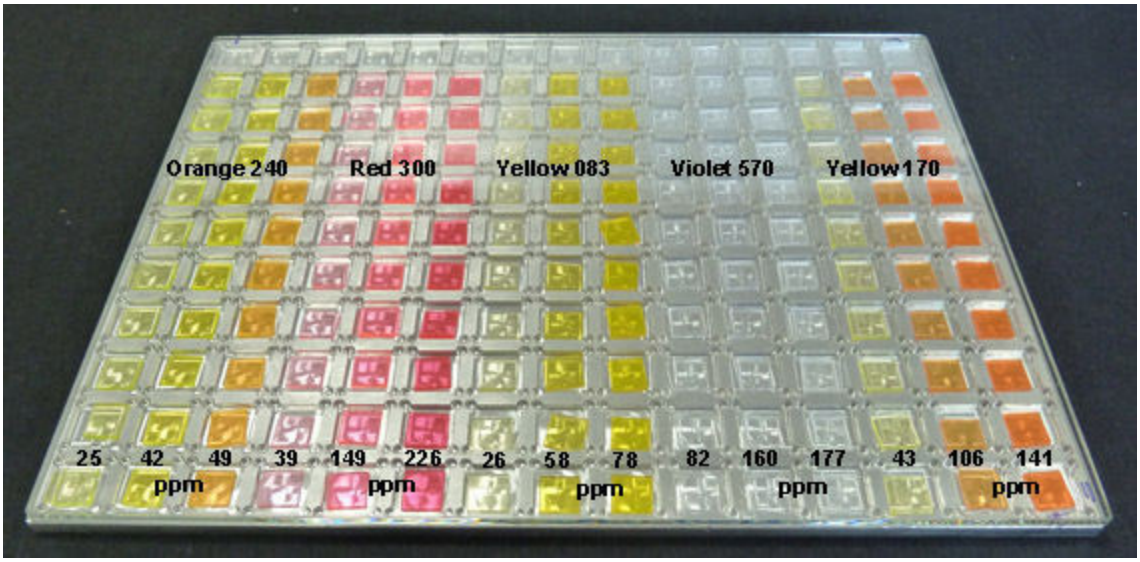

Figure 8.2: An aluminium tray containing Sylgard samples, prior to placement in the Suntest machine. The top row of the tray contains reference samples. Each three columns, from the left, contain Orange 240, Red 300, Yellow 083, Violet 570 and Yellow 170 samples. The sample concentrations in each set of three columns are from low on the left to high on the right.

The Xenon lamp was a long tube, which was installed across the centre of the top of the Suntest CPS+ test chamber. There was likely to be variation in the intensity of light across the tray, so that different rows of samples would not receive the same level of light intensity. The variation in light intensity was established by placing a calibrated, Thor Labs photodiode in nine positions on the base of the tray. The variation in current is shown in Table 8.1 below. The spread of the readings shows a maximum 3.7% variation in light intensity from the central reading. The readings in Table 8.1 were taken after the Sylgard samples had been tested. At the start of testing, the photodiode read 10.3 μA when placed in the centre of the testbed. The measured variation in intensity between the start and end of the test could have been due to ageing of the Xenon bulb or to changes in the circuitry of the Suntest CPS+, which failed after the Sylgard test.

Table 8.1: Variation in photodiode current across the test area in the Suntest CPS+ used for Sylgard sample testing after the Sylgard test

	Reading on photodiode (μA)		
Position of photodiode in Suntest CPS+	**Left**	**Centre**	**Right**
Back	11.00	10.75	10.50
Centre	10.90	10.70	10.40
Front	10.85	10.85	10.65

The EVA samples were tested in a different Suntest CPS+ due to the failure of the first machine after completion of Sylgard sample testing. The same filters were used in both machines, but a new Xenon lamp was used for each 1000 hour test, as each lamp is guaranteed for a maximum of 1500 hours [145]. The second machine was calibrated in the factory so that it emitted light at same intensity as the first Suntest machine, and this calibration was considered more accurate than the photodiode reading, which fluctuated considerably. The central readings in tables 8.1 and 8.2 are therefore different although the machines were calibrated to operate at similar levels of light intensity.

The photodiode was used to assess the variation in levels of irradiance across the bed of the second Suntest CPS+, to ascertain if the variation in light intensity across the testbed was similar to that in the first machine. The results are shown in Table 8.2. The photodiode readings fluctuated greatly when the photodiode was placed at some points on the edge of the test area, so it was not possible to obtain measurements at all points. There is a maximum 2.9% variation in the readings that were obtained. This is of the same order as the 3.7% variation for the first Suntest CPS+, showing that the two machines were likely to cause similar levels of difference in sample degradation across each test area.

Table 8.2: Variation in photodiode current across the Suntest CPS+ used for EVA sample testing. Readings were taken after sample testing.

Position of photodiode in Suntest CPS+	Reading on photodiode (μA)		
	Left	Centre	Right
Back	10.1	10.6	10.3
Centre	-	10.3	10.1
Front	-	10.1	-

This, second Suntest CPS+ had been calibrated by the manufacturers just before use, and had an irradiance level indicator. Once calibrated with the photodiode, the irradiance level was 485 Wm^{-2}. Standard test conditions are normally 1000 Wm^{-2} [146], but this lower irradiance level was considered sufficient, as it resulted in severe degradation of the samples (discussed in section 8.5). Figure 8.3 shows the EVA samples in an aluminium tray, prior to testing in the second Suntest CPS+ machine.

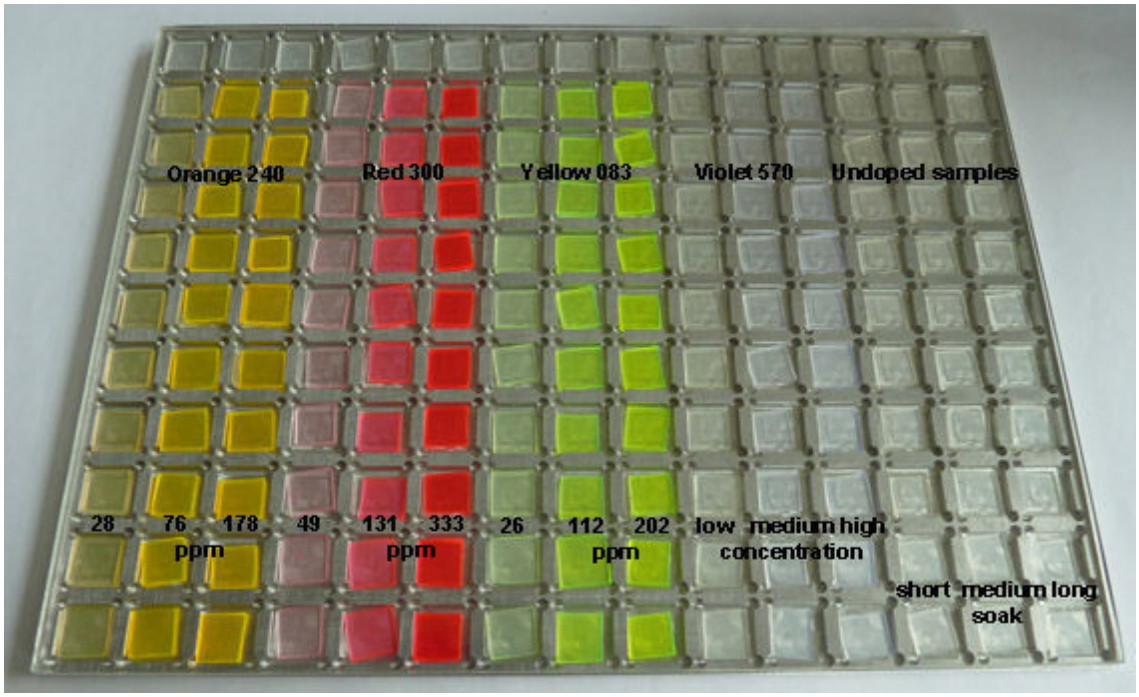

Figure 8.3: EVA samples prior to ageing tests. The top row of the tray contains reference samples. Each three columns, from the left, contain Orange 240, Red 300, Yellow 083, Violet 570 and Clear samples. The sample soak times in each set of three columns are from short on the left to long on the right.

8.4 Outdoor testing

Outdoor tests were carried out using fresh samples from the same batches as for the accelerated ageing tests. The same type of aluminium trays were used as for the accelerated ageing tests. 3.3 mm borofloat glass was also placed over the samples in the trays. The trays were placed on stands angled at 35 degrees to the horizontal, as shown in Figure 8.4. This is the optimal angle at which an inclined surface receives the maximum amount of light over one year, in Edinburgh, according to PVSOL software [147, 148]. Samples were placed in the trays in the same layout as for the accelerated ageing tests. The trays were placed in a South-facing location, in Riccarton, UK (at 55.9° North). The test was started on 13 May 2013, when there were 16’12” of daylight in Riccarton. This rose to a maximum of 17’36” on 21 June 2013 [149]. A row of samples, plus a reference sample, was removed every month. To measure the dye degradation within the samples, absorbance and emission spectra were measured, using the method described in sections 4.2.4 and 5.2.2.

Figure 8.4: Stands supporting samples held in trays, at the start of outdoor testing. An irradiance sensor is seen attached to the edge of the stand on the left of the picture. This stand contains EVA samples. Sylgard samples are in the tray on the right.

8.5 Results and discussion

There was a major loss of dye colour during accelerated and outdoor tests. Figure 8.5 shows that no colour is visible in most of the Sylgard and EVA samples after 1000 hours in the Suntest CPS+. The two reference samples in the top of each photo appear clear, without any of the expected yellow or brown colouration that could have resulted if the encapsulant material had also become degraded [118]. A little Orange 240 dye is just visible in the two groups of 3 samples on the left of each photo. Red 300 dye is still visible in both Syglard and EVA samples. This corresponds to Slooff's findings that Lumogen F Red dye is the most stable in a variety of matrices [112]. Kinderman [75] also indicates that Red 300 is one of the more stable dyes. He also notes that Yellow 083 dye stability is very dependant on the host material. This corresponds to the small amount of yellow colouring visible only in the central three EVA samples, in the lower photo.

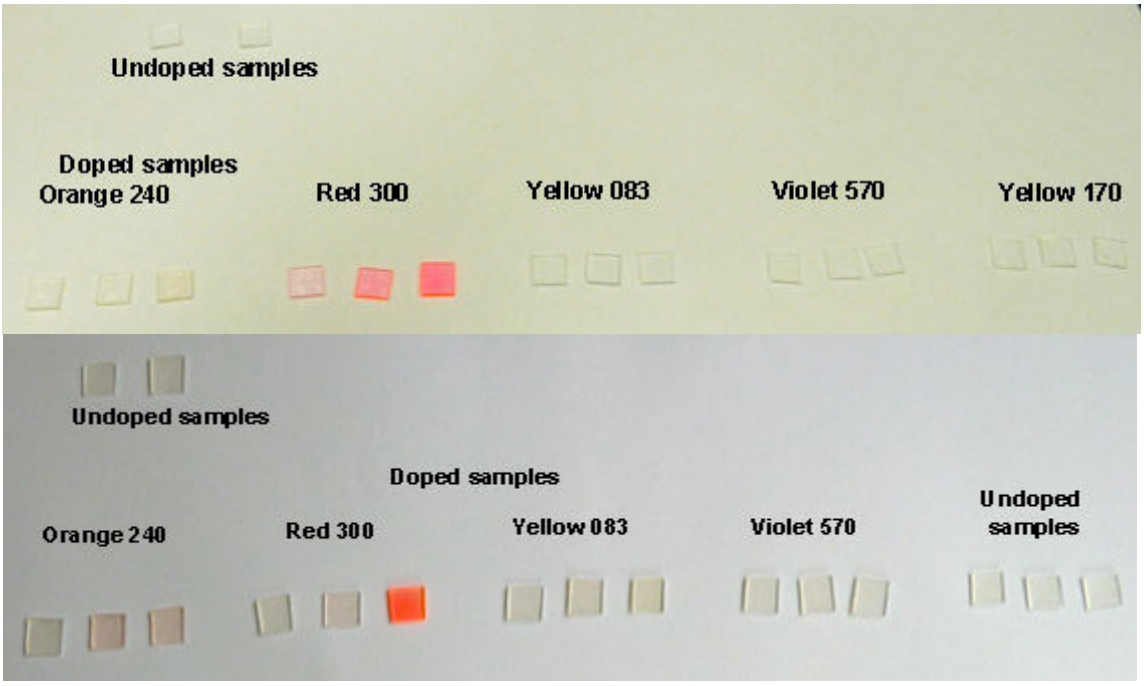

Figure 8.5: Samples of Sylgard (above) and EVA (below) after 1000 hours of accelerated ageing tests. Two un-doped samples are shown at the top of each photo. The three samples on the right of the lower photo are also un-doped EVA samples. The doped samples are in groups of three, and originally contained Lumogen dyes, from left: Orange 240; Red 300; Yellow 083; Violet 570; Yellow 170 (which is only in the Sylgard samples in the top photo).

Violet 570 samples had very little visible colour, as the violet is in the ultraviolet section of the spectrum, so not visible to the human eye. To assess the level of dye degradation, Violet samples were illuminated with a 375 nm UV lamp. Figure 8.6 shows the samples under indoor, fluorescent lighting on the left, and illuminated by the UV lamp on the right. The samples that are shown had been fabricated with the highest concentration of Violet dye. Undoped samples are at the top of each column. The second sample in each column a doped sample that has not been aged. The following samples are placed so that ageing time increases from top to bottom of the column. Fewer samples are visible in the photos taken under UV light, showing that the Violet dye has degraded to the point where it does not fluoresce after 200 hours for accelerated ageing tests. The lower photos show only two Violet Sylgard and one Violet EVA sample visible. This indicates that after 2 months of outdoor testing, the dye ceased to be active within Sylgard. This decreased to 1 month for EVA.

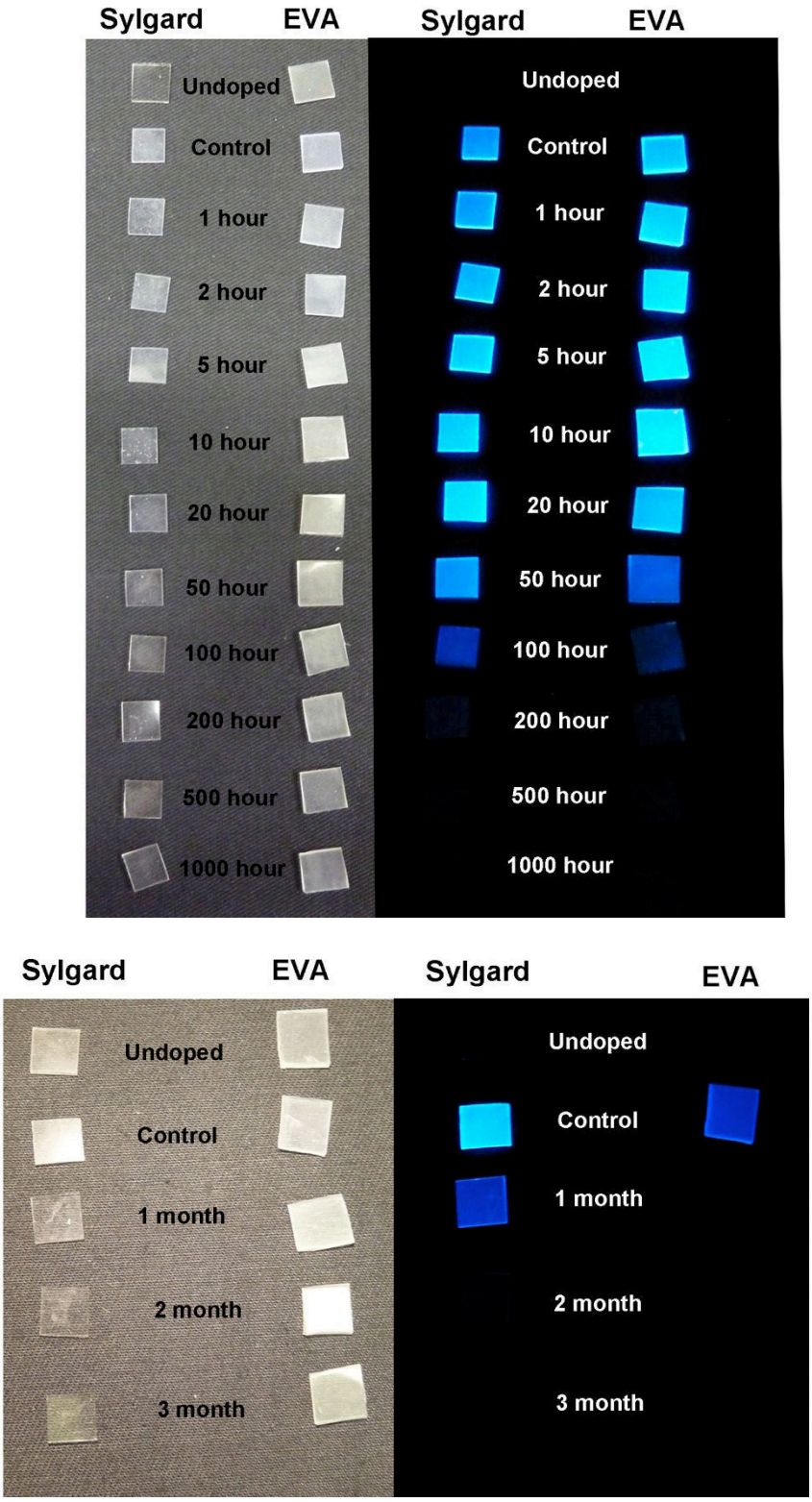

Figure 8.6: Violet 570 samples from accelerated ageing tests (above) and outdoor tests (below). Sylgard samples are on the left and EVA on the right in each photo. An un-doped sample is included at the top of each column. The photos on the right are taken in UV light. The photos on the left show the samples under indoor, fluorescent lighting. The duration of testing is shown beside each sample.

Figure 8.7 shows the outdoor sample trays after 3 months testing. Three rows of samples have been removed. The remaining samples show complete loss of colour for all except the Orange and Red EVA samples on the left. Some Red colour remains in the Sylgard samples, on the right of the figure. The samples made with Yellow 083 dye, and the Sylgard samples made with Yellow 170 dye, show no colour. The reference samples in the top row remained clear, as in the accelerated ageing tests.

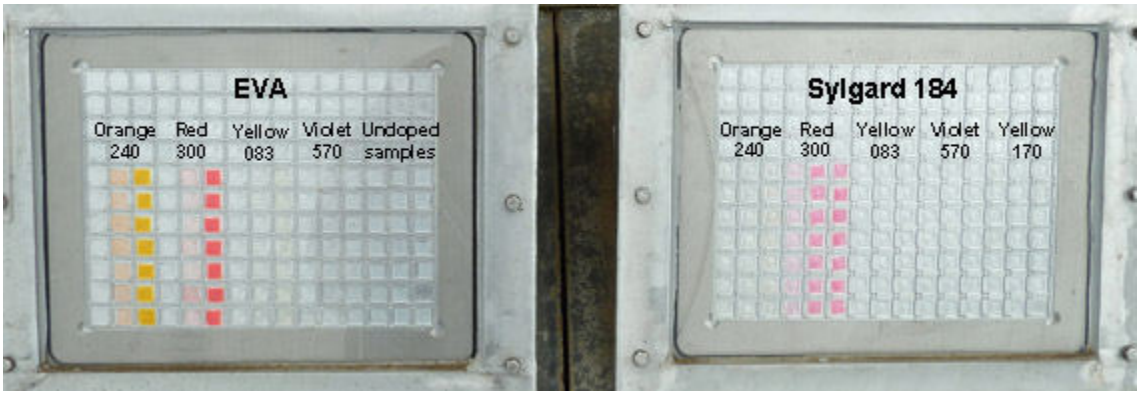

Figure 8.7: The outdoor test setup after 3 months, with the first 3 rows of doped samples removed from the trays. EVA samples are on the left, and Sylgard on the right. The severe loss of dye colour is apparent in the remaining samples, but some colour remains in the high concentration Orange 240 and Red 300 EVA samples on the left. Some Red colour is maintained in the Sylgard samples on the right.

8.5.1 Absorbance and emission spectra from aged samples

Absorbance and emission spectra of selected samples were measured to assess the way in which Lumogen dye degraded within Sylgard and EVA. Red 300 medium and high concentration samples were assessed, as these samples had retained the most colour during degradation testing with both Sylgard and EVA hosts. Emission spectra of Sylgard samples were measured using a paper sample holder. This did not have a significant effect on spectra from Red dye, as discussed in section 6.4.1.1.

Figure 8.8 shows absorbance and emission spectra for 149 ppm Red 300 dye in Sylgard. The top two graphs in the figure show the absorbance and emission from each sample after accelerated ageing testing in the Suntest CPS+. A repeat measurement of the control sample was also made at the end of each series of testing. The graph on the top left shows a close correlation between the two absorbance measurements of the control sample, indicated by the solid, black line and the red, dashed line. There is then a slight increase in absorbance for samples placed in the Suntest CPS+ for up to 10 hours or less. Initial degradation of the samples appears to increase the ability of the dyes to absorb light. This could be due to reduction in the amount of agglomerated dye, leading to dye molecules being able to absorb light more efficiently. The initial increase

in in absorbance is followed by a steady decrease in absorbance. The dotted, turquoise line shows that after 1000 hours, the dyes absorb less than half the light that is absorbed by the control samples.

The graph of dye emission, in the top right of Figure 8.8 shows a similar trend. The repeat control emission is lower than the initial measurement of emission from the control sample, as shown by the relative positions of the dashed, red line and black, solid line. This change in intensity can occur due to the difficulty in maintaining exactly the same position of the sample holder within the fluorospectrometer throughout all the measurements, or to fluctuations in emission from the Xenon lamp.

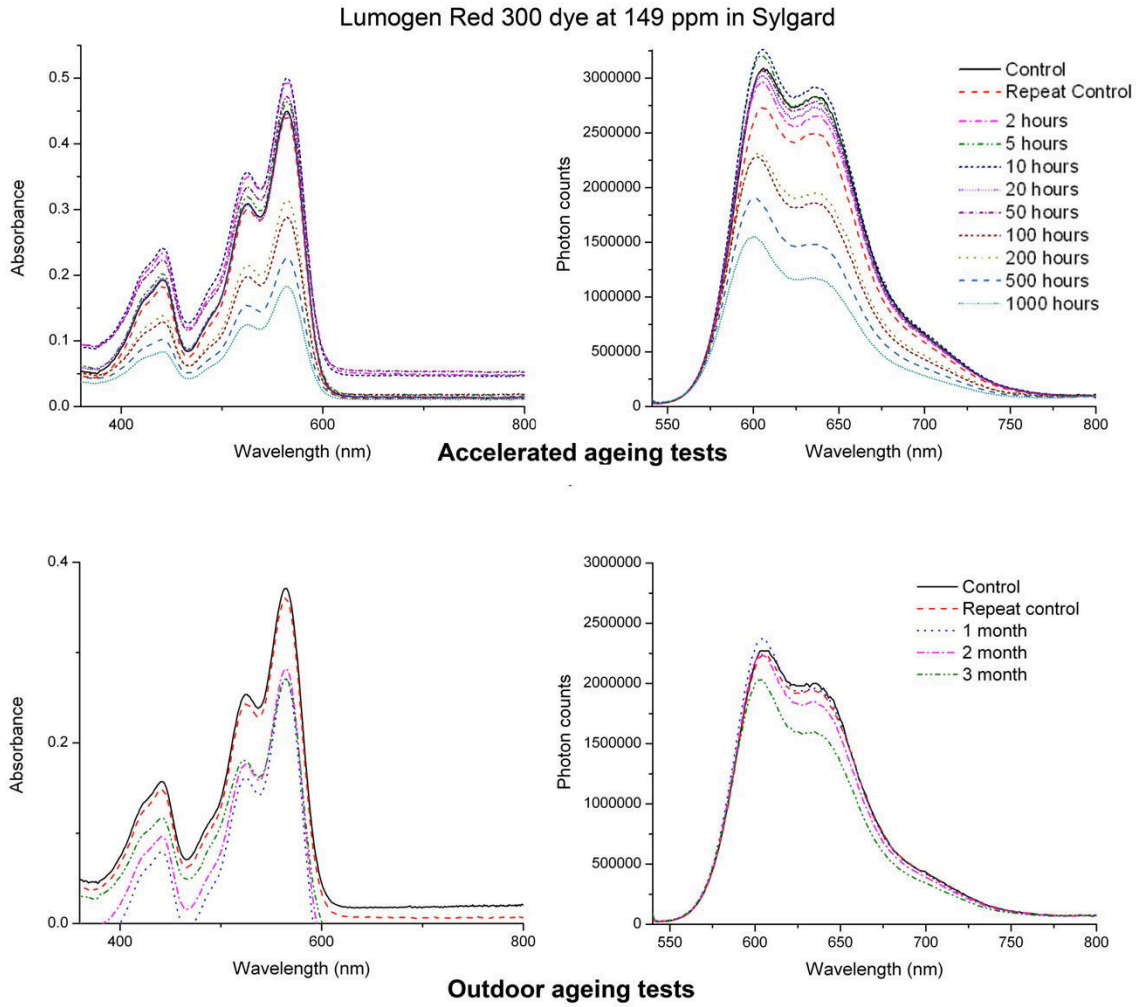

Figure 8.8: Absorbance (on the left) and emission (on the right) for Lumogen Red 300 dye at 149 ppm in Sylgard. Results from 1000 hours of accelerated testing are shown at the top of the figure. The lower section of the figure shows the results from 3 months of outdoor testing.

The general decrease in emission due to increased exposure to light from the Xenon lamp, however, is greater than the difference between the two measurements of

the control sample. 1000 hours of accelerated ageing testing is shown to decrease peak emission to approximately half of the value from the control sample.The graphs in the lower section of Figure 8.8 show the results for the samples that were tested outdoors. Generally, both absorbance and emission decrease over the 3 months of outdoor testing, although the initial decrease in absorbance outdoors is followed by little change in the peak emission in subsequent months. The slight increase in emission after 1 month of testing shows a similar trend to that in the graph of emission from samples subjected to accelerated ageing testing. Absorbance and emission of undoped Sylgard and EVA samples were also measured and found to be similar for all samples, regardless of the length of time for which they had been exposed to light, within the margins of experimental error.

Figure 8.9 shows the changes in absorbance and emission for 131 ppm samples of Red 300 dye in EVA. The larger graphs at the top and bottom of the figure show faster decreases in absorbance and emission than for Red dye in Sylgard (in Figure 8.8). There is no initial increase in sample absorbance or emission, as seen for the same dye in Sylgard. The rapid decrease in dye performance indicates that Red 300 dye is less stable within EVA than in Sylgard 184. The smaller graphs within the figure show results from the un-doped samples. There is some spread in absorbance values for un-doped samples subjected to both accelerated and outdoor testing which could be due to variations in sample thickness, as for the Sylgard samples in Figure 8.8. The emission from the un-doped, control sample used for accelerated ageing tests is greater than the emission from the aged samples. The difference is similar to that between the two, doped, reference samples in the top right of Figure 8.8, so is within the margin of error of this method.

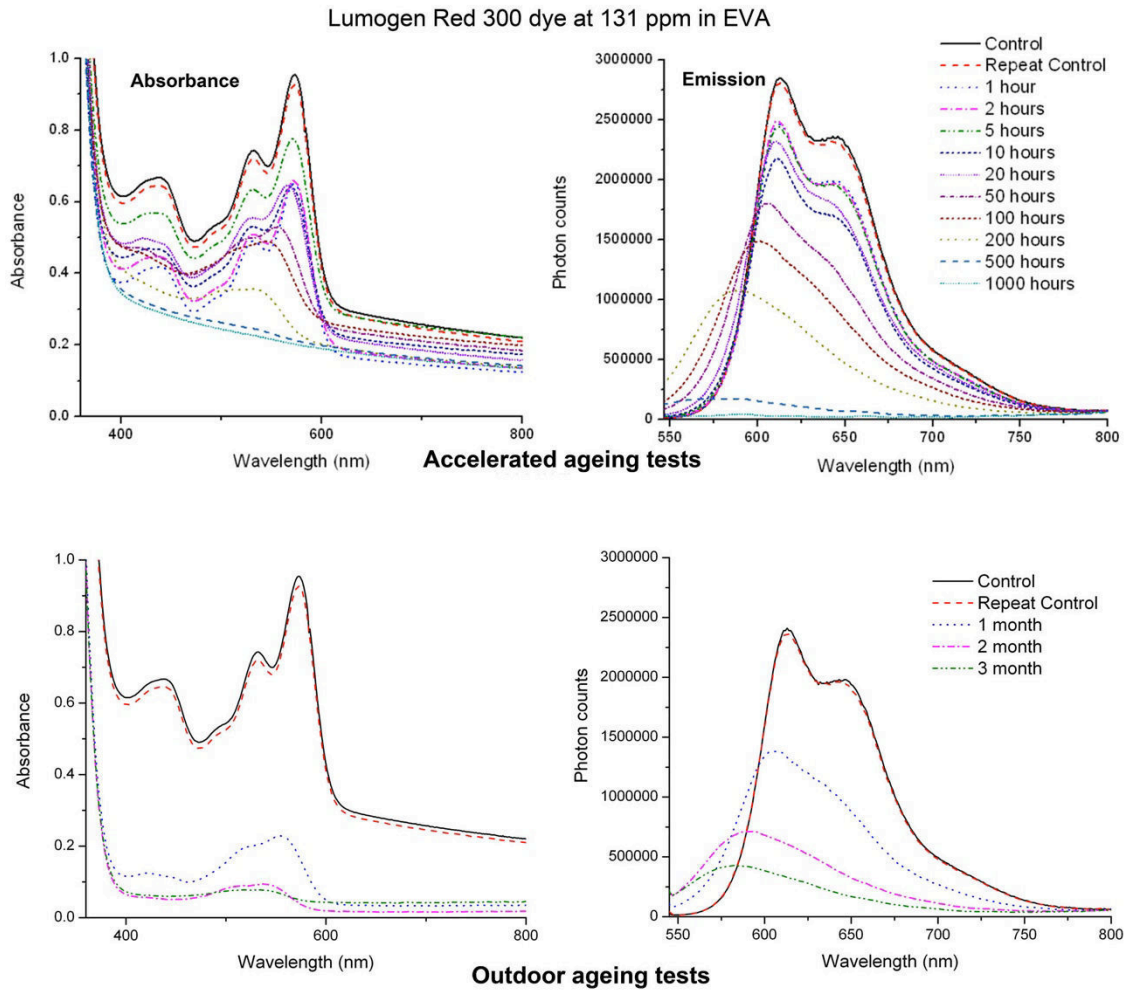

Figure 8.9: Absorbance (on the left) and emission (on the right) for Lumogen Red 300 dye at 131 ppm in EVA. Results from 1000 hours of accelerated testing are shown at the top of the figure. The lower section of the figure shows the results from 3 months of outdoor testing

Figure 8.10 and Figure 8.11 show ageing test results for higher-concentration Red 300 dye in Sylgard and EVA respectively. All the graphs show a decrease in emission intensity as a result of increasing exposure to light. At the end of both accelerated and outdoor testing, there are still significant amounts of emission from Sylgard and EVA samples. This corresponds to the significant amounts of colour retained in both sets of samples, as shown in Figure 8.5 and Figure 8.7. Starting each test with a higher concentration of dye has led to a larger amount of dye remaining active at the end of the experiment. Both graphs of emission, on the right side of Figure 8.10, show a reverse in the relative heights of the two emission peaks that occurs as ageing of Sylgard samples progresses. This indicates that increasing exposure to light leads to less dye molecules being active, so that re-absorbance of light decreases. Increasing amounts of light are emitted at shorter wavelengths, rather than being re-absorbed and emitted at longer wavelengths. The emission spectra shapes become closer

to the spectrum for low concentration of Red dye in Sylgard that are shown in Figure 6.2. In Figure 8.11, a similar effect occurs with changes in EVA emission. As sample ageing increases, emission graphs with two peaks transform to graphs with a single peak, at a lower wavelength, as for the low-concentration EVA spectrum in Figure 6.2.

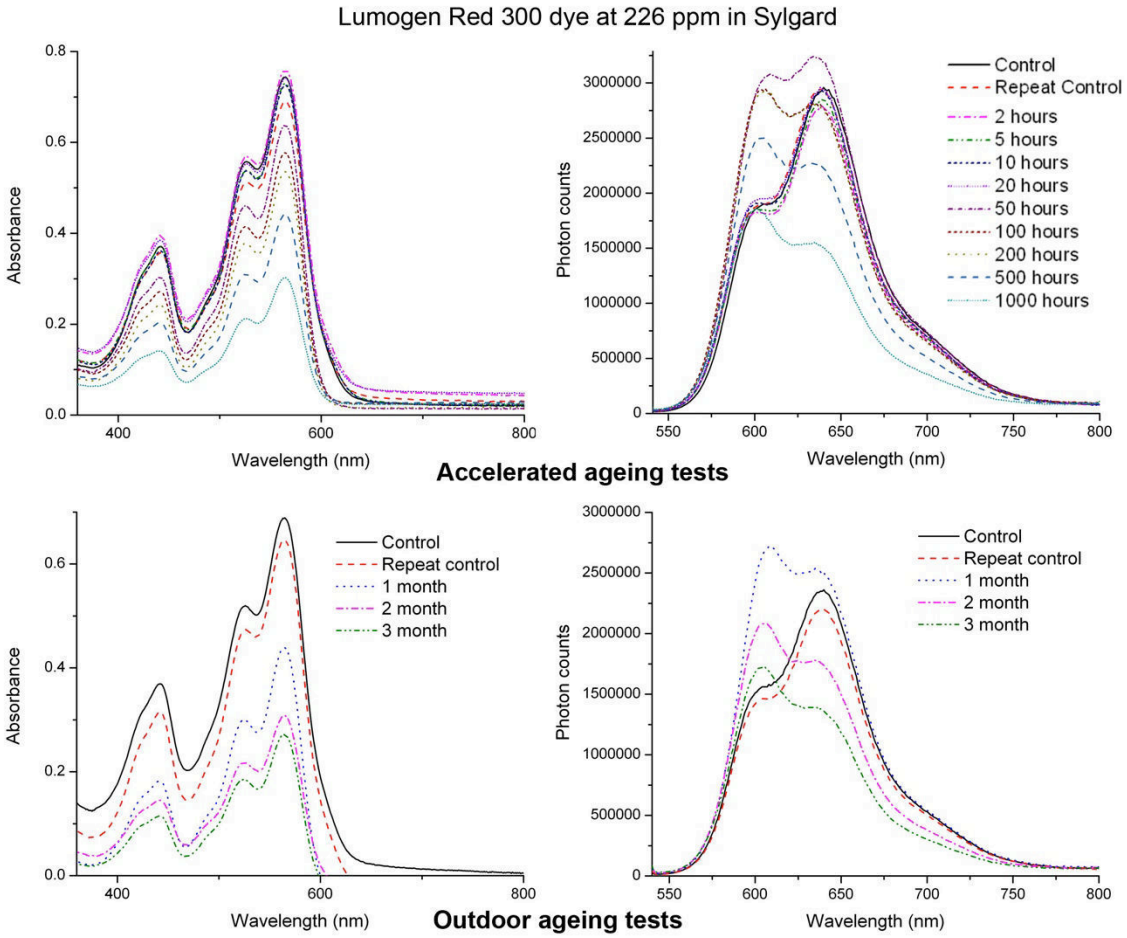

Figure 8.10: Absorbance (on the left) and emission (on the right) for Lumogen Red 300 dye at 226 ppm in Sylgard. Results from 1000 hours of accelerated testing are shown at the top of the figure. The lower section of the figure shows the results from 3 months of outdoor testing

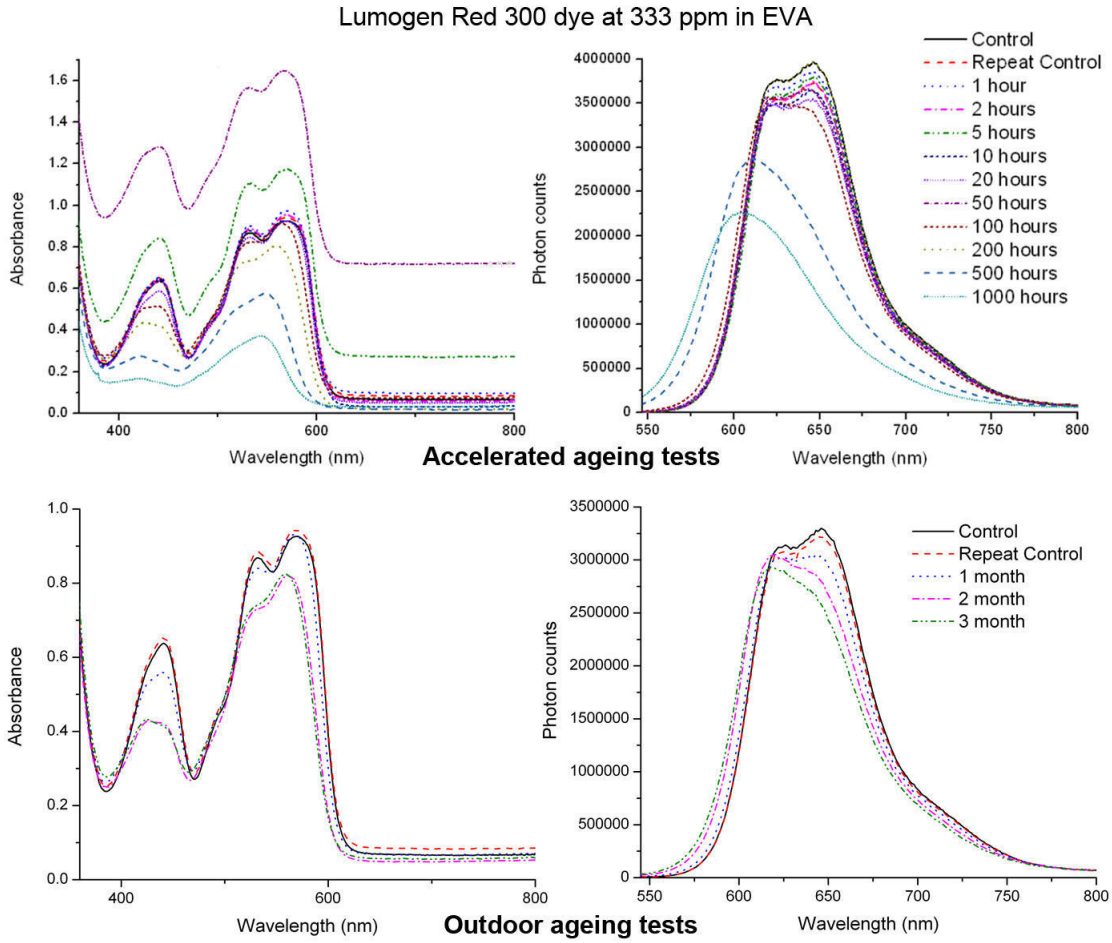

Figure 8.11: Absorbance (on the left) and emission (on the right) for Lumogen Red 300 dye at 333 ppm in EVA. Results from 1000 hours of accelerated testing are shown at the top of the figure. The lower section of the figure shows the results from 3 months of outdoor testing

The absorbance graph on the top left of Figure 8.11 shows high levels of absorbance for EVA samples aged by 5 and 50 hours. This raised absorbance occurs over the entire measured spectrum for both samples. This could indicate material within the sample, such as dirt or degradation products, obscuring the light. Alternatively, this could be due to error in the method of sample holder placement within the spectrometer leading to a decrease in the size of the lit area of the sample. The general trend, over all the sample measurements, however, is decreasing sample absorbance.

The colour degradation due to outdoor testing was sufficiently complete that a comparison with accelerated ageing tests was not necessary for all except the Lumogen Red 300 samples at higher dye concentrations. This dye did maintain significant amounts of colour after outdoor testing for 3 months. The curves in the bottom right graph of Figure 8.11 show a reduction in peak fluorescence emission of 10.7% after 3 months, for the 333 ppm Red dye in EVA.

8.5.2 Assessment of peak absorbance and emission

The peak values of absorbance and emission from Figure 8.8 to Figure 8.11 are plotted in figures 8.12 to 8.15 below, with test duration shown on a natural logarithmic scale on the x-axis. The test duration for the outdoor test was calculated from the number of daylight hours during the test [150]. Figure 8.12 shows that Red Sylgard absorbance gradually decreased during the ageing process with greater decreases after 50 hours of accelerated testing. Greater decreases in absorbance also occurred for samples with higher, initial dye concentrations, with the lower-concentration, 149 ppm samples showing little change in absorbance during outdoor testing. The EVA samples had higher, initial absorbances, with a sharper decrease in absorbance after 50 hours of accelerated testing. There are increases in peak absorbance at 5 hours of accelerated testing for both sample concentrations, and a large increase for the higher-concentration samples at 50 hours. These increases are likely to be due to a reduction in dye agglomeration caused by decay of some dye molecules, so that the remaining dye molecules are better able to absorb light effectively.

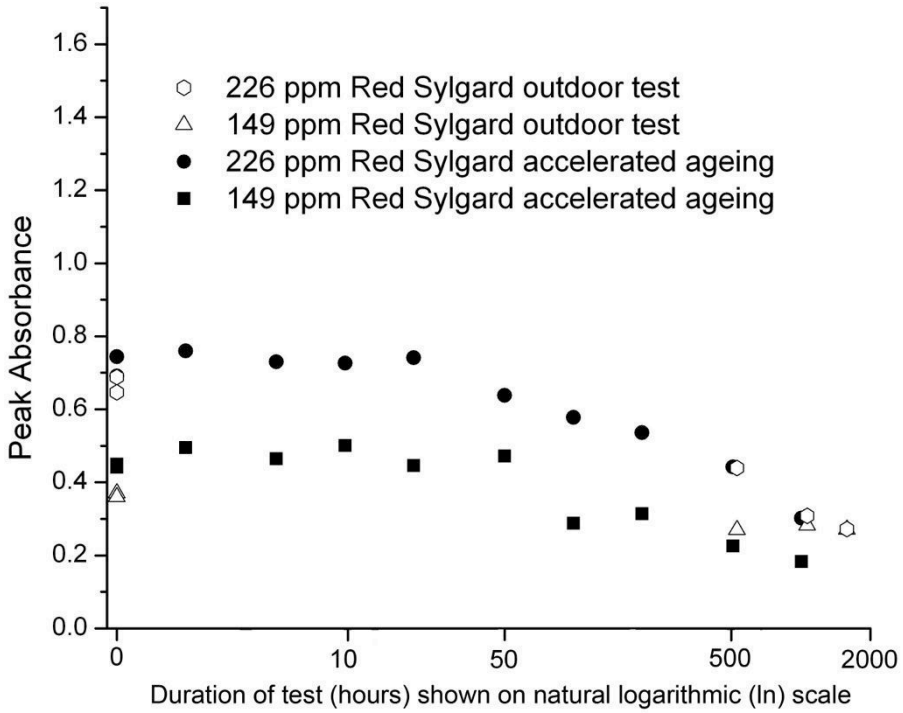

Figure 8.12: Peak absorbance values for Red Sylgard samples after accelerated and outdoor degradation testing. The test durations are shown in hours on a natural logarithmic scale

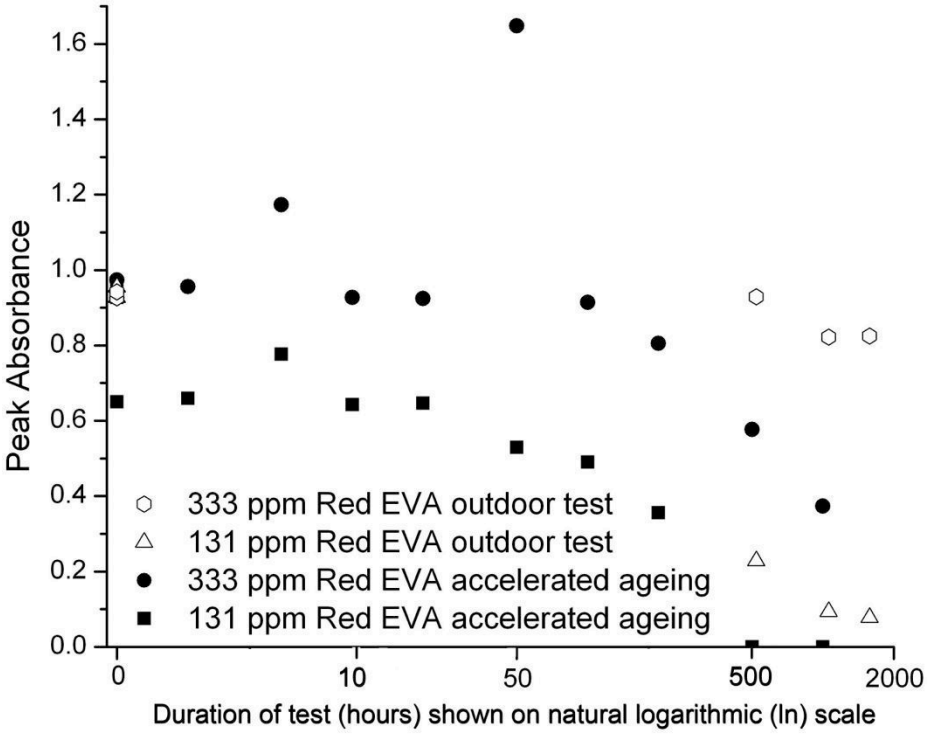

Figure 8.13: Peak absorbance values for Red EVA samples after accelerated and outdoor degradation testing. The test durations are shown in hours on a natural logarithmic scale

Figure 8.14 and Figure 8.15, below, show the peak emission values for Lumogen Red 300 dye in Sylgard and EVA. The initial peak emission values for Sylgard are lower than for EVA, indicating better solubility of the dye within the EVA. There is an initial, slight increase in emission for Sylgard samples at the start of accelerated ageing testing, then a gradual fall in emission after 50 hours of accelerated ageing. The samples with an initial dye concentration of 131 ppm have higher emission values than the 333 ppm samples at 2 to 20 hours of testing, indicating that the initial loss of dye agglomerates is faster for these, lower-concentration samples than for the higher-concentration samples, improving the fluorescence properties at the early stages of the test. This effect is observed later in the test for the samples with an initial dye concentration of 333 ppm, with a peak in emission at 50 hours of accelerated testing. The outdoor test samples were measured at a different time to the indoor samples, and the initial value of emission is lower than that for the accelerated ageing samples. This could be due to variations in intensity of the Xenon bulb within the fluorospectrometer, or to different sample-holder angles during the two, separate tests. The peak values from the outdoor tests show a similar initial rise then a steady fall in emission. The decrease in emission is much greater for the samples with a higher, initial dye concentration, with the final peak, emission values for these samples being lower than for samples with an initial lower, concentration.

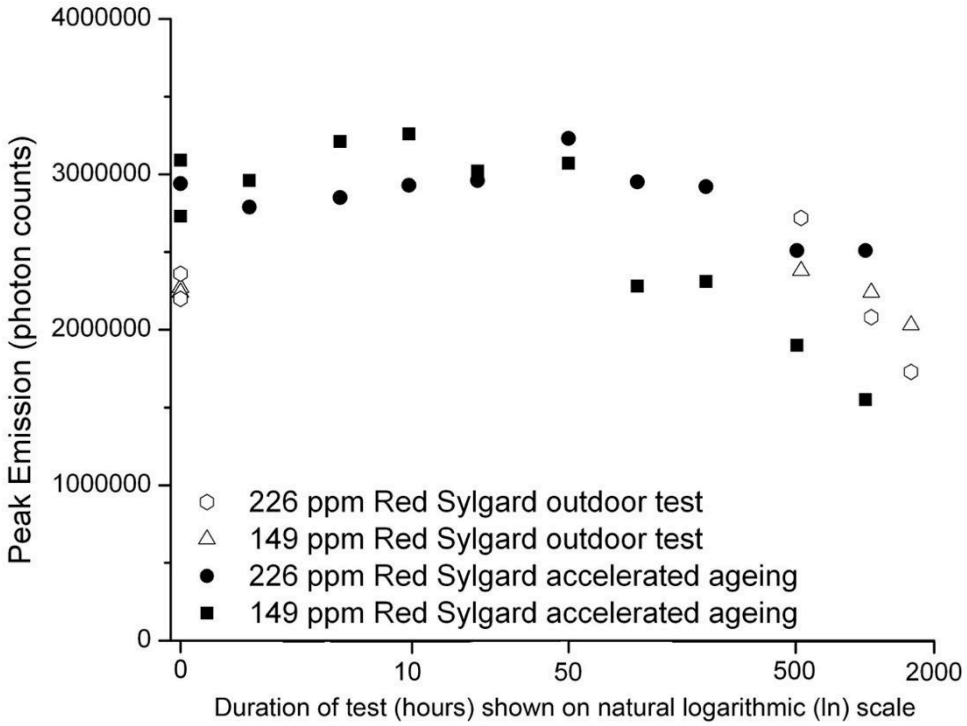

Figure 8.14: Peak emission values for Red Sylgard samples from accelerated and outdoor degradation tests. The test durations are shown in hours on a natural logarithmic scale

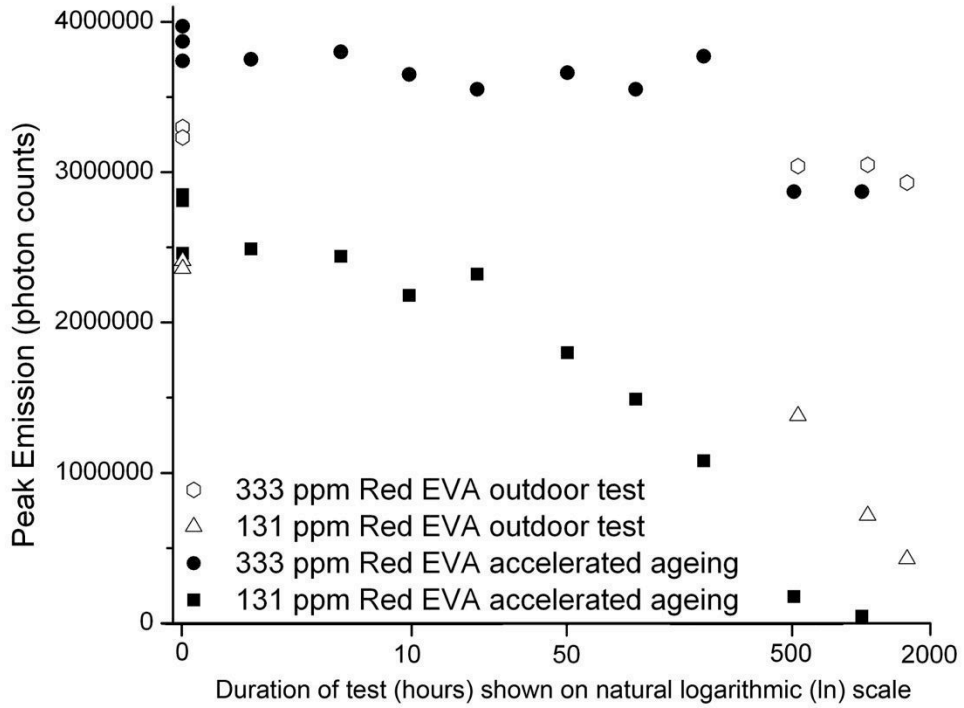

Figure 8.15: Peak emission values for Red EVA samples from accelerated and outdoor degradation tests. The test durations are shown in hours on a natural logarithmic scale

This could indicate that the presence of dye agglomerates that are likely to be contained within high concentration samples renders the dye more susceptible to ageing, even after the initial breakdown of some of these agglomerates at the start of testing.

EVA high concentration samples had greater, peak emission at the start of testing, with little change in peak emission until 500 hours of accelerated testing. There was also little change in peak emission from the higher-concentration samples during outdoor testing. This is corresponds with the significant amounts of colour retained during the outdoor testing of these EVA samples. The EVA samples with lower, initial dye concentrations show a considerable decrease in peak emission intensity after 20 hours of accelerated ageing, and throughout the outdoor ageing test. This is similar to the change in peak absorbance values shown in Figure 8.9. This, general pattern of decreasing absorbance and emission is also shown in the Sylgard graphs (Figures 8.8 and 8.10) but the decrease is less marked than for EVA.

Lumogen dyes are known to exhibit better durability when incorporated within a PMMA host [151, 74]. Data presented by BASF, who are the manufacturers of Lumogen F dyes, show that when testing 200 ppm concentrations of the four, commercially-available Lumogen dyes used in this research, Lumogen F Red 300 dye was the most durable within a PMMA host, exhibiting more than '90 % fluorescence' after 80 days accelerated ageing (in a Xenotest machine) [111]. Lumogen F Violet 570 was the least durable, exhibiting more than '80 % fluorescence' after 60 days of accelerated ageing [111]. 80 days corresponds to 1920 hours, and 60 days to 1440 hours, so these were longer than the 1000-hour, accelerated ageing tests carried out for this thesis. The maximum fluorescence values of 90% exceed the change in emission for the highest-concentration Lumogen F Red samples for which results are shown in Figure 8.10 and Figure 8.11. After 1000 hours of accelerated testing the emission is 85% of the initial value for the high-concentration Sylgard samples and 72% of the initial value for the high-concentration EVA samples.

The accelerated ageing tests of all the dye-encapsulant combinations were useful in showing that acute degradation conditions did not result in changes in transparency or colour of the host materials. This indicated that processing of the samples, through use of solvents and addition of dyes, did not appear to damage the durability of the host materials. The severe degradation of all the dyes, after 3 months of exposure outdoors, indicates that all these combinations of dye and host material are unsuitable for use in PV installations designed to last for at least 25 years. Alternative material combinations will need to be explored if coloured fluorescent materials are to be used routinely in PV

installations containing standard c-Si PV. Franklin [152] agrees that the fundamental problems of outdoor degradation must be solved if fluorescent dyes are to be of any practical use outdoors.

8.6 Chapter conclusion

Five Lumogen dyes were tested within Sylgard and EVA host materials. All the dyes exhibited severe degradation when exposed to accelerated and outdoor ageing tests. In contrast, the host materials appeared undamaged by exposure to light. This was verified by absorbance and transmission measurements that remained similar for host materials in which dye had degraded completely and for un-doped samples. Higher initial concentrations of Lumogen Red 300 dye led to the greatest amount of visible colour at the end of each test, especially within EVA. The higher levels of visible colour correlated to greater measured levels of absorbance and emission. Lumogen Red 300 dye within EVA was therefore chosen for use in the test pieces described in chapter Chapter 9.

CHAPTER 9: PV MODULES INCORPORATING REFLECTIVE AND OPAQUE BACKING MATERIALS, ETHYLENE VINYL ACETATE, AND LUMOGEN RED 300 DYE

9.1 Chapter synopsis

c-Si PV cells were both disguised and displayed within pieces of decorative glazing. A variety of designs were created through use of a mixture of black and reflective backing materials, broken c-Si PV cell pieces and EVA containing Lumogen Red 300 dye. Increases in maximum power from the PV were shown to occur due to use of reflective and fluorescent materials.

9.2 Introduction

The best of the methods and materials that have been established in this thesis were combined and developed to create a set of decorative PV glazing test pieces that were designed and fabricated by the author. Details of the design development are given in appendix 1. Chapter 3 described development of a method for incorporating PV cells within translucent glazing designs using glass paint. The aim was to develop this method further by demonstrating the variety that could be achieved through use of different materials within PV glazing, whilst ensuring that the PV cells still functioned well. The level of visibility of the PV depended on the materials used behind and in front of the PV, with the level of prominence of the square PV cells differing when viewing each panel from the front or the back in reflected or transmitted light. The materials were chosen for their ability to blend with the PV cells and to enhance the amount of light incident on the PV.

9.3 Materials and method

A series of decorative panels were made up to fulfil the aims of:

- Disguising or highlighting PV cells within decorative glazing designs
- Using the chosen materials to enhance power output from c-Si PV
- Using coloured and reflective materials to increase design variety and to optimise the amount of light reaching the PV

Glass measuring 450 x 280 mm was used for each panel. This gave ample space for six, functional c-Si PV cell pieces to be incorporated into each design. Where possible, the c-Si PV cells were contained within an area measuring 250 x 250 mm, so that the complete string of PV cells could fit within the illuminated area under the ABET solar

simulator. This made it possible to carry out measurements of IV curves at the same level of illumination for each PV cell. The larger, surrounding area of glass ensured that there was space to create a unique design in each panel. The designs differed from those developed in chapters 3 and 7 because glass paint was not used, so that the panels could be made up quickly without use of a paint kiln. This also meant that EVA could be used as the encapsulant material. This was quick to process, and Lumogen Red 300 dye within EVA could be incorporated into the panels. It was demonstrated in Chapter 8 that this is the most durable of the dye and PV encapsulant combinations that were investigated in Chapter 4 to Chapter 6. Use of this material demonstrated the best of the methods of colour addition to encapsulant materials that were developed in this thesis. Addition of Lumogen F Red 300 dye to the area surrounding each PV cell could also lead to PV efficiency increases due to total internal reflection of light, as discussed in section 1.2.6, and as demonstrated by Corrado [86]. An EETS PV laminator was used to manufacture the panels, as described in section 4.4. EVA sheet (Vistasolar 486.00) [120] was doped with Lumogen Red 300 dye at the highest concentration to give the most intense colour. The method of making these doped EVA sheets was as described in section 4.4: soaking EVA sheets in a 200 ppm of Lumogen Red dye for 68 hours.

Materials were selected as follows, in order to develop a set of PV module designs:

- c-Si PV cell pieces, measuring 52 x 52 mm were cut from monocrystalline silicon PV (Sunways AH50-H) which had a uniform, black appearance. Each piece was cut to give a central busbar for the connection of tabbing strip. Broken PV cells were used for decoration in several of the designs.
- 3.3 mm borofloat glass (Newcastle Optical) for use in front of the PV cells, to optimise the light spectrum reaching the surface of the c-Si PV
- 3 mm soda lime float glass for use behind the PV cells. This provided a rigid, transparent backing
- Tabbing strips (E Jordan Brookes) to connect the c-Si PV cells.

The materials that were chosen to disguise the functional c-Si PV cell strings were broken pieces of the same type of c-Si PV and black card (Canson). These were both straightforward to obtain and could be laminated in between sheets of glass. An alternative was required to the reflective, glass paint that was used in Chapter 3. The chosen alternative was ‘Solar film 65’ (MDP, Grangemouth): a translucent, reflective, film with a silver tint, that is designed to reflect ‘65%’ of incoming light [103]. A piece of film is shown in Figure 9.1.

Figure 9.1: 'Solar film 65' (MDP) held in a window aperture to demonstrate the limited light transmission with some reflectivity which is shown in the creases in the film

The design of the demonstration PV modules is described in appendix 1. A different material was used to hide or display the PV cell strings within each panel. The materials used were: broken c-Si PV cells; EVA doped with Lumogen Red 300 dye; 'solar film 65'; and black card (Canson). The reflective backing materials and coloured encapsulants were likely to alter the electrical power outputs from the PV strings. The extent of the changes in electrical output due to use of these, two materials was investigated by measuring the current-voltage curves from the PV in each design. Reference panels were made up with 6 c-Si PV cells in a rectangular grid arrangement in the centre of the panel. One panel contained undoped EVA, and another incorporated three layers of EVA doped with Lumogen Red 300 dye. Current-voltage curves were measured for these panels to find the effect of the addition of Lumogen Red 300 dye to the EVA. The effect of use of reflective 'solar film 65' was also tested by applying it to the backs of these panels.

9.3.1 Initial tests using single PV cell

Measurements were carried out to find the effect on c-Si PV power outputs due to use of Lumogen Red 300 dye and 'solar film 65' within laminated PV test pieces. Single c-

Si PV cell pieces were sandwiched between sheets of EVA, then laminated between pieces of borofloat and soda lime glass, using the EETS laminator and the process discussed in section 4.4. EVA sheets were doped with dye by soaking for 68 hours in a solution of Lumogen Red 300 dye. This was then used to make one of these small PV modules. Two sheets of EVA were placed in front of the PV, and one behind, to give strong red colouring in front of the PV. The 3 layers of EVA were also equivalent to the 3 layers of EVA used to make the samples described in section 4.4. Un-doped EVA was used to make the second panel, with two sheets of EVA in front of the PV and one behind. The power outputs from the c-Si PV cells were measured before and after lamination, using the IV testing procedure detailed in section 5.2.1 of Chapter 5, with a thermocouple placed under each test piece so that measurements could be carried out at a temperature of 25 °C. PV power output is temperature dependant [107], so maintenance of a constant temperature ensured that variations in power output were not due to fluctuations in temperature. The efficacy of the 'solar film 65' as a reflective backing was testing by applying this temporarily to the backs of both of the small PV modules. The IV curves measured with this backing in place were compared with those measured when a mirror was placed behind each laminated PV cell. Measurements were carried out with the PV cells placed on a black, cloth backing to minimise reflection.

9.4 Results and discussion

Figure 9.2 is a comparison of the measured IV curves for single c-Si PV pieces, before and after encapsulation with EVA. The similar values of the open-circuit voltage in Figure 9.2 and Figure 9.3 indicate that the temperature remained constant between measurements [107]. The increase in current due to encapsulation with EVA containing Red 300 dye is shown by the difference between the red dashed and solid curves in Figure 9.2 and Figure 9.3 indicate that the temperature was constant between measurements, as indicated by the thermocouple. The increase in short circuit current (I_{sc}) is 18.6%. There is a lesser increase of 10.4% for the c-Si PV encapsulated by undoped EVA. This is shown by the difference in height between the black, dotted line and the black, dashed and dotted line in Figure 9.2. For these, single c-Si PV pieces, use of EVA doped with Lumogen Red 300 dye caused an 8.2% absolute increase in short-circuit current (I_{sc}) compared with encapsulation in undoped EVA.

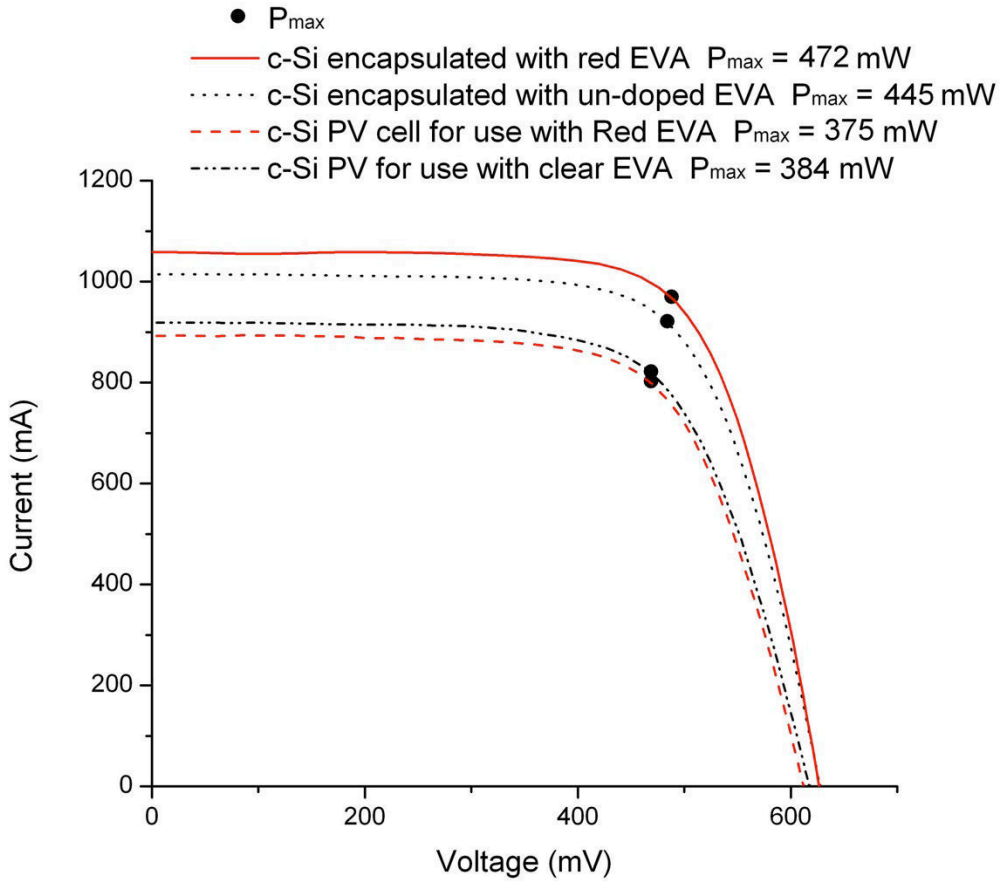

Figure 9.2: Comparison of IV measurements before and after encapsulation of c-Si PV with un-doped EVA and with EVA doped with Lumogen Red 300 dye

It was shown in section 3.4.2 that mirror backings could be used to increase the maximum power produced by c-Si PV. The effectiveness of mirror backings, and of the chosen 'solar film 65', were measured with c-Si PV encapsulated in dye-doped and undoped EVA (Figure 9.3). The black lines in Figure 9.3 show a steady increase in current output from the lowest dashed and double-dotted line, representing c-Si PV with a black backing. The dotted, black line shows an increase in the short-circuit current (I_{sc}) when 'solar film 65' is applied to the back of the encapsulated PV. The increase in I_{sc} is 5.1% compared with encapsulation with a black backing. The effect of placing a mirror behind the PV is shown by the black line with dots and short dashes. This corresponds to an increase in I_{sc} of 10.1%. The mirror reflects more light back towards the c-Si PV than the 'solar film 65', which is designed to reflect 60% of all wavelengths of incoming visible light [103].

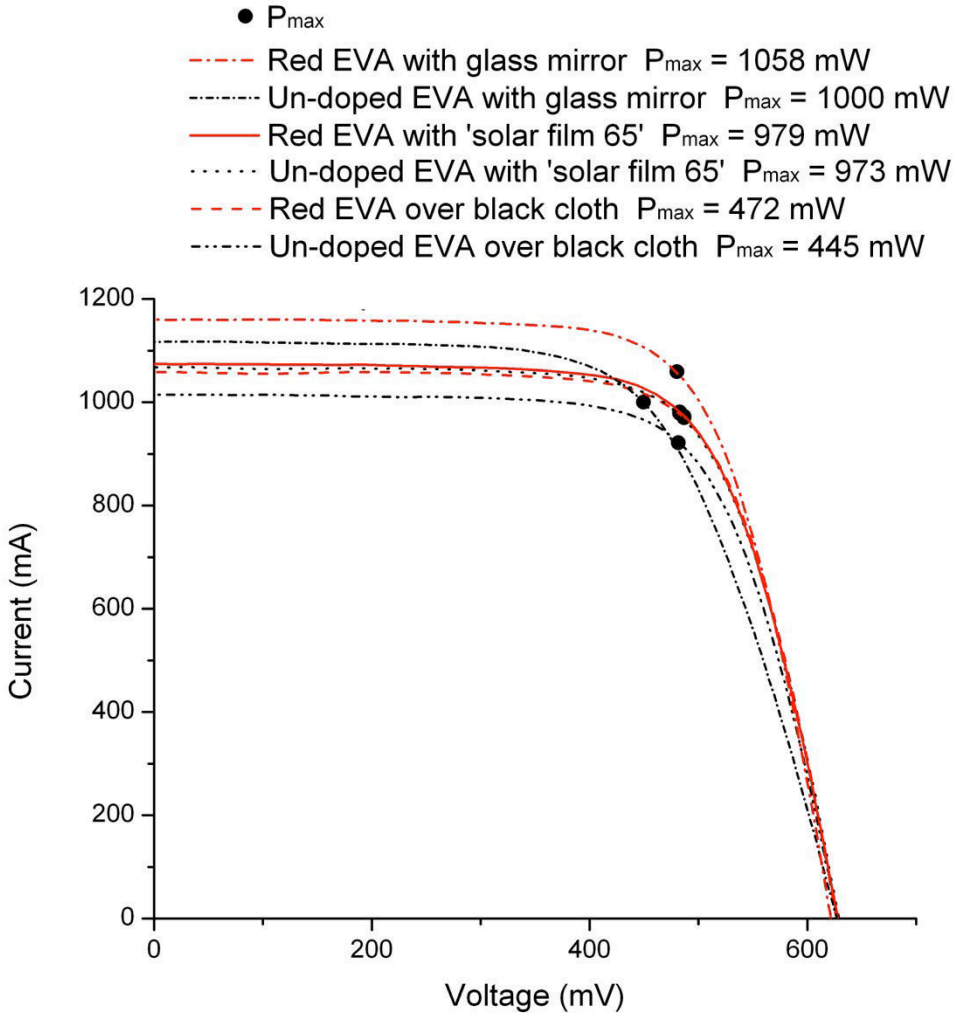

Figure 9.3: Comparison of IV curves for encapsulated c-Si PV with glass mirror backing; 'solar film 65'; and a black, cloth backing. The c-Si PV cells are encapsulated with undoped EVA and with EVA doped with Lumogen Red 300 at 333 ppm

The EVA doped with Red 300 dye is represented by the red lines in Figure 9.3. There is little difference between the lines representing c-Si with doped encapsulant on a black backing, and the result when 'solar film 65' is applied. These measurements are shown by the dashed and solid red lines, respectively. The increase in I_{sc} is only 1.5% due to use of 'solar film 65'. The top, red dotted and dashed line shows a much greater increase when a mirror backing is used. The increase in I_{sc} is 9.5% greater than the I_{sc} measured with a black backing behind the PV. This is is similar to the 10.1% increase due to use of a mirror with undoped EVA compared with that measured with a black backing behind the PV. These results show that, in general, use of reflective backings causes an increase in maximum power output from c-Si PV. EVA doped with Red 300 Lumogen dye, combined with 'solar film 65', does not cause a large power increase when used with c-Si PV. This could be due to the composition of 'solar film 65', which is designed to absorb incoming solar energy, as well as reflecting light [103]. A test was

carried out to find if the 2 sides of 'solar film 65' exhibited differing reflectance. Figure 9.4 shows measurements of reflectance from both sides of piece of 'solar film 65'. The measurements were made by placing each material at a port behind the integrating sphere of the Perkin Elmer spectrometer (as used in section 4.2.4). The graphs show that 'solar film 65' reflects light similarly from both sides. The film causes a sharp cut-off in reflectance below 400 nm, with a maximum transmission of 71% above this wavelength, so any differences in measured I-V from test pieces incorporating 'solar film 65' were not due to differing properties of different sides of the film.

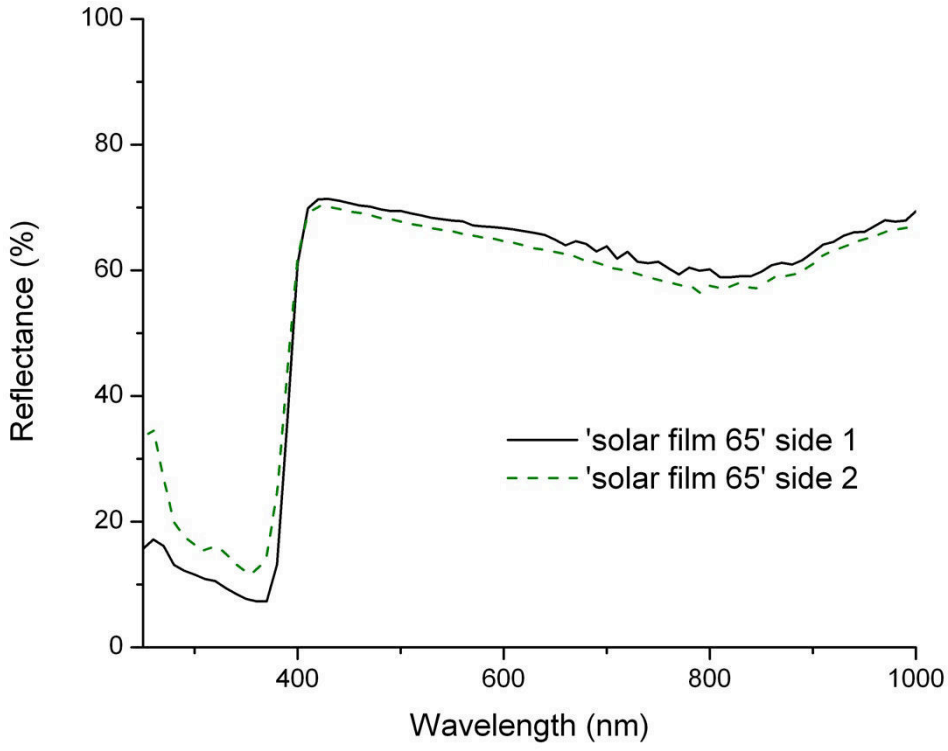

Figure 9.4: Reflectance from both sides of 'solar film 65' (MDP)

The decorative panels described in Table 9.1 to Table 9.4 each contain 6 c-Si PV cell pieces. A comparison was made between reference panels containing 6 c-Si PV pieces, with undoped EVA and with EVA doped with Red 300 dye. The red reference panel is shown on the right in Figure 9.6. The PV string is arranged in 2 straight rows, and the panel contains no additional material such as film or decal. Figure 9.5 shows IV curves for the two reference panels. The black dashed-and-dotted, as well as the dotted lines show a small increase in current for the panel containing undoped EVA when 'solar film 65' is placed underneath the panel. There is a similar, small effect for panels with doped EVA, shown by the red, dashed and solid lines. This increase in I_{sc} when

adding ‘solar film 65’ is about the same in both cases and amounts to 2.4% for both doped and undoped EVA.

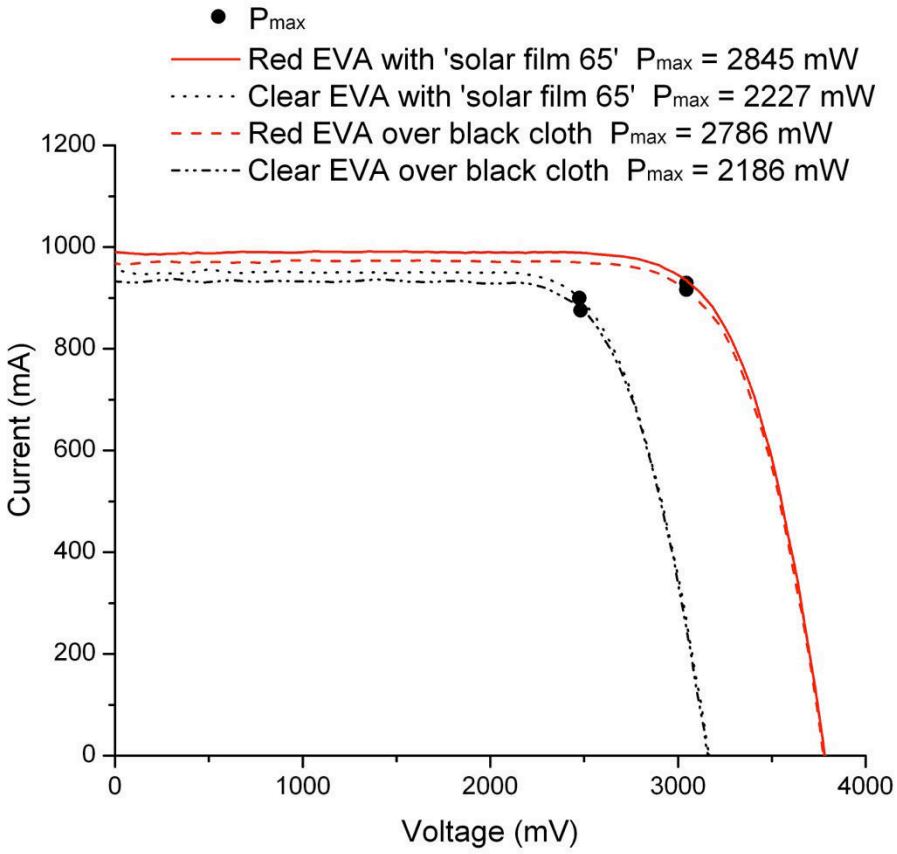

Figure 9.5: Comparison of IV curves for strings of 6 c-Si PV cells encapsulated with undoped EVA and with Red 300 dye in EVA; with black backing or ‘solar film 65’ backing

Figure 9.5 also shows dissimilarity in open circuit voltages between the panel with undoped EVA and that with Red 300 dye within the EVA. This is shown by the difference in points at which the curves meet the x-axis, and remains consistent for all the I-V tests. The difference is not due to temperature differences between measurements, as the temperature was 25 °C for each measurement. There is no corresponding difference in Figure 9.2, where doped and undoped EVA are also compared. The undoped panel containing 6 PV cells is producing approximately 1/6 less open circuit voltage than the red panel. There are 6 PV cells in the panel, so it is likely that the voltage drop is due to one PV cell not functioning within the clear panel, so that only 5/6 of the expected voltage is produced. This difference in open circuit voltage is unlikely to affect the peak current (I_{sc}) values, as these are independent of the number of PV cells within a string.

The performance of these panels can also be compared with that of the test pieces measured in Figure 9.2 and Figure 9.3, by using J_c, the current density, to allow a direct comparison to be made irrespective of the surface area of PV used in each test. J_c for the red EVA over black cloth is 172 W for the 6 cells with results shown in Figure 9.5. J_c is 174 W for the single PV cell encapsulated with red EVA and tested over black cloth, for which the results are shown in Figure 9.2 and Figure 9.3. The similarity of these two values of current density shows that the increase from 1 to 6 cells is leading to similar performance from the PV that is encapsulated with red EVA. When 'solar film 65' is used with red EVA, the values of J_c are 362 W for the single PV cell with results shown in Figure 9.3 and 175 W for the 6 PV cells with results shown in Figure 9.5. Increasing the number of c-Si PV cell pieces to six, appears to limit the effectiveness of the 'solar film 65' in increasing the maximum current on panels with doped EVA. This could be due to the placing of the 6 c-Si PV pieces in close proximity to each other, to fit into the illuminated area underneath the ABET solar simulator. The single c-Si PV pieces, for which results are shown in Figure 9.5, have a much larger surrounding area, as shown in Figure 9.6, in which the test piece with a single c-Si PV piece is shown on the left, under the light from the ABET solar simulator. The panel on the right contains 6 c-Si PV pieces contained within a similar, illuminated area. More light can reach the c-Si PV in the panel on the left, due to total internal reflection from the large area surrounding the individual PV cell. Corrado has demonstrated that the gain in power is proportional to the amount of luminescent material surrounding each PV cell within front-facing LSC's [86].

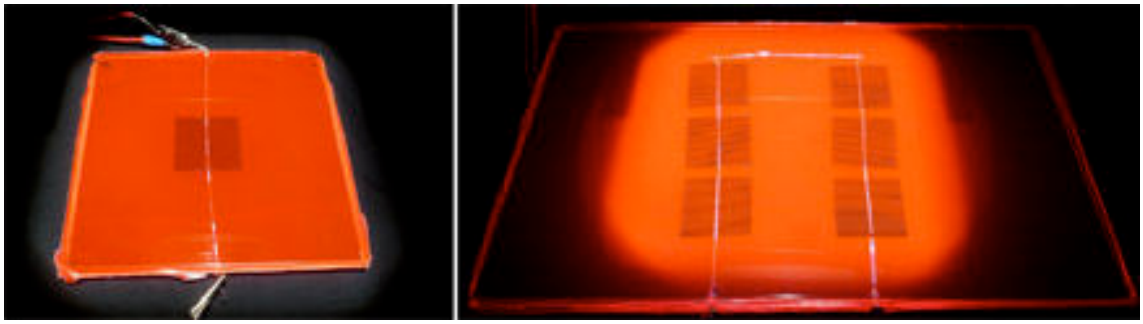

Figure 9.6: Panels under the light from the ABET solar simulator. Left: a single c-Si PV cell; Right: 6 c-Si PV cell pieces. Both are encapsulated with EVA containing Red 300 dye

9.4.1 Decorative c-Si PV panels

Four, decorative panels were constructed using the materials listed in section 9.3. Each was designed to demonstrate the use of a specific material combination. Additional, decorative features were made by selecting from the range of available materials as

required to create each artistic design. Details of three of the designs are shown in Table 9.1 to Table 9.3, below. Design A (in Table 9.1) made use of broken c-Si PV pieces, which were separated from the functional c-Si PV by a layer of EVA. Use of the same material for both functional component and decoration was particularly effective in disguising the square shapes of the functional c-Si PV cells. The beak detail was made from 'solar film 65', which was laminated into the module together with the other components. Heating during lamination caused the film to crease. This was not considered detrimental, as the reflectivity of this piece of film was not important to the functioning of the module.

Table 9.1: Front (main photo) and rear views of design A, incorporating broken c-Si PV additions

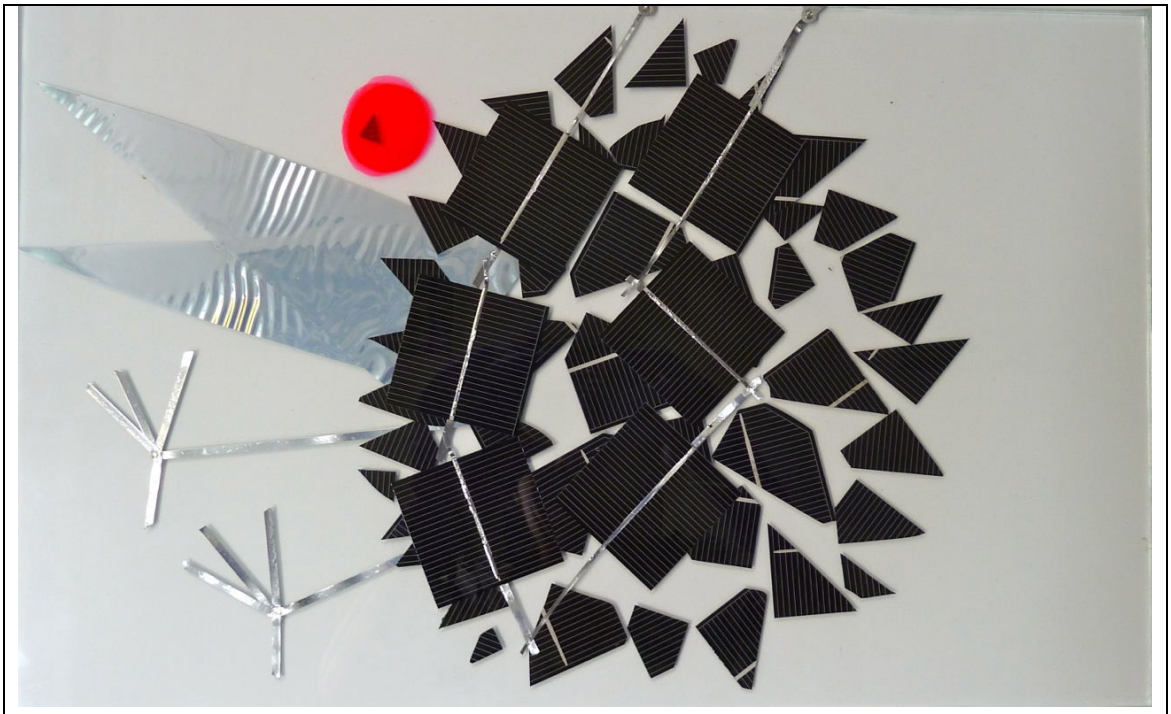

Main material: Broken c-Si PV cells behind functional c-Si PV, with a sheet of EVA between the two layers

Reason for material use: To disguise the square, functional PV cells

Additional material use: Reflective material and EVA containing Lumogen Red 300 dye used to create beak and eye details. Tabbing strip used for feet.

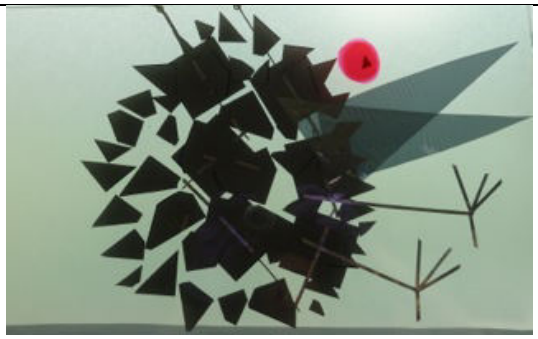

Design A back view

Table 9.2 shows design B, where the c-Si PV cells are covered in EVA doped with Lumogen Red 300. Additional details are created using tabbing strip offcuts. The PV cell shapes are displayed, but the surface colour is muted by the layers of doped EVA

placed over them.

Table 9.2: Front (main photo) and rear views of design B, incorporating Lumogen Red 300 dye within EVA

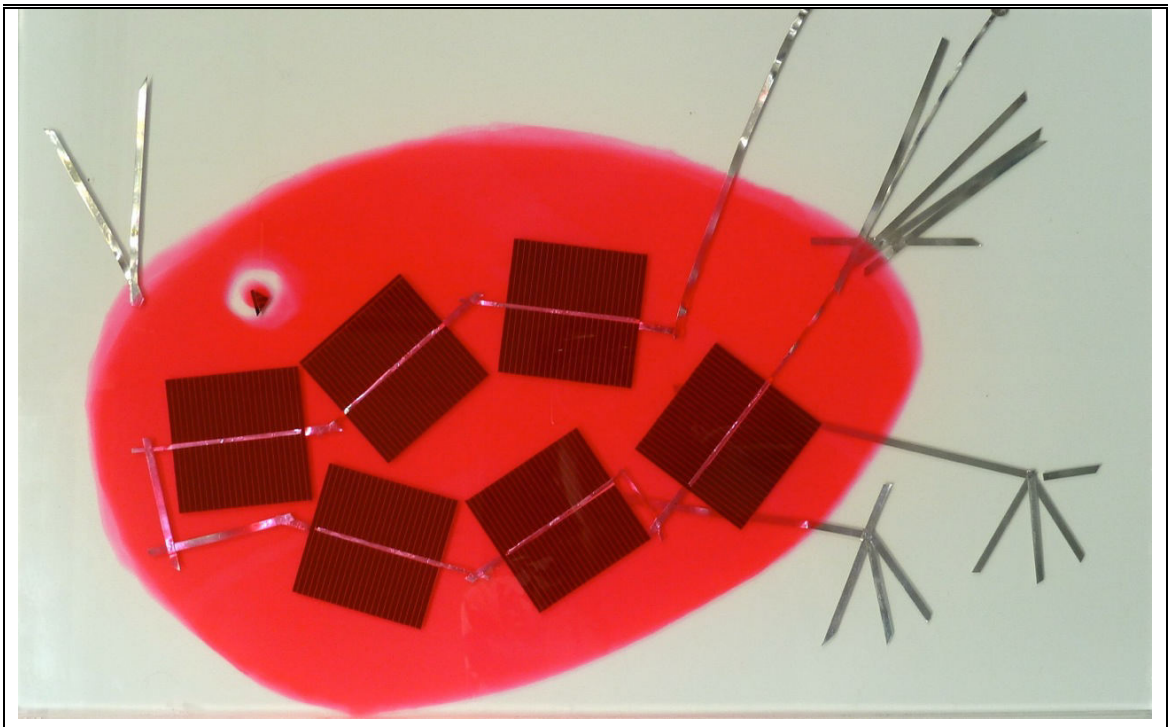

Main material: Lumogen Red 300 dye within EVA sheet

Reason for material use: To add colour and to transport light to PV cell surfaces

Additional material use: Tabbing strip to create details such as feet

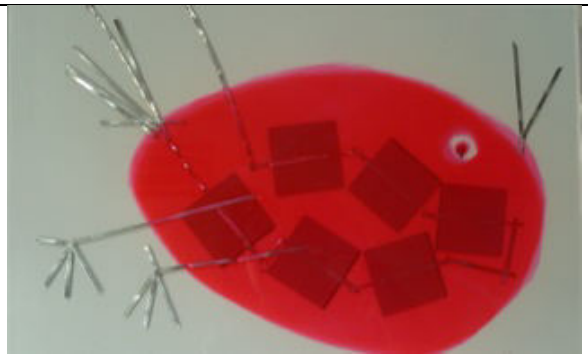

Design B back view

Design C (shown in Table 9.3) incorporates 'solar film 65' behind a string of c-Si PV cells. This covers the PV backs so that they are barely visible in reflected light, as shown by the smaller photo of the panel back, in Table 9.3. The tabbing strip details are within layers of Red-doped EVA, so appear indistinct in reflected light, unlike those in design B, where the tabbing strip is laminated between layers of undoped EVA.

Table 9.3: Design C, incorporating 'solar film 65' and EVA doped with Lumogen Red 300 dye

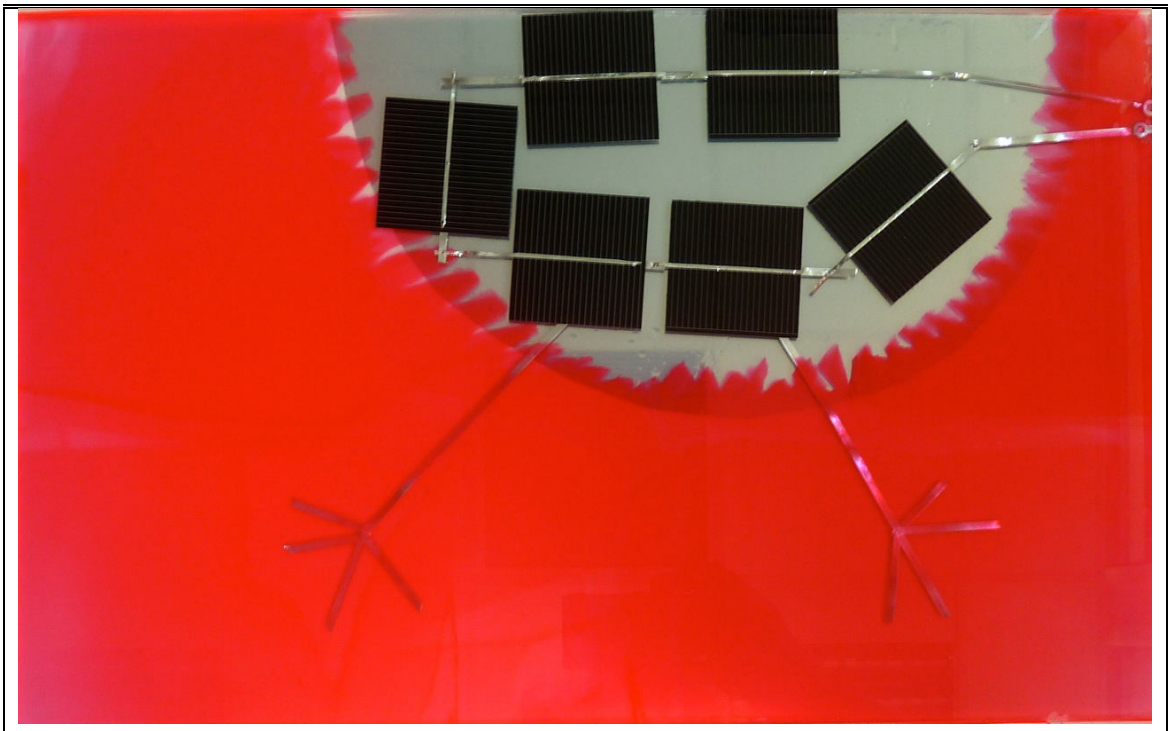

Main materials: Reflective backing, plus Lumogen Red 300 dye within EVA

Reason for use of reflective material: To disguise PV cells when viewed from behind; to reflect light back towards PV cells. **Lumogen Red 300 dye** highlights the area covered in reflective material, by providing a colour contrast

Additional material: Tabbing strip details

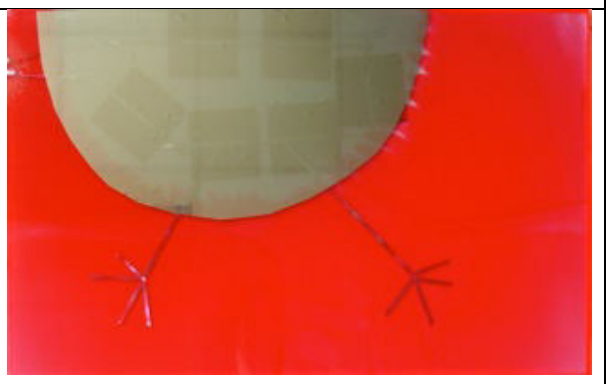

Design C back view

Design D was made up using black card laminated in place behind the c-Si PV. Table 9.4 shows the design, in which the square PV cells are effectively disguised against the dark card, when viewed from the front. The PV is completely covered from the rear. Lumogen Red dye is used within one section of the EVA, to add colour and another shape to the design, in addition to the bird silhouette. It was not possible to carry out IV tests on this design using the ABET solar simulator, as the PV cell string was too long to place under the illuminated area of the solar simulator. The concept of use of opaque material to disguise square c-Si PV shapes, was established in Chapter 3. Efficiency enhancements due to use of Lumogen Red dye within EVA are also shown previously (Figure 9.2 and Figure 9.5).

Table 9.4: Design D showing use of black card laminated within a module that contains a mixture of undoped EVA and EVA doped with Lumogen Red 300 dye

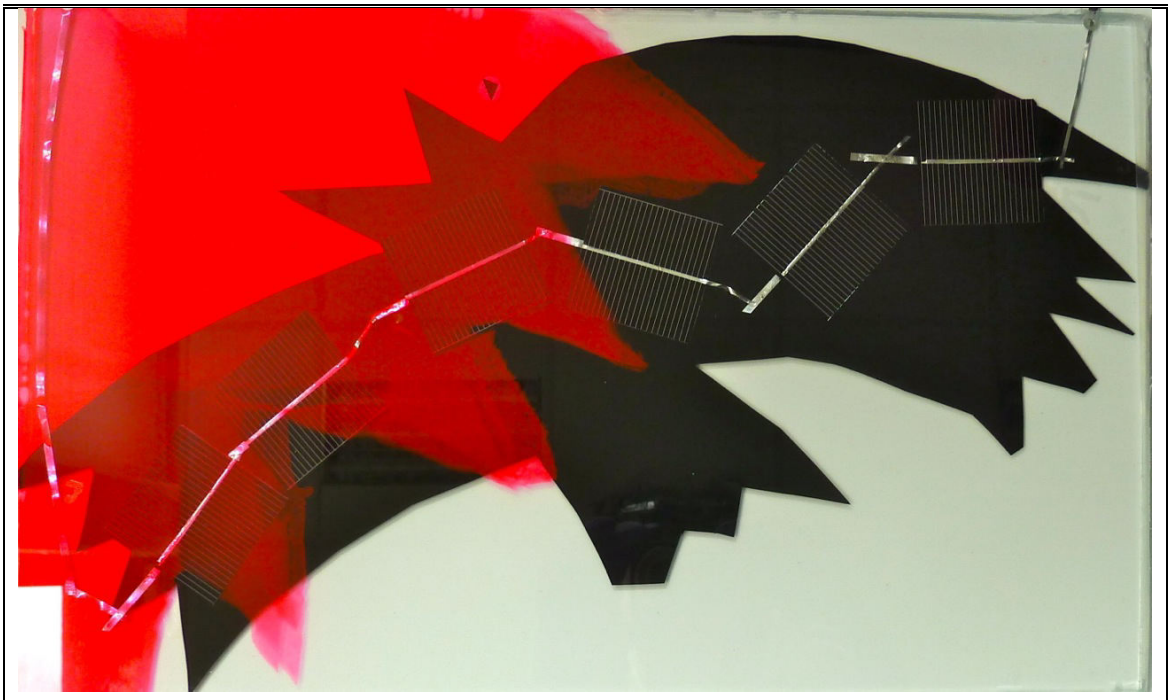

Main materials: Black card; Lumogen Red 300 dye within EVA **Reason for use of black card:** To disguise PV cells when viewed from both sides **Additional material:** Lumogen Red 300 dye. This covers 3 PV cells within the design, and is used to add a coloured shape to the design	 **Design D**

9.4.2 Comparison of current-voltage curves from designs A, B and C

The c-Si PV cell strings in designs A, B and C were placed under the ABET solar simulator before and after lamination. The graph in Figure 9.7 shows the IV curves. There is little difference between the curves, but encapsulation with the chosen materials is causing slight increases in maximum power production from the PV cells. The greatest increase is for design A, shown by the difference between the relative heights of the dashed and double-dotted lines in Figure 9.7. There is an increase in short circuit current (I_{sc}) of 5.8% compared with the I_{sc} from the unencapsulated PV cell. The proximity of the black, dotted line and red line with closely-spaced dots demonstrates that lamination of design B has led to very little increase in power output from the PV cells. This is the design in which EVA doped with Lumogen Red 300 encapsulates the central area that contains the c-Si PV. The increase in I_{sc} due to encapsulation is only

0.6%. This is very different from the single PV for which results are shown in Figure 9.2. This has a large surrounding area of red EVA, which gave an increase in I_{sc} of 18.6%. There is a trade-off between light absorbance by the Red dye, preventing light from reaching the PV cell surface, and light transport from adjacent areas, due to total internal reflection. The c-Si PV cells are closely spaced in Design B, with a comparatively small area of surrounding Red-doped EVA, accounting for the low I_{sc}.

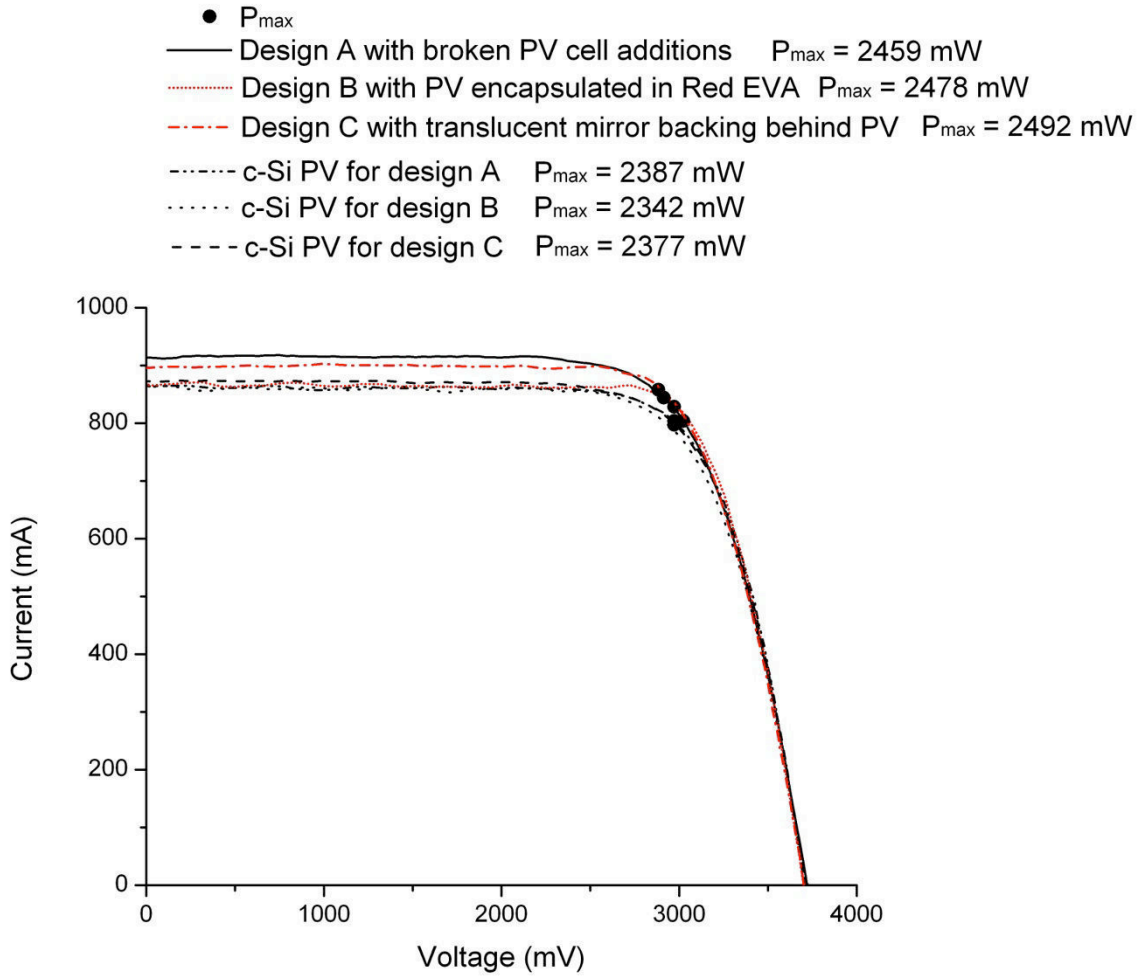

Figure 9.7: Comparison of IV measurements for c-Si PV cell strings before and after encapsulation into decorative panels

Design C gives an increase in Isc of 2.6% due to encapsulation of the PV, which has a backing of 'solar film 65'. This is similar to the 2.4% increase in I_{sc} measured from the 6 c-Si PV pieces encapsulated with both undoped and Red-doped EVA, as shown in Figure 9.5.

9.4.3 Summary of decorative panel performance

Designs A to D all demonstrate methods of applying material within the encapsulant or on the glass at the back of the PV panel. The most successful was design A, in which broken PV cell pieces were placed between layers of EVA, within the panel. This gave

the greatest efficiency increase, of 5.8% when comparing encapsulated with unencapsulated c-Si PV. This is still lower than the 10.4% increase in efficiency when encapsulating a single c-Si PV piece with a large glass surround. It appears that a large area of material surrounding each c-Si PV piece leads to greater increases in efficiency due to encapsulation. The broken c-Si PV pieces used in design A were readily available, at no extra cost, due to breakage of c-Si PV during fabrication of the panels. These PV cell pieces blended well with the functional c-Si PV cells, as they were the same material. Table 9.5 is a comparison of the materials used to make the decorative panels. The advantages and disadvantages of each material are listed in the central columns. Alternative materials are listed in the right hand column. An alternative to use of broken c-Si PV would be screen-printing directly onto the glass to be used at the back of the panel. Patterns with the appearance of broken c-Si PV cells could be used. This would be more labour-intensive to set up initially, but useful if a production run of several panels were required, as it would not be necessary to place pieces of broken PV cell within each design if screen printing were used on the glass. Screen-printing could also be applied to adhesive film to be attached to the back of the panel. Adhesive film would be less durable than screen-printing directly onto glass, but would create a design that could be replaced as required. Direct application of PV to glass could also be considered if the efficiency and lifetimes of the chosen PV are suitable for the application [153, 154].

Table 9.5, below, lists the problems associated with use of EVA doped with Lumogen Red 300 dye. Wide spacing of c-Si PV pieces is required if the dye is to cause any increase in electrical current produced by underlying PV cells. More durable methods of colour addition are listed in the right hand column, and these should be applied in situations where colouring of the front of the c-Si PV is not required. The lowest, two rows of the table indicate that ‘solar film 65’ and card could be replaced by films or coatings from a wide range of available products [155]. The levels of opacity and reflectivity can be selected as required. Further work is required to check the thermal performance of glass-glass modules in which widely-spaced c-Si PV cells will absorb heat at different rates from surrounding areas of coloured glass. Initial work by Masseck indicates that significant thermal stresses could be induced due to the differential rates of heating and cooling of PV elements, reflective materials and translucent, coloured areas of glazing [156]. Ideally PV would be combined with transparent insulation, to create light transmitting building materials with good U-values as well as electrical power generation [157, 158].

9.5 Chapter conclusion

Variety can be achieved when incorporating c-Si PV cells into decorative architectural glass. A wide range of materials can be utilised to disguise or highlight square crystalline-silicon photovoltaic cells within glazing. Careful choice of additional materials, and of their placement within a design, can ensure that good c-Si PV efficiency is obtained. Wide spacing of c-Si PV pieces is required if a combination of reflective materials and Lumogen dyes within PV encapsulants are to be effective at increasing the maximum power achieved. Issues of material durability must be to be taken into account when selecting films, coatings and inclusions.

Table 9.5: Advantages and disadvantages of materials used in the decorative c-Si PV panels

Material	Advantages	Disadvantages	Alternative material
Broken c-Si PV cells as decoration	Disguises functional c-Si PV Can be chosen to match functional PV cells Readily available	Extra layer of EVA required to provide separation from functional PV	An alternative is screen-printing directly onto glass or onto film for application to the back of the panels.
EVA doped with Lumogen Red 300 dye	Adds colour to both front and back of c-Si PV	Wide spacing of PV cells required to obtain significant efficiency increases Poor durability (discussed in Chapter 8)	Could be replaced by coloured film, paint or coloured glass to hide or add colour to c-Si PV cell backs
'solar film 65'	Disguises back of c-Si PV Can boost device efficiency	Not effective at improving device efficiency when combined with dye-doped EVA	Glass coatings or other types of film provide alternative combinations of reflectivity and light transmission
Black card	Completely disguises PV from the back in all lights Disguises PV cell fronts when viewed against the light	Durability unknown	An alternative is dark film applied to panel backs. This could be replaced as necessary Use of metal-wrap-through (MWT) c-Si PV would remove the visible tabbing strip

CHAPTER 10: THESIS CONCLUSIONS AND FURTHER WORK

It has been shown that crystalline-silicon photovoltaics (c-Si PV) can be integrated into a wide variety of decorative glazing styles through use of opaque, reflective and coloured materials. Opaque and reflective materials were used to blend square c-Si PV cells into light-transmitting designs. Both reflective and fluorescent materials were shown to be useful in increasing the amount of light incident on PV cells, so enhancing the maximum power produced by the PV. It was demonstrated that the PV encapsulants Sylgard 184 and EVA (Solutia Vistasolar Fastcure 486.00) could act as hosts for fluorescent Lumogen F dyes, but that the dyes then degraded quickly on exposure to light.

10.1 Synopsis of thesis findings

In search of new ways of making PV appear more architecturally attractive in building glazing, the aims of this thesis were to demonstrate that c-Si PV cells could be integrated into a wide variety of decorative glazing, and that maximum power from the PV could be enhanced through use of reflective and fluorescent materials. c-Si PV cells were selected from the available range of photovoltaic cells as giving the best combination of efficiency, durability and cost. Front-facing luminescent solar concentrators (LSC's) were chosen for development due to their use of front-facing PV cells and fluorescent dyes that could enhance the maximum power attained by the PV. Table 10.1 shows the materials that were selected to achieve opacity, reflectivity and colour (with these properties listed on the left of the table).

Opacity and reflectivity were initially achieved through use of glass paints, as shown in the upper part of Table 10.1. When working in a studio setting, kiln firing of the paints warped the glass so that it could not be processed in a PV laminator. Alternatives to glass paint included films and decals, which were straightforward to apply to the glass surfaces after PV lamination. These are likely to require replacement during the lifetime of a glazing installation. Further work is required to select appropriate glass coatings that can be used to create patterns as part of PV glazing designs. Ideally, PV coatings would also be applied directly to glass in any pattern, but increases in these thin-film PV efficiencies and lifetimes are required before this is a suitable alternative to use of discrete c-Si PV cells.

Colour was achieved through addition of Lumogen F dyes (BASF) into the silicone encapsulant Syglard 184 (Dow Corning) and EVA (Solutia Vistasolar Fastcure

486.00), as shown in the bottom row of Table 10.1. Lumogen F Red 300, Orange 240 and Violet 570 dyes were shown to exhibit good absorbance and emission properties within both host materials. Lumogen F Yellow 170 and Yellow 083 exhibited poor fluorescence properties within Sylgard 184. Of these two dyes, only Yellow 083 was tested within EVA, exhibiting good optical properties within this host. Exposure to sunlight caused rapid deterioration of dye colour, absorbance and fluorescence. This showed that these dye-encapsulant combinations were unsuitable for use within c-Si PV modules that are designed to last for 25 years.

Table 10.1: Materials used to enhance c-Si PV appearance and power outputs

Property	**Material**	**Advantages**	**Disadvantages**	**Further work**
Opacity	Ceramic glass paint	Established for studio use	Not suitable for processing in a PV laminator	Establish optimal glass coatings for selective application to achieve decorative effects and efficiency enhancements
	Decal	Ease of application	Short lifetime	
Reflectivity	Platinum paint	Established for studio use	Glass cannot be heat treated	
	Decal	Ease of application	Short lifetime	
Colour	Lumogen F dye within PV encapsulants Sylgard 184 and EVA (Solutia Vistasolar Fastcure 486.00)	• Minimal use of additional material • Colour is added in front of PV as well as behind	• Short dye lifetimes • Poor assimilation of dye within Sylgard 184	Select alternative methods of colour addition such as films and coatings behind PV

PV glazing test pieces were designed to demonstrate application of the properties listed on the left of Table 10.1. Use of opaque and reflective materials was combined with addition of Lumogen F dyes to PV encapsulants. Lumogen F dyes quenched within the PV encapsulant Sylgard 184 when the process of mixing was transferred to a studio setting. In contrast, the addition of Lumogen Red 300 dye to EVA was shown to be successful in both adding colour and maintaining PV efficiency, as long as wide spaces were maintained between PV cells. Maximum power from c-Si PV cells was increased when combining Lumogen Red 300 dye with the chosen ‘solar film 65’ (MDP). Further exploration of designs and materials for use in PV glazing is required.

10.2 Future work

Increasing the use of PV in glazing is one method of promoting the take-up of building-integrated PV. This thesis has demonstrated that c-Si PV can be integrated into a wide range of design styles. This is one step towards making PV into a versatile and attractive building material, which is vital in creation of more buildings that are net energy generators. The work has demonstrated that there is great potential for PV glazing to be developed further. This will require investigation of use of materials for artistic use within PV glazing, as well education about potential applications of PV for glass artists, architects, and those who commission buildings. Developments in application of durable, efficient PV to glazing materials should be coupled with artistic experimentation with the new material combinations. A feedback loop can then be set up in which new developments in PV glazing are seen as attractive and desirable due to examples of their use in architectural glass that is well designed. Further products can then be promoted for combined artistic and practical use, ensuring that new PV products are routinely exploited to their full potential as building-integrated materials. This will ensure that manufacture of future PV glazing products is carried out in ways that will allow the most creative and aesthetically-pleasing use of these products as part of architecture. This could avoid PV being seen simply as a utilitarian material like concrete, which is generally considered ugly, although it has been used in the creation of some structures that are much admired [159]. PV cells can then be seen to be part of both an artists and architects palettes of materials, not as strange and high-tech.

This PhD research has focused on development of a few designs using materials and processes that were readily available. The design processes described in the thesis have jumped from application of traditional, glass-painting techniques to use of films and card in PV glazing. Both methods were carried out on a small scale. Dye – encapsulant combinations have also been created for use in this PhD research and have been useful in demonstrating the range of colour variation that can be attained whilst maintaining adequate electrical performance from PV within glazing. These particular dye-encapsulant combinations have been shown to have short lifetimes (of less than 3 months outdoors) that are unsuitable for use in applications with the guaranteed lifetimes of at least 25 years that are expected for c-Si PV products. Development of photoluminescent materials that are commercially viable in combination with PV will require all of the following to be achieved:

- Development of fluorescent dyes with lifetimes of at least 25 years
- Maintenance of dye durability in combination with architectural materials

- Sufficient demand for coloured, fluorescent dye in combination with PV
- Demand for designs with widely-spaced PV cells or PV cell strips hidden at glazing edges
- Demand for glazing that produces low amounts of electrical power per unit area compared with 'standard' c-Si PV panels

Lumogen F dyes are currently considered the best for use in PV applications, as discussed in section 1.2.6. Development of durable combinations of dyes and other materials for use in architectural glass will require collaboration between manufacturers of dyes and of host materials for the dyes. The use of Lumogen dyes within PV encapsulant materials is also covered by a patent [160]. Sharing of patented and secret information about the molecular structure of the dyes and the materials with which they are to be amalgamated will be required if long processes of experimental trial and error in combining these materials are to be avoided. For use of fluorescent dyes with PV to be commercially viable, colouring of glazing with fluorescent dye will have to outweigh the potential for use of the many existing methods of adding durable colour to glazing that are discussed in section 10.2.1 below. PV glazing generally has lower power outputs per unit area than standard c-Si PV panels due to the need to have areas free from PV through which light can be transmitted, so any further disincentives to use, such as short lifetimes of component fluorescent dyes, will reduce the market potential of this niche product.

Fluorescent dyes are useful in public engagement activities that highlight the potential of PV within colourful designs. But as PV use expands, the associated public engagement activities will also need to develop. There is a need not only for basic education about what PV does, but also for activities that help to advance methods of incorporation of PV within building designs. Education of glass artists, architects and building commissioners is particularly important in ensuring that these groups are aware that PV can be integrated into architecture in many ways. Development of a wide range of designs for PV glazing can assist with this, as architectural glass offers great possibilities for incorporation of PV, as shown in this thesis. The ability to disguise or display PV within architectural glass can be particularly useful in demonstrating the versatility of PV. The examples of artistic use of PV in glazing test pieces that are shown in this thesis are a start point. Creation of larger-scale structures that are incorporated into building glazing schemes would assist in showing the potential for further development. There is the opportunity to carry out these developments now, while the most frequently-used type of PV is still made up from individual c-Si PV

cells. These are relatively easy to manipulate to create unique designs. Once direct application of efficient, durable PV to glass is established, then most artistic embellishment of PV is likely to become more complex, due to the need to alter the process of manufacture of the PV in order to modify the patterns in which PV is applied to substrates.

10.2.1 Alternative materials for use in PV glazing

In addition to selecting optimal PV and encapsulant combinations, there is the challenge of finding the optimal range of glass coatings, films and decals that can be used when fabricating durable, decorative PV glazing with excellent guaranteed lifetimes. Use of tinted glass [161] behind PV cells is possible when single colours are required. Screen-printing then firing of ceramics onto glass [101] offers a wide range of colour and pattern and is already carried successfully on an industrial scale by companies such as Romag [162]. These offer more durable solutions than spray-on or adhesive colour, but good selection and application could ensure that these, too, can be guaranteed for the lifetime of the PV glazing. As PV technology develops, so that direct application of durable PV to glass becomes more widespread [84, 153, 154], it will be ideal if this can be combined with selective application of coloured and other coatings to the glass to create areas of colour and pattern as required. This PhD research also highlighted the potential of reflective finishes for use with PV. Further research is required to find ideal combinations of PV and reflective coatings for glass in which thermal stresses that are likely to be set up due to selective use of reflective materials are controlled within acceptable limits. The wide range of glazing designed to reflect infrared [163, 164] can be explored, as can methods of manipulating the coatings on these types of glass [165].

The glazing test pieces fabricated for this PhD were not designed for specific locations or electrical power requirements. Design of future, building-integrated PV glazing will require careful calculation of the surface area of PV required for specific power demands. PV within architectural glass is unlikely to be installed at optimal angles to receive as much sunlight as possible, as glazing is often mounted vertically. This can be an advantage in winter, in Northerly latitudes, as the sun is then low to the horizon, so more light is received during the few hours of daylight. The need to design for specific power requirements will place an extra constraint on artistic developments, due to the need to fit a given number of PV cells into a given area of glazing. In general, the overall cost of these installations will also be higher than that of installing standard glazing or standard PV panels, but artistic use of PV glazing is intended for locations

where expensive glazing systems such as traditional stained glass would be installed [166] at costs of at least £750 per square metre [167167]. Artistic PV glazing is a niche product, but development of novel designs and material combinations could be crucial in showing that PV is a vital, adaptable building material that can then be used extensively in the creation of sustainable architecture.

10.3 Summary

PV can be integrated into decorative glazing. Individual c-Si PV cells can be blended into designs or highlighted through use of opaque, reflective and coloured materials. These materials can be applied to glass or integrated within PV encapsulants. Reflective and fluorescent materials can be used to increase the amount of light reaching PV cells. Careful consideration should be given to choice of PV cell and of additional materials to ensure that lifetimes of all components within an installation are compatible, or that replacement of less-durable elements is possible. Lumogen F, fluorescent dyes are not recommended for addition to PV encapsulant materials unless the compatibility of the dyes with each encapsulant can be established. Considerable increases in Lumogen dye durability are also required if these dyes are to be used with c-Si PV in outdoor applications with a guaranteed lifetime of at least 25 years. The existing range of reflective and opaque glass coatings and decals can be used in a wide variety of PV glazing designs. Further work is required to establish which coatings and films can be applied selectively to provide optimal combinations of reflectivity, opacity, light transmission, colour and durability.

APPENDIX A: DETAILS OF DESIGN DEVELOPMENT

This appendix gives details of the development of the design of the pieces of PV glazing that are described in chapters 3, 7 and 9. The aim is to make it straightforward for those creating their own PV glazing designs to make further improvements to the methodology. Drawings of glazing designs (which are also known as cartoons), mock-ups and preliminary test pieces are shown.

A.1 Creation of the painted test piece designs shown in Chapter 3

The aim of the work described in Chapter 3 was to blend small c-Si PV cells into a glazing design using glass paint. Figure A.1 shows initial sketches in which details are added to a square that represents a PV cell, so that both the cell colour and tabbing strip blend into the detail of the cartoon.

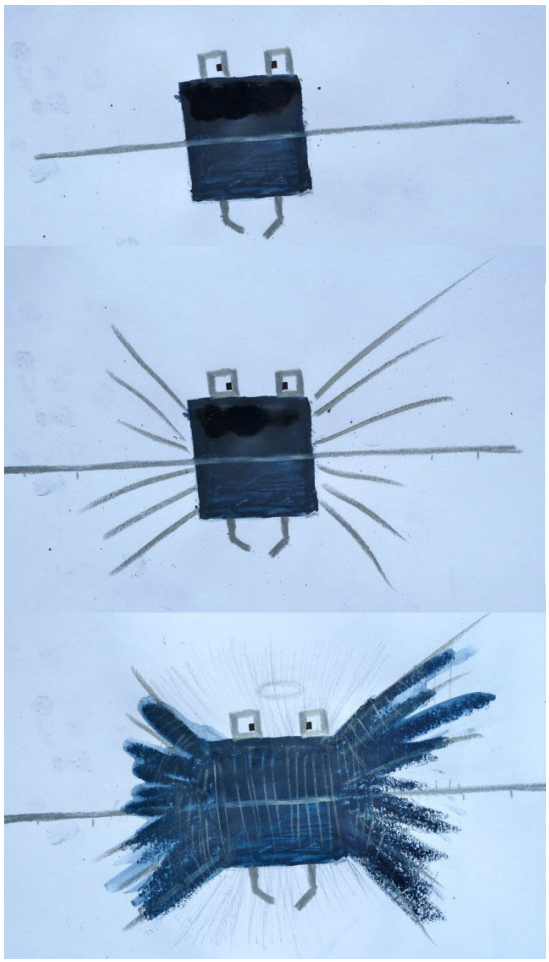

Figure A.1: Drawing of c-Si PV cell piece with addition of rectangular shapes and lines, then blue colouring, to blend the square cell shape and tabbing strip into a design.

The coloured areas representing paint do not surround the PV cell in the lowest drawing in Figure A.1, so the square cell shape is not well disguised. The design was then developed further: Figure A.2 shows a glass test piece in which the paint surrounds the square area under which the PV cell will be placed.

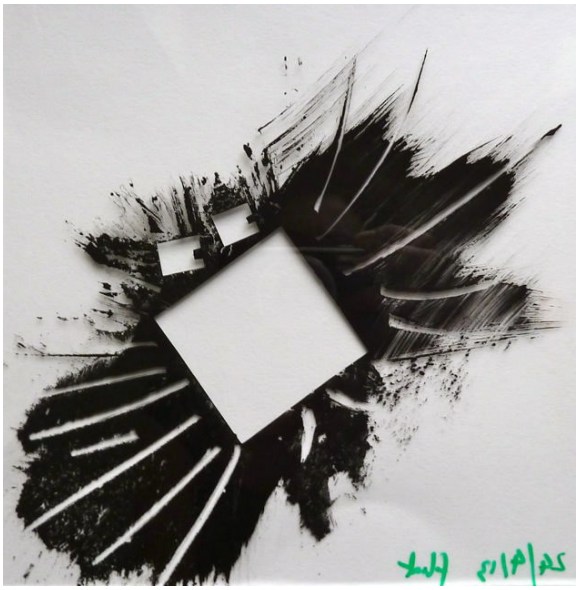

Figure A.2: Painted test piece showing the way in which masking has left a clear rectangular area to be placed over the PV cell surface.

The sketches in Figure A.3 also show drawings in which colour surrounds the PV cell shape at the front (shown in the centre of the figure).

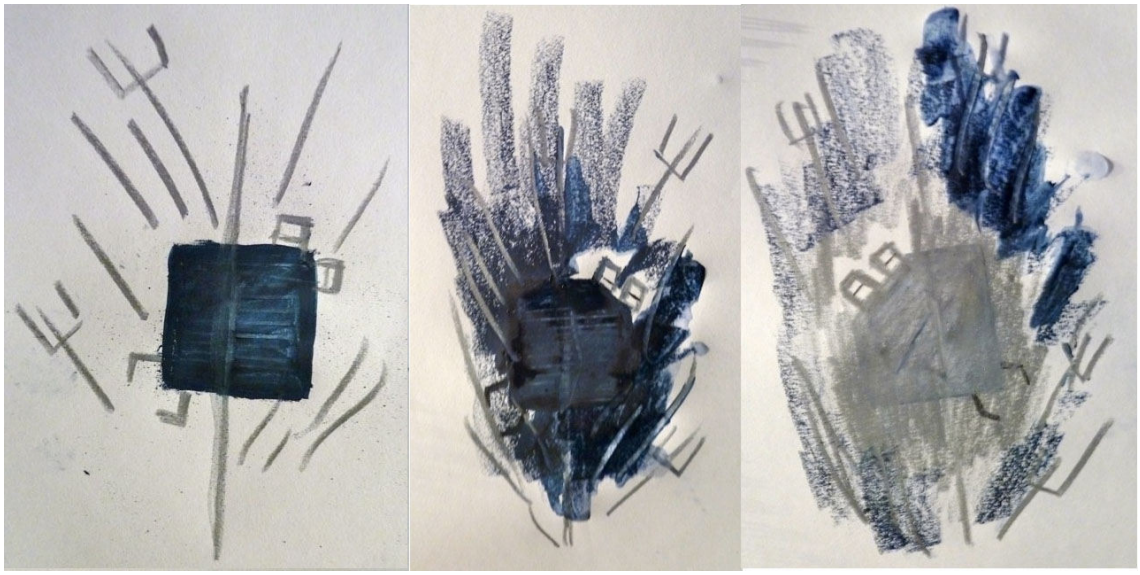

Figure A.3: The drawings on the left and at the centre of the figure show addition of tabbing strip and paint details to a PV cell. The drawing on the right shows how silver paint could be used on the reverse of the glazing design.

The grey backs of the c-Si PV cells also need to be blended into the design. These can be covered, so silver colouring is used to achieve this (shown on the right side of the figure). Figure A.4 shows glass placed on lightboxes with paint being applied according to the designs shown in Figure A.3. The photo on the left of Figure A.4 shows that adhesive plastic masking is preventing black paint from covering the area under which the PV cell will be placed. On the right, platinum paint is being used to cover an area of glass over which a PV cell has been placed. Once fired, the silver colour of the paint can then be used to hide the back of the PV cell.

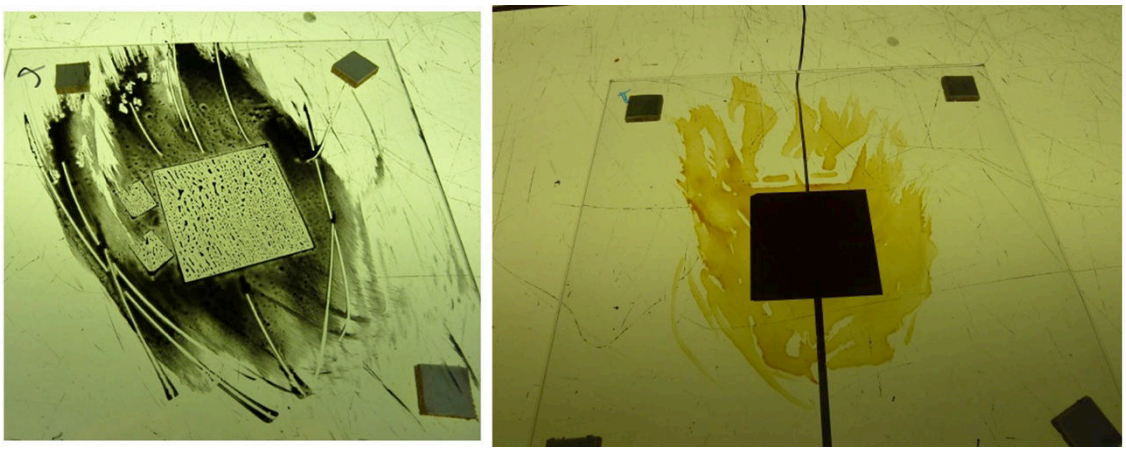

Figure A.4: Paint being applied to glass testpieces. Left: black paint with masking to retain a clear, square area. Right: Platinum paint applied to glass with a PV cell placed underneath to ensure that the paint covers the cell area.

The development of these design ideas into a full-size test piece is described in section 3.3.2 of Chapter 3. Larger cartoons (drawings of proposed glass panels) were drawn and used as templates when putting together the larger test pieces shown in chapters 3 and 9.

A.2 Use of coloured encapsulant material as described in Chapter 7

The painting techniques developed for use in Chapter 3 were also used to create a large test piece containing coloured encapsulant material, as described in Chapters 7. An initial test was made using Lumogen Yellow 083 dye within Sylgard 184 encapsulant. This is shown in Figure A.5. This, small test showed the feasibility of the method of use of coloured encapsulants with painted glass. The larger test piece is shown in Figures 7.1 and 7.2 of Chapter 7.

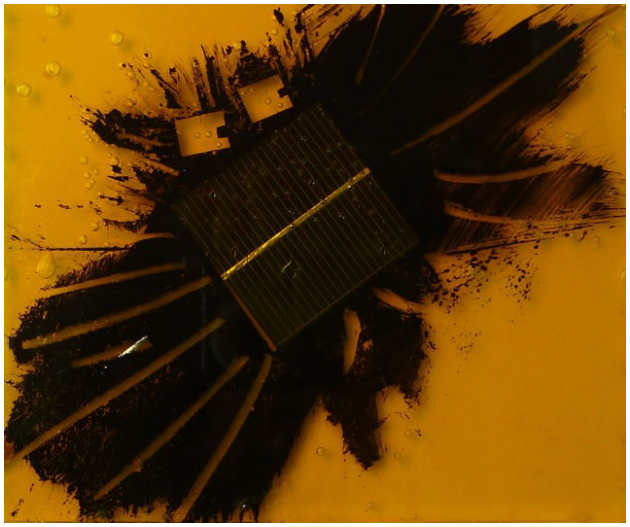

Figure A.5: Painted glass test piece with Sylgard 184 encapsulant containing Lumogen Yellow 083 dye

A.3 Development of the designs shown in Chapter 9

The above methodology was modified for the test pieces that represent birds, shown in Chapter 9. After making initial design sketches, translucent materials and paper copies of PV cells were used to mock-up designs that could then be placed in windows to see the effect of light transmitted through each design. This gave an inexpensive and relatively-quick method of testing effects such as use of broken PV cell pieces to block some light.

One of the main aims when making the designs shown in Chapter 9 was to fit the PV-cell string within the 250 x 250 mm test area of the ABET solar simulator. This proved ideal for creation of egg and body shapes for the sequence of bird designs that were made up. Figure A.6 shows a mock-up of the cell string shape made at full size, to ensure that the string fits into a 250 x 250 mm space. The photo on the left shows the layout in transmitted light, in which the square PV cell shapes dominate the design. The photo on the right of Figure A.6 shows addition of other opaque shapes, which could be made from broken pieces of PV cell. These create an overall image that is not dominated by square shapes.

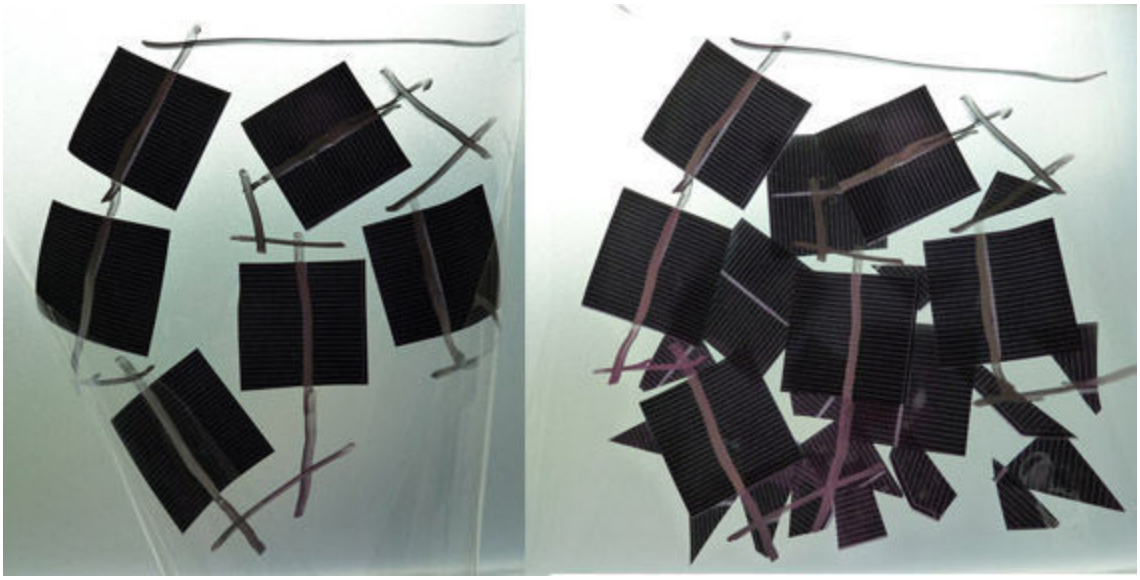

Figure A.6: Paper copies of c-Si PV cells placed on transparent plastic to show string shape (left), with addition of paper representing broken PV cell pieces (right)

The initial bird design that was created to fit with the curved PV-cell string is shown in Figure A.7. The sketch on the left shows the way in which the PV cells fit within the body of the bird, so that they are surrounded by opaque lines.

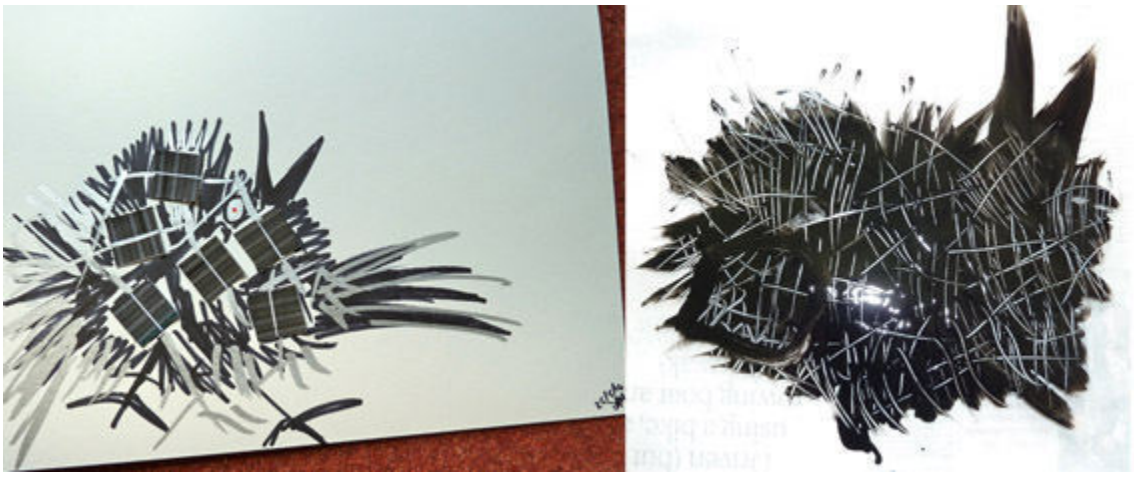

Figure A.7: The sketch on the left shows a bird design in marker pen on paper with addition of paper PV cell copies. The design on the right shows acrylic paint on transparent plastic sheet being used to mimic and disguise c-Si PV cell shapes.

The design on the right in Figure A.7 uses black acrylic paint on transparent plastic to test the way in which the screen-printed patterns on the surface of the PV cells could become part of a larger, opaque area. The use of paint has not given an accurate representation of PV cell design or shape, and the design has become very fluid and only transmits light around the edges. A crisper design was preferred, with some light transmission through the centre.

In Figure A.8, paper copies of PV cells have been used once again to create a design that resembles the sketch on the left in Figure A.8. Lines made with a silver marker pen represent tabbing strip, and grey plastic is used to add details that could be made from reflective, silver solar film, in the final design. The designs are shown in reflected light. This gives an idea of the way in which the colours and shapes will appear together in the final design. Figure A.9 shows the mock-up in transmitted light, where the opaque pieces of paper that represent PV cell pieces give a good indication of the appearance of the glass test piece as made up. The completed test piece is shown in Table 9.1 in Chapter 9.

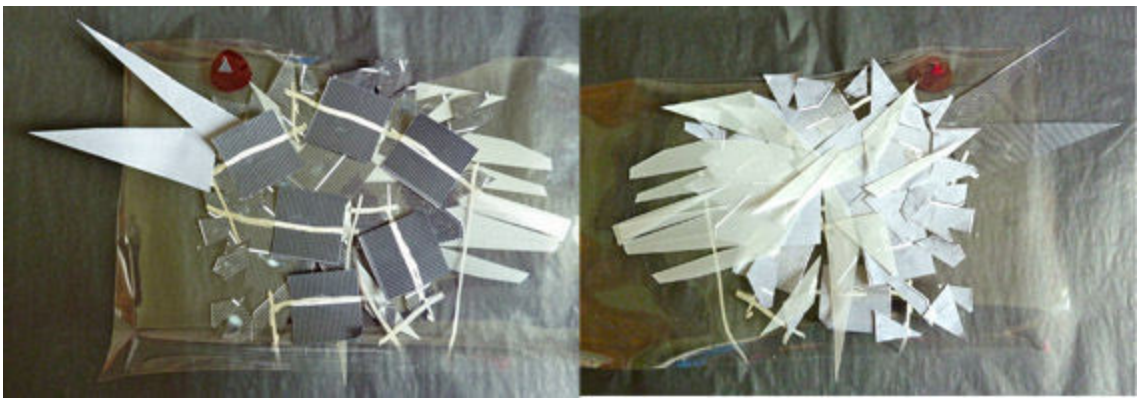

Figure A.8: Mock-ups of the front (left) and rear (right) of a PV panel. These are made up from paper and plastic shapes placed on transparent plastic, to show how the colours and shapes interact in both transmitted and reflected light. They are shown here in reflected light.

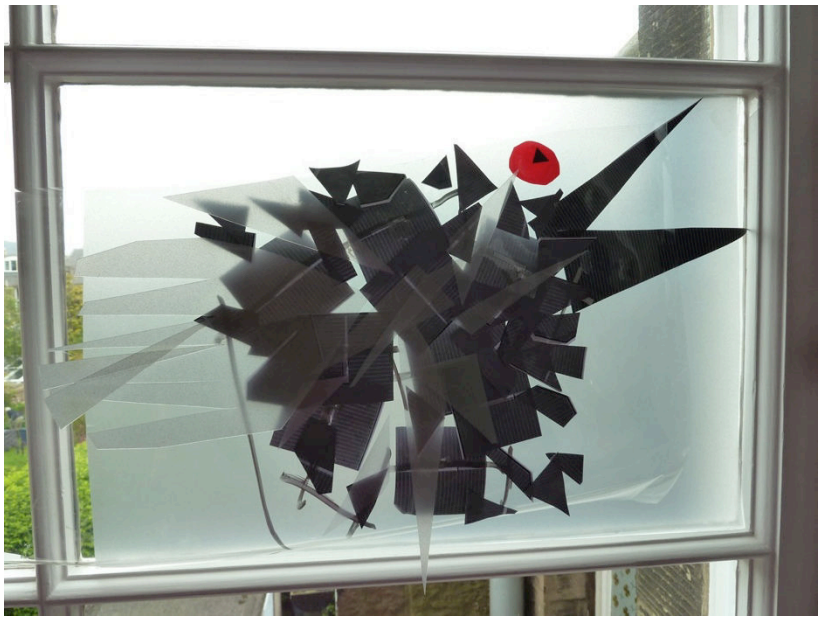

Figure A.9: Mock-up of a glass panel made with plastic, paper and marker pen. The panel is placed in a window aperture to view the design in transmitted light.

Assembly of the glass panel is shown in Figure A.10 with a piece of borofloat glass covered by a layer of EVA sheet. A PV-cell string is placed with the cell fronts facing the borofloat glass. The photo on the right shows the setup with the addition of a second sheet of EVA, which has decorative elements of broken PV cells, tabbing strip and film placed on top. This layer was then covered by a third EVA sheet and a layer of float glass before lamination.

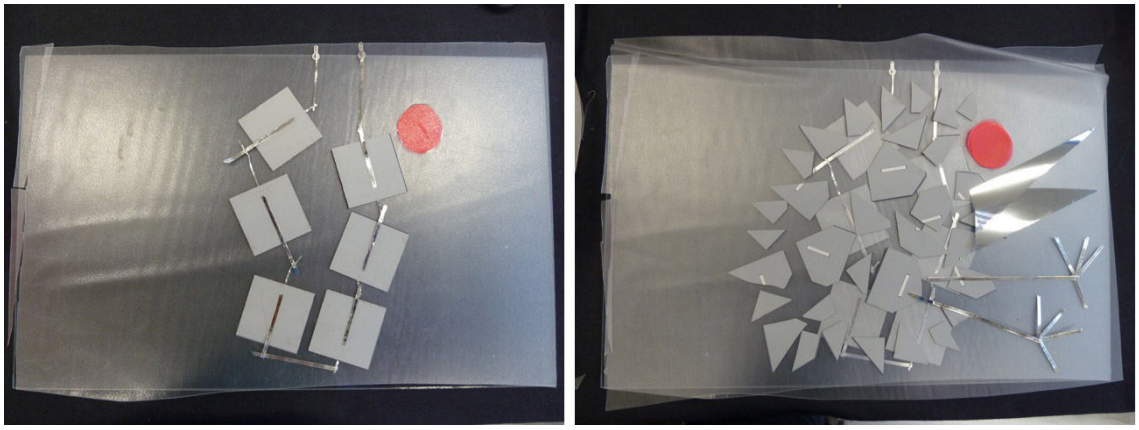

Figure A.10: Layers of PV and EVA being assembled for fabrication of a glass panel. Left: PV cell string and red EVA piece in place on top of 1 layer of EVA over glass. Right: broken PV cells, film and tabbing strip placed over a second layer of EVA

The other glass test pieces that are discussed in Chapter 9 were assembled from initial sketches such as that shown in Figure A.11, in which the PV cells are designed to fit into a small area. This is the sketch for design B, shown in Table 9.2 of Chapter 9.

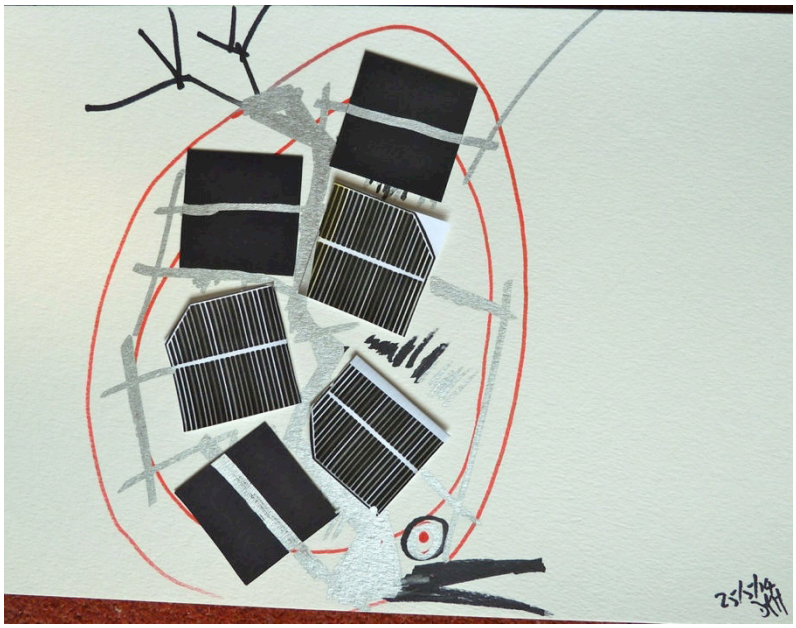

Figure A.11: Sketch for design of test piece B in Chapter 9

This sketch was relatively straightforward to assemble in glass and EVA. The assembly of materials prior to lamination is shown in Figure A.12. The central area is constructed from 3 layers of dyed EVA sheet, with no clear EVA placed in the centre, to ensure that the colour is as intense as possible. The surrounding areas contain 3 layers of clear EVA ensuring that the tabbing strip does not come into direct contact with the glass, as this would be liable to crack the glass.

Figure A.12: Layers of material assembled prior to lamination of test piece B

The assembly of materials for design D is shown in Figure A.13. This design requires a black crow shape to cover the back of the string of PV cells as shown in Table 9.4 in Chapter 9. To ensure that the black paper was cut to the correct size, a translucent material was first used to design the shape, so that the PV cell string could be seen through the material (as shown in Figure A.13).

Figure A.13: Assembly of test piece D, showing a translucent foam stencil being used to cover the PV cells prior to cutting a black, paper mask to this shape to cover the cell backs.

A.4 Conclusion

The methods described in this appendix show the advantages of experimenting with a wide range of materials to create translucent test pieces and mock-ups of PV glazing designs. Use of translucent backing materials when making mock-ups ensured that designs could be viewed in transmitted light, which was useful in ensuring that opaque PV cell shapes fitted into designs for light-transmitting glazing.

REFERENCES

[1] Hardy, D. A., Roaf, S. C. & Richards, B. S. 2015. Integrating Photovoltaic Cells into Decorative Architectural Glass Using Traditonal Glass-Painting Techniques and Fluorescent Dyes. *To be published by Wessex Institute of Technology Press in the International Journal of Sustainable Development and Planning.*

[2] Hardy, D., Kerrouche, A., Roaf, S. & Richards, B. S. 2011. The Search for Building-Integrated PV Materials with Good Aesthetic Potential: A Survey. *In:* Hutchins, M. G. & Pearsall, N. (eds.) *PVSAT-7: 7th Photovoltaic Science, Applications and Technology Conference.* Heriot-Watt University: The Solar Energy Society.

[3] Hardy, D., Kerrouche, A., Roaf, S. & Richards, B. 2012. A Silicone Host for Lumogen Dyes. *In:* Hutchins, M., Pearsall, N. & Cole, A. (eds.) *PVSAT-8: 8th Photovoltaic Science, Applications and Technology Conference.* Northumbria University, Newcastle: The Solar Energy Society.

[4] Hardy, D. A., Blekastad, S., Kerrouche, A., Roaf, S. C. & Richards, B. S. 2012. Creative Use of BIPV Materials: Barriers and Solutions. *27th European Photovoltaic Solar Energy Conference and Exhibition.* WIP.

[5] Hardy, D., Kerrouche, A., Roaf, S. C. & Richards, B. S. 2013. Improving the Aesthetics of Photovoltaics Through Use of Coloured Encapsulants. *PLEA2013 - 29th Conference: Sustainable Architecture for a Renewable Future.* Munich: Technische Universität München.

[6] Hardy, D. A., Roaf, S. C. & Richards, B. S. 2014. Improving the aesthetics of photovoltaics in decorative architectural glass. *In:* Brebbia, C. A. & Pulselli, R. (eds.) *Eco-architecture V: Fifth international conference on harmonisation between architecture and nature.* Siena: Wessex Institute of Technology Press.

[7] Baum, R. 2011. Architectural Integration of Light-Transmissive Photovoltaic (LTPV). *EU PVSEC.* Hamburg.

[8] Farkas, K., Probst, M., Cristina, M. & Horvat, M. 2010. Barriers and Needs for Building Integration of Solar Thermal and Photovoltaics. *EuroSun 2010.* Graz.

[9] German Solar Energy Society 2005. *Planning and Installing Photovoltaic Systems: A guide for installers, architects and engineers,* London, James and James (Earthscan).

[10] Roaf, S., Hyde, R., Campbell, C. & Seigert, M. 2010. Transforming markets in the built environment and adapting to climate change: an introduction. *Architectural Science Review,* 53**,** 3-11.

[11] Roaf, S., Crichton, D. & Nicol, F. 2009. *Adapting Buildings and Cities for Climate Change,* Oxford, Routledge.

[12] Oreskes, N. 2004. The Scientific Consensus on Climate Change. *Science,* 306**,** 1686-1686.

[13] HM Government 2008. Climate Change Act 2008. *In:* HM Government (ed.).

[14] Department of Energy & Climate Change. *Statistics: Energy trends section 5: electricity* [Online]. UK Government. https://http://www.gov.uk/government/statistics/electricity-section-5-energy-trends [Accessed 2 July 2015].

[15] Department of Energy & Climate Change. *Statistics: Solar photovoltaics deployment* [Online]. UK Government. https://http://www.gov.uk/government/statistics/solar-photovoltaics-deployment [Accessed 2 July 2015].

[16] Energy Saving Trust. *Our Calculations* [Online]. Energy Saving Trust. http://www.energysavingtrust.org.uk/content/our-calculations [Accessed 2 July 2015].

[17] Energy Saving Trust. *Feed-in Tariff scheme* [Online]. http://www.energysavingtrust.org.uk/domestic/feed-tariff-scheme [Accessed 2 July 2015].
[18] T. Schoen, D. P., D. Ruoss, P. Eiffert, H. Sørensen 2001. Task 7 of the IEA PV Power Systems Program - Achievements and Outlook. *17th European Photovoltaic Solar Conference* Munich.
[19] Scognamiglio, A. & Røstvik, H. N. 2012. Photovoltaics and zero energy buildings: a new opportunity and challenge for design. *Progress in Photovoltaics: Research and Applications,* 21**,** 1319-1336.
[20] Devine-Wright, P. 2005. Beyond NIMBYism: towards an integrated framework for understanding public perceptions of wind energy. *Wind Energy,* 8**,** 125-139.
[21] Scottish Natural Heritage 2009. Siting and designing windfarms in the landscape. Inverness.
[22] Pedersen, P. V., Klint, J., Kappel, K. & Pedersen, K. V. 2015. *Green Solar Cities* London, Routledge.
[23] Photon International. 2013. *Multicrystalline modules will dominate market in 2014, NPD Solarbuzz* [Online]. Aachen: Photon International. http://www.photon-international.com/news_archiv/details.aspx?cat=News_PI&sub=worldwide&pub=4&parent=7296 [Accessed 9 April 2014].
[24] Green, M. A. 2005. Silicon photovoltaic modules: a brief history of the first 50 years. *Progress in Photovoltaics: Research and Applications,* 13**,** 447-455.
[25] National Center for Photovoltaics. 2014. *Research Cell Efficiency Records* [Online]. National Renewable Energy Laboratory. http://www.nrel.gov/ncpv/index.html?print [Accessed 4 March 2014].
[26] Green, M. A. 2002. Third generation photovoltaics: solar cells for 2020 and beyond. *Physica E: Low-dimensional Systems and Nanostructures,* 14**,** 65-70.
[27] Green, M. A., Emery, K., Hishikawa, Y., Warta, W. & Dunlop, E. D. 2014. Solar cell efficiency tables (version 44). *Progress in Photovoltaics: Research and Applications,* 22**,** 701-710.
[28] Roberts, S. & Guariento, N. 2009. *Building Integrated Photovoltaics: A Handbook,* Basel, Birkhauser.
[29] Gaiddon, B., Kaan, H. & Munro, D. 2009. *Photovoltaics in the Urban Environment,* London, Earthscan.
[30] PV Upscale 2006. World PV projects database. Intelligent Energy Europe.
[31] Dunmore Corporation. *DUN-SOLAR™ PPE+ BACKSHEETS* [Online]. Bristol: Dunmore Corporation, . http://www.dunmore.com/products/polyester-pv-backsheet.html [Accessed 18 March 2015].
[32] Solar Century. *C21e tiles and slates* [Online]. London: Solar Century. http://www.solarcentury.com/uk/c21e-tiles-and-slates/ [Accessed 6 March 2015].
[33] Thurston, C. W. 2015. *Power Shingles* [Online]. PV magazine. http://www.pv-magazine.com/archive/articles/beitrag/power-shingles-_100016438/86/?tx_ttnews%5BbackCat%5D=248&cHash=42e91c43e195207bbcc8efda7d3f4c0f - axzz3TbkmH354 [Accessed 6 March 2015].
[34] Jelle, B. P. & Breivik, C. 2012. State-of-the-art Building Integrated Photovoltaics. *Energy Procedia,* 20**,** 68-77.
[35] Kaan, H. & Reijenga, T. 2004. Photovoltaics in an architectural context. *Progress in Photovoltaics: Research and Applications,* 12.
[36] Pagliaro, M., Ciriminna, R. & Palmisano, G. 2010. BIPV: merging the photovoltaic with the construction industry. *Progress in Photovoltaics: Research and Applications,* 18**,** 61-72.

[37] Prasad, D. & Snow, M. 2005. *Designing with Solar Power: A Source Book for Building Integrated Photovoltaics (BIPV),* Victoria, Australia and London, UK, Images Publishing Group and Earthscan.
[38] Farkas, K. Designing Photovoltaic Systems for Architectural Integration: Criteria and guidelines for product and system developers. *In:* Agency, I. E. (ed.) *Solar Heating and Cooling Programme.*
[39] Kanters, J., Dubois, M.-C. & Wall, M. 2012. Architects' design process in solar-integrated architecture in Sweden. *Architectural Science Review,* 56**,** 141-151.
[40] Farkas, K. 2013. *Architectural integration of photovoltaics : formal and symbolic aesthetics of photovoltaics.* Doctor of Philosophy PhD, Norwegian University of Science and Technology.
[41] Lüling, C., ed. 2009. *Energizing Architecture: Design & Photovoltaics,* Berlin, Jovis.
[42] Weller, B., Hemmerle, C., Jakubetz, S. & Unnewehr, S. 2010. *Photovoltaics: Technology Architecture Installation,* Munich/Basel, Institut für internationale Arkitektur-Dokumentation/ Birkhaüser.
[43] Scognamiglio, A., Munno, E. D., Temporin, V. & Palumbo, M. L. 2009. Use of Photovoltaics in historical buildings: an architectural approach. *In:* WIP (ed.) *24th European Photovoltaic Solar Energy Conference and Exhibition.* Hamburg: WIP-Renewable Energies.
[44] Hermannsdörfer, I. & Rüb, C. 2005. *Solar Design: Photovltaics for Old Buildings, Urban Space, Landscapes,* Berlin, Jovis.
[45] Claus, J. r. 2003. Art for the Solar Age. *Leonardo,* 36**,** 175-176.
[46] Tölle, R. & Bruton, T. 1999. Development of Bi-functional Photovoltaic Modules for Building Integration. "BIMODE". BP Solar.
[47] Devenport, S., Roberts, S., Bruton, T. M., Heasman, K., Brown, L., Cole, A. & Baistow, I. 2009. A Summary of the Havemor Project - Process Development of Shaped and Coloured Solar Cells for BIPV Applications *24th European Photovoltaic Solar Energy Conference and Exhibition.* Hamburg.
[48] Gintech. *Gintech Duoro High efficiency solar cell* [Online]. http://www.gintech.com.tw/thumb/30a92296a0c47bf3c1d7ce726ac60f5b.pdf.
[49] Baum, R. 2012. *Studies on light-transmissive photovoltaics (LTPV): patterns of integration into architectural design.* Doctor of Engineering in Architecture, Tokyo.
[50] Riedel, A. Creating electricity, letting light through. *PV magazine.* 01/2010 ed. Berlin: Karl-Heinz Remmers.
[51] Multiplying Sustainable Energy Communities 2009. Sustainable Urban Art in Valby (Denmark). *Newsletter 03/2009.*
[52] Aschehoug, Ø., Hestnes, A. G., Wyckmans, A., Stang, J., Bell, D. & Andresen, I. BP SOLAR SKIN - A FACADE CONCEPT FOR A SUSTAINABLE FUTURE. *Internationa Solar Energy Conference ISES 2003.* Göteborg, Sweden
[53] Gunnarshaug-Lien, A. & Hestnes, A. G. 2000. VISUAL STUDIES OF TRANSPARENT PV - ELEMENTS. *Eurosun 2000.* Copenhagen.
[54] Onyx Solar. *Photovoltaic Glass Patterns* [Online]. Avila, Spain: Onyx Solar Group LLC. http://www.onyxsolar.com/photovoltaic-glass-patterns.html [Accessed 27 March 2014].
[55] Masseck, T. TRANSPARENT AMORPHOUS SILICON PV-FAÇADE AS PART OF AN INTEGRATED CONCEPT FOR THE ENERGETIC REHABILITATION OF AN OFFICE BUILDING IN BARCELONA. *20th European Photovoltaic Solar Energy Conference.* Barcelona, Spain.
[56] Reyntiens, P. 1990. *The Beauty Of Stained Glass,* London, Herbert Press.
[57] Moor, A. 2006. *Colours of Architecture,* London, Octopus.

[58] Piper, J. 1968. *Stained Glass: Art or Anti-Art,* London, Studio Vista.
[59] Julie's Bicycle. *Julie's Bicycle* [Online]. London. http://www.juliesbicycle.com [Accessed 12 March 2015].
[60] BreGlobal. *BREEAM* [Online]. http://www.breeam.org/page.jsp?id=66 [Accessed 28 May 2011].
[61] Baum, R. & Liotta, S.-J. 2011. Culturally Inspired Patterns for Photovoltaics. *The Second Asian Conference on Arts & Humanities 2011.* Osaka, Japan: The International Academic Forum.
[62] Poensgen, J. *Solar-Kunst am Parkhaus Pilgrimstein* [Online]. Marburg. https://http://www.marburg.de/sixcms/detail.php?template=bild_template&id=96054&ges_id=5 [Accessed 9 April 2014].
[63] Goodpasture, L. 2011. *Art and Design: Art for Architecture* [Online]. http://www.lynngoodpasture.com/portfolio/portfolio.html [Accessed 6 August 2012].
[64] Hall, S. *'Lux Nova' wind tower with solar cells, Regent College, University of British Columbia, Vancouver, British Columbia, Canada* [Online]. Vancouver, Canada. http://www.SarahHallStudio.com/portfolio.html [Accessed 9 September 2012].
[65] Hecht, E. 2002. *Optics 4th Edition,* San Francisco, Addison Wesley.
[66] Tilley, R. J. D. 2011. *Colour and the Optical Properties of Materials,* Chichester, Wiley.
[67] Finlay, V. 2002. *Colour,* London, Hodder and Stoughton.
[68] Konica Minolta. *Precise Color Communication* [Online]. Konica Minolta Inc,. http://www.konicaminolta.com/instruments/knowledge/color/ [Accessed 26 June 2015].
[69] Kerr, D. A. 2010. *The CIE XYZ and xyY Color Spaces* [Online]. http://graphics.stanford.edu/courses/cs148-10-summer/docs/2010--kerr--cie_xyz.pdf [Accessed 15 July 2015].
[70] Technical Committee 1-48 "Revision of CIE document 15.2 Colorimetry" of CIE Division 1 "Colour and Vision". 2004. *CIE 15: Technical Report: Colorimetry, 3rd edition* [Online]. International Commission on Illumination. file:///Users/dorothyhardy/Downloads/3-publikace-cie15-2004.pdf [Accessed 15 July 2015].
[71] Weber, W. H. & Lambe, J. 1976. Luminescent greenhouse collector for solar radiation. *Appl. Opt.,* 15**,** 2299-2300.
[72] Debije, M. G. & Verbunt, P. P. C. 2012. Solar Concentrators: Thirty Years of Luminescent Solar Concentrator Research: Solar Energy for the Built Environment (Adv. Energy Mater. 1/2012). *Advanced Energy Materials,* 2**,** 1-1.
[73] Van Sark, W. G., Barnham, K. W., Slooff, L. H., Chatten, A. J., Büchtemann, A., Meyer, A., Mc.Cormack, S. J., Koole, R., Farrell, D. J., Bose, R., Bende, E. E., Burgers, A. R., Budel, T., Quilitz, J., Kennedy, M., Meyer, T., Wadman, S. H., van Klink, G. P., van Koten, G., Meijerink, A. & Vanmaekelbergh, D. 2008. Luminescent Solar Concentrators - A review of recent results. *Opt. Express,* 16**,** 21773-21792.
[74] BASF. 2005. *Colorants for plastics colorations* [Online]. BASF [Accessed 05 January 2012].
[75] Kinderman, R., Slooff, L. H., Burgers, A. R., Bakker, N. J., Buchtemann, A., Danz, R. & van Roosmalen, J. A. M. 2006. I-V Performance and Stability Study of Dyes for Luminescent Plate Concentrators. *Journal of Solar Energy Engineering,* 129**,** 277-282.

[76] Wilson, L. R. & Richards, B. S. 2009. Measurement method for photoluminescent quantum yields of fluorescent organic dyes in polymethyl methacrylate for luminescent solar concentrators. *Appl. Opt.,* 48**,** 212-220.
[77] Klampaftis, E. & Richards, B. S. 2011. Improvement in multi-crystalline silicon solar cell efficiency via addition of luminescent material to EVA encapsulation layer. *Progress in Photovoltaics: Research and Applications,* 19**,** 345-351.
[78] Klampaftis, E., Congiu, M., Robertson, N. & Richards, B. S. 2011. Luminescent Ethylene Vinyl Acetate Encapsulation Layers for Enhancing the Short Wavelength Spectral Response and Efficiency of Silicon Photovoltaic Modules. *Photovoltaics, IEEE Journal of,* 1**,** 29-36.
[79] Lakowicz, J. R. 2006. *Principles of Fluorescence Spectroscopy,* New York, Springer.
[80] British Standards Institution 2011. BS EN 410:2011 Glass in building — Determination of luminous and solar characteristics of glazing. London: BSI.
[81] British Standards Institution 2011. BS EN 673: 2011 Glass in building — Determination of thermal transmittance (U value) — Calculation method. London: BSI.
[82] British Standards Institution 2011. BS EN 674:2011 Glass in building — Determination of thermal transmittance (U value) — Guarded hot plate method London: BSI.
[83] British Standards Institution 2006. BS EN 6094-1:2006 Photovoltaic devices — Part 1: Measurement of photovoltaic current-voltage characteristics. London: British Standards Institution.
[84] Green, M. A., Basore, P. A., Chang, N., Clugston, D., Egan, R., Evans, R., Hogg, D., Jarnason, S., Keevers, M., Lasswell, P., O,ÄôSullivan, J., Schubert, U., Turner, A., Wenham, S. R. & Young, T. 2004. Crystalline silicon on glass (CSG) thin-film solar cell modules. *Solar Energy,* 77**,** 857-863.
[85] Wilson, L. R. 2010. *Luminescent Solar Concentrators: A Study of Optical Properties, Re-absorption and Device Optimisation.* PhD, Heriot-Watt University.
[86] Corrado, C., Leow, S. W., Osborn, M., Chan, E., Balaban, B. & Carter, S. A. 2013. Optimization of gain and energy conversion efficiency using front-facing photovoltaic cell luminescent solar concentrator design. *Solar Energy Materials and Solar Cells,* 111**,** 74-81.
[87] Chow, C. L., Chow, W. K., Fong, N. K., Jiang, Z. & Han, S. S. 2004. ASSESSING FIRE BEHAVIOUR OF COMMON BUILDING MATERIALS WITH A CONE CALORIMETER *International Journal on Architectural Science,* 5**,** 91 - 98.
[88] Lange, R. F. M., Luo, Y., Polo, R. & Zahnd, J. 2011. The lamination of (multi)crystalline and thin film based photovoltaic modules. *Progress in Photovoltaics: Research and Applications,* 19**,** 127-133.
[89] Moor, A. 2013-15. *Glass Art Technology* [Online]. London: Andrew Moor Associates. http://andrewmoor.co.uk/technology.html [Accessed 20 March 2015].
[90] Ketola, B., McIntosh, K. R., Norris, A. & Tomalia, M. K. 2008. Silicones for Photovoltaic Encapsulation. *23rd European Photovoltaic Solar Energy Conference and Exhibition.* Valencia, Spain.
[91] Dow Corning. 2007. *Sylgard® 184 Silicone Elastomer* [Online]. Dow Corning. http://www.dowcorning.com/applications/search/default.aspx?R=131EN [Accessed 22 December 2011].
[92] Dross, F., Labat, A., Antonio Perez Lopez, M., Antonio Perez Lopez, M., Raudez, R., Bruce, A., Kinne, S. & Komp, R. 2006. Vacuum-free, cost-effective,

developing-country-material-available solar cell encapsulation. *Solar Energy Materials and Solar Cells,* 90**,** 2159-2166.
[93] Dow Corning. 5 November 2011 2011. *RE: Use of toluene with Sylgard 184.* Personal communication with Richards, B. S.
[94] Coe, B. 1981. *Stained Glass in England, 1150 - 1550,* London, W H Allen.
[95] Reyntiens, P. 1977. *The Technique of Stained Glass,* London, Batsford Ltd.
[96] Pilkington. *Pilkington Optiwhite™ Literature* [Online]. NSG Group. http://www.pilkington.com/products/bp/bybenefit/solarenergy/optiwhitese/literature.htm [Accessed 13 March 2015].
[97] Schott Technical Glass Solutions GmbH. *SCHOTT BOROFLOAT ® 33* [Online]. Jena, Germany. http://psec.uchicago.edu/glass/borofloat_33_e.pdf [Accessed 17 December 2014].
[98] Cuttle, C. 2007. *Light for Art's Sake: Lighting for Artworks and Museum Displays,* London, Routledge.
[99] Benemann, J., Chehab, O. & Schaar-Gabriel, E. 2001. Building-integrated PV modules. *Solar Energy Materials and Solar Cells,* 67**,** 345-354.
[100] DeBergalis, M. 2004. Fluoropolymer films in the photovoltaic industry. *Journal of Fluorine Chemistry,* 125**,** 1255-1257.
[101] Petrie, K. 2005. *Glass and print,* London, A and C Black.
[102] Straumal, B., Vershinin, N., Filonov, K., Dimitriou, R. & Gust, W. 1999. Masked deposition of decorative coatings on large area glass and plastic sheets. *Thin Solid Films,* 351**,** 204-208.
[103] MDP Supplies. *Solar Film 65* [Online]. Bromborough. http://www.mdpsupplies.co.uk/solarfilm65.asp [Accessed 13 June 2014].
[104] Cowen, P. 1985. *A guide to Stained Glass in Britain,* London, Michael Joseph.
[105] Creative Glass. *Detecting the Tin Side of Float Glass* [Online]. Rochester: Creative Glass UK. http://www.creativeglassshop.co.uk/page/27/uv-tin-side-detector.html [Accessed 24 March 2015].
[106] Halliday, D., Resnick, R. & Walker, J. 2005. *Fundamentals of Physics 7th Edition,* Hoboken, New Jersey, John Wiley and Sons.
[107] Honsberg, C. & Bowden, S. *Effect of Temperature* [Online]. pveducation.org. http://www.pveducation.org/pvcdrom/solar-cell-operation/effect-of-temperature [Accessed 15 July 2015].
[108] Kerschaver, E. V. & Beaucarne, G. 2006. Back-contact solar cells: a review. *Progress in Photovoltaics: Research and Applications,* 14**,** 107-123.
[109] Heraeus Precious Metals GmbH. 15 July 2015. *RE: Price of GP 205 B platinum paint.* Personal communication with Hardy, D.
[110] Klampaftis, E., Ross, D., McIntosh, K. R. & Richards, B. S. 2009. Enhancing the performance of solar cells via luminescent down-shifting of the incident spectrum: A review. *Solar Energy Materials and Solar Cells,* 93**,** 1182-1194.
[111] BASF. 1997. *Lumogen F Collector Dyes: Technical Information* [Online]. Ludwigshafen, Germany: BASF. http://www2.basf.us/additives/pdfs/p3201e.pdf [Accessed 20 April 2012].
[112] Slooff, L. H., Bakker, N. J., Sommeling, P. M., Büchtemann, A., Wedel, A. & van Sark, W. G. J. H. M. 2014. Long-term optical stability of fluorescent solar concentrator plates. *physica status solidi (a)*.
[113] Richards, B. S. 7 October 2011 2011. *RE: BASF Update.* Personal communication with Ross, D.
[114] McIntosh, K. R., Cotsell, J. N., Norris, A. W., Powell, N. E. & Ketola, B. M. An optical comparison of silicone and EVA encapsulants under various spectra. Photovoltaic Specialists Conference (PVSC), 2010 35th IEEE, 20-25 June 2010 2010. 000269-000274.

[115] Thompson, R. B. 2006. *Fluroescence Sensors and Biosensors,* Boca Raton, Florida, Taylor and Francis.
[116] Lee, J. N., Park, C. & Whitesides, G. M. 2003. Solvent Compatibility of Poly(dimethylsiloxane)-Based Microfluidic Devices. *Analytical Chemistry,* 75**,** 6544-6554.
[117] Klampaftis, E., Ross, D., Hardy, D. A., Scanlan, P. & Richards, B. S. 2013. Adding Colour and Opening-Up Graphic Design Possibilities for Photovoltaic Modules in the Urban Landscape. *In:* Mine, A., Jäger-Waldau, A. & Helm, P. (eds.) *28th European Photovoltaic Solar Energy Conference and Exhibition.* Paris: WIP.
[118] Pern, F. J. 1997. Ethylene-vinyl acetate (EVA) encapsulants for photovoltaic modules: Degradation and discoloration mechanisms and formulation modifications for improved photostability. *Die Angewandte Makromolekulare Chemie,* 252**,** 195-216.
[119] Peike, C., Purschke, L., Weiss, K. A., Kohl, M. & Kempe, M. Towards the origin of photochemical EVA discoloration. 39th IEEE Photovoltaic Specialists Conference (PVSC), 16-21 June 2013 2013. 1579-1584.
[120] Solutia Solar GmbH. 2010. *VISTASOLAR® EVA Encapsulant Type: 486.00 / 486.10 Fast cure, transparent* [Online]. Solutia Solar GmbH. http://www.enfsolar.com/ApolloF/solar/Product/pdf/EVA/520c6d375f649.pdf [Accessed 5 Mar 2013].
[121] Slooff, L. H., Bende, E. E., Burgers, A. R., Budel, T., Pravettoni, M., Kenny, R. P., Dunlop, E. D. & Büchtemann, A. 2008. A luminescent solar concentrator with 7.1% power conversion efficiency. *physica status solidi (RRL) – Rapid Research Letters,* 2.
[122] Richards, B. 2011. *RE: Mass absorptivites of Lumogen dyes.* Personal communication with Hardy, D.
[123] Edelenbosch, O. Y., Fisher, M., Patrignani, L., van Sark, W. G. J. H. M. & Chatten, A. J. 2013. Luminescent solar concentrators with fiber geometry. *Optics Express,* 21**,** A503-A514.
[124] Heipieper, A. 2012. *Encapsulation of fluorescent organic dyes in poly-ethylene-vinyl-acetate for luminescent solar concentrators.* Renewable Energy Engineering MSc, Heriot-Watt University.
[125] Powell, N. E., Hwang, B. K., Norris, A. W., Ketola, B. M., Beaucarne, G. & McIntosh, K. R. Improved spectral response of silicone encapsulanted photovoltaic modules. 35th IEEE Photovoltaic Specialists Conference (PVSC), 20-25 June 2010 2010. 002791-002794.
[126] Abrisa Technologies. *Speciality Glass Materials Products and Specifications* [Online]. http://abrisatechnologies.com/wp-content/uploads/2014/03/Soda-Lime-Low-Iron.pdf [Accessed 15 July 2015].
[127] Sunways AG. *Sunways Solar Cells Mono 156 (AH50-H)* [Online]. ArchiExpo: The Online Architecture and Design Exhibition. http://pdf.archiexpo.com/pdf/sunways-photovoltaic-technology/sunways-solar-cells-mono-156-ah50-h/84132-90855.html [Accessed 13 March 2015].
[128] Seiffert, S., Dubbert, J., Richtering, W. & Weitz, D. A. 2011. Reduced UV light scattering in PDMS microfluidic devices. *Lab on a Chip,* 11**,** 966-968.
[129] Wilbur, J. L., Jackman, R. J., Whitesides, G. M., Cheung, E. L., Lee, L. K. & Prentiss, M. G. 1996. Elastomeric Optics. *Chemistry of Materials,* 8**,** 1380-1385.
[130] Cesaro-Tadic, S., Dernick, G., Juncker, D., Buurman, G., Kropshofer, H., Michel, B., Fattinger, C. & Delamarche, E. 2004. Supplementary information for: High-sensitivity miniaturized immunoassays for tumor necrosis factor [small alpha] using microfluidic systems. *Lab on a Chip,* 4**,** 563-569.

[131] Sharma, A. & Schulman, S. G. 1999. *Introduction to Fluorescence Spectroscopy,* New York, Wiley.
[132] Buffa, M., Carturan, S., Debije, M. G., Quaranta, A. & Maggioni, G. 2012. Dye-doped polysiloxane rubbers for luminescent solar concentrator systems. *Solar Energy Materials and Solar Cells,* 103**,** 114-118.
[133] Carnegie Mellon University 2006. Modern Biology / Biochemistry Flash Tutorials. Carnegie Mellon University.
[134] Pålsson, L. O. & Monkman, A. P. 2002. Measurements of Solid-State Photoluminescence Quantum Yields of Films Using a Fluorimeter. *Advanced Materials,* 14**,** 757-758.
[135] Wilson, L. R., Rowan, B. C., Robertson, N., Moudam, O., Jones, A. C. & Richards, B. S. 2010. Characterization and reduction of reabsorption losses in luminescent solar concentrators. *Applied Optics,* 49**,** 1651-1661.
[136] Porrès, L., Holland, A., Pålsson, L.-O., Monkman, A., Kemp, C. & Beeby, A. 2006. Absolute Measurements of Photoluminescence Quantum Yields of Solutions Using an Integrating Sphere. *Journal of Fluorescence,* 16**,** 267-273.
[137] Rowan, B. C., Wilson, L. R. & Richards, B. S. 2008. Advanced Material Concepts for Luminescent Solar Concentrators. *Selected Topics in Quantum Electronics, IEEE Journal of,* 14**,** 1312-1322.
[138] Ahn, T.-S., Al-Kaysi, R. O., Müller, A. M., Wentz, K. M. & Bardeen, C. J. 2007. Self-absorption correction for solid-state photoluminescence quantum yields obtained from integrating sphere measurements. *Review of Scientific Instruments,* 78.
[139] Pravettoni, F. 2009. External Quantum Efficiency Measurements Of Luminescent Solar Concentrators: A Study Of The Impact Of Backside Reflector Size And Shape. *24th European Photovoltaic Solar Energy Conference.* Hamburg, Germany: WIP.
[140] British Standards Institution 2005. BS 6262-4:2005 Glazing for buildings — Part 4: Code of practice for safety related to human impact. London: British Standards Institution.
[141] Photon.info 2014. Solar Module-Database. Photon Publishing.
[142] Madreperla. *Madreperla* [Online]. Milan: Madreperla s.p.a. . http://www.madreperlaspa.com/EN/chi.htm [Accessed 13 January 2014].
[143] French, R. H., Murray, M. P., Wei-Chun, L., Shell, K. A., Brown, S. A., Schuetz, M. A. & Davis, R. J. Solar radiation durability of materials components and systems for Low Concentration Photovoltaic Systems. Energytech, 2011 IEEE, 25-26 May 2011 2011. 1-5.
[144] Ametek measurement and calibration technologies. *Atlas material testing solutions: Suntest CPS+* [Online]. http://atlas-mts.com/products/product-detail/pid/237/ [Accessed 13 January 2015].
[145] Atlas Material Testing Solutions. *SUNTEST CPS / CPS+ Operating Manual* [Online]. Linsengericht / Altenhaßlau: ATLAS Material Testing Technology GmbH. http://www.severnsaleslabequip.com/manual-PDFs/G General/3 light & colour/Suntest_CPS_CPS_Opr_Manual1.pdf [Accessed 23 January 2015].
[146] Gueymard, C. A., Myers, D. & Emery, K. 2002. Proposed reference irradiance spectra for solar energy systems testing. *Solar Energy,* 73**,** 443-467.
[147] The Solar Design Company. *Software for Photovolatics* [Online]. Machynlleth: The Very Efficient Heating Company Limited, . http://www.solardesign.co.uk/pv.php [Accessed 14 January 2014].
[148] Solar Century. 12 March 2013 2013. *RE: Optimal inclination angle for PV in Edinburgh.* Personal communication with Hardy, D.

[149] timeanddate.com. *Edinburgh, United Kingdom — Sunrise, sunset and daylength, June 2013* [Online]. Stavanger: Time and Date AS. http://www.timeanddate.com/sun/uk/edinburgh?month=6&year=2013 [Accessed 14 January 2015].
[150] Astronomical Applications Department. 2014. *Sun or Moon Rise/Set Table for One Year* [Online]. Washington DC: US Navy. http://aa.usno.navy.mil/data/docs/RS_OneYear.php [Accessed 15 July 2015].
[151] BASF. 2011. *RE: Weathering of Lumogen Dyes.* Personal communication with Richards, B.
[152] Franklin, J. B., Smith, G. B. & Earp, A. E. A critical hurdle to widespread use of polymer based luminescent solar concentrators. 2013. 88250N-88250N-9.
[153] Green, M. A. 2003. Crystalline and thin-film silicon solar cells: state of the art and future potential. *Solar Energy,* 74**,** 181-192.
[154] Po, R., Bernardi, A., Calabrese, A., Carbonera, C., Corso, G. & Pellegrino, A. 2014. From lab to fab: how must the polymer solar cell materials design change? - an industrial perspective. *Energy & Environmental Science,* 7**,** 925-943.
[155] Pilkington. *Surface coatings* [Online]. Nippon Sheet Glass Co., Ltd. . https://http://www.pilkington.com/en-gb/uk/architects/glass-information/energycontrolthermalsolarproperties/coatings [Accessed 6 February 2015].
[156] Masseck, T. *Monitoring Results and Overall Evaluation of a Multifunctional, Transparent, Coloured PV-Façade for the Energetic Rehabilitation of an Office Building in Barcelona* [Online]. http://upcommons.upc.edu/e-prints/bitstream/2117/603/1/127_ES06-T05-0365_paper.pdf [Accessed 11 April 2011].
[157] Hutchins, M. G. & Platzer, W. J. 1996. The thermal performance of advanced glazing materials. *Renewable Energy,* 8**,** 540-545.
[158] Gunnarshag Lien, A. 1995. *Transparent Insulation Materials for Low Energy Dwellings in a Cold Climate.* PhD, Universitetet i Trondheim: Norges tekniske høgskole.
[159] Miodownik, M. 2013. *Stuff Matters: The Strange Stories of the Marvellous Materials that Shape Our Man-Made World,* London, Viking.
[160] Boehm, A., Grimm, A. & Richards, B. 2010. *Photovoltaic modules with improved quantum efficiency*. PCT/EP2008/052912.
[161] Pilkington. 2015. *Tinted Glass* [Online]. Tokyo: Nippon Sheet Glass Co., Ltd. https://http://www.pilkington.com/en-gb/uk/architects/glass-information/energycontrolthermalsolarproperties/glass-tints [Accessed 15 July 2015].
[162] Romag. 2015. *Romag* [Online]. Consett, Co Durham: Romag. http://www.romag.co.uk/ [Accessed 15 July 2015].
[163] Mohelnikova, J. 2009. Materials for reflective coatings of window glass applications. *Construction and Building Materials,* 23**,** 1993-1998.
[164] Gordon, R. 1997. Chemical vapor deposition of coatings on glass. *Journal of Non-Crystalline Solids,* 218**,** 81-91.
[165] Leatherland, E. 2012. *Possibilites for the use of Low Emissivity Glass by Surface Coating Manipulation Within a Creative Contex.* PhD PhD, University of Sunderland.
[166] The British Society of Master Glass Painters. *The British Society of Master Glass Painters* [Online]. London: The British Society of Master Glass Painters. http://www.bsmgp.org.uk/Home/ [Accessed 15 July 2015].
[167] Foley Stained Glass. *Terms of Trade* [Online]. http://www.foleystainedglass.com/Terms+of+trade/ [Accessed 15 July 2015].